On the distribution and biogeochemical cycling of bioactive trace metals in the Southern Ocean

by
Ryan Cloete

Dissertation presented for the degree of Doctor of Philosophy in the Faculty of Science at Stellenbosch University

Supervisor: Prof. Alakendra N. Roychoudhury

December 2020

Declaration

By submitting this dissertation electronically, I declare that the entirety of the work contained therein is my own, original work, that I am the sole author thereof (save to the extent explicitly otherwise stated), that the reproduction and publication thereof by Stellenbosch University will not infringe any third party rights and that I have not previously in its entirety or in part submitted it for obtaining any qualification.

This dissertation includes one original paper published in a peer-reviewed journal and two papers which are under peer-review yet are unpublished at the time of the submission of this dissertation. The development and writing of the papers (published and unpublished) were the principle responsibility of myself and, for each of these cases where this is not the case, a declaration is included in the dissertation indicating the nature and extent of the contributions of co-authors.

Ryan Cloete

Abstract

Bioactive trace metals, including copper (Cu), zinc (Zn), nickel (Ni) and cadmium (Cd), are essential micronutrients to marine phytoplankton and their availability in the surface ocean has been shown to influence phytoplankton community composition and abundance. Through photosynthesis, phytoplankton are the primary drivers of the marine carbon cycle therefore constraining trace metal – phytoplankton dynamics, as well as other biogeochemical processes controlling trace metal distributions, is critical to understanding the greater carbon cycle. Owing to logistical constraints, less attention has been directed toward trace metal cycling on a seasonal basis. This is particularly important in the high latitude ocean regions where large seasonal fluctuations in environmental conditions e.g. light, wind and temperature, are likely to impact trace metal distributions directly or indirectly. To this end, this study focuses on the data scarce Southern Ocean and investigates the distribution and biogeochemical cycling of Cu, Zn, Ni and Cd in summer and in winter, two seasons with contrasting environmental conditions for phytoplankton growth. This framework provided a unique opportunity to characterise the Southern Ocean winter reset period and to assess the role of deep winter mixing as a potential in-situ physical trace metal supply mechanism to aid surface productivity.

In order to address these questions, research cruises were conducted in summer and winter in the Atlantic sector of the Southern Ocean (0 - 8°E) while a third cruise took place in winter in the Indian Sector of the Southern Ocean (30°E). In the Atlantic sector, first winter measurements of dissolved (0.2 µm filtered seawater) Cu (dCu), Zn (dZn) and Ni (dNi) were compared with corresponding summer measurements from the same locations. Differences in trace metal distributions were most evident in the surface mixed layer where winter concentrations were consistently greater compared to summer. Variations in trace metal seasonality were also linked to latitude whereby seasonal variations observed near the Sub-Antarctic Front (SAF; ~ 46°S) were negligible for all three trace metals and largest variations, up to 2.0 nmol kg^{-1} for dCu, 1.2 nmol kg^{-1} for dZn and 0.3 nmol kg^{-1} for dNi, were observed near the southern extent of the Antarctic Circumpolar Current (ACC; ~ 54°S). The primary driver of these variations was through differences in biological activity with lower trace metal utilisation during winter. Sub-optimal growth conditions experienced by phytoplankton during the winter were further confirmed through calculated trace metal uptake ratios and estimations of phytoplankton productivity. Our results further suggest that deep winter mixing, i.e. the mixing of depleted summer surface waters with nutrient enriched sub-surface waters, constitutes a potentially significant surface water source of dCu, dZn and dNi with implications for phytoplankton productivity over the subsequent spring and summer seasons.

In the Indian sector of the Southern Ocean (30°E longitude), winter measurements of dZn and dissolved cadmium (dCd) were coupled with particulate (> 0.45 µm filter) zinc (pZn) and cadmium (pCd) in an effort to investigate winter trace metal cycling in more detail. Distinct changes in dissolved and particulate Cd and Zn cycling were observed between the various frontal regions encountered and were related to changes in phytoplankton community composition and physical circulation patterns. Our data suggests diatoms are major drivers of the observed trace metal gradients through their preferential consumption of dCd and dZn, relative to the major nutrient phosphate (PO_4), in the Antarctic Zone (AAZ). Here, high dCd/PO_4 and dZn/PO_4 uptake ratios set the high ratios of pCd and pZn to phosphorous (P; pCd/P; pZn/P) observed in surface waters. Ultimately, the uptake characteristics of diatoms at higher latitudes influences Cd and Zn cycling at lower latitudes as a result of the northward flow of surface waters depleted in dCd and dZn. In addition, because diatoms require silicic acid ($Si(OH)_4$), the export of their cells below the winter mixed layer provides additional insights as to the observed deep water coupling of dZn and $Si(OH)_4$. Below the surface, Cd and Zn cycling is predominantly controlled by remineralisation, vertical mixing and upwelling. We conclude that winter Southern Ocean surface waters are not biologically dormant and that trace metal cycling is influenced by biological productivity during winter.

Opsomming

Bio-aktiewe spoormetale, insluitend koper (Cu), sink (Zn), nikkel (Ni) en kadmium (Cd), is noodsaaklike mikrovoedingstowwe vir mariene fitoplankton. Daar word getoon dat die beskikbaarheid van hierdie bio-aktiewe spoormetale in die oppervlakwater van die oseaan die fitoplanktongemeenskappe se samestelling en weligheid beïnvloed. Fitoplankton is die primêre dryfveer vir die mariene koolstofsiklus deur fotosintese. Die ontleding van die dinamika tussen spoormetale en fitoplankton, asook die ander biogeochemiese prosesse wat die verspreiding van spoormetale beheer, is kritiek tot die verstaan van die groter koolstofkringloop. Seisoenaal word daar minder aandag gegee aan spoormetaal-siklussering as gevolg van logistieke beperkinge, veral in die hoë breedtegraad oseaanstreke. In hierdie streke is die kanse groter dat die verspreiding van spoormetale direk of indirek beïnvloed word deur die groot seisoenale skommelinge in omgewingstoestande soos lig, wind en temperatuur. Derhalwe fokus hierdie studie op die Suidelike Oseaan waaroor daar ‘n skaarste aan data is en ondersoek dit die verspreiding en biogeochemiese siklussering van Cu, Zn, Ni en Cd in die somer en winter, twee seisoene met uiteenlopende omgewingstoestande vir die groei van fitoplankton. Hierdie raamwerk bied ‘n unieke geleentheid om die tydperk van herset tydens die winter in die Suidelike Oseaan te karakteriseer en die rol van diepte-vermenging in die winter as ‘n potensiële meganisme om ter plaatse spoormetale te voorsien wat produktiwiteit in die oppervlakwater van die oseaan bevorder, te bepaal.

Ten einde hierdie vrae aan te spreek, is navorsingsvaarte tydens somer- en wintermaande in die Atlantiese gedeelte van die Suidelike Oseaan (0 - 8°E) uitgevoer. ‘n Derde navorsingsvaart het tydens die winter in die Indiese gedeelte van die Suidelike Oseaan (30°E) plaasgevind. In die Atlantiese gedeelte is die metings van opgeloste (0.2 µm gefiltreerde seewater) Cu (dCu), Zn (dZn) and Ni (dNi), wat vir die eerste keer tydens die winter geneem is, vergelyk met die ooreenstemmende metings wat in die somer by dieselfde ligging geneem is. Die verskil in die verspreiding van die spoormetale was die duidelikste in die oppervlakmenglaag. Hier was die konsentrasies, wat in die winter gemeet is, deurgaans hoër as in die somer. Variasies in die seisoensgebondenheid van spoormetale is ook aan breedteligging verbind. Die veranderinge wat tydens die seisoenskommeling by die Subantarktiese Front (SAF; ~ 46°S) waargeneem is, was weglaatbaar klein vir al drie spoormetale. Die grootste variasies, tot 2.0 nmol kg^{-1} vir dCu, 1.2 nmol kg^{-1} vir dZn en 0.3 nmol kg^{-1} vir dNi, is naby die suidelike reikwydte van die Antarktiese Sirkumpolêre Seestroom (ACC; ~ 54°S) waargeneem. Die hoofdryfveer van hierdie variasies was deur die verskil in biologiese aktiwiteit, met ‘n laer benutting van spoormetale in die winter. Die fitoplankton het in die winter suboptimale toestande vir groei ervaar, iets wat verder bevestig is deur die berekening van die verhoudings van spoormetale se opname en die skattinge rakende die produktiwiteit van die fitoplankton. Ons uitslae dui verder daarop dat die diepte-

vermenging in die winter, m.a.w. die vermenging van die uitgeputte oppervlakwater van die oseaan van die somerseisoen met die dieper water wat verryk is met voedingstowwe, moontlik ‘n beduidende bron van dCu, dZn and dNi in die oppervlakwater van die oseaan uitmaak. Dit het implikasies vir fitoplanktonproduktiwiteit gedurende die daaropvolgende lente en somer.

In die Indiese gedeelte van die Suidelike Oseaan (30°E lengtegraad), is die metings van dZn en opgeloste kadmium (dCd) wat in die winter gemeet is, verbind met partikulêre (> 0.45 µm filter) sink (pZn) en kadmium (pCd) in ‘n poging om spoormetaal-siklussering in die winter in meer diepte te ondersoek. Onmiskenbare veranderinge in die opgeloste en partikulêre Cd en Zn siklussering is tussen die verskeie frontale streke waargeneem. Dit is verwant aan die veranderinge in die samestelling van die fitoplanktongemeenskappe en die fisiese sirkulasiepatrone. Volgens ons data is diatomeë die hoofaandrywers van die gradiënte van die spoormetale se konsentrasies wat waargeneem is. Dit is oorwegend as gevolg van diatomeë se voorkeur vir die verbruik van dCd and dZn, relatief tot fosfaat (PO_4) as die vername voedingstof in die Antarktiese Zone (AAZ). Hier word daar in die oppervlakwater van die oseaan waargeneem dat hoë verhoudings van dCd/PO_4 en dZn/PO_4 se opname lei tot hoë verhoudings van pCd en pZn tot fosfor. Uiteindelik beïnvloed die kenmerkende manier waarop diatomeë hierdie spoormetale opneem by hoër breedteliggings die siklussering van Cd en Zn by laer breedteliggings as gevolg van die noordwaartse vloei van die oppervlakwater van die oseaan wat uitgeput is aan dCd en dZn. Boonop verskaf die besinking van diatomeë tot onder die menglaag in die winter verdere insigte oor die aankoppeling wat tussen dZn en kieselsuur ($Si(OH)_4$) waargeneem word, aangesien diatomeë kieselsuur benodig. Onder die oppervlak menglaag word die siklussering van Cd en Zn oorwegend deur hermineralisering, vertikale vermenging en opwelling beheer.

Ons kom tot die gevolgtrekking dat die oppervlakwater van die Suidelike Oseaan nie in die winter biologies onaktief is nie en dat spoormetaal-siklussering gedurende die winter deur biologiese produktiwiteit beïnvloed word.

Acknowledgements

Naturally, undertaking a project on this scale would never be possible without the guidance, support and input from not just my supervisor and research group members, but also from family and friends. Words will never truly express my gratitude in this regard however the following is my best attempt:

To my supervisor, Prof Alakendra Roychoudhury, you deserve so much credit for the success of this project as well as that of our research group. Your vision and hard work has guided the development of the TracEx research group and in so doing has put South Africa on the map in terms of trace metal geochemistry. Thank you also for guiding my development as a young scientist, there is no doubt in my mind that your supervision has been the biggest influence in my scientific career thus far. Your supervision style was such that I was completely accountable for every step of my project, be it in decision making or time management, however your open-door policy meant that I was never far from advice. This has taught me the ability to think critically, to break up mammoth tasks into smaller, more manageable goals and to never give up, lessons which I intend to carry with me not just in a scientific context but also in everyday life. Lastly, thank you for all the opportunities you have provided me. I have been fortunate to travel to places I never dreamed of during this project. Through this project, my horizons have broadened significantly and I can confidently say that it has developed a curiosity and passion for oceanography that I never knew I had.

To Dr Susanne Fietz, much of the credit for the success of the TracEx group goes to you aswell. I, as well as this project, have benefitted hugely from your logical and methodical approach to science. Your expertise from a biology point of view, especially in terms of phytoplankton, has proved invaluable. Your leadership, particularly during cruise preparations and while at sea, was largely responsible for the successful collection of seawater samples and ultimately the project as a whole. Thank you for encouraging us to pursue a career in science, I think you eventually got through to me.

To Jean Loock, where to even start. To get to where we are today would have simply been impossible without each other. From the early days, we spent day after day developing methodologies, to days and nights spent putting this into action and finally to days and mostly nights spent trying to make sense of all the data. What a journey it has been so far. Through our research we have explored oceans and traversed countries to present our research. Your general knowledge is remarkable and through this, you have taught me to question and form my own opinions. I am equally grateful for our friendship outside of research. Your passion for Africa, travel, camping and mountain biking has meant that for every hour spent in the lab, another hour (sometimes two) has been spent engaging in other interests. I

believe much of our success has resulted from this balance and I hope it continues wherever our paths lead us.

To the TracEx team and the many other researchers I have met along the way, Thato Mtshali, Natasha van Horsten, Johan Viljoen, Jan-Lukas Menzel Barraqueta, Saumik Samanta, Andrea Baker, Ishmael Kangueehi, Tara de Jong, Margaret Ogundare and Andile Mkandla. What a team we've made! Thank you for your contributions to this project. From playing your part in ensuring successful cruises to feedback sessions during lab meetings, it has been a pleasure working and interacting with you all. A special thank you to Riana Rossouw from the Central Analytical Facility (CAF) whose tireless work cleaning, calibrating, optimising and operating the ICP-MS was instrumental in providing high quality data.

To everyone in the PhD lab at the Earth Science department, thank you the countless daily interactions and many impromptu lunch breaks. A special mention to Jared van Rooyen and Andrew Watson for many afternoon mountain bike rides where my sanity was often restored, frustrations vented and small victories celebrated.

My sincere appreciation extends to the technical and administrative staff whose work is often not tangible yet is absolutely essential. I would like to thank in particular George Olivier, Martina Frei, Gillian Strydom and Faizel for their behind the scenes work, especially in the months leading up to the various scientific cruises.

To Captain Gavin Syndercombe and Captain Knowledge Bengu as well crew from the SA Agulhas II research vessel, your professionalism and 'make a plan' mentality was key to successful voyages. Thank you for being our eyes and keeping us safe whilst braving the Southern Ocean. Thank you also to the Department of Environmental Affairs (DEA) and the South African National Antarctic programme (SANAP) for providing the platforms and infrastructure necessary to conduct this research. A special mention to the Antarctic Legacy of South Africa (ALSA) for their constant interest and doing such great work in promoting and communicating Antarctic related sciences to the public.

The South African National Research Foundation (NRF) has supported me financially, through a scholarship and through travel allowances. The NRF has made this project, and countless others, possible and for this I extend my sincere gratitude. I am also grateful for the support of Rozelle Peterson, the NRF coordinator at Stellenbosch University.

To my mom, dad and sister, I will never be able to fully express how thankful I am to have your love, support encouragement in my life. From the moment I was born you have sacrificed for me, placed an importance on health, communication and education and have provided me with every tool necessary

to make a success of the opportunities you have afforded me. Thank you for encouraging me to pursue my interests and for being the best support system during this project and in life. I couldn't have done it without you three. To my extended family, in particular my nana, your interest and support during the past 3 years was greatly appreciated. I look back at the many times I tried to explain my research to you and can't help but to smile. Thanks also goes to our spaniel, Bronty, who sat at my feet day in and day out during the final months of write up and provided endless entertainment and necessary distractions.

To my partner Saskia, as someone who is also involved in research, your advice and perspective was always appreciated and often provided the inspiration I was searching for. Your love of nature and appreciation for the tiniest details and interactions happening all around us has given me a fresh lens through which I view my surroundings and also the nano-scale interactions between trace metals and phytoplankton. Research aside, the many weekends spent adventuring outdoors, camping, climbing and hiking provided the perfect escape to recharge, breathe fresh air and relax. Thank you for your support always and for showing such interest in this work.

Lastly, while this PhD was largely a personal endeavour, I believe the ocean is ours to share, enjoy, understand and respect. Thank you to all my friends who showed interest, not just in the work I have been involved in, but to marine research in general. I have come to find the ocean is a truly magical place. Long may its beauty and complexity keep us enthralled. Finally, to the friends who made my university years some of the best of my life, may the fun continue….

Table of contents

List of figures

Chapter 1: Introduction to ocean biogeochemistry

Chapter 2: Winter and summer distributions of Copper, Zinc and Nickel along the International GEOTRACES Section GIPY05: Insights into deep winter mixing

Appendix A

List of tables

Chapter 1: Introduction to ocean biogeochemistry

Chapter 2: Winter and summer distributions of Copper, Zinc and Nickel along the International GEOTRACES Section GIPY05: Insights into deep winter mixing

Chapter 3: Winter dissolved and particulate cadmium in the Indian sector of the Southern Ocean (GEOTRACES GIpr07 transect)

Chapter 4: Winter dissolved and particulate zinc in the Indian sector of the Southern Ocean: Distribution and relation to major nutrients (GEOTRACES GIpr07 transect)

Appendix A

Chapter 1
Introduction to ocean biogeochemistry

1. Trace metals as micronutrients in the ocean

The modern ocean ecosystem is driven by photosynthesis, a biochemical process that converts carbon dioxide (CO_2) and water (H_2O) to glucose (sugar) and oxygen (O_2) using sunlight (photons) as the energy source. Phytoplankton are photo-autotrophic organisms, i.e. they are capable of performing photosynthesis, and form the base of the marine food web such that all other organisms in the marine ecosystem are dependent on them. Phytoplankton cannot function on light, CO_2 and H_2O alone. Major nutrient elements and trace nutrient elements are also essential for vitality. Chief among the required major nutrients are nitrogen (N) and phosphorous (P) although diatoms, a major group of phytoplankton, require additional silicon (Si) with which they build their protective frustules. Phytoplankton assimilate these major nutrients, as well as carbon (C), in a more or less uniform ratio referred to as the Redfield ratio (Redfield et al., 1963) with an elemental ratio of:

C:N:P = 106:16:1. Eq. 1

In addition to the major nutrients, several trace nutrient elements or "trace metals" including iron (Fe), zinc (Zn), copper (Cu), manganese (Mn), nickel (Ni), cobalt (Co) and cadmium (Cd) are essential for phytoplankton growth and reproduction. Trace metals are used as co-factors in a myriad of different enzymatic processes (Sunda, 1989) responsible for the uptake and transformation of C, N and P including photosynthesis and respiration. The Redfield ratio was later extended to include trace metals (e.g. Bruland et al., 1991) with an approximate elemental ratio of:

C:N:P:Fe:Zn:Cu,Mn,Ni,Co,Cd = 106:16:1:0.005:0.002:0.0004. Eq.2

From Eq.2 it is clear that phytoplankton require micronutrients in quantities far smaller compared to the macronutrients and that there are large differences between individual micronutrient requirements. The trace metal sufficiency (or deficiency) of phytoplankton cells depends on the specific enzymatic requirement and the cellular metal concentration (cell quota). As such, deviations from the extended Redfield ratio are observed throughout the global ocean.

Changes in the abundance and cycling of trace metals influences the distributions of phytoplankton such that major chemical elements, most importantly C, are re-proportioned between the ocean and atmosphere. The transfer of C from the atmosphere to the surface ocean and eventually to the deep ocean storage reservoir is a process collectively referred to as the biological carbon pump (Marinov and Sarmiento, 2004). To expand upon this, the uptake of CO_2 by phytoplankton for photosynthesis and subsequent sinking/export of organic particles e.g. dead organisms and faecal pellets, results in the

export or 'pumping' of C to the deep ocean. Simplified, once CO_2 is utilised in the surface ocean by phytoplankton the water becomes undersaturated and the CO_2 is replenished through atmosphere/surface ocean exchange. Ultimately, the amount of C that is brought to the deep ocean via the biological pump affects the atmospheric CO_2 concentration and therefore the global climate. Perhaps the best example of trace metals affecting the carbon cycle is the "iron hypothesis" (Martin, 1990). Here, changes in the supply of dust (Fe) to the surface Southern Ocean, and the resulting stimulation of algal growth, increased photosynthesis and carbon uptake, are thought to be a primary control of atmospheric CO_2 levels, ultimately driving glacial/interglacial periods on earth. Considering the critical role trace metals play in the global biosphere, it is of utmost importance to fully understand their biogeochemical cycling, particularly in marine systems. This thesis aims to contribute to the growing body of knowledge on the role trace metals play in the global biosphere and furthermore, to serve future models in assessing the sensitivity of trace metal cycling to climatic changes.

2. The global importance of the Southern Ocean

The Southern Ocean is geographically constrained to waters between the Antarctic continent and the 40°S latitude (Orsi et al., 1995). The Southern Ocean plays a central role in the global thermohaline circulation which ultimately impacts Earth's climate over decadal to centennial timescales (see review by Carter et al., 2009) as the Antarctic Circumpolar Current (ACC) and its offshoots provide direct communication to the major ocean basins. Around the margins of Antarctica, cold and dense surface water sinks to abyssal depths and is transported northwards via deep boundary currents into the other major ocean basins (Figure 1; (Meredith, 2019)). Through vertical exchange processes (upwelling and mixing), these deep waters rise, increase in temperature and contribute to warm surface circulation that extends from the Pacific and Indian Oceans into the Atlantic Ocean. In the Atlantic, the warm and saline surface waters flow north where the water cools and sinks at high latitudes to form deep waters which flow south and eventually upwell in the Southern Ocean thereby completing one cycle of thermohaline circulation (Broecker, 1991). Through the physical transport of Antarctic derived water masses, the Southern Ocean has the potential to influence the biogeochemical cycling of elements on a global scale (Sarmiento et al., 2004).

Apart from functioning as a central hub for thermohaline circulation, the Southern Ocean is characterised by a unique interplay between phytoplankton productivity and nutrient availability. The high latitude Southern Ocean is classified as a High Nutrient Low Chlorophyll (HNLC; Figure 2; (Garcia et al., 2019)) region whereby an incomplete utilisation of the major nutrients (N, P), hence 'high nutrient', in surface waters results in phytoplankton, represented by chlorophyll-*a* (chl-*a*), not growing to their full potential, i.e. 'low chlorophyll'. Portions of the north and tropical Pacific Ocean are also classified as HNLC however the Southern Ocean is by far the largest such region. The limitation of biological productivity in the Southern Ocean stems from trace nutrient/metal availability, most notably

Fe (Boyd et al., 2000; Croot et al., 2004; de Baar et al., 2005; Martin et al., 1990), while light is also a major potential factor inhibiting phytoplankton growth in the Southern Ocean (Mitchell et al., 1991; Viljoen et al., 2018). Because the Southern Ocean is a key sink for anthropogenic CO_2 (Sabine et al., 2007), variations in the efficiency of the biological carbon pump, as a result of trace metal availability, may have consequences for the oceanic uptake of CO_2. The research presented here contributes to the global effort in understanding the impact of trace metal distributions on the efficiency of the biological carbon pump.

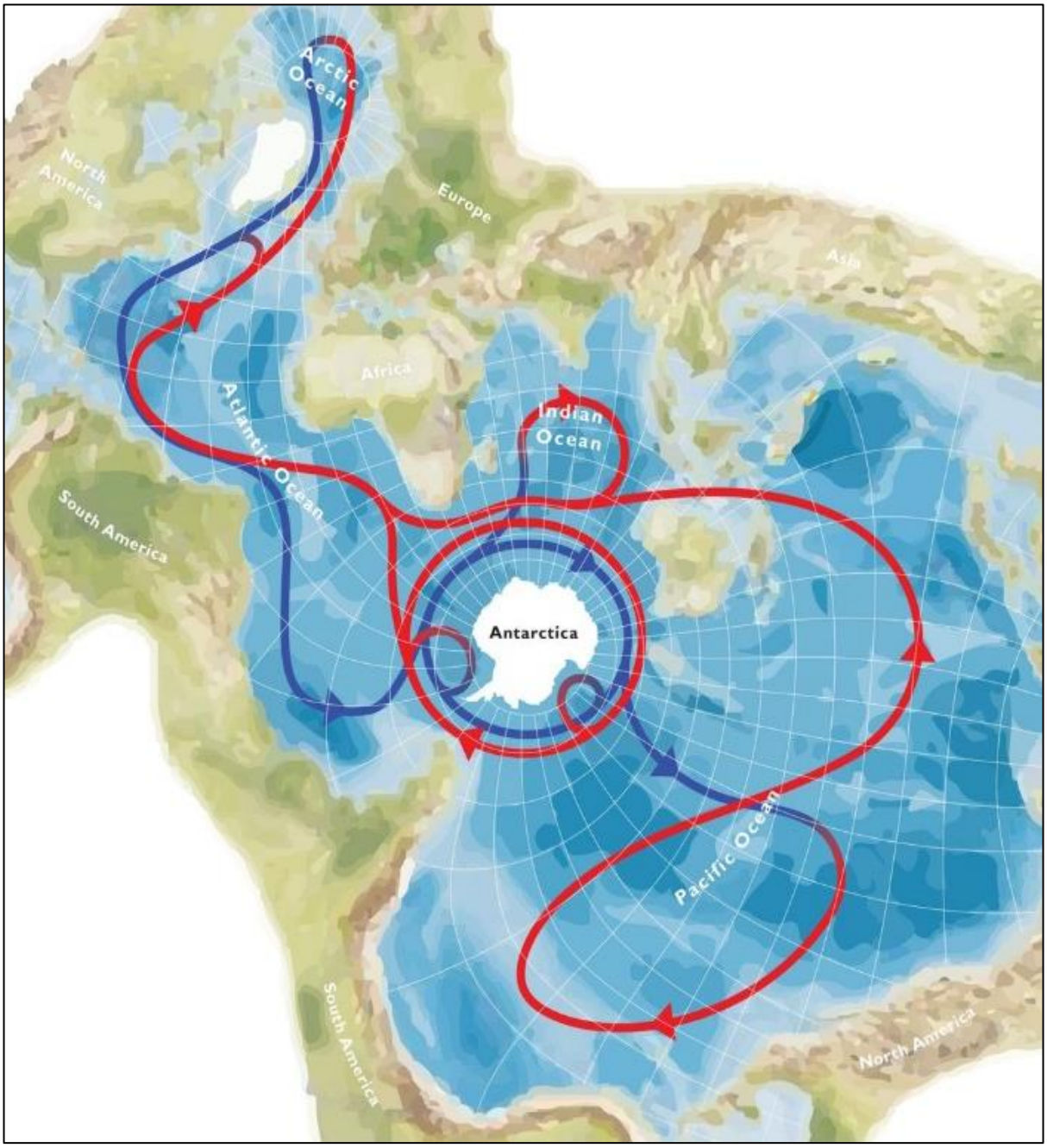

Figure 1. *Spilhaus projection, centered on Antarctica, showing the upper flow (red) and lower flow (blue) components of the global thermohaline circulation system. Figure from Meredith, (2019).*

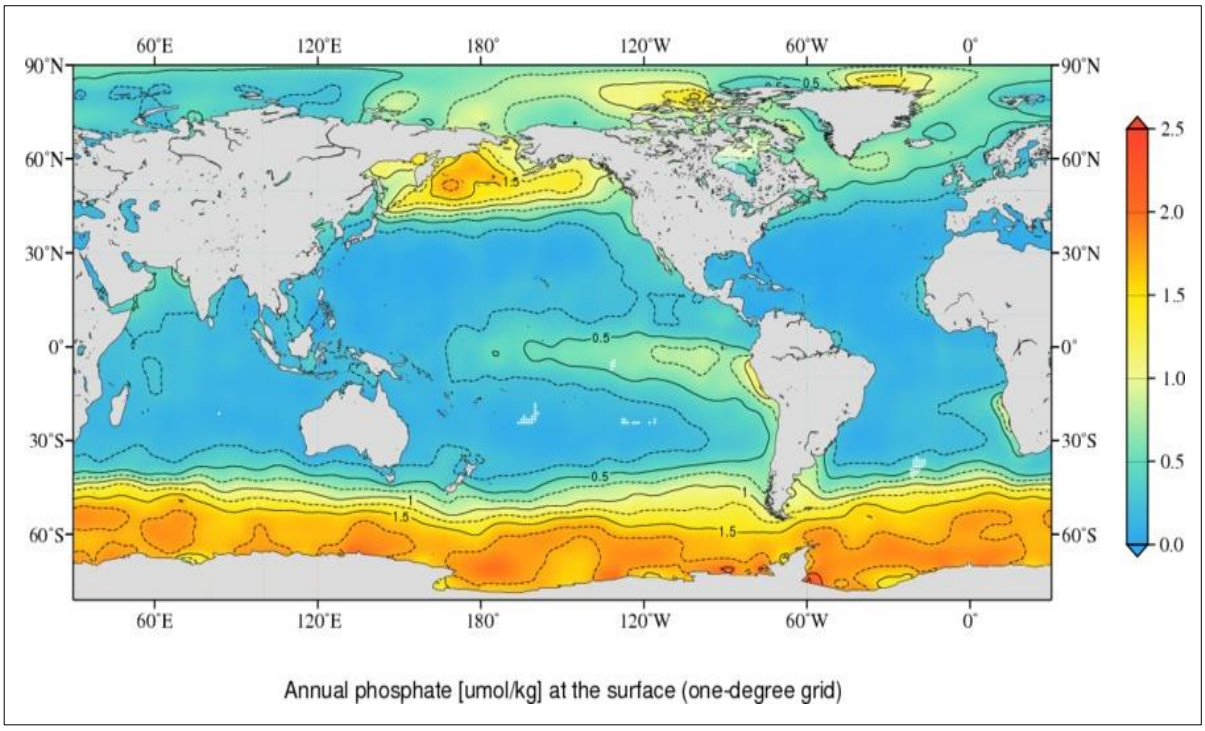

***Figure 2**. Global surface distributions of the major nutrient phosphate (P; µM) showing elevated concentrations particularly throughout the Southern Ocean and also in the north and sub-Arctic Pacific Ocean. Figure from Garcia et al., (2019).*

3. Biogeochemical cycling in the Southern Ocean

Naturally, one may ask the question of why is there a shortage of micronutrient trace metals in the Southern Ocean? This is especially perplexing given that some trace metals e.g. Fe and Mn, constitute relatively significant abundances in Earth's crust (Rudnick and Gao, 2013) yet are present in sub-to-nanomolar concentrations in the open Southern Ocean (e.g. Klunder et al., 2011; Middag et al., 2011). Recent evidence suggests this phenomenon revolves around the supply of trace metal micronutrients and the availability thereof. When considering that the major surface trace metal sources (Figure 3) are river discharge (Little et al., 2014; Rijkenberg et al., 2014; Samanta and Dalai, 2018) and continentally derived atmospheric deposition of aerosols (Chance et al., 2015; Jickells and Moore, 2015; Jickells et al., 2016), it comes as no surprise that little direct influence is brought upon the remote open Southern Ocean. However, the Southern Ocean does benefit from the seasonal melting of icebergs (Duprat et al., 2016; Raiswell et al., 2008) and seasonal ice (Tovar-Sánchez et al., 2010; Wadham et al., 2013) laden with entrained trace metals, a source unique to the polar oceans. The data however suggests that this source is highly variable and often localised. Resuspension of sediment from continental margins (Hawco et al., 2016; Nishioka and Obata, 2017; Noble et al., 2017), mixing of watermasses with different preformed nutrient signatures, (Middag et al., 2019), mid-ocean ridge hydrothermal systems (Noble et al., 2017; Resing et al., 2015; Roshan et al., 2016; Tagliabue et al., 2010) and seabed interactions (Noble et al., 2017) represent variable mid-to-deepwater sources for select trace metals. Furthermore, while acting as a source for certain trace metals, hydrothermal vent plumes and seafloor

processes may act to remove others, e.g. Cu (Jacquot and Moffett, 2015), from the water column thereby acting as a trace metal sink. In addition to limited trace metal supply, a host of processes relating to the chemical speciation and physical form act to decrease trace metal micronutrient bioavailability. Micronutrient elements exist in the ocean primarily in the form of strong organic complexes which have fundamentally different biogeochemical properties compared to their respective bioavailable free dissolved inorganic species (Bruland et al., 2014). This being said, the role of metal binding ligands in complexing trace metals (Gledhill and Buck, 2012) and the processes controlling the partitioning between varies trace metal size fractions, i.e. soluble (0.02µm filtered seawater), colloidal (0.02 – 0.2µm filtered seawater), dissolved (0.2µm filtered seawater) and particulate (>0.45µm) phases, are areas of trace metal chemistry that require further investigation. These questions can be better resolved through the production of large volumes of high quality trace metal data from targeted areas. In this regard, the data presented here contributes substantially to the data scarce Atlantic and Indian sectors of the Southern Ocean (Schlitzer et al., 2018).

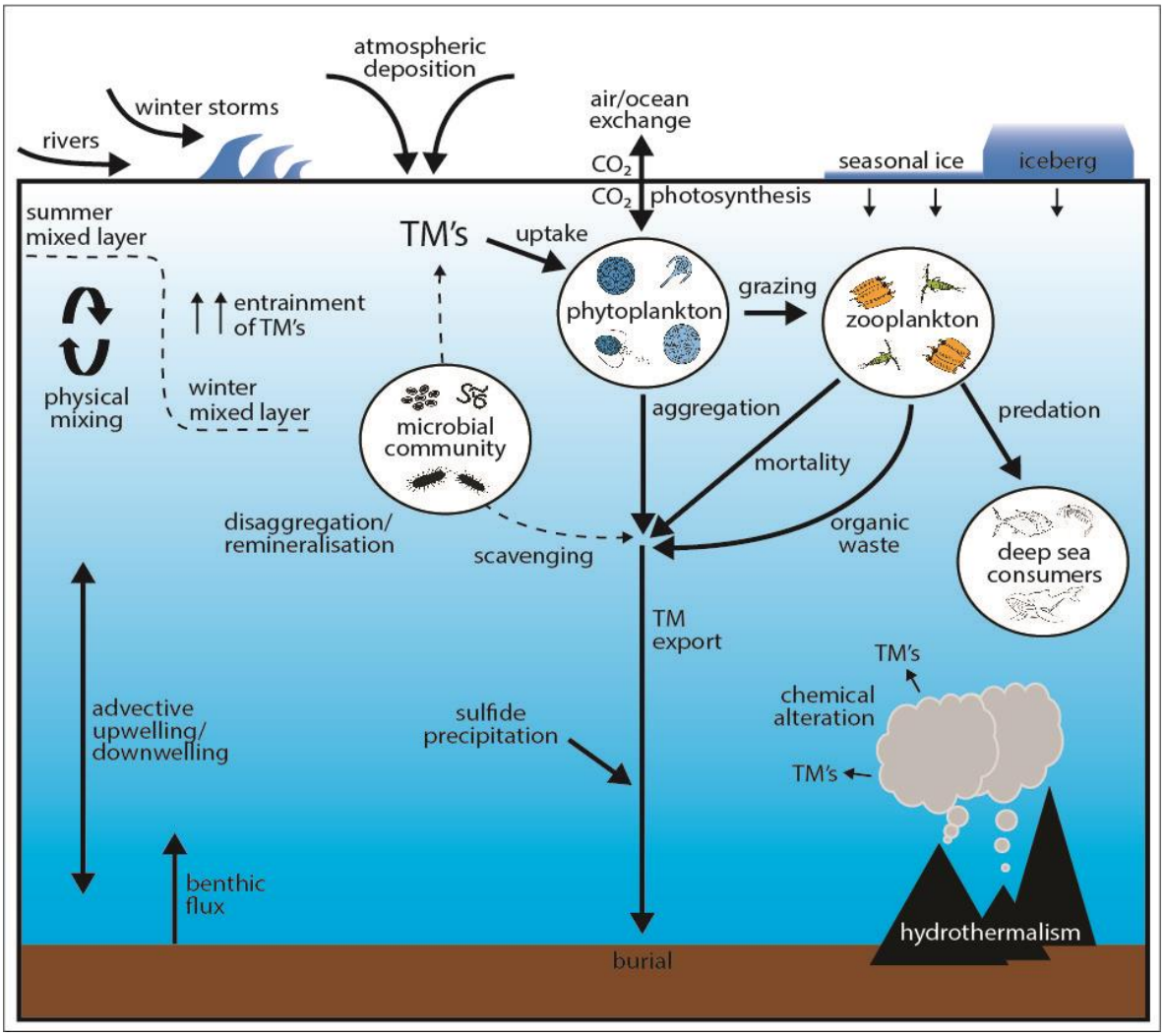

***Figure 3**. Schematic illustrating the dominant sources and sinks of trace metals (TM's) in the ocean as well as major process governing TM cycling.*

4. Accelerating trace metal research

The GEOTRACES programme (https://www.geotraces.org/) is the latest in a series of international collaboration efforts aimed at progressing our understanding of the ocean. Previous oceanographic programs such as the Geochemical Ocean Sections Study (GEOSECS), the World Ocean Circulation Experiment (WOCE) and the Joint Global Ocean Flux Study (JGOFS), are the backbone upon which our understanding of the biogeochemical cycles of carbon and major nutrients is based. The primary aim of the GEOTRACES programme is to extend this knowledge to micronutrients by identifying processes and quantifying fluxes that control the distributions of key trace elements and isotopes, and to establish the sensitivity of these distributions to changing environmental conditions (Anderson, 2020). Under the GEOTRACES framework, the number of datasets and spatial coverage has increased significantly which has certainly led to an acceleration of our trace metal understanding. This is largely thanks to a central, open access data management system, referred to as the Intermediate Data Product (IDP, e.g. Schlitzer et al. 2018), to which all trace metal and ancillary data is quality checked and stored. The research manuscripts (chapters 2, 3 and 4) in this thesis benefited from the IDP in that it allowed for the targeting of data scarce areas, both spatially and seasonally, as well as for data comparison purposes.

5. Knowledge gaps

The Southern Ocean is the most understudied of all the major oceans with respect to trace metal biogeochemistry (Schlitzer et al., 2018). A spatial and seasonal summary of all published Cu, Ni, Zn and Cd datasets in the Southern Ocean is shown in Table 1. Two important observations are clear from the literature. Firstly, existing data is heavily skewed toward the austral spring and summer seasons (October-March). Secondly, the Indian Sector of the Southern Ocean is more data scarce compared to the Atlantic and Pacific sectors. In this context, the primary objectives of this thesis were formed.

6. Objectives of this research

The research for this PhD project was conducted under the framework of the GEOTRACES programme. With an overarching focus on identifying processes which control the distributions of key trace elements, the primary objective of this research was to measure the distributions and investigate the subsequent seasonal cycling of copper (Cu), zinc (Zn), nickel (Ni) and cadmium (Cd) in the data scarce Southern Ocean (red blocks in Table 1). It is important to mention that this thesis forms part of a broader project incorporating other key trace elements such as iron (Fe), manganese (Mn) and cobalt (Co). In order to achieve this, several objectives were posed:

- To assess the role of deep winter mixing in re-supplying nutrient-type micronutrients Cu, Zn and Ni to aid spring/summer phytoplankton blooms.

Table 1. *A spatial and seasonal summary of all published Cu, Ni, Zn and Cd datasets in the Southern Ocean. Blocks outlined in red represent data contributed by this thesis. References as follows: [1]*(Boye et al., 2012)*; [2]*(Cloete et al., 2019)*; [3]*(Heller and Croot, 2015)*; [4]*(Löscher, 1999)*; [5]*(Martin et al., 1990)*; [6]*(Nolting et al., 1991)*; [7]*(Nolting and de Baar, 1994)*; [8]*(Westerlund and Ohman, 1991)*; [9]*(Sañudo-Wilhelmy et al., 2002)*; [10]*(Croot et al., 2011)*; [11]*(Sieber et al., 2019a)*; [12]*(Zhao et al., 2014)*; [13]*(Abouchami et al., 2014)*; [14]*(Baars et al., 2014)*; [15]*(Hendry et al., 2008)*; [16]*(Sieber et al., 2019b)*; [17]*(Janssen et al., 2020)*; [18]*(Castrillejo et al., 2013)*; [19]*(Wang et al., 2018)*; [20]*(Abollino et al., 2004)*; [21]*(Butler et al., 2013)*; [22]*(Corami et al., 2005)*; [23]*(Ellwood, 2008a)*; [24]*(Fitzwater et al., 2000)*; [25]*(Frew et al., 2001)*; [26]*(Grotti et al., 2001)*; [27]*(Lai et al., 2008)*; [28]*(Coale et al., 2005).

Sector	trace metal	Jan	Feb	Mar	Apr	May	Jun	Jul	Aug	Sep	Oct	Nov	Dec	References
Atlantic	Cu													1,2,3,4,5,6,7,8,9
	Ni													2,4,7,8,9
	Zn													2,4,5,7,8,9,10,11,12
	Cd													1,5,6,7,8,9,13,14,15,16
Indian	Cu													17
	Ni													17,18,19
	Zn													17,18,19
	Cd													17,18
Pacific	Cu													17,20,21,22,23,24,25,26,27
	Ni													17,20,21,23,24,25,27
	Zn													11,17,21,22,23,24,25,28
	Cd													16,17,20,21,22,23,24,25,26

- Measure the winter distributions of Cd and Zn (both dissolved and particulate phases) in the Indian sector of the Southern Ocean thereby contributing a unique spatial and seasonal dataset to the global trace element database
- Identify processes controlling the biogeochemical cycling and speciation of the micronutrients Cd and Zn.
- Characterise the Southern Ocean winter reset state, when conditions are theoretically unfavourable for phytoplankton growth compared to summer.

7. Major themes and thesis structure

This thesis consists of five chapters and includes three stand-alone scientific papers. Each scientific paper deals with a separate aspect pertaining to the study of trace metal biogeochemistry yet are linked spatially, seasonally and through mutual objectives.

Chapter 2 presents distributions of Cu, Zn and Ni measured across a consecutive summer-winter cycle along the Zero Meridian (between African and Antarctica) in the Atlantic sector of the Southern Ocean. These three specific elements were chosen due to their similar global ocean distribution patterns. This dataset represents the first winter Cu, Zn and Ni data from this monitoring line (and in fact first from this sector) and also contributes the first summer measurements of Ni. Comparing seasonal distributions, both latitudinally and vertically throughout the water column, provided a unique platform to assess the role of deep winter mixing in resupplying trace metals to surface waters which would otherwise remain depleted after the summer phytoplankton growth season. Results not only show that deep winter mixing may entrain significant amount of these micronutrients but also that the winter season is not as biologically dormant as expected. These results have been published in a special GEOTRACES edition of Chemical Geology (Cloete et al., 2019).

In 2017, the decision to conduct a winter oceanographic expedition along the 30°E longitude again provided a unique opportunity to measure winter trace metal distributions for the first time in the Indian sector of the Southern Ocean. Chapters 3 and 4 present the distributions of dissolved and particulate Cd and dissolved and particulate Zn respectively. Consistent with our observations from the Atlantic sector, our data suggest that biological uptake exerts an important control on trace metal cycling during the winter months. Results show distinct latitudinal trends in Cd and Zn cycling, particularly in the Antarctic Zone where the preferential uptake of Cd and Zn (relative to P) by diatoms coupled with physical circulation patterns in the region of upwelling has implications for Cd and Zn cycling in surface waters to the north. Chapter 3 has been prepared for submission to Frontiers in Marine Science: Marine Biogeochemistry. Chapter 4 has been prepared for submission to Marine Chemistry.

The concluding chapter, Chapter 5, presents a brief synopsis of the thesis, providing a summary of the key findings outlined in the preceding chapters. To close, possible avenues for future research and outstanding gaps in knowledge regarding trace metal biogeochemistry, particularly the seasonality thereof, are identified.

There are 4 appendices included at the end of the thesis. Appendix A contains a detailed description of the full sample collection and sample analysis protocol including data pertaining to the validation thereof. Appendix B (summer) and C (winter) contain the datasets of dissolved Cu, Zn and Ni presented in chapter 2. The data is accompanied by physical parameters (temperature and salinity) as well as macronutrient data. Appendix D contains the complete dissolved and particulate Cd dataset presented in chapter 3. Physical parameters (temperature and salinity) as well as macronutrient data are also tabled. Appendix E contains the complete dissolved and particulate Zn dataset presented in chapter 4. Physical parameters (temperature and salinity) as well as macronutrient data are also tabled.

8. References

Abollino, O., Aceto, M., Buoso, S., La Gioia, C., Sarzanini, C., Mentasti, E., 2004. Distribution of major, minor and trace elements in Antarctic offshore and coastal seawaters: Correlation among sites and variables by pattern recognition. Int. J. Environ. Anal. Chem. 84, 471–492. https://doi.org/10.1080/03067310310001637667

Abouchami, W., Galer, S.J.G., De Baar, H.J.W., Middag, R., Vance, D., Zhao, Y., Klunder, M., Mezger, K., Feldmann, H., Andreae, M.O., 2014. Biogeochemical cycling of cadmium isotopes in the Southern Ocean along the Zero Meridian. Geochim. Cosmochim. Acta 127, 348–367. https://doi.org/10.1016/j.gca.2013.10.022

Anderson, R.F., 2020. GEOTRACES: Accelerating Research on the Marine Biogeochemical Cycles of Trace Elements and Their Isotopes. Ann. Rev. Mar. Sci. 12, 9.1-9.37. https://doi.org/10.2138/gselements.14.6.377

Baars, O., Abouchami, W., Galer, S., Boye, M., Croot, P., 2014. Dissolved cadmium in the Southern Ocean: Distribution, speciation, and relation to phosphate. Limnol. Ocean. 59, 385–399. https://doi.org/10.4319/lo.2014.59.2.0385

Boye, M., Wake, B.D., Lopez Garcia, P., Bown, J., Baker, A.R., Achterberg, E.P., 2012. Distributions of dissolved trace metals (Cd, Cu, Mn, Pb, Ag) in the southeastern Atlantic and the Southern Ocean. Biogeosciences 9, 3231–3246. https://doi.org/10.5194/bg-9-3231-2012

Broecker, W.S., 1991. The Great Ocean Conveyor. Oceanography 4, 79–89. https://doi.org/10.1016/s0262-4079(08)61198-7

Bruland, K., Middag, R., Lohan, M., 2014. Controls of trace metals in seawater, in: Turekian, K., Holland, H. (Eds.), Treatise on Geochemistry. Elsevier, Oxford, UK, pp. 19–51.

Bruland, K.W., Donat, J.R., Hutchins, D.A., 1991. Interactive influences of bioactive trace metals on biological production in oceanic waters. Limnol. Oceanogr. 36, 1555–1577. https://doi.org/10.4319/lo.1991.36.8.1555

Butler, E.C. V, O'Sullivan, J.E., Watson, R.J., Bowie, A.R., Remenyi, T.A., Lannuzel, D., 2013. Trace metals Cd, Co, Cu, Ni, and Zn in waters of the subantarctic and Polar Frontal Zones south of Tasmania during the "SAZ-Sense" project. Mar. Chem. 148, 63–76. https://doi.org/10.1016/j.marchem.2012.10.005

Carter, L., McCave, I.N., Williams, M.J.M., 2009. Chapter 4: Circulation and Water Masses of the Southern Ocean: A Review, in: Florindo, F., Siegert, M. (Eds.), Developments in Earth and Environmental Sciences Series. Antarctic Climate Evolution. Elsevier, Amsterdam, pp. 85–114. https://doi.org/10.1016/S1571-9197(08)00004-9

Castrillejo, M., Statham, P.J., Fones, G.R., Planquette, H., Idrus, F., Roberts, K., 2013. Dissolved trace metals (Ni, Zn, Co, Cd, Pb, Al, and Mn) around the Crozet Islands, Southern Ocean. J. Geophys. Res. Ocean. 118, 5188–5201. https://doi.org/10.1002/jgrc.20359

Chance, R., Jickells, T.D., Baker, A.R., 2015. Atmospheric trace metal concentrations , solubility and deposition fl uxes in remote marine air over the south-east Atlantic. Mar. Chem. 177, 45–56. https://doi.org/10.1016/j.marchem.2015.06.028

Cloete, R., Loock, J.C., Mtshali, T., Fietz, S., Roychoudhury, A.N., 2019. Winter and summer distributions of Copper, Zinc and Nickel along the International GEOTRACES Section GIPY05: Insights into deep winter mixing. Chem. Geol. 511, 342–357. https://doi.org/10.1016/j.chemgeo.2018.10.023

Coale, K.H., Michael Gordon, R., Wang, X., 2005. The distribution and behavior of dissolved and particulate iron and zinc in the Ross Sea and Antarctic circumpolar current along 170°W. Deep Sea Res. Part I Oceanogr. Res. Pap. 52, 295–318. https://doi.org/10.1016/j.dsr.2004.09.008

Corami, F., Capodaglio, G., Turetta, C., Soggia, F., Magi, E., Grotti, M., 2005. Summer distribution of trace metals in the western sector of the Ross Sea, Antarctica. J. Environ. Monit. 7, 1256–1264. https://doi.org/10.1039/b507323p

Croot, P.L., Baars, O., Streu, P., 2011. The distribution of dissolved zinc in the Atlantic sector of the Southern Ocean. Deep Sea Res. Part II Top. Stud. Oceanogr. 58, 2707–2719. https://doi.org/10.1016/j.dsr2.2010.10.041

de Baar, H.J.W., La Roche, J., 2003. Trace Metals in the Oceans: Evolution, Biology and Global Change. Mar. Sci. Front. Eur. 79–105. https://doi.org/10.1007/978-3-642-55862-7_6

Duprat, L.P.A.M., Bigg, G.R., Wilton, D.J., 2016. Enhanced Southern Ocean marine productivity due to fertilization by giant icebergs. Nat. Geosci. 9, 219–221. https://doi.org/https://doi.org/10.1038/ngeo2633

Ellwood, M.J., 2008. Wintertime trace metal (Zn, Cu, Ni, Cd, Pb and Co) and nutrient distributions in the Subantarctic Zone between 40-52°S; 155-160°E. Mar. Chem. 112, 107–117. https://doi.org/10.1016/j.marchem.2008.07.008

Fitzwater, S.E., Johnson, K.S., Gordon, R.M., Coale, K.H., Smith, J., 2000. Trace metal concentrations in the Ross Sea and their relationship with nutrients and phytoplankton growth. Deep. Res. Part II Top. Stud. Oceanogr. 47, 3159–3179. https://doi.org/10.1016/S0967-0645(00)00063-1

Frew, R., Bowie, A., Croot, P., Pickmere, S., 2001. Macronutrient and trace-metal geochemistry of an in situ iron-induced Southern Ocean bloom. Deep. Res. Part II Top. Stud. Oceanogr. 48, 2467–2481. https://doi.org/10.1016/S0967-0645(01)00004-2

Garcia, H.E., Weathers, K.W., Paver, C.R., Smolyar, I., Boyer, T.P., Locarnini, R.A., Zweng, M.M., Mishonov, A.V., Baranova, O.K., Seidov, D., Reagan, J.R. (2019). World Ocean Atlas 2018. Vol. 4:

Dissolved Inorganic Nutrients (phosphate, nitrate and nitrate+nitrite, silicate). A. Mishonov Technical Editor, NOAA Atlas NESDIS 84, 35pp.

Gledhill, M., Buck, K.N., 2012. The organic complexation of iron in the marine environment: A review. Front. Microbiol. 3, 1–17. https://doi.org/10.3389/fmicb.2012.00069

Grotti, M., Soggia, F., Abelmoschi, M.L., Rivaro, P., Magi, E., Frache, R., 2001. Temporal distribution of trace metals in Antarctic coastal waters.

Hawco, N.J., Ohnemus, D.C., Resing, J.A., Twining, B.S., Saito, M.A., 2016. A dissolved cobalt plume in the oxygen minimum zone of the eastern tropical South Pacific. Biogeosciences 13, 5697–5717. https://doi.org/10.5194/bg-13-5697-2016

Heller, M.I., Croot, P.L., 2015. Copper speciation and distribution in the Atlantic sector of the Southern Ocean. Mar. Chem. 173, 253–268. https://doi.org/10.1016/j.marchem.2014.09.017

Hendry, K.R., Rickaby, R.E.M., de Hoog, J.C.M., Weston, K., Rehkämper, M., 2008. Cadmium and phosphate in coastal Antarctic seawater: Implications for Southern Ocean nutrient cycling. Mar. Chem. 112, 149–157. https://doi.org/10.1016/j.marchem.2008.09.004

Jacquot, J.E., Moffett, J.W., 2015. Copper distribution and speciation across the International GEOTRACES Section GA03. Deep. Res. Part II 116, 187–207. https://doi.org/10.1016/j.dsr2.2014.11.013

Janssen, D.J., Sieber, M., Ellwood, M.J., Conway, T.M., Barrett, P.M., Chen, X., de Souza, G.F., Hassler, C.S., Jaccard, S.L., 2020. Trace metal and nutrient dynamics across broad biogeochemical gradients in the Indian and Pacific sectors of the Southern Ocean. Mar. Chem. 221, 103773. https://doi.org/10.1016/j.marchem.2020.103773

Jickells, T., Moore, C.M., 2015. The Importance of Atmospheric Deposition for Ocean Productivity. Annu. Rev. Ecol. Evol. Syst. 46, 481–501. https://doi.org/10.1146/annurev-ecolsys-112414-054118

Jickells, T.D., Baker, A.R., Chance, R., 2016. Atmospheric transport of trace elements and nutrients to the oceans. Philos. Trans. R. Soc. A Math. Phys. Eng. Sci. 374. https://doi.org/10.1098/rsta.2015.0286

Klunder, M.B., Laan, P., Middag, R., Baar, H.J.W. De, Ooijen, J.C. Van, 2011. Dissolved iron in the Southern Ocean (Atlantic sector). Deep. Res. Part II 58, 2678–2694. https://doi.org/10.1016/j.dsr2.2010.10.042

Lai, X., Norisuye, K., Mikata, M., Minami, T., Bowie, A.R., Sohrin, Y., 2008. Spatial and temporal distribution of Fe, Ni, Cu and Pb along 140??E in the Southern Ocean during austral summer 2001/02. Mar. Chem. 111, 171–183. https://doi.org/10.1016/j.marchem.2008.05.001

Little, S.H., Vance, D., Walker-Brown, C., Landing, W.M., 2014. The oceanic mass balance of copper and zinc isotopes, investigated by analysis of their inputs, and outputs to ferromanganese oxide sediments. Geochim. Cosmochim. Acta 125, 673–693. https://doi.org/10.1016/j.gca.2013.07.046

Löscher, B.M., 1999. Relationship among Ni, Cu, Zn, and major nutrients in the Southern Ocean. Mar. Chem. 67, 67–102. 10.1016/S0304-4203(99)00050-X

Marinov I., Sarmiento J.L., 2004. The Role of the Oceans in the Global Carbon Cycle: An Overview. In: Follows, M., Oguz, T., (eds) The Ocean Carbon Cycle and Climate. NATO Science Series (Series IV: Earth and Environmental Sciences), vol 40. Springer, Dordrecht. https://doi.org/10.1007/978-1-4020-2087-2_8

Martin, J.H., 1990. Glacial-Interglacial CO2 changes: The Iron Hypothesis. Paleoceanography 5, 1–13. https://doi.org/doi:10.1029/PA005i001p00001

Martin, J.H., Gordon, R.M., Fitzwater, S.E., 1990. Iron in Antarctic waters. Nature 349, 156. https://doi.org/https://doi.org/10.1038/345156a0

Meredith, M.P. (2019). The global importance of the Southern Ocean, and the key role of its freshwater cycle. Ocean Challenge, 23(2), 27-32.

Middag, R., De Baar, H.J.W., Laan, P., Cai, P.H., Van Ooijen, J.C., 2011. Dissolved manganese in the Atlantic sector of the Southern Ocean. Deep Sea Res. Part II Top. Stud. Oceanogr. 58, 2661–2677. https://doi.org/10.1016/S0967-0645(96)00064-1

Mitchell, B.G., Brody, E.A., Holm-hansen, O., Mcclain, C., Bishop, J., 1991. Light limitation of phytoplankton biomass and macronutrient utilization in the Southern Ocean. Limnol. Ocean. 36, 1662–1677. https://doi.org/https://doi.org/10.4319/lo.1991.36.8.1662

Morel, F.M.M., Reinfelder, J.R., Roberts, S.B., Chamberlain, C.P., Lee, J.G., Yee, D., 1994. Zinc and carbon co-limitation of marine phytoplankton. Nature 369, 740–742.

Nishioka, J., Obata, H., 2017. Dissolved iron distribution in the western and central subarctic Pacific: HNLC water formation and biogeochemical processes. Limnol. Oceanogr. 62, 2004–2022. https://doi.org/https://doi.org/10.1002/lno.10548

Noble, A.E., Ohnemus, D.C., Hawco, N.J., Lam, P.J., Saito, M.A., 2017. Coastal sources, sinks and strong organic complexation of dissolved cobalt within the US North Atlantic GEOTRACES transect GA03. Biogeosciences 14, 2715–2739. https://doi.org/10.5194/bg-14-2715-2017

Nolting, R.F., de Baar, H.J.W., 1994. Behaviour of nickel, copper, zinc and cadmium in the upper 300m of a transect in the Southern Ocean (57°-62°S, 49°W). Mar. Chem. 45, 225–242.

Nolting, R.F., Debaar, H.J.W., Vanbennekom, A.J., Masson, A., 1991. Cadmium, Copper and Iron in the Scotia Sea, Weddell Sea and Weddell Scotia Confluence (Antarctica). Mar. Chem. 35, 219–243. https://doi.org/10.1016/S0304-4203(09)90019-6

Orsi, A.H., Whitworth, T., Nowlin, W.D., 1995. On the meridional extent and fronts of the Antarctic Circumpolar Current. Deep. Res. Part I 42, 641–673. https://doi.org/10.1016/0967-0637(95)00021-W

Raiswell, R., Benning, L.G., Tranter, M., Tulaczyk, S., 2008. Bioavailable iron in the Southern Ocean: The significance of the iceberg conveyor belt. Geochem. Trans. 9, 1–9. https://doi.org/10.1186/1467-4866-9-7

Redfield, A.C., Ketchum, B.H., Richards, F.A., 1963. The influence of organisms on the composition of seawater, in: Hill, M.N. (Ed.), The Sea. Wiley Interscience, New York, USA, pp. 26–77.

Resing, J.A., Sedwick, P.N., German, C.R., Jenkins, W.J., Moffett, J.W., Sohst, B.M., Tagliabue, A., 2015. Basin-scale transport of hydrothermal dissolved metals across the South Pacific Ocean. Nature 523, 200–203. https://doi.org/10.1038/nature14577

Rijkenberg, M.J.A., Middag, R., Laan, P., Gerringa, L.J.A., Van Aken, H.M., Schoemann, V., De Jong, J.T.M., De Baar, H.J.W., 2014. The distribution of dissolved iron in the West Atlantic Ocean. PLoS One 9, 1–14. https://doi.org/10.1371/journal.pone.0101323

Roshan, S., Wu, J., Jenkins, W.J., 2016. Long-range transport of hydrothermal dissolved Zn in the tropical South Pacific. Mar. Chem. 183, 25–32. https://doi.org/10.1016/j.marchem.2016.05.005

Rudnick, R.L., Gao, S., 2013. Composition of the Continental Crust, 2nd ed, Treatise on Geochemistry: Second Edition. Elsevier Ltd. https://doi.org/10.1016/B978-0-08-095975-7.00301-6

Samanta, S., Dalai, T.K., 2018. Massive production of heavy metals in the Ganga (Hooghly) River estuary, India: Global importance of solute-particle interaction and enhanced metal fluxes to the oceans. Geochim. Cosmochim. Acta 228, 243–258. https://doi.org/10.1016/j.gca.2018.03.002

Sañudo-Wilhelmy, S.A., Olsen, K.A., Scelfo, J.M., Foster, T.D., Flegal, A.R., 2002. Trace metal distributions off the antarctic peninsula in the weddell sea. Mar. Chem. 77, 157–170. https://doi.org/10.1016/S0304-4203(01)00084-6

Schlitzer, R., Anderson, R.F., Dodas, E.M., Lohan, M., Geibert, W., Tagliabue, A., Bowie, A., Jeandel, C., Maldonado, M.T., Landing, W.M., Cockwell, D., Abadie, C., Abouchami, W., Achterberg, E.P., Agather, A., Aguliar-Islas, A., van Aken, H.M., Andersen, M., Archer, C., Auro, M., de Baar, H.J., Baars, O., Baker, A.R., Bakker, K., Basak, C., Baskaran, M., Bates, N.R., Bauch, D., van Beek, P., Behrens, M.K., Black, E., Bluhm, K., Bopp, L., Bouman, H., Bowman, K., Bown, J., Boyd, P., Boye, M., Boyle, E.A., Branellec, P., Bridgestock, L., Brissebrat, G., Browning, T., Bruland, K.W., Brumsack, H.J., Brzezinski, M., Buck, C.S., Buck, K.N., Buesseler, K., Bull, A., Butler, E., Cai, P., Mor, P.C., Cardinal, D., Carlson, C., Carrasco, G., Casacuberta, N., Casciotti, K.L., Castrillejo, M., Chamizo, E., Chance, R., Charette, M.A., Chaves, J.E., Cheng, H., Chever, F., Christl, M., Church, T.M., Closset, I., Colman, A., Conway, T.M., Cossa, D., Croot, P., Cullen, J.T., Cutter, G.A., Daniels, C., Dehairs, F., Deng, F., Dieu, H.T., Duggan, B., Dulaquais, G., Dumousseaud, C., Echegoyen-Sanz, Y., Edwards, R.L., Ellwood, M., Fahrbach, E., Fitzsimmons, J.N., Russell Flegal, A., Fleisher, M.Q., van de Flierdt, T., Frank, M., Friedrich, J., Fripiat, F., Fröllje, H., Galer, S.J.G., Gamo, T., Ganeshram, R.S., Garcia-Orellana, J., Garcia-Solsona, E., Gault-Ringold, M., George, E., Gerringa, L.J.A., Gilbert, M., Godoy, J.M., Goldstein, S.L., Gonzalez, S.R., Grissom, K., Hammerschmidt, C., Hartman, A., Hassler, C.S., Hathorne, E.C., Hatta, M., Hawco, N., Hayes, C.T., Heimbürger, L.E., Helgoe, J., Heller, M., Henderson, G.M., Henderson, P.B., van Heuven, S., Ho, P., Horner, T.J., Hsieh, Y. Te, Huang, K.F., Humphreys, M.P., Isshiki, K., Jacquot, J.E., Janssen, D.J., Jenkins, W.J., John, S., Jones, E.M., Jones, J.L., Kadko, D.C., Kayser, R., Kenna, T.C., Khondoker, R., Kim, T., Kipp, L., Klar, J.K., Klunder, M., Kretschmer, S., Kumamoto, Y., Laan, P., Labatut, M., Lacan, F., Lam, P.J., Lambelet, M., Lamborg, C.H., Le Moigne, F.A.C., Le Roy, E., Lechtenfeld, O.J., Lee, J.M., Lherminier, P., Little, S., López-Lora, M., Lu, Y., Masque, P., Mawji, E., Mcclain, C.R., Measures, C., Mehic, S., Barraqueta, J.L.M., van der Merwe, P., Middag, R., Mieruch, S., Milne, A., Minami, T., Moffett, J.W., Moncoiffe, G., Moore, W.S., Morris, P.J., Morton, P.L., Nakaguchi, Y., Nakayama, N., Niedermiller, J., Nishioka, J., Nishiuchi, A., Noble, A., Obata, H., Ober, S., Ohnemus, D.C., van Ooijen, J., O'Sullivan, J., Owens, S., Pahnke, K., Paul, M., Pavia, F., Pena, L.D., Peters, B., Planchon, F., Planquette, H., Pradoux, C., Puigcorbé, V., Quay, P., Queroue, F., Radic, A., Rauschenberg, S., Rehkämper, M., Rember, R., Remenyi, T., Resing, J.A., Rickli, J., Rigaud, S., Rijkenberg, M.J.A., Rintoul, S., Robinson, L.F., Roca-Martí, M., Rodellas, V., Roeske, T., Rolison, J.M., Rosenberg, M., Roshan, S., Rutgers van der Loeff, M.M., Ryabenko, E., Saito, M.A., Salt, L.A., Sanial, V., Sarthou, G., Schallenberg, C., Schauer, U., Scher, H., Schlosser, C., Schnetger, B., Scott, P., Sedwick, P.N., Semiletov, I., Shelley, R., Sherrell, R.M., Shiller, A.M., Sigman, D.M., Singh, S.K., Slagter, H.A., Slater, E., Smethie, W.M., Snaith, H., Sohrin, Y., Sohst, B., Sonke, J.E., Speich, S., Steinfeldt, R., Stewart, G., Stichel, T., Stirling, C.H., Stutsman, J., Swarr, G.J., Swift, J.H., Thomas, A., Thorne, K., Till, C.P., Till, R., Townsend, A.T., Townsend, E., Tuerena, R., Twining, B.S., Vance, D., Velazquez, S., Venchiarutti, C., Villa-Alfageme, M., Vivancos, S.M., Voelker, A.H.L., Wake, B., Warner, M.J., Watson, R., van Weerlee, E., Alexandra Weigand, M., Weinstein, Y., Weiss, D., Wisotzki, A., Woodward, E.M.S., Wu, J., Wu, Y., Wuttig, K., Wyatt, N., Xiang, Y., Xie, R.C., Xue, Z., Yoshikawa, H., Zhang, J., Zhang, P., Zhao, Y., Zheng, L., Zheng, X.Y., Zieringer, M., Zimmer, L.A., Ziveri, P., Zunino, P., Zurbrick, C., 2018. The GEOTRACES Intermediate Data Product 2017. Chem. Geol. 493, 210–223. https://doi.org/10.1016/j.chemgeo.2018.05.040

Sieber, M., Conway, T.M., Souza, G.F. De, Hassler, C.S., Ellwood, M.J., Vance, D., 2019a. Cycling of zinc and its isotopes across multiple zones of the Southern Ocean : Insights from the Antarctic Circumnavigation Expedition. Geochim. Cosmochim. Acta. https://doi.org/10.1016/j.gca.2019.09.039

Sieber, M., Conway, T.M., Souza, G.F. De, Hassler, C.S., Ellwood, M.J., Vance, D., 2019b. High-resolution Cd isotope systematics in multiple zones of the Southern Ocean from the Antarctic Circumnavigation Expedition. Earth Planet. Sci. Lett. 527, 115799. https://doi.org/10.1016/j.epsl.2019.115799

Sunda, W.G., 1989. Trace Metal Interactions with Marine Phytoplankton. Biol. Oceanogr. 6, 411–442. https://doi.org/10.1080/01965581.1988.10749543

Tagliabue, A., Bopp, L., Dutay, J., Bowie, A.R., Chever, F., Jean-baptiste, P., Bucciarelli, E., Lannuzel, D., Remenyi, T., Sarthou, G., Aumont, O., Gehlen, M., Jeandel, C., 2010. Hydrothermal contribution to the oceanic dissolved iron inventory. Nat. Geosci. 3, 252–256. https://doi.org/10.1038/ngeo818

Tovar-Sánchez, A., Duarte, C.M., Alonso, J.C., Lacorte, S., Tauler, R., Galban-Malagón, C., 2010. Impacts of metals and nutrients released from melting multiyear Arctic sea ice. J. Geophys. Res. C Ocean. 115, 1–7. https://doi.org/10.1029/2009JC005685

Wadham, J.L., De'Ath, R., Monteiro, F.M., Tranter, M., Ridgwell, A., Raiswell, R., Tulaczyk, S., 2013. The potential role of the Antarctic Ice Sheet in global biogeochemical cycles. Earth Environ. Sci. Trans. R. Soc. Edinburgh 104, 55–67. https://doi.org/10.1017/S1755691013000108

Wang, R.M., Archer, C., Bowie, A.R., Vance, D., 2018. Zinc and nickel isotopes in seawater from the Indian Sector of the Southern Ocean: The impact of natural iron fertilization versus Southern Ocean hydrography and biogeochemistry. Chem. Geol. https://doi.org/10.1016/j.chemgeo.2018.09.010

Westerlund, S., Ohman, P., 1991. Cadmium, Copper, Cobalt, Nickel, Lead, and Zinc in the Water Column of the Weddell Sea, Antarctica. Geochim. Cosmochim. Acta 55, 2127–2146. https://doi.org/10.1016/0016-7037(91)90092-j

Zhao, Y., Vance, D., Abouchami, W., de Baar, H.J.W., 2014. Biogeochemical cycling of zinc and its isotopes in the Southern Ocean. Geochim. Cosmochim. Acta 125, 653–672. https://doi.org/10.1016/j.gca.2013.07.045

Chapter 2

Winter and summer distributions of Copper, Zinc and Nickel along the International GEOTRACES Section GIPY05: Insights into deep winter mixing

A presentation of the published research paper

This research manuscript was published in a special issue of the journal Chemical Geology entitled "Cycles of trace elements and isotopes in the ocean – GEOTRACES and beyond". I was the lead author of the manuscript. J.C. Loock, T. Mtshali, S. Fietz and A.N. Roychoudhury were co-authors.

This manuscript contributes the first winter measurements of labile dissolved copper (LdCu), dissolved zinc (dZn) and dissolved nickel (dNi) in the Atlantic sector of the Southern Ocean. This dataset is compared with the corresponding summer dataset in order to assess the significance of deep winter mixing in supplying essential trace metals to phytoplankton in surface waters following the intense spring/summer growth periods. This internal supply mechanism is particularly important in sustaining phytoplankton stocks in the open Southern Ocean where external trace metal supply is extremely limited.

I was responsible for the collection of seawater samples on both winter and summer research cruises, analysis of seawater samples, data processing and writing of the manuscript.

Full citation: Cloete, R., Loock, J.C., Mtshali, T., Fietz, S., Roychoudhury, A.N., 2019. Winter and summer distributions of Copper, Zinc and Nickel along the International GEOTRACES Section GIPY05: Insights into deep winter mixing. Chem. Geol. 511, 342–357. https://doi.org/10.1016/j.chemgeo.2018.10.023

Winter and summer distributions of Copper, Zinc and Nickel along the International GEOTRACES Section GIPY05: Insights into deep winter mixing

R.Cloete[1], J.C. Loock[1], T. Mtshali[1,2], S. Fietz[1] and A.N. Roychoudhury[1*]

[1]Centre for Trace Metal and Experimental Biogeochemistry (TracEx), Department of Earth Sciences, Stellenbosch University, Stellenbosch 7600, South Africa

[2]Southern Ocean Carbon and Climate Observatory, Natural Resources and Environment, CSIR, Stellenbosch, 7600, South Africa

Abstract

First measurements of labile dissolved copper (LdCu) and dissolved zinc (dZn) and nickel (dNi) in the Atlantic sector of the Southern Ocean in winter are compared with summer data at reoccupied stations in order to better understand the winter reset state and supply of these trace metals to support productivity. In summer, vertical profiles of zinc behaved similarly to silicate (Si) and increased from sub-nanomolar surface concentrations to 8 nmol kg^{-1} in bottom waters. Copper profiles also resembled Si and were typically 1nmol kg^{-1} in surface waters and increased to 3 nmol kg^{-1} at depth. First summer nickel data reported from this transect displayed comparatively higher surface concentrations of ~4.6 nmol kg^{-1} increasing more rapidly to local intermediate depth maximums between 6.5 and 7.0 nmol kg^{-1}, similar to phosphate (PO_4). Trace metal seasonality was most apparent in the mixed layer where the average of winter concentrations within the mixed layer exceeded summer values by approximately 0.2 nmol kg^{-1} for LdCu, 1.2 nmol kg^{-1} for dZn and 0.3 nmol kg^{-1} for dNi owing to low utilization under unfavourable growth conditions for phytoplankton. In an effort to estimate the winter reserve, two scenarios were considered. Scenario 1 accounted for in-situ mixed layer depths (MLD) where the winter reserve inventory was calculated by subtracting the summer depth integrated metal inventory (surface to summer MLD) from the winter equivalent (surface to winter MLD). Scenario 2 assumed a constant mixed layer (taken as the depth of the maximum winter mixed layer) where summer depth integrated metal inventories (surface to maximum winter MLD) were subtracted from the winter equivalents (surface to maximum winter MLD). Results for scenario 1 were predominantly dependant on the mixed layer depth which varied spatially and seasonally. Scenario 2 showed a southwards increase in the winter reserve inventory suggesting a greater role for entrainment at higher latitudes in this region. This is however heavily dependent on other physical processes controlling vertical trace metal supply e.g. diapycnal diffusion, Ekman upwelling/downwelling. Zinc ($r^2 > 0.75$) and copper ($r^2 > 0.73$) were strongly correlated with Si throughout the study implicating diatoms as strong controllers of their biogeochemical cycling. Nickel was more strongly correlated with PO_4 in the upper water column ($r^2 > 0.75$), as compared to the whole water column ($r^2 > 0.52$), while in the deep ocean nickel appears to

correlate with Si although more deep ocean data is needed to confirm this. Trace metal to major nutrient ratios were higher in winter suggesting reduced micronutrient requirement relative to macronutrients under stressed but low productivity conditions.

1. Introduction

Copper (Cu), zinc (Zn) and nickel (Ni) have been shown to exert important controls on phytoplankton productivity and community composition (William G. Sunda, 1989). These metals serve as cofactors in enzymes responsible for key metabolic functions such as photosynthetic electron transport via the copper containing enzyme plastocyanin, uptake of carbon dioxide via the zinc containing enzyme carbonic anhydrase and the acquisition of nitrogen from urea via the nickel containing enzyme urease (Bruland, 1980; William G. Sunda, 1989). The ongoing advancement of 'clean' sampling and analytical techniques since the late 1970's (Bruland and Franks, 1979) has permitted scientists to investigate the distributions of bio-active trace metals far more rapidly and accurately. Despite this, the Southern Ocean remains relatively data scarce (Boye et al., 2012), particularly in winter (Ellwood, 2008b). Expeditions into the Atlantic Sector of the Southern Ocean over a successive summer-winter cycle has provided the unique opportunity to investigate the biogeochemical cycling of copper, zinc and nickel over seasonal cycles.

1.1. Deep winter mixing as a nutrient supply mechanism

Winter deep mixing (or entrainment) has been identified as a major physical process supplying essential trace metals to depleted surface waters which then sustains phytoplankton productivity over the subsequent spring and summer seasons (Moore et al., 2002; Tagliabue et al., 2014). For the Southern Ocean, a key player in the global carbon cycle, this sub-surface supply mechanism may be extremely important given the inherently low trace metal concentrations and lack of major exogenous sources (Bruland et al., 1991). In winter, deeper mixing compared to summer, arises from an annual reset in the Southern Ocean's upper water column processes when net heat losses, elevated wind stresses and sea ice formation lead to an increase in the Mixed Layer Depth (MLD; Swart et al., 2015). This supply mechanism is envisioned as winter deep mixing accessing a reserve micro – and macronutrient source pool in more nutrient rich water masses below the summer stratified layer. Subsequent shoaling of the mixed layer as the season progresses from winter, through spring, to summer may replenish surface nutrient stocks through mixing. The quantity of trace metal entrainment will thus depend on the maximum depth of the mixed layer (MLD_{max}) and the trace metal concentration within the stratum (Tagliabue et al., 2014). Another important aspect to consider is the possibility that the nutricline, (the depth at which the vertical nutrient concentration gradient, ∂nutrient/∂z, is maximum), of LdCu, dZn and dNi (hereafter Z_{Cu}, Z_{Zn} and Z_{Ni} respectively), may be deeper than that of the MLD and major nutrients. A deeper 'ferricline' (Z_{Fe}) for dissolved iron (dFe) in relation to nitrate has been previously noted and is dependent on physical mixing, metal demand, organic complexation and scavenging in surface waters (Croot et al., 2007). This can have important implications for the magnitude of vertical trace metal supply with obvious implications for phytoplankton productivity. Additional major vertical supply mechanisms include diapycnal diffusion and Ekman upwelling/downwelling (Law, 2003; Moore

et al., 2002). Based on the vertical distribution of iron in the Southern Ocean it has been shown that deep winter mixing supplies on average ten times more iron to the surface ocean each year compared to diapycnal diffusion (Tagliabue et al., 2014).

1.2. Trace metal – major nutrient coupling in the Southern Ocean

Evidence for the involvement of Cu, Zn and Ni in the oceanic biological cycle stems from the coupled cycling of trace metals and the major nutrients (NO_3, PO_4 and Si). This 'nutrient type' behaviour is induced by biological removal in the surface euphotic zone and deeper remineralization (Croot et al., 2011; Heller and Croot, 2015; Löscher, 1999; Nolting and de Baar, 1994). There are, however, deviations from the major nutrient/trace metal coupling. For example, the tight correlation between Zn and Si, as compared to that of Zn and PO_4, has received much attention in recent times. Culture studies (M J Ellwood and Hunter, 2000) and synchrotron data show that Zn is co-located with phosphate (PO_4) in the organic tissue of diatom cells (Twining et al., 2003; Twining and Baines, 2013) and only contributes 1 - 3% of the total cellular inventory of diatom opaline frustules (M J Ellwood and Hunter, 2000). We would therefore expect that Zn is regenerated with PO_4 from the rapidly dissolvable organic material in the upper ocean while the depth profile of Si is controlled by the less readily dissolvable diatom frustules leading to deeper ocean maximums. Underlying reasons behind this paradox have previously been attributed to an absolute biological control. Twining et al. (2014) proposed the simultaneous release of Zn and Si from sinking diatom cells packaged with other detrital material. Alternatively, scavenging of dissolved Zn onto marine organic matter and subsequent deeper dissolution may generate depth profiles similar to Si (John and Conway, 2014). More recently, a non-mechanistic approach involving physical ocean circulation through the Southern Ocean hub and the result of preferential biological uptake of Zn and Si has been put forward (Vance et al., 2017). It is evident that the interplay between micro- and macronutrients requires further investigation.

1.3. Aim of this study

This study was undertaken as part of the International GEOTRACES program which aims at improving our understanding of the large scale distribution of trace elements in the ocean. The data presented here focuses on the summer and winter distributions of labile dissolved copper (LdCu) and dissolved zinc (dZn) and nickel (dNi), three potentially important bio-active elements for primary production in the Southern Ocean. The primary aim of this study was to investigate the biogeochemical cycling of these metals over seasonal cycles by measuring their distributions in summer, when conditions are favourable for phytoplankton growth (e.g. high light levels and a stable, shallow mixed layer), and in winter when conditions limit their growth (e.g. low light levels and a deep mixed layer). Furthermore, an effort was made to investigate variation in micro-to-macronutrient ratios in different water masses and with depth.

2. Materials and methods

2.1. Sample collection

Seawater samples were collected on-board the R.V. SA Agulhas II during the 54th South African National Antarctic Expedition (SANAE 54) summer cruise (January 2015) and the third Southern Ocean Seasonal Cycle Experiment (SOSCEx III) winter expedition (July 2015). The transect followed the GIPY05 GEOTRACES section, from Cape Town to Antarctica along the Zero Meridian (Figure 1). Of the six locations sampled between 46°S and 68°S during summer, three overlapping locations at 46°S, 50°S and 54°S, were sampled in winter to allow direct seasonal comparisons in different water masses.

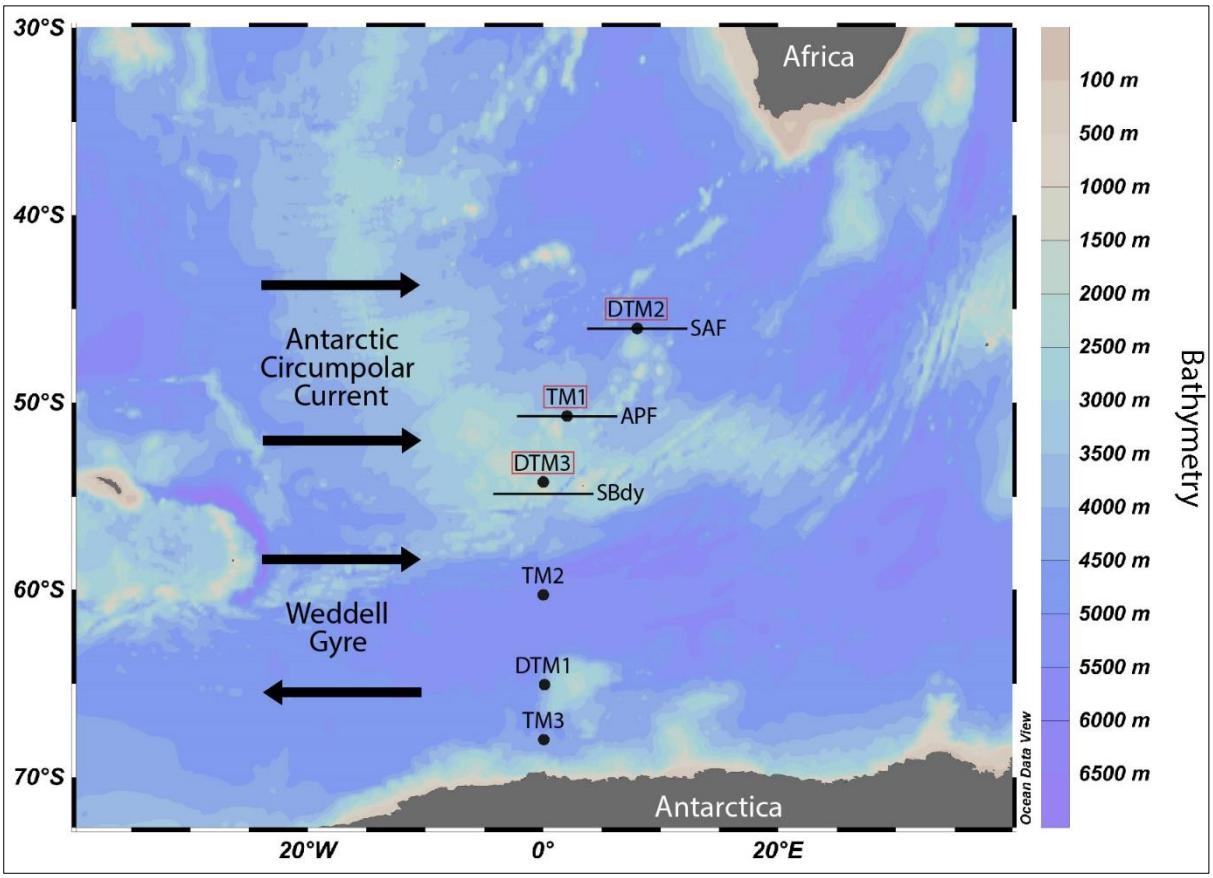

Figure 1. *Location of stations sampled for copper, zinc and nickel during the 54th South African National Antarctic Expedition (SANAE54) summer cruise along the GEOTRACES GIPY05 transect. Stations outlined in red were re-occupied during winter. The positions of the frontal systems encountered are shown as found during summer. APF: Antarctic Polar Front; SAF: Sub-Antarctic Front; SBdy: Southern Boundary. Figure made using Ocean Data View (ODV) (Schlitzer, 2017).*

A vertical profile sampling method was employed at all sampling stations. Seawater samples were collected following a strict clean protocol, as per the GEOTRACES cookbook (Cutter and Bruland, 2012), using a GEOTRACES compliant CTD and rosette. Directly upon recovery of the rosette, the GO-FLO bottles were covered in a polyvinyl chloride (PVC) plastic wrap in addition to their ends being covered in plastic (PVC) shower caps, and were transported into a class 100 clean lab for sub-sampling. Samples for dissolved trace metal determination were collected in 125 ml acid-

cleaned low density polyethylene (LDPE) bottles after online filtration through 0.2 µm Sartobran filters and under slight N_2 (99.9999% N_2, BIP technology) overpressure. Samples were acidified (pH = 1.7) on-board under a laminar flowhood using hydrochloric acid (Ultrapur HCL, Merck) and stored for later analysis in Stellenbosch, South Africa.

2.2. Reagents and materials

All plasticware used for storage, and subsequent analysis, of samples was extensively acid cleaned following the protocols outlined by GEOTRACES. Prior to analyses, samples were pre-concentrated using a SeaFAST-pico SC-4 DX module (see section 2.4 for details) where the required buffer solution (pH 6.0 ± 0.2) was prepared using ammonium hydroxide solution (NH_4OH) (suprapur, Merck) and glacial acetic acid (CH_3COOH) (suprapur, Merck), the eluent was prepared using nitric acid (HNO_3) (ultrapure, Merck) and all reagents were diluted using 18MΩ Milli-Q water (Millipore system) dispensed through a Q-POD system for removal of trace metals and organics.

2.3. Intercalibration and reference standards

As required by GEOTRACES, a cross-over station was performed to ensure data produced in this study is intercalibrated. The location and sample depths of the summer station, DTM1 (65°S), were chosen to coincide with previous studies investigating copper and zinc (Croot et al., 2011; Heller and Croot, 2015). At present no data exists for nickel along this transect preventing any comparisons. The accuracy of the analytical procedure was evaluated by measurement of the SAFe D2 (bottle number 98) reference standard, the GEOTRACES reference standards, GSC (bottle number 1-19) and GSP (bottle number 62), and the certified seawater standard NASS-5 (National Research Council of Canada). To monitor ICP-MS precision and instrumental drift, Stellenbosch University (SU) internal control standards were placed in the run sequence and results compared to consensus. The SU internal control calibrated mean was created by repeat analysis (n = 10) of a large volume seawater sample collected from surface water (50 m) at 36°S; 13°E.

2.4. Dissolved trace metal determination

Prior to analysis, seawater samples were pre-concentrated by solid phase extraction. Pre-concentration was carried out offline on a seaFAST-pico SC-4 DX module (elemental scientific Inc.) in a class 100 laboratory at Stellenbosch University. The module makes use of a metal chelating resin column comprising ethylenediaminetriacetic acid (EDTriA) and iminodiacetic acid (IDA) functional groups immobilized on a hydrophilic methacrylate polymer (60 µm bead diameter). The method was set for 4 elution cycles resulting in a final pre-concentrated seawater volume of 250 µL and a pre-concentration factor of 40. The pre-concentrated seawater samples were analysed in duplicate (n = 2) for a suite of trace metals (Cu, Zn, Ni, Fe, Mn, Cd, Co, Pb) by Inductively Coupled Plasma Mass Spectrometry

(Agilent 7900 quadrupole ICP-MS) using the standard configuration quartz spray chamber and torch. The calibration curve was constructed using an Inorganic Ventures (IV) 0, 1, 10 and 20 ppb multi-element standard (MES) and verified with a MES supplied by Merck Millipore. Samples were introduced using a low self-aspirating perfluoroalkoxy (PFA) nebulizer with a flow rate of ~0.2 µL min^{-1}. Isotopes of ^{63}Cu, ^{66}Zn and ^{60}Ni were measured using the Agilent Octopole Reaction System (ORS) in helium (He) collision mode to eliminate plasma and matrix based interferences, extensively reduced by the aforementioned seaFAST matrix removal module. The instrument was optimised for best sensitivity and low oxide ratios (<0.3%). Continuous check standards, comprising ^{45}Sc and ^{89}Y, were continuously analysed to monitor any instrumental drift as well as matrix differences between samples and standards. To determine the blank contribution from the method, a solution of HNO_3 (ultrapur, Merck) diluted to 2% with ultra-pure deionized water, the same composition as the eluent used in sample pre-concentration, was analysed. The blank was subjected to the same pre-concentration procedure as the seawater samples. Detection limits were calculated as 3 times the standard deviation of the pre-concentrated blank. Nickel plated sample and skimmer cones were used on the instrument however the Ni blanks associated with the cone were determined not to be significant in relation to the Ni signal of the samples. Estimates for resin recovery were carried out by comparing the results of replicate analysis of pre-concentrated SU internal control standards with and without the addition of a 200ppt Cu (3.07 nmol kg^{-1}), Zn (2.98 nmol kg^{-1}) and Ni (3.32 nmol kg^{-1}) spike (Inorganic Ventures IV-28).

2.5. Additional parameters

Major nutrients, NO_3 and Si, were measured from filtered seawater collected from the same GO-FLO bottles using a Lachat Flow Injection analyser following methods 31-107-04-1-E, 31-107-04-1-C and 31-144-27-2-A. PO_4 was measured using a Genesys 30 spectrophotometer (Thermo scientific) following the method described by (Grasshoff, 1983). Salinity (conductivity), temperature and pressure (depth) were measured using a Seabird 9+ CTD recorder attached to the rosette. Samples (400 - 600 mL) for chlorophyll-a analysis were collected and processed under dim light. The samples were filtered through Whatman GF/F filters (0.7 um nominal pore size), extracted in 90% acetone for 24h at -25°C. The extract was analysed using a Turner fluorometer calibrated with an Anacystis nidulans chl-a standard (Sigma).

3. Results

3.1. Method validation

3.1.1. Cross over station

Copper ranged between 1.45 ± 0.06 and 2.50 ± 0.08 nmol kg^{-1} in this study, well within the range of 1.56 and 2.90 nmol kg^{-1} reported by Heller and Croot, (2015) (Figure 2a). Likewise for zinc, the range

of 2.21 ± 0.11 and 6.05 ± 0.01 nmol kg^{-1} reported here agrees well with the values of 2.32 and 6.25 nmol kg^{-1} measured by Croot et al. (2011) (Figure 2b).

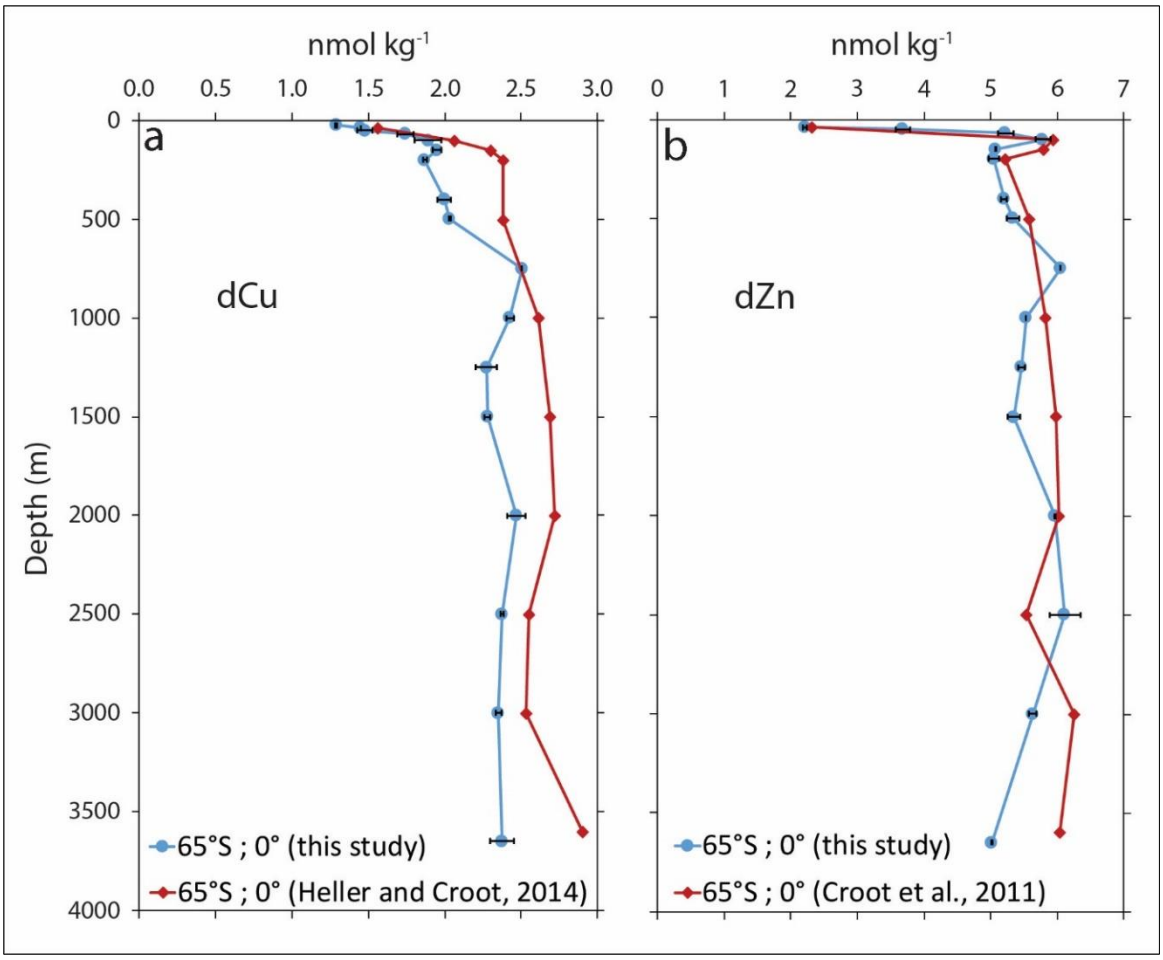

Figure 2. *Results of a crossover station performed at 65°S; 0° for a) dissolved labile copper (LdCu) and b) dissolved zinc (dZn). Cu data obtained from Heller and Croot, (2015) and Zn data obtained from Croot et al., (2011). There is currently no data available for dissolved nickel (dNi) along the GEOTRACES GIPY05 transect.*

3.1.2. Reference standards

Results from the analysis of GEOTRACES reference seawater was in good general agreement with consensus values (Table 1). For SAFe D2, our Ni (8.10 ± 0.11 nmol kg^{-1}) and Cu (2.04 ± 0.03 nmol kg^{-1}) are slightly underestimated according to their respective consensus values however agree well with the values of 8.10 ± 0.50 nmol kg^{-1} and 2.20 ± 0.2 nmol kg^{-1} published by Quéroué et al. (2014). The omission of UV irradiation on the SAFe D2 samples, deemed necessary to liberate Cu from strong organic complexes, resulted in the approximate 10% underestimation (relative to the consensus value) reported here and previously (Milne et al., 2010). It is for this reason that copper is reported as the labile dissolved fraction and not the dissolved fraction. Our GSP Zn value was higher than the current consensus value. For the NASS 5 certified seawater standard (Table 1), values of 4.40 ± 0.23 nmol kg^{-1} (Cu), 1.63 ± 0.04 nmol kg^{-1} (Zn) and 4.02 ± 0.37 nmol kg^{-1} (Ni) were in agreement with the corresponding consensus values. The results of the SU internal standard compared favourably with their respective consensus values and confirmed the precision of the analysis over time.

Table 1. *Results of the ICP-MS analysis of four sets of seawater reference standards namely SAFe (SAFe D2), GEOTRACES (GSP 62 and GSC 1-19), NASS-5 and our Stellenbosch University (SU) internal control are displayed alongside their respective consensus values. Consensus values for the GEOTRACES standards (www.geotraces.org) as of 2013 (SAFe) and 2019 (GSC and GSP). Consensus values for the NASS-5 standard as of 1998 (www.gbcpolska.pl/me/crm/pdf/certyf_woda_morska_nass_5.pdf). Calibrated mean values for the SU internal control calculated by repeat analysis (n=10) of a large volume surface seawater sample.*

	Ni	**Cu**	**Zn**
SAFe D2	*nmol kg^{-1}*	*nmol kg^{-1}*	*nmol kg^{-1}*
Consensus	8.63 ± 0.25	2.28 ± 0.15	7.43 ± 0.25
Average (n = 5)	8.10 ± 0.11	2.04 ± 0.03	7.23 ± 0.25
GSC			
Consensus	4.39 ±0.21	1.10 ±0.15	1.43 ± 0.10
Average (n = 5)	3.91 ± 0.16	1.14 ± 0.04	1.41 ± 0.10
GSP			
Consensus	2.60 ± 0.10	0.57 ± 0.05	0.03 ± 0.05
Average (n = 5)	2.37 ± 0.11	0.56 ± 0.02	0.10 ± 0.05
NASS-5			
Certified	4.21 ± 0.47	4.56 ± 0.71	1.52 ± 0.58
Average (n = 3)	4.02 ± 0.37	4.40 ± 0.23	1.63 ± 0.04
SU internal control			
Cal. mean (n = 10)	5.80 ± 0.11	1.57 ± 0.03	5.83 ± 0.07
Average (n = 8)	5.96 ± 0.16	1.65 ± 0.02	5.72 ± 0.10

3.1.3. Blanks and detection limits

The precision for replicate analysis was between 1.18 and 3.00% for Ni, 1.74 and 3.77% for Cu and 2.15 and 4.69% for Zn at the concentrations observed in this study (Table 2). Detection limits ranged between 0.003, 0.228 and 0.024 nmol kg^{-1} for Cu, Zn and Ni respectively while the analytical blank values ranged between 0.049, 0.070 and 0.041 nmol kg^{-1} for the three metals. Blank values fell well within previously published ranges (Minami et al., 2015; Quéroué et al., 2014; Sohrin et al., 2008; Wang et al., 2014) for Ni, Cu and Zn (Table 2). All metals demonstrated >97% recovery through the pre-concentration procedure ensuring the resin column was performing optimally.

3.2. Hydrographic setting

The summer cruise track crossed the Antarctic Circumpolar Current (ACC) and entered the Weddell Gyre (WG) at ~55.5°S. The three overlapping sampling locations (DTM2, TM1 and DTM3) coincided broadly with three frontal regions, as described by Orsi et al., 1995, namely the Subantarctic Front (SAF), the Antarctic Polar Front (APF) and the Southern Boundary (SBdy) respectively, within the eastward flowing ACC (Figure 1). The position of these fronts fluctuates seasonally due to large variations in wind stress fields. The SAF was located at 46°38’S for summer compared to 43°49’S for winter indicating a large (~330 km) northward migration. A mean position of 46°23’S has been

Table 2. *Detection limits and procedural blanks for the intercalibration station. [a] 3SD of blank. [b] Data sourced from Sohrin et al., (2008). [c] 40 times pre-concentration. [d] not analysed.*

element	measured isotope	detection limit without preconc.[a] (nmol kg^{-1})	mean conc. in the open ocean[b] (nmol kg^{-1})	mean conc. after preconc.[c] (nmol kg^{-1})	detection limit comparisons				blank		blank comparisons			
					Minami et al.	Sohrin et al.	Quéroué et al.	Wang et al.	n	mean	Minami et al.	Sohrin et al.	Quéroué et al.	Wang et al.
Ni	60	0.024	8.519	340.76	0.070	0.010	0.003	0.030	6	0.041	0.017	<0.01	0.013	0.040
Cu	63	0.003	3.147	125.89	0.020	0.005	0.030	0.190	6	0.049	0.017	<0.005	0.053	0.020
Zn	66	0.228	4.589	183.54	0.100	0.060	n.a.[d]	0.210	6	0.070	0.120	0.071	n.a.[d]	0.090

previously identified for the SAF (Lutjeharms, 1985) while a more recent study suggested the SAF is often found as a broad frontal feature present between 43°38'S - 47°17'S with a number of narrow reversals (S. Swart et al., 2008). The locations of the APF (~50°36'S) and SBdy (~55°49'S) showed negligible variation between summer and winter. The three additional summer stations (TM2, DTM1 and TM3) were all located in the WG.

Seawater surface temperatures (SST) decreased poleward from 6.4°C to -1.8°C during summer indicating the transition from Sub Antarctic Surface Water (SASW) to Antarctic Surface Water (AASW) (Figure 3a). This observation persisted during winter with SST decreasing from 5.5°C to -0.6°C across the ACC, equating roughly to a 1 – 1.5 °C decrease from the comparative summer stations. Below the surface, seasonal differences in potential temperature and salinity were minor. A colder (0.5°C < Θ <2.9°C), more saline (34.2 PSU) water mass, termed Antarctic Intermediate Water (AAIW), was found subducting northwards below SASW (Le Moigne et al., 2013). Intermediate and deepwaters throughout the transect were characterised by a relatively homogenous salinity (34.7 PSU) and potential temperature (0°C < Θ < 1°C) signature indicating the presence of nutrient rich Upper Circumpolar Deep Water (UCDW) and Lower Circumpolar Deepwater (LCDW) which was seen upwelling in the WG (Le Moigne et al., 2013). Beneath LCDW, between 2500 and 3500 m depth, Weddell Sea Deep Water (Θ < 0.7°C) was found (Baars et al., 2014). North Atlantic Deepwater (NADW) was observed as a tongue of slightly saltier (PSU > 34.7) water at intermediate depths in the ACC (Figure 3b). Bottom waters across the transect were identified as Antarctic Bottom Waters (AABW) and had characteristic temperature minimums (Boye et al., 2012).

The formation of Sub Antarctic Mode Water (SAMW) in winter was traced using the Si* tracer (Si* = [Si] – [NO_3]; Sarmiento et al., 2004). SAMW is thought to be the main conduit of nutrients from the Southern Ocean to most of the global upper ocean (Vance et al., 2017). The Si* signature of SAMW was observed in the northern ACC between depths of 300 and 450 m (Figure 3c) consistent with the location of previously observed SAMW (Sarmiento et al., 2004).

3.3. Biogeochemical features along the transect

In summer, low surface silica (Si) concentrations (<10 µM) in the northern ACC were maintained until the APF whereafter concentrations increased to ~90 µM in the southern WG. Phosphate (PO_4) behaved similarly with concentration increasing southwards from ~1.2 to ~2.0 µM. Seasonal differences between major nutrients were most notable in the surface mixed layer where winter concentrations exceeded those of summer by an order of ~5 µM for Si and ~0.2 µM for PO_4. The summer and winter Mixed Layer Depth (MLD), calculated using a fixed density criterion of 0.03 kg m^{-3} (de Boyer Montégut et al., 2004), reached a maximum of 102 and 193 m respectively at 50°S. At 46°S (SAF) and 54°S (SBdy), the winter MLD was 41 and 27 m deeper compared to summer. In summer, the lowest MLD of 58 m at 65°S coincided with a subsurface chl-a maximum of 3.8 µg L^{-1}. Here, maximum

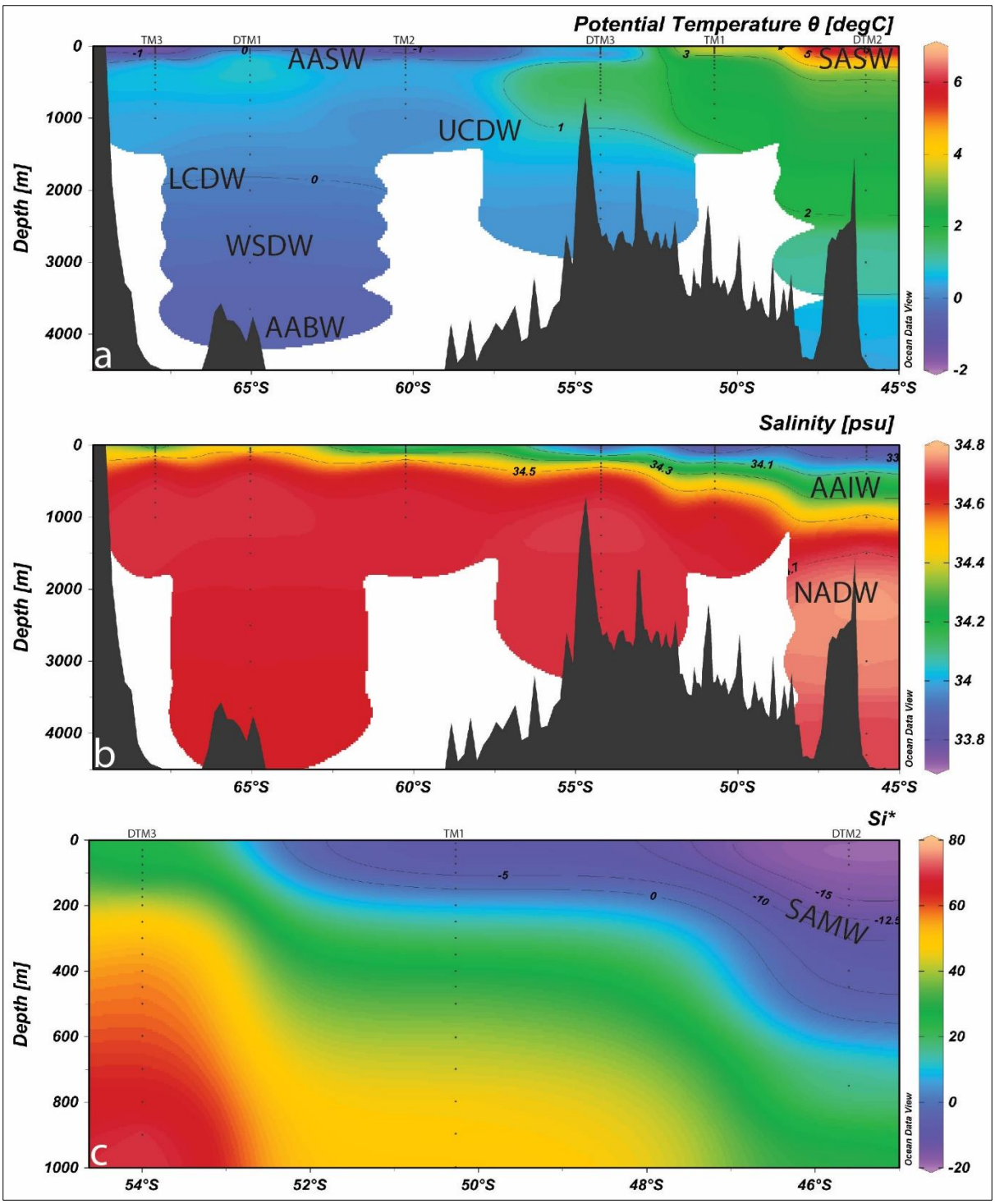

Figure 3. *Distribution of a) summer potential temperature and b) summer salinity defining the water mass regime. AABW: Antarctic Bottom Water; AAIW: Antarctic Intermediate Water; AASW: Antarctic Surface Water; LCDW: Lower Circumpolar Deepwater; NADW: North Atlantic Deepwater; SASW: Sub Antarctic Surface Water; UCDW: Upper Circumpolar Deepwater. Figure 3c) Si*values [Si* = [Si] – [NO_3]] calculated for winter defining SAMW (Sub Antarctic Mode Water). Figure made using Ocean Data View (ODV) (Schlitzer, 2017). Dots represent depths sampled. Data displayed using weighted average gridding.*

observed major nutrient gradients for PO_4 and for Si coincided with the transition to nutrient rich UCDW. Phosphate displayed intermediate depth peaks of approximately 2.5 µM which shallowed southwards from 1000 m in the northern ACC to 250 m in the southern WG. Deepwater (>1000 m) phosphate distributions throughout the study ranged between 2 and 2.25 µM. In contrast to PO_4, Si increased steadily through the water column obtaining maximum concentrations approaching ~130µM in AABW. Estimates of seasonal variability in phytoplankton biomass, calculated by depth integrating chl-a concentrations between surface and 100 metres, were most pronounced at the APF where total summer chl-a (~1.00 µg cm^{-2}) was fivefold that of winter. Chl-a concentrations never exceeded 0.45 µg L^{-1} at the SAF with phytoplankton biomass in summer (0.41 µg cm^{-2}) higher compared to winter (0.39 µg cm^{-2}). Chl-a profiles in the southern ACC showed little seasonal difference in phytoplankton biomass (~0.40 µg cm^{-2}).

Note: As a result of issues pertaining to sample loss through freezing (tubes were overfilled such that when frozen, their caps popped off) in our macronutrient analysis during the summer expedition, Si, NO_3 and PO_4 data at 50°S has been used from previously published work (Klunder et al., 2011). Additionally, PO_4 data from 46°S has also been taken from this work due to inconsistencies in sample labelling.

3.4. Distributions of labile dissolved copper and dissolved zinc and nickel

3.4.1. Summer

At all stations, vertical profiles of LdCu, dZn and dNi displayed a nutrient type behaviour consistent with low surface concentrations and higher deepwater values. Vertically, LdCu ranged between 0.91 nmol kg^{-1} at the surface and 3.15 nmol kg^{-1} in bottom waters of the ACC (Figure 4a). dZn displayed sub nanomolar surface concentrations throughout the northern ACC and increased to deepwater maximums (Figure 4b). dNi had comparatively high surface concentrations of >4.65 nmol kg^{-1} throughout the study and a dNi maximum of ~7 nmol kg^{-1} in the bottom waters of the ACC (Figure 4c). In surface waters (<35 m), metal concentrations showed little variation in SASW whereafter concentrations increased southward through AASW and obtained maximum surface concentrations of 2.79 (LdCu), 4.56 (dZn) and 6.02 (dNi) nmol kg^{-1} near the Antarctic continental shelf. The north-south gradient coincided with the frontal systems with the APF acting as a physical divide between lower metal concentrations to the north and higher concentrations to the south. Highest removal ratios, defined as the slope of the correlation between metal and phosphate (metal/PO_4), for all three metals were calculated in the mixed layer at 65°S. Removal ratios indicated that Zn was most strongly removed, with a maximum Zn/PO_4 ratio of 8.6 nmol $µmol^{-1}$, followed by Ni (Ni/PO_4 – 2.5 nmol $µmol^{-1}$) and Cu (Cu/PO_4 – 1.3 nmol $µmol^{-1}$). In general, the order i.e. Zn > Ni > Cu, of trace metal removal in the mixed layer was consistent throughout the summer season. In the intermediate and deepwaters (>500 m), vertical concentration gradients for all three metals were less steep compared to the mixed layer. Localised enrichments in excess of 2.5 nmol kg^{-1} for LdCu and 7.0 nmol kg^{-1} for dZn and dNi were observed in UCDW down-

current of the mid-Atlantic ridge. dNi displayed intermediate depth peaks, similar to that of phosphate, between 6 and 7 nmol kg^{-1}.

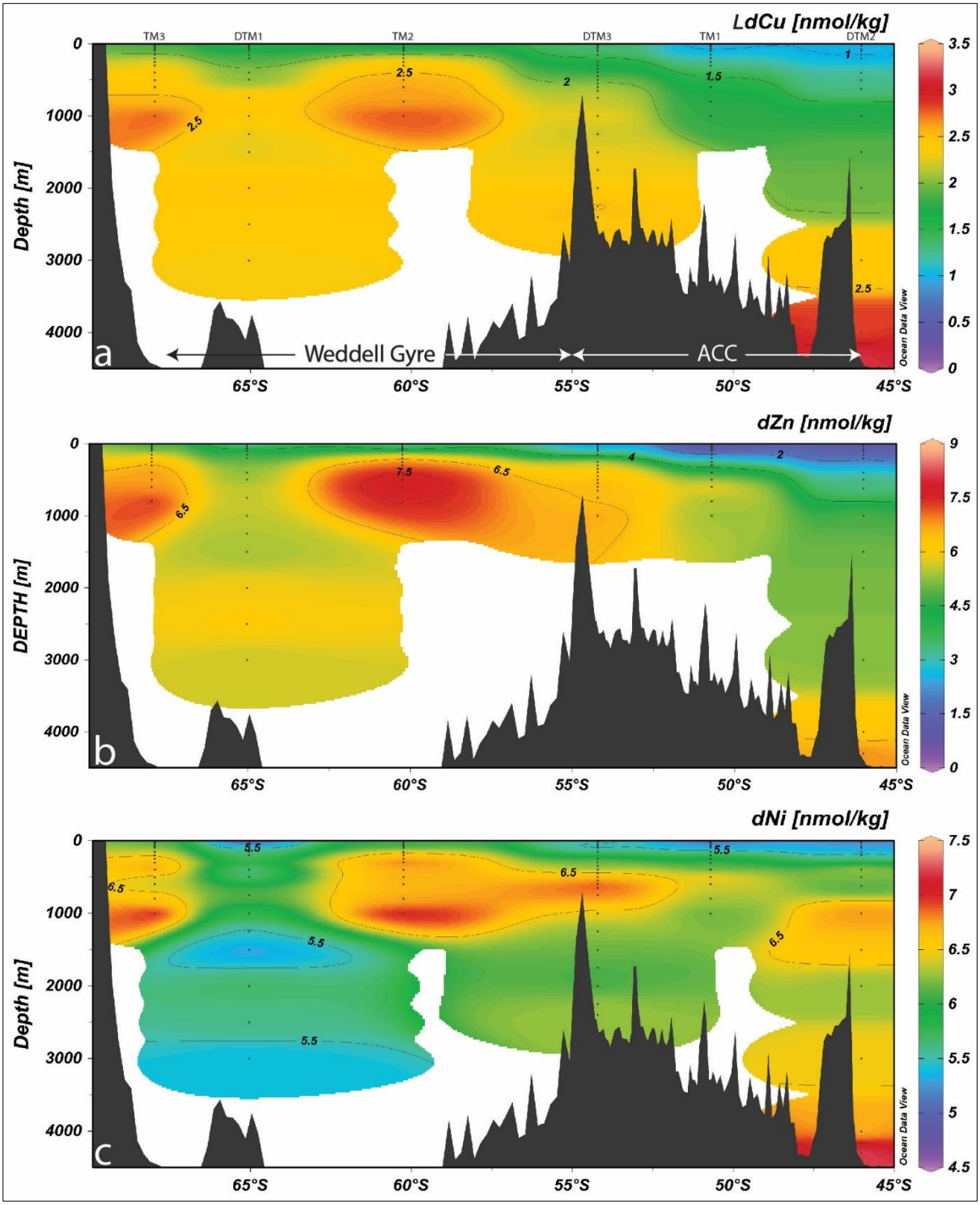

Figure 4. *Summer distributions of a) dissolved labile copper (LdCu), b) dissolved zinc (dZn) and c) dissolved nickel (dNi). Figures generated in Ocean Data View (ODV) (Schlitzer, 2017) using weighted average gridding method based on 6 sampling stations between 46°S and 68°S. Dots represent depths sampled. Data displayed using weighted average gridding.*

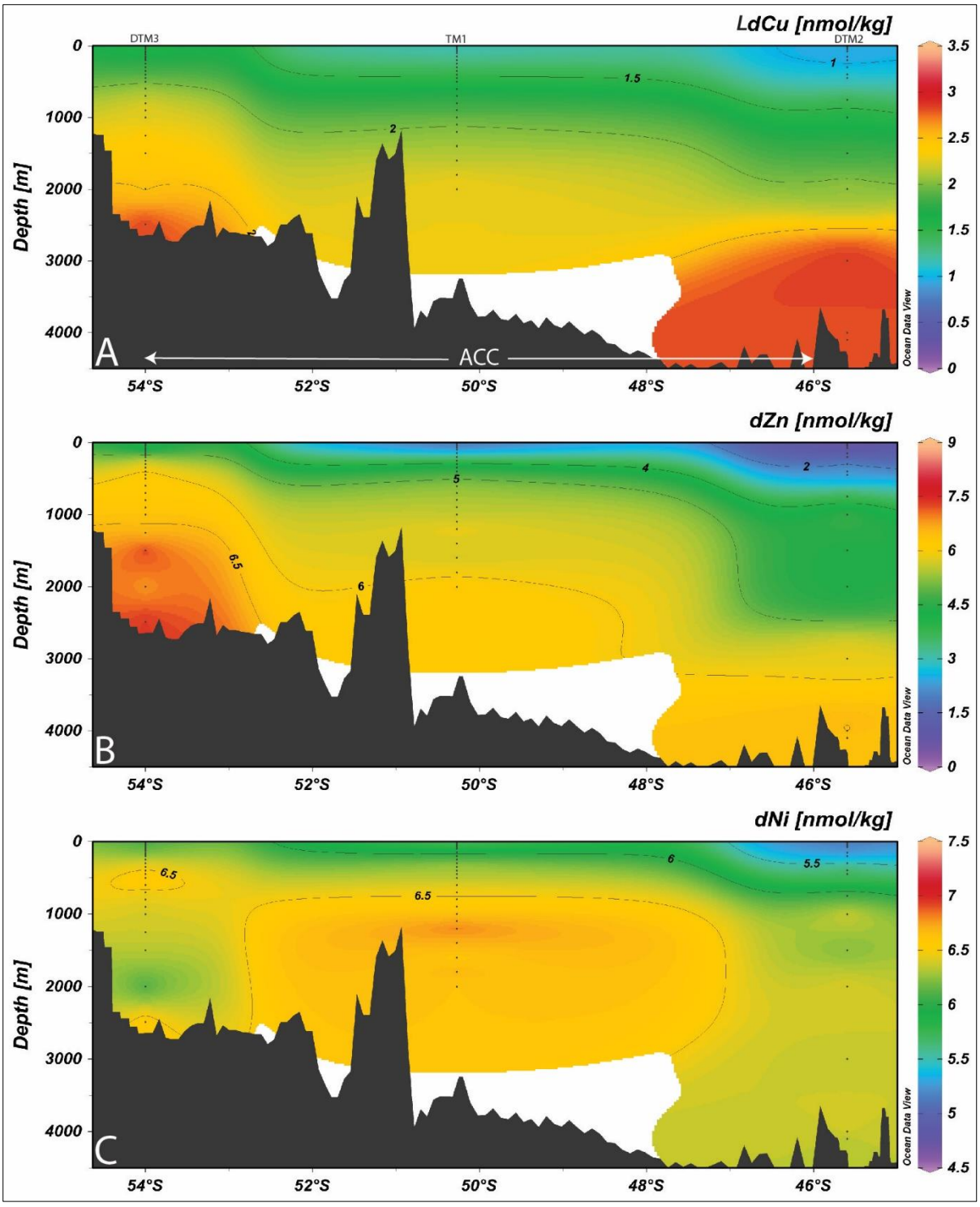

***Figure 5**. Winter distributions of a) dissolved labile copper (LdCu), b) dissolved zinc (dZn) and c) dissolved nickel (dNi). Figures generated in Ocean Data View (ODV) (Schlitzer, 2017) using weighted average gridding method based on 3 sampling stations between 46°S and 54°S. Dots represent depths sampled. Data displayed using weighted average gridding.*

3.4.2. Winter

Throughout the winter transect (46°S – 54°S), nutrient type behaviour persisted for LdCu, dZn and dNi. Surface (<35 m) concentrations showed distinct southward increases across the transect. dZn showed the greatest north - south surface gradient of 0.47 to 3.38 nmol kg^{-1}, while LdCu and dNi increased from

1.06 to 1.48 nmol kg^{-1} and 5.05 to 5.99 nmol kg^{-1} respectively. LdCu increased steadily down the water column and reached maximum observed concentrations approaching 3 nmol kg^{-1} in bottom waters at all stations (Figure 5a). dZn behaved similarly reaching deep ocean maximums at each station and a maximum observed concentration of 7.78 nmol kg^{-1} in close proximity to the ocean floor at 54°S (Figure 5b). dNi concentrations fell between 5 nmol kg^{-1} near the surface and 7 nmol kg^{-1} at intermediate (500 - 1500 m) depths (Figure 5c). Removal ratios (metal/PO_4) reveal that, like summer, zinc was most strongly removed from the winter mixed layer followed by nickel and copper. Within the ACC, winter removal ratios were lower compared to those in summer with maximum observed ratios of 3.4, 1.2 and 0.2 nmol $\mu mol^{-1}$for Zn, Ni and Cu respectively.

4. Discussion

There is a general paucity of trace metal data in the Southern Ocean. To our knowledge, no prior Ni data exists along the Zero Meridian in summer and certainly these are the first profiles of dissolved labile Cu and dissolved Zn and Ni produced for winter. The only other sub-Antarctic winter profiles were produced in the Tasman Sea therefore data is not directly comparable. High resolution Cu (Boye et al., 2012; Heller and Croot, 2015) and Zn (Croot et al., 2011) profiles are directly comparable with our summer dataset and show a good general agreement in both Cu and Zn distributions. Nickel distributions have been investigated along the 6°W meridian in summer with reported concentrations generally ranging between 4 nmol kg^{-1} at the surface and 7 nmol kg^{-1} at depth (Löscher, 1999), similar to the dNi range of between 5 and 7 nmol kg^{-1} reported here.

4.1. Summer trace metal distributions

It is well established that the observed nutrient type behaviour of Cu, Zn and Ni is induced predominantly by biological (phytoplankton) utilization in the surface euphotic zone and remineralization of sinking organic matter at depth , consider the early work of Bruland and co-workers (Bruland, 1980; Bruland and Franks, 1983). Highest metal/PO_4 removal ratios were calculated at 65°S coinciding with the chl-a maximum of >3.5 µg L^{-1} (50 m) indicating increased biological uptake. These nutrient signatures indicate higher productivity, perhaps initiated by the retreating ice edge and the release of trace metals and major nutrients from remineralised diatoms entrained in melting sea ice (Croot et al., 2011, 2004). In addition, trace metal gradients throughout the transect appeared to follow those of the macronutrients. This coupling further suggests that common biological processes control their distributions (Sunda, 2012, 1989). As such the downward flux of phytoplankton, in particularly diatoms, appears to be the main transfer mechanism of Cu, Zn and Ni from AASW (Heller and Croot, 2015; Löscher, 1999). Local maxima in all three metal profiles, between 100 and 150 m depth, from the central WG (65°S) suggests a zone of shallow remineralization as has been previously noted for Zn

(Croot et al., 2011), Cu (Heller and Croot, 2015) and a number of other elements including cadmium (Baars et al., 2014), iron (Klunder et al., 2014, 2011) and barium (Hoppema et al., 2010a).

The southward increase in trace metal and major nutrient concentrations in AASW is a reflection of the underlying water mass regime where lateral advection of waters from the Drake Passage via the eastwards flowing ACC combined with upwelling of nutrient enriched UCDW south of the APF is a likely cause of these elevated concentrations (Coale et al., 2005). The downward trace metal flux, mediated by sinking biogenic detritus from AASW, contributed toward the maintenance of high LdCu (~2.5 nmol kg^{-1}) as well as dZn and dNi (>6.0 nmol kg^{-1}) below the euphotic zone (Löscher, 1999) although this term is less significant, in terms of magnitude, compared to the opposing upwelling flux. Additionally, surface metal concentrations may be augmented in the southern WG due to seasonal melting of the dust laden Antarctic ice sheet and drifting icebergs, as has been shown for Fe (Croot et al., 2004; Klunder et al., 2011). Associated with ice melt is a lower surface salinity signature which was evident at 68°S (Figure 3b), suggesting meltwater was present, however the magnitude of this highly variable surface supply mechanism is poorly constrained. Enrichments of all three metals at ~1000 m depth near to the Antarctic shelf make it convenient to suggest a continental margin source as has been observed near other continental margins for multiple elements including Cu e.g southwest African continental margin (Boye et al., 2012). Interestingly the absence of a continental margin source for typical proxy elements such as Mn, Fe and Al (Klunder et al., 2011; Middag et al., 2011) in this region has been noted and attributed to the protruding continental ice-sheet preventing nutrient supply (from shelf sediments) to surface waters. It therefore seems unlikely that preferential resupply of Cu, Zn and Ni would occur here. As samples to a maximum depth of 1000 m were collected it is difficult to assess whether this is a localised enrichment or whether these seemingly elevated concentrations persist with depth. Enrichments, most notably in Zn, above the mid-Atlantic ridge and at shallowing depths to the south are possibly the result of episodic hydrothermal activity, the signatures of which are transported southwards by upwelling circumpolar deepwaters. Iron (Fe) and manganese (Mn), two hydrothermal proxy elements, have shown enrichments over the mid-Atlantic ridge during previous occupations of this transect, e.g. Klunder et al., (2011) and Middag et al., (2011).

4.2. Winter trace metal distributions

With respect to the deepwaters, comparatively low surface concentrations persisted for Cu, Zn and Ni in winter indicating that biological utilisation remains a major control on surface trace metal distributions despite seemingly unfavourable conditions for phytoplankton growth (Ellwood, 2008b). Distinct north-south increases in surface LdCu, dZn and dNi concentrations across the ACC, similar to that of silica and phosphate, suggests that the major source of trace metals to surface waters is upwelling and vertical mixing of nutrient enriched UCDW. In addition to these bottom-up supply mechanisms, vertical trace metal gradients below the MLD were supplemented by remineralization of sinking

biogenic particles from surface waters. Compared to Cu and Zn, Ni appeared to have a shallower recycling mechanism, like that of PO_4, consistent with a portion of dNi being incorporated into the soft tissue of diatoms (Twining et al., 2012) and flagellated cells from the Southern Ocean (Twining et al., 2004). Copper and zinc increased to bottom water maximums at all stations with highest concentrations of >2.5 and >7.0 nmol kg^{-1} respectively measured above the mid-Atlantic ridge at 54°S. Although Ni did not display a bottom water maximum here, there was an enrichment of >6.5 nmol kg^{-1}. Given the proximity of the ocean floor to the deepest depth sampled at this station, these high concentrations may be attributed to resuspension of sea floor sediment or flux from metal rich porewaters.

4.3. Seasonal variation in the upper water column (<500 m)

In general, average winter mixed layer concentrations were between 0.20 - 0.22 nmol kg^{-1} for LdCu, 1.15 – 1.24 nmol kg^{-1} for dZn and 0.25 – 0.30 nmol kg^{-1} for dNi higher compared to summer in the central and southern ACC (Figure 6). Interestingly, the seasonal signal at the SAF was virtually negligible. Previously, in the subantarctic waters east of New Zealand, seasonal variations showed a 0.1 – 0.2 nmol kg^{-1} increase in copper from winter to summer, 0.2 - 0.3 nmol kg^{-1} for zinc and no seasonal variation for nickel (Ellwood, 2008b). The winter deepening of the mixed layer, to between depths of 120 and 193 m (Figure 6), resulted from an approximate cooling of surface waters by between 1.2 and 1.6°C and the formation of a more dense (σ_Θ > 26.7) water mass, termed Sub-Antarctic Mode Water (SAMW) (Figure 3C), in the vicinity of the SAF (Sarmiento et al., 2004). During the onset of summer the production of SAMW ceased as surface waters warmed and stratified leading to a 40 – 100 m shoaling of the mixed layer.

In winter, deeper mixed layers combined with lower light levels provide unfavourable growth conditions for phytoplankton when compared to summer. Considering biological uptake as the primary sink for surface metal concentrations, the results here indicate decreased biological consumption during winter months. Using Chl-*a* concentrations as an indicator of phytoplankton biomass confirms a higher abundance of phytoplankton present during summer (and hence a greater drawdown of Cu, Zn and Ni), particularly at the APF where estimated summer biomass was 1.0 µg cm^{-2} compared to 0.2 µg cm^{-2} in winter. Interestingly, seasonal variation in phytoplankton biomass was not as readily apparent at the other two re-occupied stations where Chl-*a* was approximately 0.4 µg cm^{-2} for both seasons. This outcome is however complicated by numerous adaptation strategies adopted by phytoplankton when exposed to a dynamic irradiance regime coupled with nutrient (particularly Fe) stresses, as is the case in the Southern Ocean (Alderkamp et al., 2010). Additional complications arise when accounting for phytoplankton mortality due to grazing via zooplankton and viral lysis (Evans and Brussaard, 2012). The following serves to discuss these factors.

Under low light/high Fe conditions (i.e. winter), phytoplankton are known to produce more Chl-*a* per cell compared to high light/low Fe (i.e. summer) conditions (Van De Poll et al., 2005; Van Leeuwe and

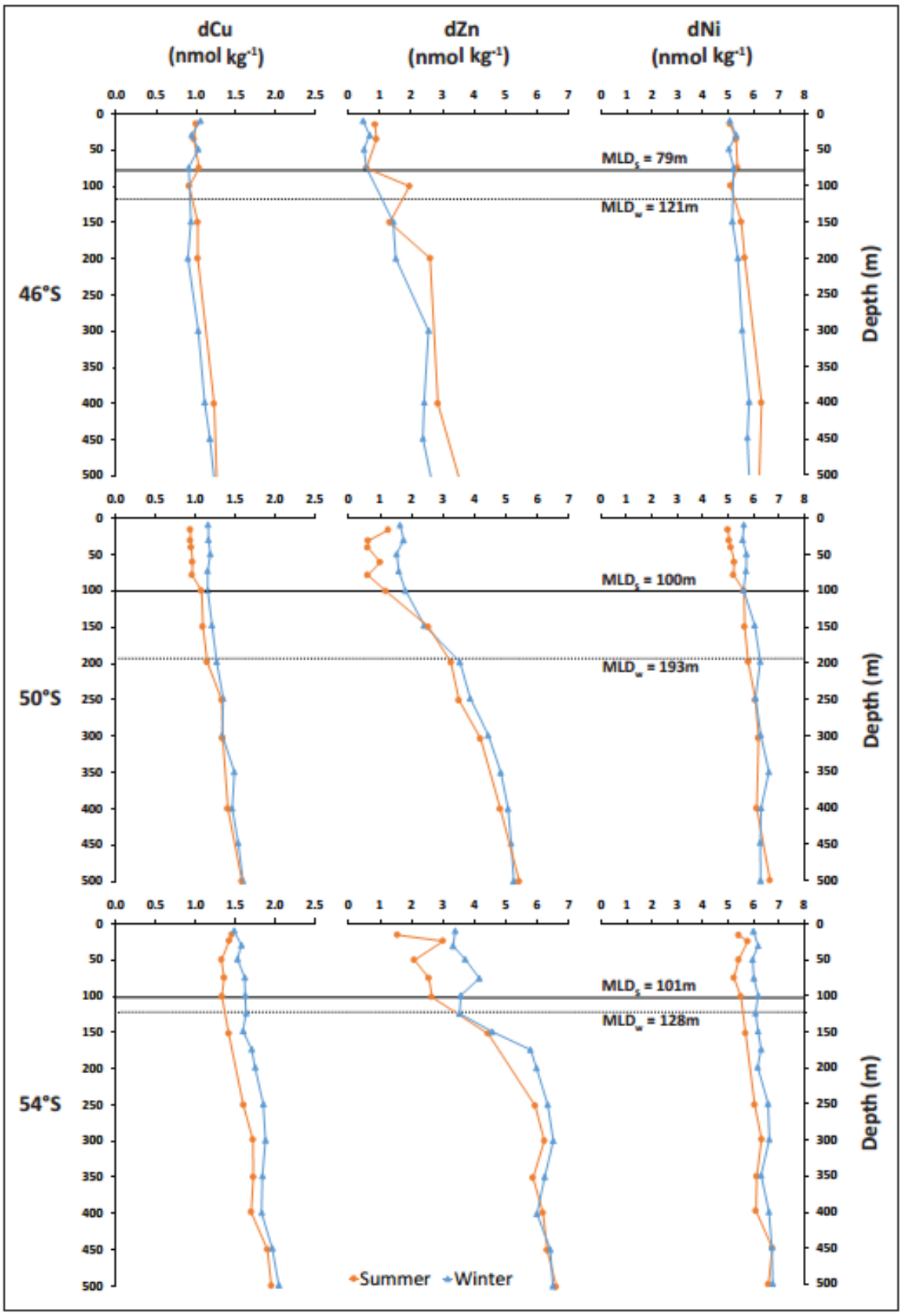

Figure 6. *Seasonal comparisons of dissolved labile copper (LdCu) (left column), dissolved zinc (dZn) (middle column) and dissolved nickel (dNi) (right column) in the upper 500 metres of the water column at each overlapping station. The solid line (MLD_S) represents the calculated summer MLD. The dotted line (MLD_W) represents the calculated winter MLD.*

Stefels, 2007). Consequently, winter phytoplankton biomass may be overestimated. This is particularly important for stations at the SAF and SBdy in the summer. Considering the approximately equal depth integrated Chl-*a* values at the SAF and SBdy for both seasons, the greater drawdown of trace metals in summer vs winter at the SBdy suggest that this apparent overestimation might be greater in the south, perhaps a consequence of larger diurnal and seasonal light cycles at higher latitudes. At the APF, where there was a large difference in phytoplankton biomass and mixed layer depth (100 m in summer vs 193 m in winter), variability in seasonal irradiance regimes i.e. more stable, higher irradiance in summer vs more unstable, dynamic irradiance in winter, will favour certain species of phytoplankton due to their photoacclimaition strategies. For example, bloom forming Antarctic diatoms (Cailliau et al., 1997) and haptophytes (*Phaeocystis Antarctica*; Van Leeuwe and Stefels, 2007). In addition, low summer grazing pressures exerted by copepods at the APF (Dubischar and Bathmann, 1997) agree with high summer phytoplankton biomass. During the same study, increased grazing pressures by salps at the SBdy were shown to constrain phytoplankton biomass providing additional reasoning behind the seemingly paradoxical results presented at the SBdy during this study i.e. increased summer trace metal uptake yet lack of observed seasonal difference in phytoplankton abundances. The effects of viral lysis on phytoplankton biomass has been deemed as comparatively minor in the Southern ocean (Evans and Brussaard, 2012). Ultimately, increased biological uptake in the summer is the underlying driver between the observed seasonal trace metal profiles, particularly at the APF. Winter trace metal depletion, although comparatively smaller, is driven by a smaller phytoplankton standing stock which are well acclimatized to dynamic irradiance regimes due to increased mixing e.g. flagellates (Van Leeuwe et al., 2005).

4.4. Seasonal variation in intermediate and deepwaters

In waters below 500 m, there existed a complete lack of seasonal signal for Cu, Zn and Ni throughout the study region. Several studies have commented on the intense turbulent mixing in the abyssal Southern Ocean where diapycnal diffusivity constants exceed the global average by factors of 10 to 1000 (Garabato et al., 2010). The mixing of the intermediate and deepwaters acts to homogenize the distributions of trace metals and major nutrients alike, irrespective of season. In the Atlantic sector of the Southern Ocean, the high basin-wide mixing rates are the result of a complex bathymetry and contributes significantly to the upward transport of water thus closing the oceans meridional circulation (Heywood et al., 2002).

4.5. Quantifying the winter reserve reservoir

In an effort to assess the quantity and importance of deep winter mixing, we propose two different scenarios with respect to the relationship between summer and winter mixed layers. Scenario 1 takes into account ocean dynamics, specifically mixed layer depth variability, the drivers of which as well as the subsequent effects on phytoplankton biomass are highly variable, both spatially and temporally

(Fauchereau et al., 2011; Swart et al., 2015). Here, the subsurface inventory was calculated by subtracting the summer mixed layer depth integrated inventory from the winter mixed layer depth integrated inventory for each re-occupied station. Scenario 2 adopts a more static approach where both summer and winter trace metal profiles were integrated over a fixed mixed layer, chosen as the depth of maximum winter mixing i.e. 193 m, at all re-occupied stations. Given the temporal sampling resolution, scenario 1 cannot be deemed representative of a full seasonal cycle however it does provide insight into the interplay between ocean dynamics and nutrient stocks. The purpose of scenario 2 is to negate the effect which integrating over different summer and winter mixed layers has on the trace metal inventories. From this, a more accurate estimation of trace metal stock available for potential entrainment can be quantified. It must be noted here that the mixed layer by no means acts as a solid physical boundary whereby all nutrients above the mixed layer depth are entrained and concentrated into a shallower layer with the onset of summer shoaling. Additional supply terms, chiefly vertical diapycnal diffusion and Ekman upwelling, and loss terms, e.g. biological metal uptake and particulate export (Bown et al., 2011; Tagliabue et al., 2014), act across the mixed layer density gradient. The purpose of the following discussion is to provide estimates for what is potentially available for entrainment taking into account these fluxes.

For scenario 1, results of the depth integrations are shown in Figure 7 (a - c). Relative to their respective summer inventories, smallest sub-surface reservoirs for all 3 metals were calculated at 54°S (Figure 7c) coinciding with the smallest difference between winter and summer mixed layer depths (Figure 6). At 50°S, the station with the largest difference between summer and winter mixed layers, subsurface inventories of 143 µmol m^{-2} Cu, 353 µmol m^{-2} Zn and 693 µmol m^{-2} Ni were calculated (Figure 7b). The outcome of scenario 2 (Figure 7d - f) showed smaller differences between winter and summer trace metal inventories, between 31 – 38 µmol m^{-2} for Cu, 129 – 174 µmol m^{-2} for Zn and 42 – 95 µmol m^{-2} for Ni at stations 50°S and 54°S. Interestingly, at 46°S, summer inventories for all 3 metals were slightly greater than winter inventories (Figure 7d). Here, the summer nutriclines of copper, zinc and nickel (Z_{Cu}, Z_{Zn} and Z_{Ni}) were located below the summer mixed layer depth yet within the depth of maximum winter mixing and largely accounts for the observed difference between scenario 1 and 2 at 46°S. Had scenario 2 represented in situ mixed layers, it would suggest slow physical mixing of trace metals with remineralization length scales slow enough to maintain these gradients as has been shown for Fe (Croot et al., 2007). It must be noted that Fe is highly particle reactive resulting in a deep remineralization cycle such that Z_{Fe} may be deeper than that of other nutrients and the mixed layer (Frew et al., 2006). In contrast to Fe, very low amounts of Cu, Zn and Ni are associated with particles, (Frew et al., 2001) such that they may be remineralised more rapidly to dissolved form within the mixed layer. The remineralization length scales of these metals therefore means it is unlikely they would show strong gradients below the depth of maximum winter mixing. At 50°S (APF) and 54°S (SBdy), Z_{Cu}, Z_{Zn} and Z_{Ni} were shallower than the summer mixed layer and may be related to increases in Ekman flux and

upwelling velocities, and hence vertical diapycnal diffusion, with latitude (Sokolov and Rintoul, 2007). Implications for this suggest the role of entrainment may increase southwards although it is recognised that there is a degree of overlap with the other bottom-up nutrients sources.

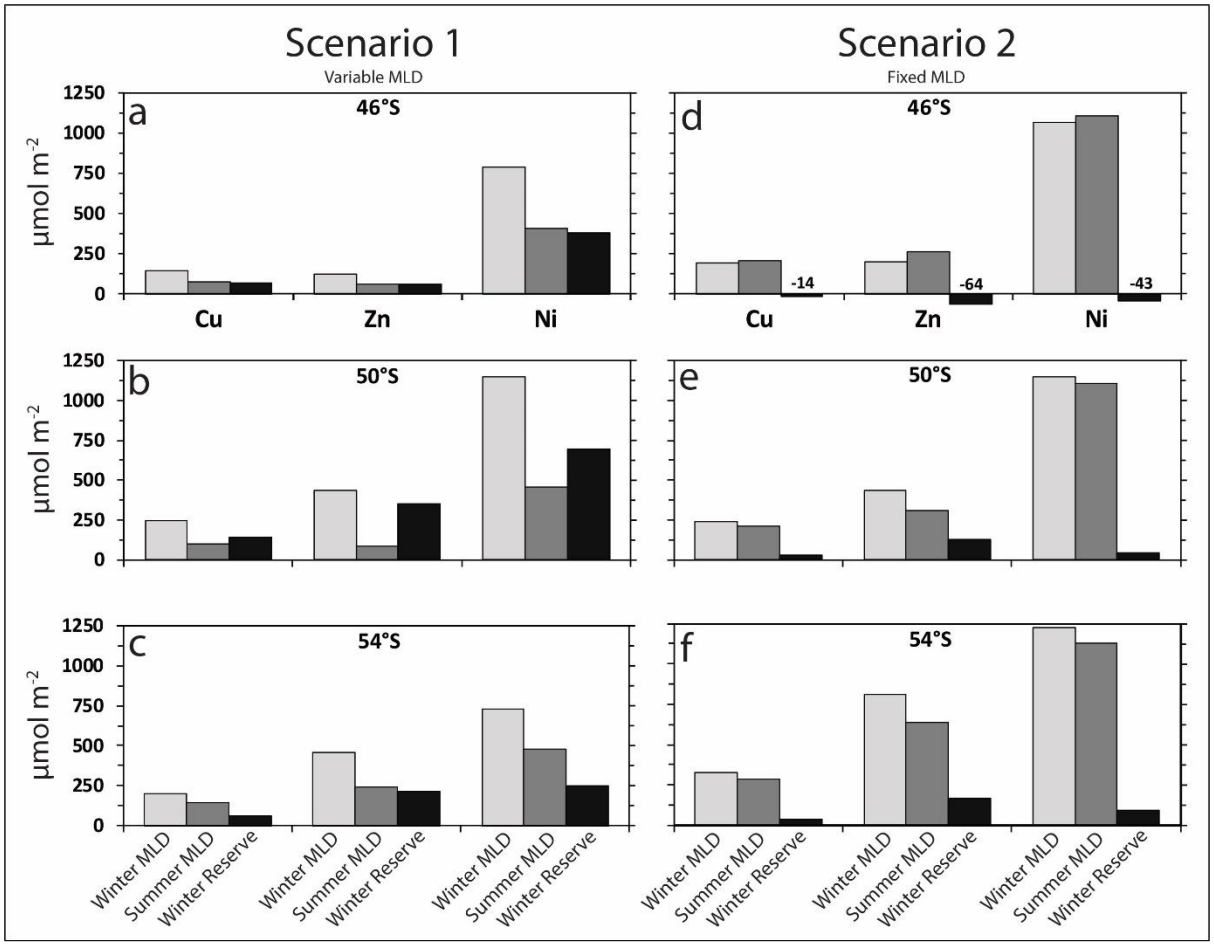

Figure 7. *Estimates of winter reserve inventories for scenario 1 at a) 46°S, b) 50°S, c) 54°S and for scenario 2 at d) 46°S, e) 50°S, f) 54°S. Depth integration calculations were carried out as follows: for scenario 1 the winter reserve inventory was calculated by subtracting the summer depth integrated metal inventory (surface to summer MLD) from the winter depth integrated metal inventory (surface to winter MLD). For scenario 2 the winter reserve inventory was calculated by subtracting the summer depth integrated metal inventory (surface to maximum winter MLD) from the winter depth integrated metal inventory (surface to maximum winter MLD).*

4.6. Micro- to macronutrient relationships

Our understanding of the relationship between trace elements and major nutrients in the Southern ocean has been hindered by a distinct scarcity of reliable trace metal data yet these interplays yield important information regarding the biogeochemical cycling of both parameters. Note that metal/macronutrient refers to the uptake ratio where metal:macronutrient refers to the dissolved ratio.

4.6.1. Trace metal – silicate relationships

Relationships between silicate and Cu (Figure 8a), Zn (Figure 8b) and Ni (Figure 8c) for summer and winter are shown. Strong linear correlations for Cu/Si have been previously found in the Atlantic sector of the Southern Ocean (Boye et al., 2012; Heller and Croot, 2015; Löscher, 1999). The close Zn and Si

coupling is comparable to previous work in the region in summer (Croot et al., 2011; Wyatt et al., 2014) and winter (Ellwood, 2008b). For Ni/Si, the only comparable data was from a single station at the APF where Ni (nmol kg^{-1}) = 0.026 [Si(µmol kg^{-1})] + 5.386 (r^2 = 0.95, n = 6; Löscher, 1999). That these trace metals show similarities to profiles of Si is evidence of the important role diatoms exert, through their biological uptake and subsequent remineralization, on the vertical distributions of Cu, Zn and Ni.

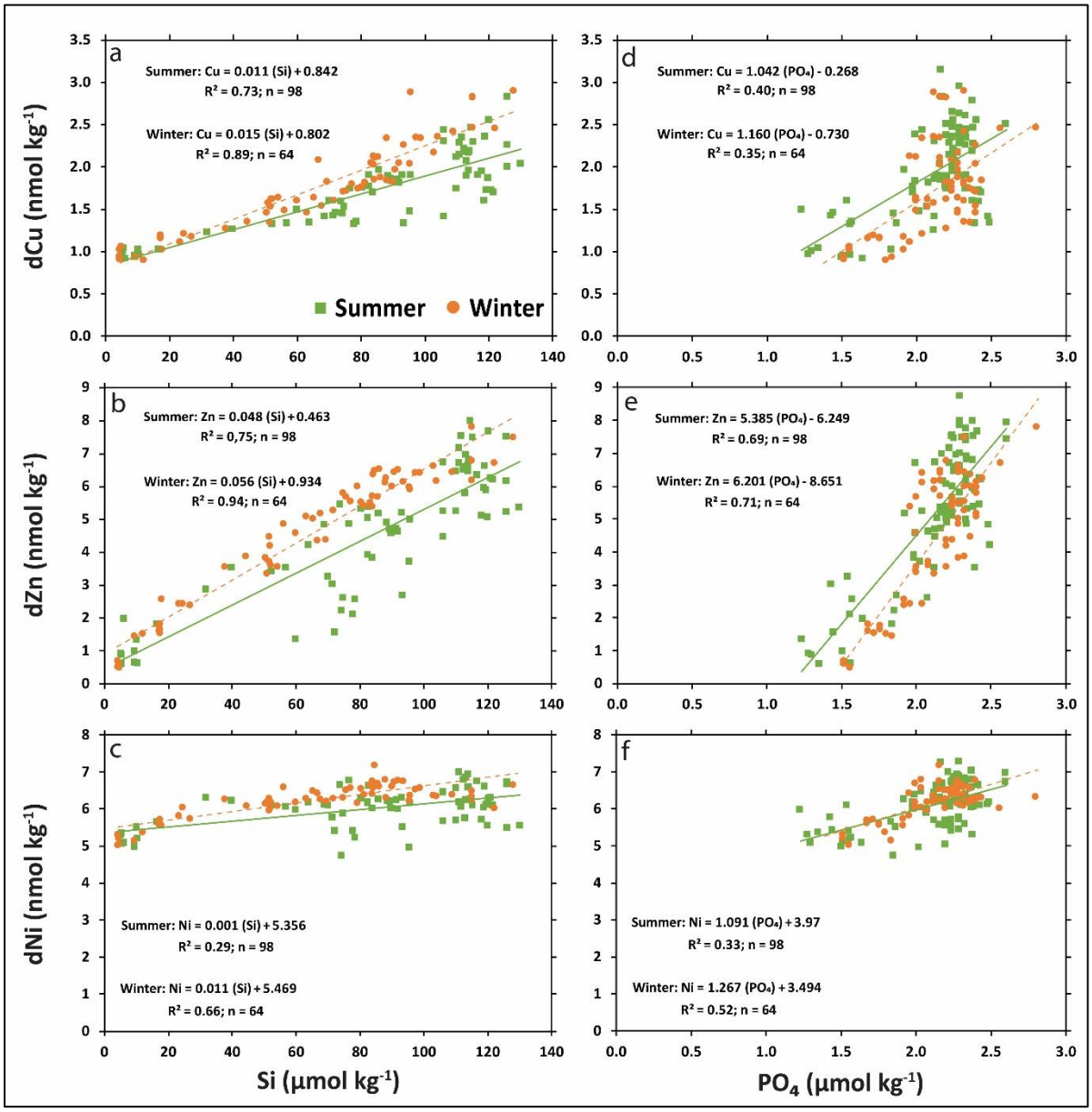

Figure 8. *Plots of a) copper versus silicate, b) zinc versus silicate, c) nickel versus silicate, d) copper versus phosphate, e) zinc versus phosphate and f) nickel versus phosphate for the whole water column for summer and winter.*

For both seasons, Cu:Si and Ni:Si dissolved ratios decreased southward across the transect and with depth through the water column (Table 3). A distinct drop in dissolved Cu:Si and Ni:Si ratios was seen below the mixed layer at ~200 m, coinciding with the transition between surface waters (SASW and AASW) and deeper water masses (AAIW and UCDW) which have higher Si gradients in comparison

to Cu and Ni. Dissolved Zn:Si ratios did not show any clear southward decreasing trend. Furthermore, dissolved Zn:Si ratios generally increased until 100 – 150 m depth before decreasing below the mixed layer (Table 3). This may suggest rapid, shallow recycling of diatoms with high Zn/Si uptake stoichiometries. In the WG, this notion is consistent with TCO_2 enrichments and reduced O_2 found in surface waters (< 200 m) (Usbeck et al., 2002), as well as the shallow remineralization cycle of Barium, which is highly correlated with silicate in this region (Hoppema et al., 2010b). Further north, in the ACC, a greater proportion of picoplankton (0.2 – 2 µm) groups compared to larger size classes e.g. nanoplankton (2 – 20 µm) in the WG (Doolittle et al., 2008), may be controlling dissolved Zn:Si ratios via their slower sinking rates and hence shallower regeneration cycle.

Table 3. *Summer (left column) and winter (right column) dissolved ratios for copper to silica (top row), zinc to silica (middle row) and nickel to silica (bottom row).*

	Summer Cu:Si (nmol µmol^{-1})						**Winter Cu:Si (nmol µmol^{-1})**		
Depth (m)	46°S	50°S	54°S	60°S	65°S	68'S	46°S	50°S	54°S
15	0.194	0.169	0.050	0.025	0.020	0.020	0.222	0.067	0.031
40	0.189	0.173	0.043	0.023	0.020	0.020	0.237	0.067	0.030
100	0.148	0.186	0.028	0.020	0.017	0.021	0.211	0.066	0.030
150	0.101	0.029	0.020	0.018	0.017	0.019	0.099	0.050	0.027
200	0.062	0.025	0.017	0.018	0.016	0.019	0.075	0.034	0.022
> 300	0.019	0.011	0.015	0.008	0.035	0.004	0.035	0.024	0.022
	Summer Zn:Si (nmol µmol^{-1})						**Winter Zn:Si (nmol µmol^{-1})**		
15	0.159	0.173	0.054	0.022	0.016	0.051	0.098	0.095	0.065
40	0.175	0.113	0.068	0.046	0.030	0.056	0.114	0.088	0.072
100	0.317	0.204	0.055	0.052	0.051	0.055	0.134	0.104	0.069
150	0.131	0.066	0.064	0.059	0.043	0.058	0.152	0.099	0.076
200	0.159	0.070	0.064	0.055	0.042	0.059	0.126	0.094	0.076
> 300	0.073	0.057	0.066	0.054	0.042	0.052	0.088	0.074	0.067
	Summer Ni:Si (nmol µmol^{-1})						**Winter Ni:Si (nmol µmol^{-1})**		
15	0.951	0.896	0.189	0.100	0.072	0.067	1.056	0.324	0.121
40	1.031	0.929	0.175	0.087	0.064	0.068	1.167	0.331	0.115
100	0.828	0.964	0.115	0.064	0.051	0.070	1.206	0.324	0.118
150	0.546	0.148	0.082	0.053	0.048	0.060	0.551	0.248	0.103
200	0.345	0.124	0.065	0.051	0.046	0.058	0.448	0.166	0.078
> 300	0.127	0.067	0.068	0.047	0.044	0.049	0.162	0.091	0.069

4.6.2. Trace metal - phosphate relationships

Relationships between phosphate and Cu (Figure 8d), Zn (Figure 8e) and Ni (Figure 8f) for summer and winter are shown. Cu/PO_4 removal ratios are comparable with results from summer (Löscher, 1999) and winter (Ellwood, 2008b). Zn/PO_4 show good agreement with previous work along this transect (Croot et al., 2011). Considering the metal/PO_4 slope values for each metal, a 0.2 µmol kg^{-1} drawdown

of phosphate from winter to summer would result in a 0.21 nmol kg^{-1} (Cu), 1.10 nmol kg^{-1} (Zn) and 0.22 nmol kg^{-1} (Ni) drawdown of micronutrients, consistent with observed seasonal differences.

As a comparative exercise, metal/PO_4 removal ratios were calculated for the upper 500 m along the transect (Figure 9). Cu/PO_4 and Zn/PO_4 ratios generally increased southwards and is suggested to be a result of iron or iron/light limitation (Croot et al., 2011). Contrastingly, Ni/PO_4 ratios generally decreased southwards likely the reflection of a weaker surface Ni gradient compared to PO_4. The sharp increase of all metal/PO_4 ratios at 65°S is consistent with increased uptake by diatoms with high metal/PO_4 stoichiometries (Twining and Baines, 2013).

While there is little comparative data for Ni/PO_4, early investigations found that Ni is remineralised at shallow depths, like PO_4, and in deep water, like Si (Sclater et al., 1976). Our results indeed indicate a closer Ni/PO_4 correlation in the upper 500 m [summer: Ni(nmol kg^{-1}) = 1.030[PO_4(µmol kg^{-1})] + 3.836 (r^2 = 0.49) winter: Ni(nmol kg^{-1}) = 1.406[PO_4(µmol kg^{-1})] + 3.086 (r^2 = 0.79)] compared to the whole water column (Figure 8f). Correlations between Ni/Si were investigated below 1000 metres however, owing to few deepwater data points, comparisons are limited. Assuming Ni/Si were correlated in deepwaters, it would suggest an important role for diatoms in Ni biogeochemical cycling whereby the association of Ni and PO_4 within the diatom, and co-localization of Ni and Si in the outer frustule of the diatom (Twining et al., 2012) would result in nickel resembling a combination of PO_4 and Si profiles.

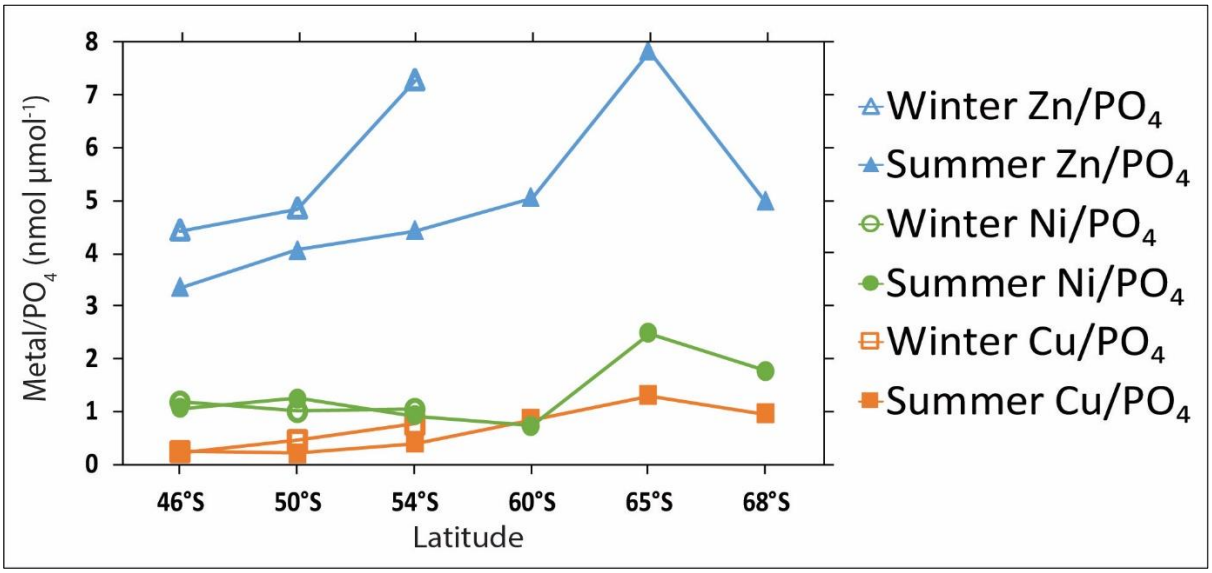

***Figure 9**. Metal/PO_4 removal ratios calculated for the upper 500m of the water column at all stations during summer (solid markers) and winter (open markers) transects.*

4.6.3. The zinc-silicate/zinc-phosphate paradox

Of particular interest in recent times is the seemingly paradoxical coupling between Zn and Si and decoupling between Zn and PO_4, as observed in this study (Figure 10). This paradox stems from the association of Si and PO_4 in the internal organic parts of diatom cells while the Zn content in the Si

based diatom frustule is negligible (Michael J Ellwood and Hunter, 2000; Twining et al., 2003; Twining and Baines, 2013). Here the reader is referred to recent investigations (de Souza et al., 2018; Vance et al., 2017) where the Zn-Si-PO_4 relationship was shown to be a result of the interaction between ocean biogeochemistry and physical circulation, highlighting the importance of AAIW and SAMW.

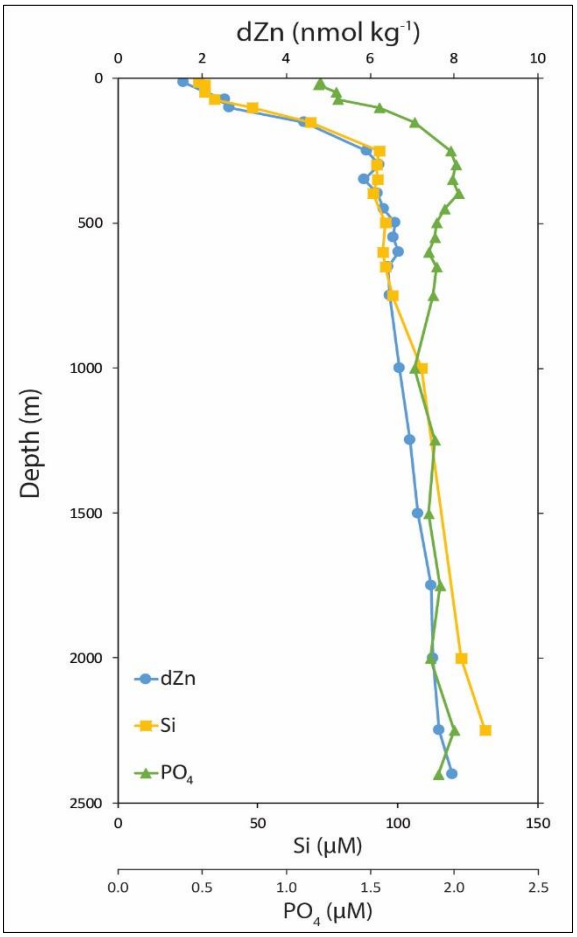

***Figure 10**. Vertical profiles showing the close similarity between the distribution of dissolved zinc (dZn) and silicate (Si). Both increase to deepwater maximums, whereas phosphate (PO_4), shows an intermediate depth maximum.*

5. Conclusion

This study presents the first winter trace metal (Cu, Zn, Ni) data along the GIPY05 transect and contributes a new dataset for Ni. Nutrient like behaviour of each element suggests an active role in biological uptake, albeit comparatively smaller in winter. Differences in trace metal seasonality were most pronounced in the surface mixed layer where winter concentrations were consistently greater as one moves further south. Stations close to SAF; however, showed little change over the two seasons. Chl-*a* data and calculated trace metal removal ratios confirm the sub-optimal growth conditions experienced by phytoplankton during winter. At the APF, biological uptake in summer was likely facilitated by high, photoacclimated phytoplankton biomass in conjunction with low grazing pressure. Low trace metal requirement and augmentation through remineralization in a deep mixed layer characterises the winter reset state. Our results further suggest that deep winter mixing may entrain

significant amounts of Cu, Zn and Ni, as shown previously for Fe (Tagliabue et al., 2014), and constitutes a potentially important micronutrient supply mechanism in the initiation and maintenance of spring/summer phytoplankton production. Strong similarities between metal profiles, particularly Zn, and silica provides evidence for the role of diatoms in controlling their biogeochemical cycling. The control over dissolved Cu:Si and Ni:Si ratios with depth was however imparted predominantly by changes in watermass. Near the surface, Cu/PO_4 and Zn/PO_4 uptake ratios increased southwards, suspected to be the result of iron and iron/light limitation while Ni/PO_4 decreased owing to a weaker surface Ni gradient with respect to PO_4.

6. Acknowledgements

We would like to thank the South African National Antarctic Programme (SANAP) and the captain and crew of the R/V SA Agulhas II for their professionalism and support during the cruises. The “Iron” team is acknowledged for their help in collecting trace-clean samples. The authors would like to thank Rob Middag and Peter Croot for their constructive reviews, the results of which improved this manuscript. Ryan Cloete was supported through NRF Innovation PhD studentship. This research was supported by NRF grants (UID# 93069, 105826 and 110715) to AR. This is TracEx publication #1.

7. References

Alderkamp, A.C., De Baar, H.J.W., Visser, R.J.W., Arrigo, K.R., 2010. Can photoinhibition control phytoplankton abundance in deeply mixed water columns of the Southern Ocean? Limnol. Oceanogr. 55, 1248–1264. https://doi.org/10.4319/lo.2010.55.3.1248

Baars, O., Abouchami, W., Galer, S., Boye, M., Croot, P., 2014. Dissolved cadmium in the Southern Ocean: Distribution, speciation, and relation to phosphate. Limnol. Ocean. 59, 385–399. https://doi.org/10.4319/lo.2014.59.2.0385

Bown, J., Boye, M., Baker, A., Duvieilbourg, E., Lacan, F., Le Moigne, F., Planchon, F., Speich, S., Nelson, D.M., 2011. The biogeochemical cycle of dissolved cobalt in the Atlantic and the Southern Ocean south off the coast of South Africa. Mar. Chem. 126, 193–206. https://doi.org/10.1016/j.marchem.2011.03.008

Boye, M., Wake, B.D., Lopez Garcia, P., Bown, J., Baker, A.R., Achterberg, E.P., 2012. Distributions of dissolved trace metals (Cd, Cu, Mn, Pb, Ag) in the southeastern Atlantic and the Southern Ocean. Biogeosciences 9, 3231–3246. https://doi.org/10.5194/bg-9-3231-2012

Bruland, K.W., 1980. Oceanographic distribution of cadmium, zinc, nickel, and copper in the North Pacific. Earth Planet. Sci. Lett. 47, 176–198. https://doi.org/https://doi.org/10.1016/0012-821X(80)90035-7

Bruland, K.W., Donat, J.R., Hutchins, D.A., 1991. Interactive influences of bioactive trace metals on biological production in oceanic waters. Limnol. Oceanogr. 36, 1555–1577. https://doi.org/10.4319/lo.1991.36.8.1555

Bruland, K.W., Franks, R.P., 1983. Mn, Ni, Cu, Zn and Cd in the Western North Atlantic. Trace Met. Sea Water. NATO Conf. Ser. (IV Mar. Sci. 9, 395–396.

Bruland, K.W., Franks, R.P., 1979. Sampling and analytical methods for the determination of copper,

cadmium, zinc and nickel at the nanogram per litre level in seawater. Anal. Chim. Acta 28, 367–376. https://doi.org/https://doi.org/10.1016/S0003-2670(01)83754-5

Cailliau, C., Claustre, H., Giannino, S., 1997. Chemotaxonomic analysis of phytoplankton distribution in the Indian sector of the Southern Ocean during late Austral summer. Oceanol. Acta 20, 721–732.

Coale, K.H., Michael Gordon, R., Wang, X., 2005. The distribution and behavior of dissolved and particulate iron and zinc in the Ross Sea and Antarctic circumpolar current along 170°W. Deep Sea Res. Part I Oceanogr. Res. Pap. 52, 295–318. https://doi.org/10.1016/j.dsr.2004.09.008

Croot, P.L., Andersson, K., Öztürk, M., Turner, D.R., 2004. The distribution and speciation of iron along 6°E in the Southern Ocean. Deep. Res. Part II Top. Stud. Oceanogr. 51, 2857–2879. https://doi.org/10.1016/j.dsr2.2003.10.012

Croot, P.L., Baars, O., Streu, P., 2011. The distribution of dissolved zinc in the Atlantic sector of the Southern Ocean. Deep Sea Res. Part II Top. Stud. Oceanogr. 58, 2707–2719. https://doi.org/10.1016/j.dsr2.2010.10.041

Croot, P.L., Frew, R.D., Sander, S., Hunter, K.A., Ellwood, M.J., Pickmere, S.E., Abraham, E.R., Law, C.S., Smith, M.J., Boyd, P.W., 2007. Physical mixing effects on iron biogeochemical cycling: FeCycle experiment. J. Geophys. Res. Ocean. 112, 1–18. https://doi.org/10.1029/2006JC003748

Cutter, G.A., Bruland, K.W., 2012. Rapid and noncontaminating sampling system for trace elements in global ocean surveys. Limnol. Oceanogr. Methods 10, 425–436. https://doi.org/10.4319/lom.2012.10.425

de Boyer Montégut, C., Madec, G., Fischer, A.S., Lazar, A., Iudicone, D., 2004. Mixed layer depth over the global ocean: An examination of profile data and a profile-based climatology. J. Geophys. Res. C Ocean. 109, 1–20. https://doi.org/10.1029/2004JC002378

de Souza, G.F., Khatiwala, S.P., Hain, M.P., Little, S.H., Vance, D., 2018. On the origin of the marine zinc–silicon correlation. Earth Planet. Sci. Lett. 492, 22–34. https://doi.org/10.1016/j.epsl.2018.03.050

Doolittle, D.F., Li, W.K.W., Wood, A.M., 2008. Wintertime abundance of picoplankton in the Atlantic sector of the Southern Ocean by 147–160.

Dubischar, C.D., Bathmann, U. V, 1997. Grazing impact of copepods and salps on phytoplankton in the Atlantic sector of the Southern OCean. Deep. Res. Part II.

Ellwood, M.J., 2008. Wintertime trace metal (Zn, Cu, Ni, Cd, Pb and Co) and nutrient distributions in the Subantarctic Zone between 40-52??S; 155-160??E. Mar. Chem. 112, 107–117. https://doi.org/10.1016/j.marchem.2008.07.008

Ellwood, M.J., Hunter, K.A., 2000. The incorporation of zinc and iron into the frustule of the marine diatom Thalassiosira pseudonana. Limnol. Oceanogr. 45, 1517–1524. https://doi.org/10.4319/lo.2000.45.7.1517

Ellwood, M.J., Hunter, K.A., Si, Z., 2000. Variations in the Zn / Si record over the last interglacial glacial transition. Paleoceanography 15, 506–514.

Evans, C., Brussaard, C.P.D., 2012. Viral lysis and microzooplankton grazing of phytoplankton throughout the Southern Ocean. Limnol. Oceanogr. 57, 1826–1837. https://doi.org/10.4319/lo.2012.57.6.1826

Fauchereau, N., Tagliabue, A., Bopp, L., Monteiro, P.M.S., 2011. The response of phytoplankton biomass to transient mixing events in the Southern Ocean. Geophys. Res. Lett. 38, 1–6. https://doi.org/10.1029/2011GL048498

Frew, R., Bowie, A., Croot, P., Pickmere, S., 2001. Macronutrient and trace-metal geochemistry of an in situ iron-induced Southern Ocean bloom. Deep. Res. Part II Top. Stud. Oceanogr. 48, 2467–2481. https://doi.org/10.1016/S0967-0645(01)00004-2

Frew, R.D., Hutchins, D.A., Nodder, S., Sanudo-Wilhelmy, S., Tovar-Sanchez, A., Leblanc, K., Hare, C.E., Boyd, P.W., 2006. Particulate iron dynamics during FeCycle in subantarctic waters southeast of New Zealand. Global Biogeochem. Cycles 20, 1–15. https://doi.org/10.1029/2005GB002558

Garabato, a, Ferrari, R., Polzin, K., 2010. Eddy-induced mixing in the Southern Ocean. J. Phys. Oceanogr. 303, 210–214.

Grasshoff, K., 1983. Automated chemical analysis, in: Grasshoff, K., Ernhardt, M., Kremling, K. (Eds.), Methods of Seawater Analysis. Verlag Chemie Weinhein, New York, pp. 263–289.

Heller, M.I., Croot, P.L., 2015. Copper speciation and distribution in the Atlantic sector of the Southern Ocean. Mar. Chem. 173, 253–268. https://doi.org/10.1016/j.marchem.2014.09.017

Heywood, K.J., Naveira Garabato, A.C., Stevens, D.P., 2002. High mixing rates in the abyssal Southern Ocean. Nature 415, 1011–1014. https://doi.org/10.1038/4151011a

Hoppema, M., Dehairs, F., Navez, J., Monnin, C., Jeandel, C., Fahrbach, E., Baar, H.J.W. De, 2010a. Distribution of barium in the Weddell Gyre : Impact of circulation and biogeochemical processes. Mar. Chem. 122, 118–129. https://doi.org/10.1016/j.marchem.2010.07.005

Hoppema, M., Dehairs, F., Navez, J., Monnin, C., Jeandel, C., Fahrbach, E., Baar, H.J.W. De, 2010b. Distribution of barium in the Weddell Gyre : Impact of circulation and biogeochemical processes. Mar. Chem. 122, 118–129. https://doi.org/10.1016/j.marchem.2010.07.005

John, S.G., Conway, T.M., 2014. A role for scavenging in the marine biogeochemical cycling of zinc and zinc isotopes. Earth Planet. Sci. Lett. 394, 159–167. https://doi.org/10.1016/j.epsl.2014.02.053

Klunder, M.B., Laan, P., De Baar, H.J.W., Middag, R., Neven, I., Van Ooijen, J., 2014. Dissolved Fe across the Weddell Sea and Drake Passage: Impact of DFe on nutrient uptake. Biogeosciences 11, 651–669. https://doi.org/10.5194/bg-11-651-2014

Klunder, M.B., Laan, P., Middag, R., Baar, H.J.W. De, Ooijen, J.C. Van, 2011. Dissolved iron in the Southern Ocean (Atlantic sector). Deep. Res. Part II 58, 2678–2694. https://doi.org/10.1016/j.dsr2.2010.10.042

Law, C.S., 2003. Vertical eddy diffusion and nutrient supply to the surface mixed layer of the Antarctic Circumpolar Current. J. Geophys. Res. 108, 1–14. https://doi.org/10.1029/2002JC001604

Le Moigne, F.A.C., Boye, M., Masson, A., Corvaisier, R., Grossteffan, E., Gueneugues, A., Pondaven, P., 2013. Description of the biogeochemical features of the subtropical southeastern Atlantic and the Southern Ocean south of South Africa during the austral summer of the International Polar Year. Biogeosciences 10, 281–295. https://doi.org/10.5194/bg-10-281-2013

Löscher, B.M., 1999. Relationship among Ni, Cu, Zn, and major nutrients in the Southern Ocean. Mar. Chem. 67, 67–102.

Lutjeharms, J.R.E., 1985. Location of frontal systems between Africa and Antarctica: some preliminary results. Deep Sea Res. Part A, Oceanogr. Res. Pap. 32, 1499–1509. https://doi.org/10.1016/0198-0149(85)90100-1

Middag, R., De Baar, H.J.W., Laan, P., Cai, P.H., Van Ooijen, J.C., 2011. Dissolved manganese in the Atlantic sector of the Southern Ocean. Deep Sea Res. Part II Top. Stud. Oceanogr. 58, 2661–2677. https://doi.org/10.1016/S0967-0645(96)00064-1

Milne, A., Landing, W., Bizimis, M., Morton, P., 2010. Determination of Mn, Fe, Co, Ni, Cu, Zn, Cd and Pb in seawater using high resolution magnetic sector inductively coupled mass spectrometry (HR-ICP-MS). Anal. Chim. Acta 665, 200–207. https://doi.org/10.1016/j.aca.2010.03.027

Minami, T., Konagaya, W., Zheng, L., Takano, S., Sasaki, M., Murata, R., Nakaguchi, Y., Sohrin, Y., 2015. An off-line automated preconcentration system with ethylenediaminetriacetate chelating resin for the determination of trace metals in seawater by high-resolution inductively coupled plasma mass

spectrometry. Anal. Chim. Acta 854, 183–190. https://doi.org/10.1016/j.aca.2014.11.016

Moore, J.K., Doney, S.C., Glover, D.M., Fung, I.Y., 2002. Iron cycling and nutrient-limitation patterns in surface waters of the world ocean. Deep. Res. Part II Top. Stud. Oceanogr. 49, 463–507. https://doi.org/10.1016/S0967-0645(01)00109-6

Nolting, R.F., de Baar, H.J.W., 1994. Behaviour of nickel, copper, zinc and cadmium in the upper 300m of a transect in the Southern Ocean (57°-62°S, 49°W). Mar. Chem. 45, 225–242.

Orsi, A.H., Whitworth, T., Nowlin, W.D., 1995. On the meridional extent and fronts of the Antarctic Circumpolar Current. Deep. Res. Part I 42, 641–673. https://doi.org/10.1016/0967-0637(95)00021-W

Quéroué, F., Townsend, A., van der Merwe, P., Lannuzel, D., Sarthou, G., Bucciarelli, E., Bowie, A., 2014. Advances in the offline trace metal extraction of Mn, Co, Ni, Cu, Cd, and Pb from open ocean seawater samples with determination by sector field ICP-MS analysis. Anal. Methods 6, 2837–2847. https://doi.org/10.1039/c3ay41312h

Sarmiento, J.L., Gruber, N., Brzezinski, M.A., Dunne, J.P., 2004. High-latitude controls of thermocline nutrients and low latitude biological productivity. Nature 427, 56–60. https://doi.org/10.1038/nature10605

Schlitzer, R., 2017. Ocean Data View. https://doi.org/10.1017/CBO9781107415324.004

Sclater, F.R., Boyle, E., Edmond, J.M., 1976. On the marine geochemistry of nickel. Earth Planet. Sci. Lett. 31, 119–128. https://doi.org/10.1016/0012-821X(76)90103-5

Sohrin, Y., Urushihara, S., Nakatsuka, S., Kono, T., Higo, E., Minami, T., Norisuye, K., Umetani, S., 2008. Multielemental determination of GEOTRACES key trace metals in seawater by ICPMS after preconcentration using an ethylenediaminetriacetic acid chelating resin. Anal. Chem. 80, 6267–6273. https://doi.org/10.1021/ac800500f

Sokolov, S., Rintoul, S.R., 2007. On the relationship between fronts of the Antarctic Circumpolar Current and surface chlorophyll concentrations in the Southern Ocean. J. Geophys. Res. Ocean. 112, 1–17. https://doi.org/10.1029/2006JC004072

Sunda, W., 1989. Trace metal interactions with marine phytoplankton. Biol. Oceanogr. 6, 411–442. https://doi.org/10.1080/01965581.1988.10749543

Sunda, W.G., 2012. Feedback interactions between trace metal nutrients and phytoplankton in the ocean. Front. Microbiol. 3, 1–22. https://doi.org/10.3389/fmicb.2012.00204

Swart, S., Speich, S., Ansorge, I.J., Goni, G.J., Gladyshev, S., Lutjeharms, J.R.E., 2008. Transport and variability of the Antarctic circumpolar current south of Africa. J. Geophys. Res. Ocean. 113, 1–24. https://doi.org/10.1029/2007JC004223

Swart, S., Thomalla, S.J., Monteiro, P.M.S., 2015. The seasonal cycle of mixed layer dynamics and phytoplankton biomass in the Sub-Antarctic Zone: A high-resolution glider experiment. J. Mar. Syst. 147, 103–115. https://doi.org/10.1016/j.jmarsys.2014.06.002

Tagliabue, A., Sallée, J.B., Bowie, A.R., Lévy, M., Swart, S., Boyd, P.W., 2014. Surface-water iron supplies in the Southern Ocean sustained by deep winter mixing. Nat. Geosci. 7, 314–320. https://doi.org/10.1038/ngeo2101

Twining, B.S., Baines, S.B., 2013. The trace metal composition of marine phytoplankton. Ann. Rev. Mar. Sci. 5, 191–215. https://doi.org/10.1146/annurev-marine-121211-172322

Twining, B.S., Baines, S.B., Fisher, N.S., 2004. Element stoichiometries of individual plankton cells collected during the Southern Ocean Iron Experiment (SOFeX). Limnol. Oceanogr. 49, 2115–2128. https://doi.org/10.4319/lo.2004.49.6.2115

Twining, B.S., Baines, S.B., Fisher, N.S., Maser, J., Vogt, S., Jacobsen, C., Tovar-Sanchez, A., Sañudo-

Wilhelmy, S.A., 2003. Quantifying trace elements in individual aquatic protist cells with a synchrotron X-ray fluorescence microprobe. Anal. Chem. 75, 3806–3816. https://doi.org/10.1021/ac034227z

Twining, B.S., Baines, S.B., Vogt, S., Nelson, D.M., 2012. Role of diatoms in nickel biogeochemistry in the ocean. Global Biogeochem. Cycles 26, 1–9. https://doi.org/10.1029/2011GB004233

Twining, B.S., Nodder, S.D., King, A.L., Hutchins, D.A., Lecleir, G.R., Debruyn, J.M., Maas, E.W., Vogt, S., Wilhelm, S.W., Boyd, P.W., 2014. Differential remineralization of major and trace elements in sinking diatoms. Limnol. Oceanogr. 59, 689–704. https://doi.org/10.4319/lo.2014.59.3.0689

Usbeck, R., Loeff, M.R. van der L., Hoppema, M., Schltzer, R., 2002. Shallow remineralization in the Weddell Gyre. Geochemistry Geophys. Geosystems 3.

Van De Poll, W.H., Van Leeuwe, M.A., Roggeveld, J., Buma, A.G.J., 2005. Nutrient limitation and high irradiance acclimation reduce par and UV-induced viability loss in the antarctic diatom Chaetoceros brevis (Bacillariophyceae). J. Phycol. 41, 840–850. https://doi.org/10.1111/j.1529-8817.2005.00105.x

Van Leeuwe, M.A., Stefels, J., 2007. Photosynthetic responses in *Phaeocystis antarctica* towards varying light and iron conditions. Biogeochemistry 83, 61–70. https://doi.org/10.1007/978-1-4020-6214-8_6

Van Leeuwe, M.A., Van Sikkelerus, B., Gieskes, W.W.C., Stefels, J., 2005. Taxon-specific differences in photoacclimation to fluctuating irradiance in an Antarctic diatom and a green flagellate. Mar. Ecol. Prog. Ser. 288, 9–19. https://doi.org/10.3354/meps288009

Vance, D., Little, S.H., De Souza, G.F., Khatiwala, S., Lohan, M.C., Middag, R., 2017. Silicon and zinc biogeochemical cycles coupled through the Southern Ocean. Nat. Geosci. 10, 202–206. https://doi.org/10.1038/ngeo2890

Wang, B.-S., Lee, C.-P., Ho, T.-Y., 2014. Trace metal determination in natural waters by automated solid phase extraction system and ICP-MS: the influence of low level Mg and Ca. Talanta 128, 337–44. https://doi.org/10.1016/j.talanta.2014.04.077

Wyatt, N.J., Milne, A., Woodward, E.M.S., Rees, A.P., Browning, T.J., Bouman, H.A., Worsfold, P.J., Lohan, M.C., 2014. Biogeochemical cycling of dissolved zinc along the GEOTRACES South Atlantic transect GA10 at 40°S. Global Biogeochem. Cycles 28, 44–56. https://doi.org/10.1002/2013GB004637

Chapter 3

Winter dissolved and particulate cadmium in the Indian sector of the Southern Ocean (GEOTRACES GIpr07 transect)

A presentation of the prepared research paper

This research manuscript has been prepared for submission to Frontiers in Marine Science: Marine Biogeochemistry. I am the lead author of the manuscript. J.C. Loock, N.R. van Horsten, S. Fietz, T.N. Mtshali, H. Planquette and A.N. Roychoudhury are co-authors.

This manuscript contributes the first winter measurements of dissolved cadmium (dCd) and particulate cadmium (pCd) along the 30°E longitude in the Indian sector of the Southern Ocean. This dataset, in combination with major nutrient phosphate (PO_4) and phosphorous (P) data, is used to investigate Cd biogeochemical cycling during a period generally thought to be biologically dormant. In so doing, we aim to gain a better understanding of processes governing Cd over seasonal cycles.

I was responsible for the collection and analysis of seawater samples for dCd, data processing and writing of the manuscript.

Winter dissolved and particulate cadmium in the Indian sector of the Southern Ocean (GEOTRACES GIpr07 transect)

R.Cloete[a], J.C. Loock[a], N.R. van Horsten[a,b,c], S. Fietz[a], T.N. Mtshali[a,b], H. Planquette[c], A.N. Roychoudhury[a, *]

[a]Centre for Trace Metal and Experimental Biogeochemistry (TracEx), Department of Earth Sciences, Stellenbosch University, Stellenbosch 7600, South Africa.

[b]Southern Ocean Carbon and Climate Observatory, Smart Places, CSIR, Stellenbosch, 7600, South Africa.

[c]Univ Brest, CNRS, IRD, Ifremer, LEMAR, F-29280 Plouzane, France

Abstract

Winter distributions of dissolved cadmium (dCd) and particulate cadmium (pCd) were measured for the first time in the Indian sector of the Southern Ocean thereby contributing a unique spatial and seasonal dataset. Seven depth profiles, between 41°S and 58°S, were collected along the 30°E longitude during the 2017 austral winter to investigate the biogeochemical cycling of Cd and to characterise the Southern Ocean winter reset state. Our results support an important role for biological uptake during winter months albeit weaker compared to summer. In the remineralisation zone (between 1500 m and 250 m), dCd was closely correlated with the major nutrient phosphate (PO_4) where dCd (pmol kg^{-1}) = 426 ± 44 PO_4 (µmol kg^{-1}) – 195 (r^2 = 0.91 n = 89) while the distribution of pCd closely matched that of phosphorous (P) where pCd (pmol kg^{-1}) = 1.08 ± 0.11 P (nmol kg^{-1}) - 0.29 (r^2 = 0.92; n = 80). In the surface mixed layer (SML), dCd was between 10 – 100 pmol kg^{-1} higher compared to summer measurements reflecting a combination of weaker biological uptake and increased recharge through deep winter mixing. There were distinct, biologically driven changes in Cd cycling across the transect. For example, uptake ratios of dCd/PO_4 (calculated from the slope of correlation between dCd and PO_4 in the SML) increased from between 434 - 513 pmol µmol^{-1} in the Sub Tropical Zone (STZ) and Sub Antarctic Zone (SAZ) to between 886 - 1058 pmol µmol^{-1} in the Polar Frontal Zone (PFZ) and Antarctic Zone (AAZ). A similar southward increase was observed for pCd/P remineralisation ratios (calculated from the slope of correlation between pCd and P between the SML and remineralisation depth), where slope values were between 0.25 – 0.67 pmol nmol^{-1} in the STZ and SAZ and 1.48 – 1.76 pmol nmol^{-1} in the PFZ and AAZ. Changes in uptake and remineralisation rates were consistent with the observed shift in phytoplankton community structure. In the PFZ and AAZ, elevated Cd requirements by diatoms may be linked to Fe-limitation. The strong southward increase in surface dCd, from approximately 20 to 700 pmol kg^{-1}, reflected the combination of preferential uptake and regeneration of diatoms with high Cd content and the upwelling of Cd enriched watermasses in the AAZ. Furthermore, there were distinct water mass dependent correlations between plots of dCd versus PO_4 in intermediate and deep waters suggesting that dCd distributions at depth are largely the result of

physical water mass mixing. Lastly, the formation and export of SAMW with low depleted dCd* and pCd* signatures has potential implications for low latitude Cd cycling and productivity.

1. Introduction

It is well established that numerous trace metals are required nutrients for phytoplankton and that trace metal availability in the world's oceans can influence phytoplankton growth and community structure (Twining and Baines, 2013) with potential consequences for the global carbon cycle. Data pertaining to the trace metal cadmium (Cd) is scarce, particularly in the Southern Ocean (Schlitzer et al., 2018), however it has allowed for a basic model of Cd cycling to be developed. The dominant external sources of Cd to the surface ocean are riverine discharge (Lambelet et al., 2013), natural and anthropogenic derived atmospheric deposition (Duce et al., 1991) as well as seasonal ice melt in the polar oceans (Hölemann et al., 1999). The internal cycling of Cd in the Southern Ocean is further controlled by complexation with natural organic ligands in surface waters (Ellwood, 2004), year-round mixing between water masses with different preformed Cd concentrations and upwelling at higher latitudes(Abouchami et al., 2014; Sieber et al., 2019). Additionally, deep winter mixing (or entrainment) is a seasonally constrained physical supply mechanism whereby deeper mixing in winter compared to summer allows access to nutrient rich sub-surface water masses found below the summer stratified layer (Ellwood, 2008; Tagliabue et al., 2014).

This model can be extended to differentiate between various size fractions of trace metals. The dissolved fraction (<0.2µm pore size filtered seawater), denoted as "d", e.g. dCd hereafter, is often recognised as the nutrient reservoir available for phytoplankton uptake. The particulate fraction (>0.45µm pore size filter), denoted as "p", e.g. pCd hereafter, is not considered bioavailable to phytoplankton yet contributes significantly to the total Cd inventory in the ocean (Turekian, 1977). A host of biophysicochemical processes control the cycling and exchange between dissolved and particulate cadmium in the ocean**.** In the surface ocean, uptake of dCd by phytoplankton is the primary process which facilitates the exchange between inorganic dCd and organic pCd. Subsequent processes, such as zooplankton grazing, result in the formation of larger particles which either sink and contribute to the vertical export of pCd, or disaggregate via remineralisation, desorption and dissolution, resulting in a source of dCd to the surface ocean (Lam and Marchal, 2015). Scavenging (or adsorption) of dCd onto organic or hydrothermally sourced particles may enhance export of Cd through formation of more rapidly sinking particulate phases (Conway and John, 2015). Similarly, precipitation of solid Cd sulphides in low oxygen environments increases pCd export in localised regions (Janssen et al., 2014). As a result of the interplay of all these processes, an increase in water column dCd typically leads to a decrease in pCd and vice versa. However, dissolved and particulate phases are not exact mirror images of each other considering that water column processes lead to differences in their respective oceanic residence times, e.g. years to thousands of years for dissolved phases and days to months for particulate phases (Lam and Marchal, 2015).

The first reliable open ocean dCd measurements (Boyle et al., 1976; Bruland et al., 1978) were well correlated with the major nutrient phosphate (PO_4) and showed a surface depletion (<2 pmol kg^{-1}) relative to the deeper waters (>1000 pmol kg^{-1}), as is typical of nutrient-type behaviour. Indeed, a diatom specific carbonic anhydrase (CA) enzyme containing Cd (CDCA) has been identified, supporting the role of Cd as a micronutrient (Lane et al., 2005; Lane and Morel, 2000). Furthermore, Cd may stimulate the growth of zinc (Zn) limited diatoms through a substitutive mechanism (Price and Morel, 1990). The substitution of Cd for Zn under low Zn conditions has also been observed in other phytoplankton groups which do not contain the CDCA enzyme, notably coccolithophores and chlorophytes (Lee and Morel, 1995; Xu et al., 2007). These findings provide a potential mechanism responsible for the observed coupling of Cd and PO_4. However, there are divergences in the global oceanic Cd-PO_4 relationship, with a pronounced break ('kink') in the slope at PO_4 ~1.3 µmol kg^{-1}, indicating a net preferential removal of Cd from surface waters (Elderfield and Rickaby, 2000). Many studies have investigated the assimilation of PO_4 and Cd in phytoplankton and revealed different factors influencing the uptake of Cd relative to PO_4. For example, a diatom dominated phytoplankton assemblage showed decreases in cellular Cd in response to the addition of the key micronutrient iron (Fe) suggesting Cd uptake is directly linked to Fe availability (Cullen et al., 2003). Subsequent experiments have shown that increased cellular Cd in response to low Fe availability appears related to reduced growth rates (Cullen, 2006) or increased dCd uptake through non-specific Fe(II) transporters (Lane et al., 2009, 2008). Increased cellular Cd is also inversely related to the availability of other essential micronutrients such as Zn and manganese (Mn; Cullen and Sherrell, 2005; Sunda and Huntsman, 2000). In sum, the role of Cd as a micronutrient is dependent on the availability of other bio-essential trace metals concentrations, notably Fe, Zn and Mn.

Understanding the biogeochemical cycling of Cd in the Southern Ocean is particularly important given that water masses formed in this region are the primary communication channels to the low latitude oceans (Broecker, 1991). The far reaching influence of the Southern Ocean has been shown in terms of macronutrients distributions (Sarmiento et al., 2004) as well as for Cd (Middag et al., 2018; Xie et al., 2015) highlighting the combination of biological uptake in the surface Southern Ocean, lateral transport and mixing between water masses with different preformed nutrient signatures. While significant strides have been made in identifying and understanding processes controlling oceanic Cd distributions, spatial and seasonal gaps in the global database still exist. For example, the Indian sector of the Southern Ocean is particularly data scarce (Janssen et al., 2020). Additionally, most observations to date represent spring/summer seasons with few winter Cd measurements available (Ellwood, 2008). We therefore have little understanding of Cd cycling over seasonal cycles and of the conditions that characterise the Southern Ocean winter reset state, a period which may be critical in supplying Cd and other nutrients (e.g. Fe) to sustain phytoplankton growth over the subsequent spring and summer seasons (Tagliabue et al., 2014). Under the GEOTRACES framework, this study aims to improve our understanding of Cd

biogeochemical cycling in the ocean by contributing first winter dissolved and particulate measurements of Cd from the western Indian sector (WOCE meridional section IO6S; GEOTRACES section GIpr07) of the Southern Ocean.

2. Methodology

2.1. Sample collection

Seawater samples were collected on-board the SA Agulhas II polar research vessel during the 2017 Winter Cruise (WC-17; 28/06/2017 – 13/07/2017). The cruise transect followed the World Ocean Circulation Experiment (WOCE) I06 transect along the 30°E meridian in the Indian sector of the Southern Ocean (Figure 1). Seven stations, consisting of four deep and three shallow, were sampled between 41°00'S and 58°30'S allowing observations to be investigated over important frontal systems and in different water masses. "Deep" stations were sampled from near the surface (25 m) to near sea-floor (< 4500 m) while "shallow" stations were sampled between near surface and 1500 m depth.

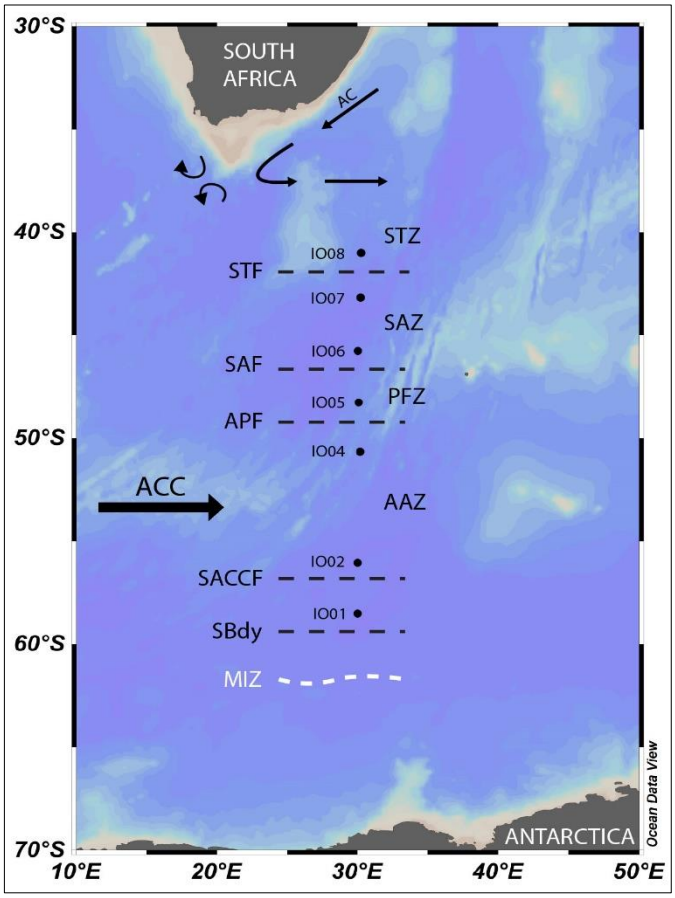

Figure 1. *Sample station locations during the 2017 Winter Cruise along the GEOTRACES GIpr07 transect (30°E Longitude). Positions of the frontal systems intersected, and corresponding oceanic zones, are shown as well as the main surface currents. Acronyms in alphabetical order are as follows; AAZ: Antarctic Zone; AC: Agulhas Current; ACC: Antarctic Circumpolar Current; APF: Antarctic Polar Front; MIZ: Marginal Ice Zone; PFZ: Polar Frontal Zone; SACCF: Southern Antarctic Circumpolar Current Front; SAZ: Sub-Antarctic Zone; SAF: Sub-Antarctic Front; SBdy: Southern Boundary; STF: Sub-Tropical Front; STZ: Sub-Tropical Zone. Figure constructed using Ocean Data View (ODV; Schlitzer, 2017).*

Seawater samples were collected following a strict 'trace metal clean' GEOTRACES protocol (Cutter and Bruland, 2012). A vertical profile sampling method was employed, using 24 trace clean, internally Teflon-coated polyvinyl chloride (PVC) 12 l GO-FLO sampling bottles attached on an epoxy coated aluminium frame CTD rosette. A Kevlar hydrowire with internal signal cables allowed for the transfer of data between the CTD and the on-board control room. The GO-FLO bottles were triggered at predetermined depths during the up cast. Directly upon recovery of the rosette, the GO-FLO bottles were covered in a PVC plastic wrap in addition to their ends being covered in plastic (PVC) shower caps, and were transported into a class 100 clean container lab for sub-sampling. Samples for dissolved trace metal determination were collected into 125 ml acid-cleaned low density polyethylene (LDPE) bottles after online filtration through 0.2 µm pore size capsule filters (Sartobran) and under slight N_2 gas (99.9999% N_2, BIP technology) overpressure. Samples were acidified (pH ~ 1.7) under laminar flow using hydrochloric acid (30% Ultrapur HCL, Merck) and stored at room temperature for later analysis. Thereafter, previously cleaned filters (25mm diameter, Supor, 0.45 µm pore size) were mounted on acid-washed swinnex (Millipore) filter holders which were then attached to the GO-FLO spigots and used for filtration (5 - 10 L) of samples for particulate trace metal determination (Planquette and Sherrell, 2012). After filtration, filter holders were removed and disassembled before the sampled filter was transferred to an acid-washed polystyrene Petri-dish using clean plastic forceps. Sampled filters were subsequently frozen at -20°C for transport back to land. All handling of filters, filter holders and samples was done under a laminar flow hood.

2.2. Dissolved Cd determination

2.2.1. sea*FAST* and ICP-MS

Samples were analysed by Inductively Coupled Plasma Mass Spectrometry (ICP-MS, Agilent 7900), after offline preconcentration by Solid Phase Extraction (SPE) on a sea*FAST* SC-4 DX module (Cloete et al., 2019). Briefly, 10 ml of seawater was taken up by the sea*FAST* (ESI) module, buffered with an ammonium acetate buffer to a pH of 6.0 ± 0.2, and loaded onto a high affinity metal chelating resin column (Nobias PA1). Here the metal ions including Cd were bound to the resin and separated from the seawater matrix elements e.g. Na, Mg and Cl which passed through the column. The metal ions were subsequently eluted from the resin column in low volumes (250 µl) resulting in a preconcentration factor of 40. On the ICP-MS, samples were introduced using a low self-aspirating perfluoroalkoxy (PFA) nebulizer with a flow rate of 0.2 µl min^{-1}. Isotopes of ^{111}Cd were measured using the instruments Octopole Reaction System (ORS) in helium (He) collision mode to eliminate plasma and matrix based interferences although the latter was extensively reduced by the sea*FAST* matrix removal system. Online internal standard addition for drift correction was not possible using the self-aspirating nebulizer. Instead, instrument drift was monitored by running a multi-element standard (MES; verified by Inorganic Ventures) calibration standard every 6 samples. Where drift exceeded 5% relative to the starting concentration of the MES for a specific element, a drift correction was applied using the

formula: $2*Conc_{MES\_start}/ (Conc_{MES\_a} + Conc_{MES\_b})*Conc_{Sample}$, where *a* and *b* are the MES before and after each set of 6 samples.

2.2.2. Accuracy and precision

The accuracy of the method was verified by the analysis of numerous community reference seawater samples for dCd (Table 1). For the GEOTRACES SAFe D2, GSC and GSP reference seawater (https://www.geotraces.org/standards-and-reference-materials/), our dCd concentrations were within analytical uncertainty estimates of consensus values confirming the methods accuracy over a wide concentration range. Our mean dCd value from the analysis of the NASS-7 certified reference material (CRM) was within analytical uncertainty of the certified dCd value. To monitor ICP-MS precision, the Winter Indian Southern Ocean Seawater (WISOS) internal control seawater was placed in the analysis sequence and results compared against each other and the calibrated mean (Table 1). The WISOS internal control was collected in bulk (20 L) from surface water at 55°S; 28°E during the 2017 Winter Cruise after filtration through a 0.2 µm filter into an acid cleaned LDPE container. Sub-samples (1 L) of the bulk seawater were then acidified (pH = 1.7) using hydrochloric acid (30% HCl, ultrapure, Merck). The calibrated dCd mean (888 ± 21 pmol kg^{-1}) concentration was established by replicate analysis (n = 10) of the WISOS internal control seawater in conjunction with the SAFe and NASS-7 reference materials. Results from the analysis of the in-run WISOS control sample were 899 ± 27 pmol kg^{-1} (n > 30) confirming the methods precision over multiple analyses.

2.2.3. Blanks and Limits of Detection

The instrument (ICP-MS) blank was quantified by introducing a solution of un-preconcentrated 2% HNO_3, identical to the seaFAST eluent, in ultrapure deionized water. Instrument blanks were below detection limits. To determine the blank contribution from the method, a solution of HNO_3 (ultrapur, Merck) diluted to 2% with ultra-pure deionized water, the same composition as the eluent used in sample pre-concentration, was analysed. The blank was subjected to the same pre-concentration procedure as the seawater samples. The mean method blank was 1.22 ± 0.30 pmol kg^{-1} (n = 5). The limit of detection (LOD) of the instrument, calculated as 3 times the standard deviation of the preconcentrated blanks, was 0.89 pmol kg^{-1} (n = 5).

2.2.4. Data processing

Samples for dCd were analysed in duplicate. The final values represent the mean of duplicate measurements. In the two cases where the percentage relative standard deviation (%RSD) between the duplicate measurements was > 10%, one of the values was deemed a suspected outlier and not used further. This was determined by curve fitting the data points based on the values above (shallower depth) and below (deeper depth) the suspect value as well as by comparison with other parameters (salinity, temperature, and nutrients) measured from the same GO-FLO bottle.

Table 1. *Results for dCd from the ICP-MS analysis of GEOTRACES SAFE D2, GSC and GSP seawater reference materials (https://www.geotraces.org/standards-and-reference-materials/), NASS-7 certified seawater reference material and our own WISOS internal reference seawater are compared with respective consensus values. Consensus values for SAFe D2 as of 2013 and GSC and GSP as of 2019. Calibrated mean values for WISOS calculated by repeat analysis (n > 10) of a large volume surface seawater sample collected from 55°S; 28°E. Instrument and method blanks as well as ICP-MS limit of detection are also shown.*

	dCd
	pmol/kg
SAFe D2	
Consensus	986 ± 23
TracEx (n = 4)	982 ± 10
TracEx %RSD	6.28
GSC	
consensus	355 ± 21
TracEx (n = 5)	345 ± 21
TracEx %RSD	6.09
GSP	
Consensus	2.00 ± 2.00
TracEx (n = 5)	4.07 ± 0.48
TracEx %RSD	11.70
NASS-7	
Certified	141.50 ± 14.40
TracEx (n = 5)	132.69 ± 3.08
TracEx %RSD	2.32
WISOS reference seawater	
TracEx Calibration (n = 10)	888.02 ± 21.22
TracEx (n > 30)	899.41 ± 27.55
TracEx %RSD	3.06
Blanks	
Instrument (n = 5)	< LOD
Method (n = 5)	1.22 ± 0.30
Limit of Detection (n = 5)	0.89

2.3. Phosphate and silicic acid determination

Seawater samples for macronutrient analysis were collected from GO-FLO bottles, filtered immediately after collection using a 0.2 µm pore size syringe filter (Anatop) into 50 mL Falcon® tubes and frozen at -20°C. Post cruise, the major nutrient phosphate (PO_4) was determined manually by colorimetric method (Grasshoff, 1983) at the Marine Biogeochemistry Laboratory at the University of Cape Town (MBL-UCT; Weir et al. in revision). The analytical error of the PO_4 measurements was ± 0.06 µmol kg^{-1} (Weir et al., in revision).

2.4. Particulate Cd and P determination

Samples for particulate trace metals were analysed at the Université de Bretagne Occidentale (UBO) according to the previously described (Planquette and Sherrell, 2012). Briefly, collected filters were digested by total acid reflux digestion in an equal part mixture of 8.0 M HNO_3 and 2.9 M HF (both Fisher Optima grade), in 15 ml trace-metal clean Teflon PFA vials (Savillex®), on a hot plate at ~110°C for 4 hours, under a fume hood. To eliminate fluorides, 100 µl of concentrated ultra-pure HNO_3 was added to the vials and evaporated to near dryness. Samples were then taken up in a 3.0 mL solution of 0.08 M HNO_3, spiked with 1 µg L^{-1} indium (In) to monitor instrumental drift, heated at 60°C for 1 hour to ensure complete redissolution of any dried residue and then transferred into acid-cleaned 15 ml PP tubes (Corning®) before analysis. Trace element analysis was performed using a Sector Field Inductively coupled Plasma Mass Spectrometer (SF-ICP-MS; Element XR™ ThermoFisher Scientific) at the Pole Spectrométrie Océans. Three certified reference materials (PACS 3, MESS 4 and BCR 414) were processed as samples and analysed for pCd and P to assess the accuracy of the methodology (Table 2). The certified reference materials yielded mean percentage recoveries of 108 %, 188% and 115% for pCd and 100%, 106% and 95% for P (PACS 3, MESS 4 and BCR 414, respectively). Filter blanks were determined by digesting and analysing an acid washed filter. The detection limits, defined as three times the standard deviation of the blanks, for pCd and P were 0.07 pmol kg^{-1} and 0.03 nmol kg^{-1}, respectively (n = 5).

Table 2. *Results for pCd and P from the ICP-MS analysis of PACS 3, MESS 4 and BCR 414 certified references materials. Filter blanks as well as ICP-MS limit of detection are also shown.*

	pCd *µmol kg^{-1}*	**P** *mmol kg^{-1}*
PACS 3		
Certified	19.84 ± 1.16	29.38 ± 2.91
Measured	21.32 ± 0.44	29.41 ± 0.31
% recovery	108	100
MESS 4		
Certified	2.49 ± 0.36	33.58 ± 5.17
Measured	4.69 ± 1.21	35.58 ± 0.51
% recovery	188	106
BCR 414		
Certified	3.41 ± 0.12	428.84 ± 51.20
Measured	3.93 ± 0.60	409.34 ± 52.14
% recovery	115	95
Filter Blank *(n = 5)*	0.09 *pmol kg^{-1}*	0.08 *nmol kg^{-1}*
Limit of Detection	0.07 *pmol kg^{-1}*	0.03 *nmol kg^{-1}*

2.5. Calculation of dCd* and pCd* tracers

The deviation of dCd and pCd from expected concentrations, based on the average deepwater dCd:PO_4 and pCd:P ratios respectively, can be visualised by calculating dCd* and pCd*. Positive values represent excess dCd or pCd while negative values represent depletion of dCd or pCd relative to PO_4 or P respectively. Because the absolute value of dCd* and pCd* will vary depending on the chosen deep water dCd:PO_4 or pCd:P value, we focus on the trends in dCd* and pCd*.

dCd* was calculated following a previous method (Janssen et al., 2014): $dCd^* = dCd_{measured} - (PO_{4\ measured} \times (dCd:PO_4)_{deep\ water})$, where $dCd:PO_{4\ deep\ water}$ = 334 pmol µmol^{-1}, similar to previous calculations (350 pmol µmol^{-1}; Janssen et al., 2014).

pCd* was calculated in a similar fashion: $pCd^* = Cd_{measured} - (P_{measured} \times (pCd:P)_{deep\ water})$, where $pCd:P_{deep\ water}$ = 0.264 pmol µmol^{-1}.

Note that the term $dCd:PO_{4\ deep\ water}$ refers to average spot ratio of dissolved Cd to PO_4 in seawater below 1000 m whereas the term $pCd:P_{deep}$ refers to the average ratio of particulate Cd to P in the particles.

3. Results

3.1. Hydrographic setting

3.1.1. Frontal positions

The transect intersected several frontal systems which, in turn, separated the study area into physically and biogeochemically distinct regions (Figure 1). Frontal positions were determined previously (Weir et al., in revision) following temperature, salinity and oxygen criteria outlined in the literature (Belkin and Gordon, 1996; Orsi et al., 1995; Pollard et al., 2002). These parameters were measured using a Seabird 9+ conductivity-temperature-depth (CTD) recorder attached to the rosette. The Sub-Tropical Front (STF) located at 42.4°S, defined the boundary between the Sub-Tropical Zone (STZ) to the north and the Sub-Antarctic Zone (SAZ) to the south. The Sub-Antarctic Front (SAF) was identified at 46.2°S and separated the SAZ in the north from the Polar Frontal Zone (PFZ) to the south which was bounded in the south by the Antarctic Polar front (APF) at 49.3°S. Further south, the Antarctic Zone (AAZ) extended until the Southern Boundary (SBdy) at 58.5°S, incorporating the southern Antarctic Circumpolar Current Front (sACCF) at 56.5°S. The Marginal Ice Zone (MIZ), defined by 30% ice cover, was encountered at 61.7°S (de Jong et al., 2018). The location of the sample stations meant that, from north to south, station IO08 was found in the STZ, stations IO07 and IO06 in the SAZ, station IO05 in the PFZ and stations IO04, IO02 and IO01 were within the AAZ.

3.1.2. Water mass classification

Water masses (Figure 2) were identified using potential temperature, salinity and oxygen criteria outlined in the literature (Anilkumar et al., 2006; Orsi et al., 1995). The high temperature and salinity

signature of surface waters at the northernmost station reflected Subtropical Surface Water (STSW; Θ > 15°C, S > 35.25 PSU). Moving southward, the decrease in surface water temperature marked the transition from STSW to Sub-Antarctic Surface Water (SASW) and Antarctic Surface Water (AASW). Below the surface waters in the STZ, a layer of South Indian Central Water (SICW) was sampled. This water mass was underlain by the northwards subducting Sub-Antarctic Mode Water (SAMW; 12 - 15°C; 26.4 - 26.8 kg m^{-3}) which was sampled between ~ 300 - 500 m at 41°S. Similarly, Antarctic Intermediate Water of Indian origin (i-AAIW), transported from the east via the Agulhas Current (AC) and identified by a salinity minimum (S < 34.25 PSU), was found subducting northwards below SAMW. Together with Antarctic Intermediate Water of Atlantic origin (a-AAIW), transported from the west via the Antarctic Circumpolar Current (ACC), i-AAIW dominated intermediate waters along the entire transect. In contrast to the intermediate waters, sampled deep waters consisted predominantly of southward upwelling Upper Circumpolar Deep water (UCDW) and the deeper lying North Atlantic Deepwater (NADW). UCDW had low salinity (S < 34.80 PSU) and an O_2 minimum (155- 180 µmol kg^{-1}) while NADW was identified by deep salinity (S > 34.80 PSU) and O_2 maxima (180 - 200 µmol kg^{-1}) centered at approximately 2500 m depth, at the northern stations. Below NADW, a northward flowing LCDW was characterised by lower temperatures (~ 1°C) and a core depth around 3000 m at all deep stations. Finally, bottom waters, termed Antarctic Bottom Waters (AABW), distinguished by characteristic local temperature minimums (< 0.5°C) were sampled at depth in the AAZ (IO02 and IO04).

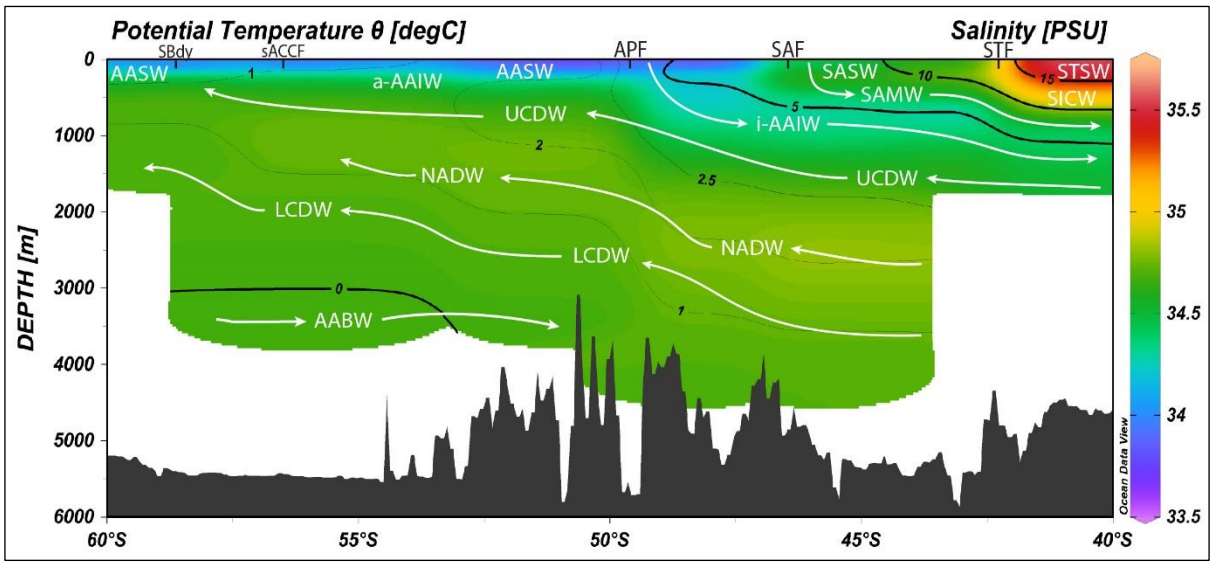

Figure 2. *Distribution plot of salinity overlain by potential temperature used to characterise the water mass regime. Acronyms in alphabetical order are as follows; AABW: Antarctic Bottom Water; AASW: Antarctic Surface Water; a-AAIW: Antarctic Intermediate Water of Atlantic origin; i-AAIW: Antarctic Intermediate Water of Indian origin; ISW: Intermediate Surface Water; LCDW: Lower Circumpolar Deepwater; NADW: North Atlantic Deepwater; SASW: Sub-Antarctic Surface Water; SAMW: Sub-Antarctic Mode Water; SICW: South Indian Central Water; STSW: Sub-Tropical Surface Water; UCDW: Upper Circumpolar Deepwater; WW: Winter Water. Figure constructed using Ocean Data View (ODV; Schlitzer, 2017). Data displayed using weighted average gridding.*

3.1.3. Surface mixed layer and remineralisation depth

The Surface Mixed Layer (SML) at each station was defined as the area between the sea surface and the Mixed Layer Depth (MLD) which was calculated according to the fixed density criterion ($\Delta\sigma\theta$ = 0.03 kg m^{-3}) using 10 m as a reference depth (de Boyer Montégut et al., 2004). The MLD was shallowest at 122 m in the STZ, deepest in the SAZ at 190 - 220 m and shallower again in the PFZ (134 m) and AAZ (125 -161 m). The remineralisation depth was defined as the depth interval below the SML for which O_2 decreased for a corresponding PO_4 increase. Remineralisation depths decreased from north to south, however physical mixing associated with upwelling of UCDW in the AAZ may overprint the actual depth of remineralisation in this zone. In the STZ, the remineralisation depth was between the SML and 1500 m, in the SAZ between SML and 1250 m, in the PFZ between SML and 1000 m and in the AAZ between SML and 250 - 450 m.

3.2. Distribution of dissolved nutrients

3.2.1. dCd

Depth profiles of dCd concentrations along the transect are shown in Figure 3a. At each station, dCd profiles displayed typical nutrient-type behaviour consistent with low surface concentrations and increased concentrations at depth. Across the transect, dCd was fairly uniform in the SML and was characterised by a strong north-south gradient which was associated with the frontal positions. Within the SML, dCd concentrations were 19 ± 2 pmol kg^{-1} in the STZ and increased rapidly across the APF to 758 ± 16 pmol kg^{-1} in the southern AAZ**.** The difference between surface and deep water concentrations was most apparent at the northern stations and decreased southwards. For example, the mean dCd in STSW was 42 ± 21 pmol kg^{-1}, ~ 17 times lower than the concentration of 697 pmol kg^{-1} (n = 1) in UCDW. At the southernmost station, this factor was ~ 1.5 between AASW (722 ± 30 pmol kg^{-1}) and UCDW (1027 ± 65 pmol kg^{-1}). Intermediate depth maxima in dCd varied in concentration and with depth and coincided with local maxima in PO_4 and minima in O_2. The mid-depth dCd maximum ranged between 700 pmol kg^{-1} at 1250 m depth in the STZ and 1150 pmol kg^{-1} at 200 m depth in the AAZ. Below the mid-depth peak, concentrations were typically lower in NADW (607 ± 47 pmol kg^{-1}) and showed increases in the LCDW (809 ± 120 pmol kg^{-1}) and AABW (865 ± 88 pmol kg^{-1}).

3.2.2. Phosphate

Major nutrient concentrations have been previously reported (Weir et al., in revision). Here we briefly describe the distribution of PO_4 (Figure 3b) because of the extensive reference made to the dCd - PO_4 relationship. There was a strong southward increase in SML PO_4 concentrations, from 0.28 ± 0.08 µmol kg^{-1} in STSW to 1.85 ± 0.09 µmol kg^{-1} in AASW. Below the SML, PO_4 increased to maximum concentrations in UCDW at each station. The intermediate depth PO_4 maximum was most evident around the APF where PO_4 reached 2.43 ± 0.16 µmol kg^{-1}. The underlying NADW (2.10 ± 0.16 µmol

kg^{-1}) and LCDW (2.14 ± 0.14 µmol kg^{-1}) were characterised by local PO_4 minima before slight increases in PO_4 in AABW (2.20 ± 0.02 µmol kg^{-1}).

3.3. Distribution of particulate nutrients

3.3.1. pCd

The depth profiles of pCd (Figure 3c) generally showed the opposite vertical distribution in comparison to dCd. Highest pCd concentrations were typically found within the surface water masses at each station, while strong negative gradients through sub-surface water masses resulted in pCd concentrations having uniformly low concentrations below 1000 m at all stations. UCDW, LCDW and AABW had mean pCd concentrations of 1.34 ± 1.08, 0.35 ± 0.21 and 0.39 ± 0.12 pmol kg^{-1} respectively. In the SML, pCd did not show any consistent latitudinal trend. Near the APF (48°S), pCd was 18.83 ± 3.76 pmol kg^{-1}, the highest SML value measured, while in the STZ, pCd in the SML was the lowest at 6.18 ± 3.49 pmol kg^{-1}. In general, concentrations in the SML were higher to the north of the APF and lower to the south.

3.3.2. Phosphorous

The depth profiles of P (Figure 3d) resembled those of pCd whereby surface waters were characterised by high P concentrations which decreased rapidly in sub surface water masses to extremely low values at depth. Like pCd, highest SML P concentrations (14.29 ± 1.78 nmol kg^{-1}) were measured near the APF. North of the APF, concentrations in the SML ranged between 9.77 ± 3.26 and 12.84 ± 4.49 nmol kg^{-1} in the SAZ and STZ respectively. South of the APF, concentrations in the SML were between 8.54 ± 1.19 and 12.98 ± 0.53 nmol kg^{-1}. At greater depths, mean P concentrations in UCDW, LCDW and AABW were 2.47 ± 1.40, 1.93 ± 0.87 and 1.48 ± 0.25 nmol kg^{-1}, respectively.

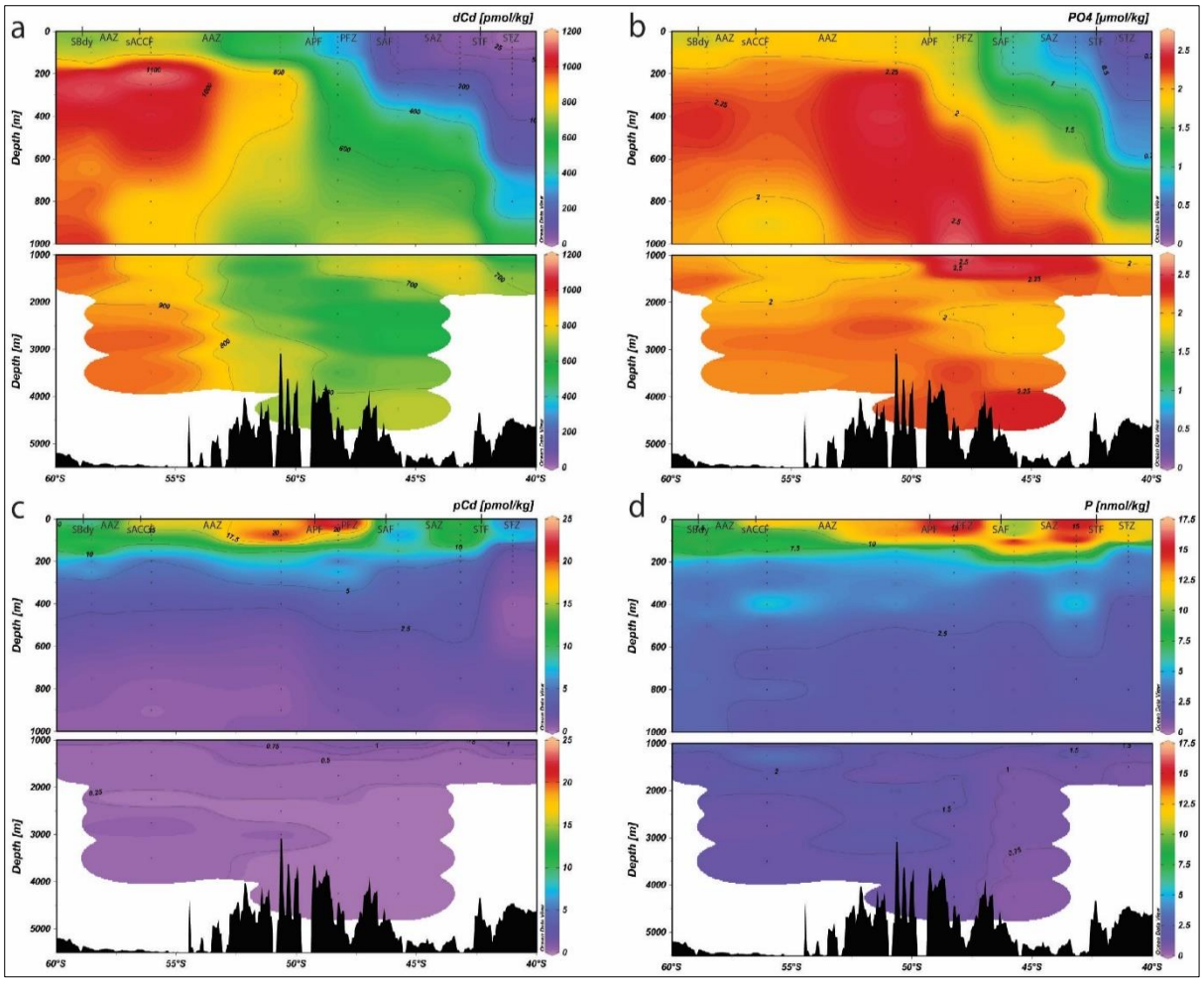

Figure 3. *Distribution plots of a) dCd, b) PO_4, c) pCd and d) P. Each figure is separated into upper 1000 m (upper panel) and below 1000 m (bottom panel). Frontal position and corresponding zones are shown. Figure constructed using Ocean Data View (ODV; Schlitzer, 2017). PO_4 data from Weir et al., in revision. Dots represent depths sampled. Data displayed using weighted average gridding.*

4. Discussion

4.1. Comparison with previously reported dCd and pCd

The data presented here contributes the first measurements of dCd and pCd from the 30°E longitude in the Indian sector of the Southern Ocean and one of only a handful of winter trace metal datasets produced globally, thus closing key spatial and seasonal gaps in the global database. For comparative purposes, a global compilation of dCd and pCd measurements (Figure 4) has been created from all available data included in the GEOTRACES Intermediate Data Product (IDP) 2017 (Schlitzer et al., 2018; see figure caption for full list of references) The data was separated into full depth profiles from surface to near sea floor for dCd (Figure 4a) and pCd (Figure 4b) and profiles from surface to 1000 m depth for dCd (Figure 4c) and pCd (Figure 4d).

For dCd, concentrations in the Indian sector of the Southern Ocean (this study) fell within the range of concentrations found in other ocean basins. In terms of dCd, the overwhelming majority of vertical

profiles showed surface minima, between 0.04 pmol kg^{-1} (Mediterranean Sea; Gerringa et al., unpublished) and 36 pmol kg^{-1} (Atlantic Southern Ocean, Baars et al., 2014) and intermediate to deep dCd maxima, between 368 pmol kg^{-1} (Mediterranean Sea, Gerringa et al., unpublished) and 1246 pmol kg^{-1} (North Pacific Ocean, Minami et al., 2015). For the full depth profiles, the Indian sector of the Southern Ocean dCd data had a range of 18 – 1160 pmol kg^{-1} which compared most similarly to that of the Atlantic Southern Ocean (36 – 970 pmol kg^{-1}; Baars et al., 2014)) and Indian Ocean (10 – 1100 pmol kg^{-1}; Thi Dieu Vu and Sohrin, 2013). In the Atlantic sector of the Southern Ocean, dCd showed strong summer surface gradients associated with the frontal positions (Baars et al., 2014; Boye et al., 2012), similar to the gradients observed here. However, surface dCd in winter was between 10 - 100 pmol kg^{-1} higher compared to summer values (Baars et al., 2014; Boye et al., 2012), and more closely resembled the comparative winter surface gradients (Ellwood, 2008). Furthermore, dCd at our northernmost station (41°S; 30°E) was similar to a station at a similar latitude but further east (60°E; Thi Dieu Vu and Sohrin, 2013). Here, dCd profiles were characterized by low (< 80 pmol kg^{-1}) surface concentrations and a mid-depth maximum of around 800 pmol kg^{-1}, were similar to the northern stations along this transect.

For pCd, concentrations in the Indian sector of the Southern Ocean fell within the range of concentrations found in other ocean basins and most closely resembled those observed in the South Atlantic, particularly in the upper 1000 m. Highest pCd concentrations were found in surface waters of all datasets while extremely low values, between 0.02 pmol kg^{-1} (South Atlantic; Henderson et al., unpublished) and 0.06 pmol kg^{-1} (Indian sector of Southern Ocean) characterised deep ocean distributions. For the upper 1000 m, mean pCd concentrations were between 1.13 and 5.04 pmol kg^{-1} in the North Atlantic (Hayes et al., 2018) and Equatorial Pacific (Lee et al., 2018) respectively while the mean value for the Indian sector of the Southern Ocean was 5.92 pmol kg^{-1}.

4.2. Distribution of dCd and pCd in the upper water column

4.2.1. Relation with PO_4, P and O_2

Seawater samples were collected in early to mid-July and therefore represent early winter conditions. Owing to increased surface mixing and decreased light exposure (Dong et al., 2008; Swart et al., 2015), the winter months are generally considered biologically dormant in comparison to the spring and summer months. However, estimates of productivity (inferred through measurements of Chl-*a*), were comparable to spring measurements and were at the lower end of summer measurements. For example, north of the APF, our early winter (July) Chl-*a* concentrations averaged over the SML (0.31 - 0.54 µg kg^{-1}) were similar to Chl-*a* concentrations measured to the east during spring (0.34 µg kg^{-1}; Becquevort et al., 2000) and summer (0.39 - 1.23 µg kg^{-1}; Rembauville et al., 2016). In the AAZ, our SML Chl-*a* (0.20 - 0.30 µg kg^{-1}) was within the range of previous spring concentrations (0.10 - 0.39 µg kg^{-1}; Becquevort et al., 2000) and below previous summer concentrations (0.49 - 0.98 µg kg^{-1}; Rembauville

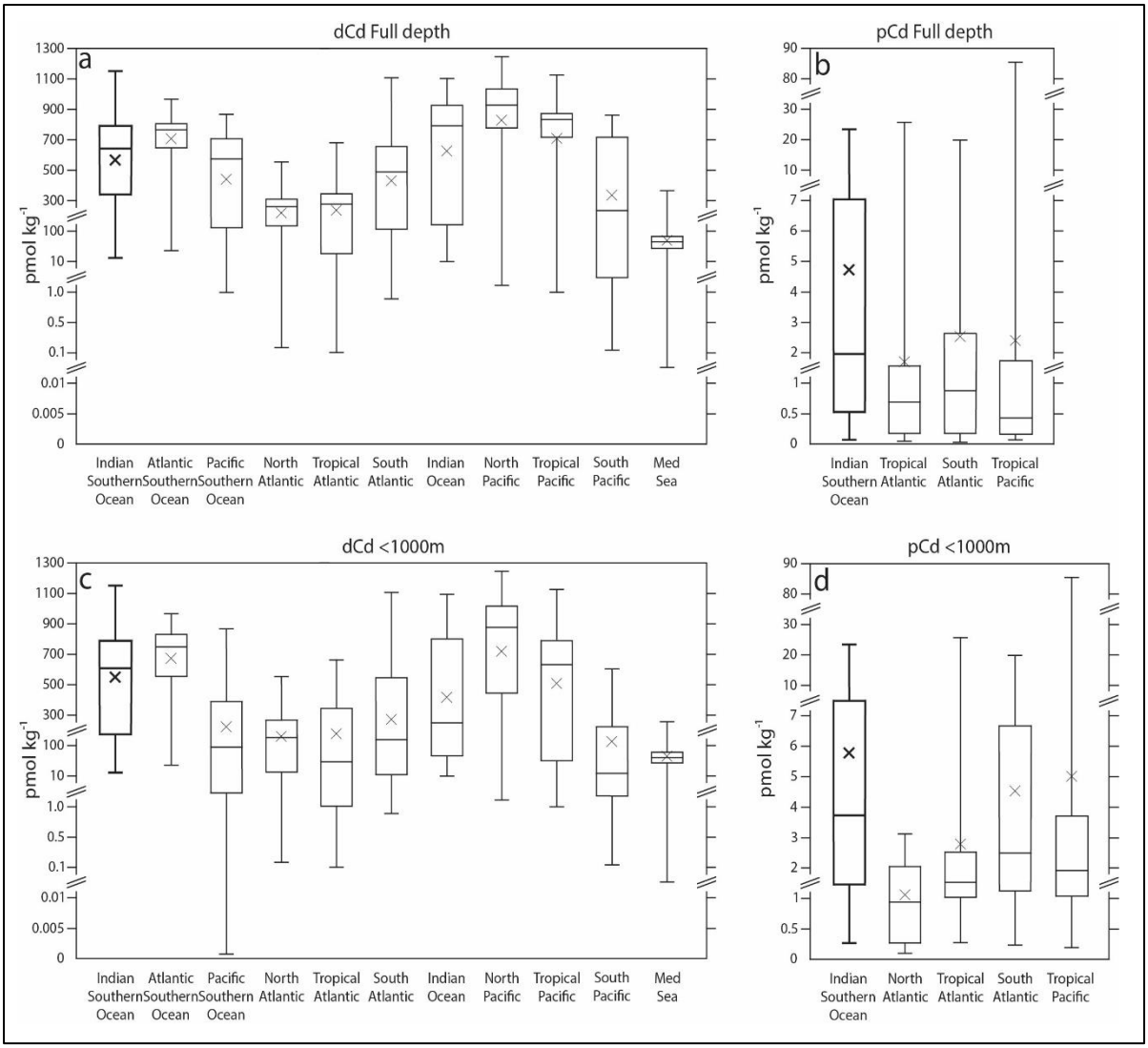

Figure 4. *Box and whisker plots of a) dCd for full depth profiles, b) pCd for full depth profiles, c) dCd for profiles to 1000 m and d) pcd for profiles to 1000 m. Data compiled from all available data from the GEOTRACES intermediate data product (IDP) 2017 (Schlitzer et al., 2018). Plots in bold are data from this study. From bottom to top, plots are structured as follows: minimum, quartile 1, median, quartile 3, maximum. The cross (x) represents the mean value. Note the changes in the vertical scale. For dCd data references are as follows, Indian Southern Ocean data [this study (n = 132 full depth; 103 < 1000 m)], Atlantic Southern Ocean [transect GIPY05 (n = 177 full depth; 116 < 1000 m) (Baars et al., 2014)], Pacific Southern Ocean [transect GIPY06 (n = 82 full depth; 223 < 1000 m) (Butler et al., 2013), transect GIPY02 (n = 0 full depth; 109 < 1000 m) (Butler et al., 2013), transect GPpr01 (n = 0 full depth; 34 < 1000 m) (Hassler and Ellwood, unpublished), transect GPpr02 (n = 77 full depth; 168 < 1000 m (Ellwood, 2008)], North Atlantic Ocean [transect GA02 (n = 407 full depth; 227 < 1000 m) (Middag et al., 2018), transect GA03 (n = 588 full depth; 303 < 1000 m) (Hayes et al., 2018)], Tropical Atlantic Ocean [transect GA02 (n = 479 full depth; 259 < 1000 m) (Middag et al., 2018), transect GA11 (n = 57 full depth; 27 < 1000 m) (Xie et al., 2018)], South Atlantic Ocean [transect GA02 (n = 482 full depth; 261 < 1000 m) (Middag et al., 2018; Xie et al., 2015), transect GA10 (n = 340 full depth; 159 < 1000 m (Achterberg, Henderson, Schlosser, unpublished), transect GIPY04 (n = 86 full depth; 103 < 1000 m) (Boye et al., 2012)], Indian Ocean [transect GI04 (n = 167 full depth; 94 < 1000 m) (Thi Dieu Vu and Sohrin, 2013)], North Pacific Ocean [transect GP02 (n = 256 full depth; 137 < 1000 m) (Minami et al., 2015), transect GP18 (n = 94 full depth; 49 < 1000 m) (Minami et al., 2015), transect GPpr07 (n = 25 full depth; 68 < 1000 m) (Janssen et al., 2017)], Tropical Pacific Ocean [transect GP16 (n = 667 full depth; 350 < 1000 m) (John et al., 2017)], South Pacific Ocean [transect GP13 (n = 342 full depth; 544 < 1000 m) (Bowie, Boyd, Ellwood, van der Merwe, Queroue, Townsend, unpublished)] and Mediterranean Sea [transect GA04 (n = 1376 full depth; 1057 < 1000 m) (Gerringa, Middag, Rijkenberg, Rolison, Stirling, unpublished)]. For pCd, references are as follows, Indian Southern Ocean data [this study (n = 122 full depth; 94 < 1000 m)], North Atlantic Ocean [transect GA03 (n = 0 full depth; 34 < 1000 m) (Hayes et al., 2018)], Tropical Atlantic Ocean [transect GA06 (n = 103 full depth; 82 < 1000 m) (Achterberg, unpublished)], South Atlantic Ocean [transect GA10 (n = 231 full depth; 134 < 1000 m) (Henderson, Achterberg, Milne, Lohan, unpublished)] and Tropical Pacific Ocean [transect GP16 (n = 703 full depth; 397 < 1000 m) (Lee et al., 2018)].*

et al., 2016). This suggests that the winter euphotic layer was not biologically dormant (Weir et al., in revision) and that biological uptake by phytoplankton could potentially play an important role in controlling dCd and pCd distributions during winter.

Further evidence for biological activity in winter stems from the closely coupled distribution of Cd and the major nutrient P, particularly in the remineralisation zone where a strong linear relationship between dCd vs PO_4 [dCd (pmol kg^{-1}) = 426 ± 44 PO_4 (µmol kg^{-1}) - 195; r^2 = 0.91; n = 89] and pCd vs P [pCd (pmol kg^{-1}) = 1.08 ± 0.11 P (nmol kg^{-1}) - 0.29; r^2 = 0.92; n = 80] were observed. Assuming that all P is of biogenic origin, and considering the close coupling of pCd and P, it is reasonable to assume that pCd is majorly biogenic in composition. Low dCd and PO_4 and high O_2 concentrations in the SML and enrichments in oxygen depleted subsurface waters (Figure 5a; in Figure 5 we plot only stations from the SAZ where O_2 profiles were very similar) are widely accepted to result from biological uptake by phytoplankton in the euphotic zone and subsequent remineralisation at depth (Abouchami et al., 2014). Biological uptake and assimilation of dCd and PO_4 drives the production of organic pCd and P as observed by the high surface pCd and P concentrations in the surface waters (Figure 5b). In the subsurface, low pCd and P coincide with low O_2 and correspond to depths at which dCd and PO_4 show local maxima reflecting the aerobic remineralisation of sinking phytoplankton cells by the microbial community. The extremely low (<1 pmol kg^{-1}) concentrations of pCd, and relatively high concentrations of dCd (>500 pmol kg^{-1}), below 1000 m depth suggests that Cd cycling at depth is controlled by the dissolved fraction. In sum, the lower dCd in surface waters coincides with low PO_4 and high O_2 while in the subsurface, dCd maxima coincides with PO_4 maxima and O_2 minima reflecting uptake at the surface and subsurface regeneration respectively.

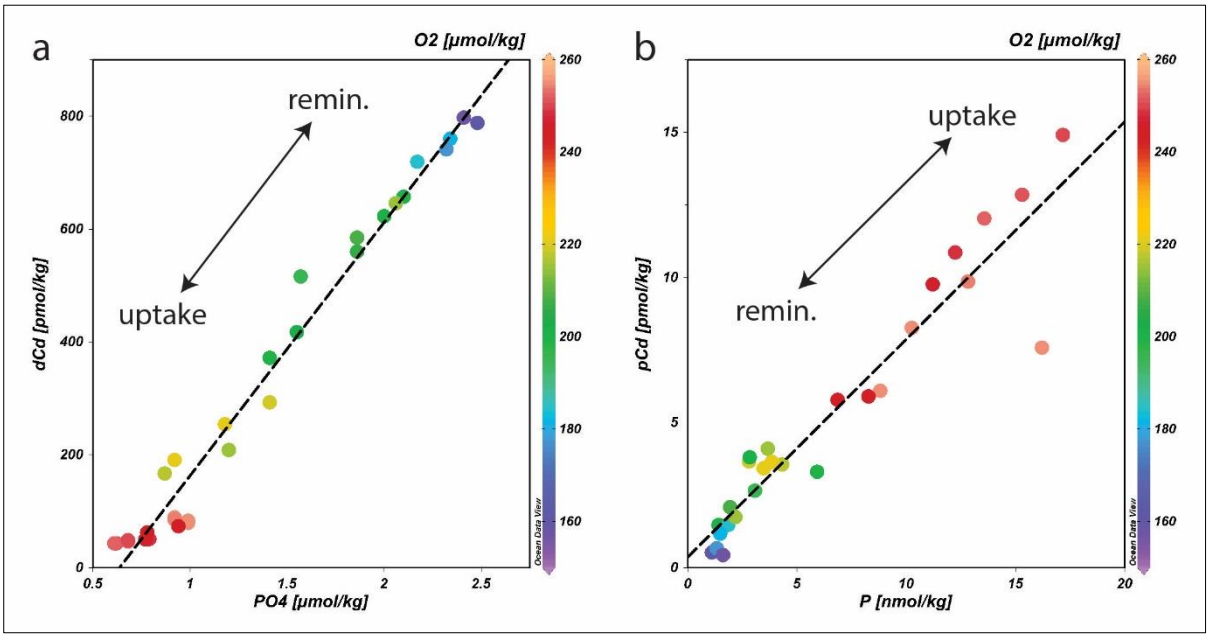

Figure 5. *Plots of a) dCd vs PO_4 overlain with O_2 and b) pCd vs P overlain with O_2. Data from both plots is from the SML and remineralisation zone in the SAZ. Figure constructed using Ocean Data View (ODV; Schlitzer, 2017).*

4.2.2. Regional variations in uptake and regeneration

Phytoplankton cellular Cd quotas are reported to range by a factor of 100 (0.01 – 1 mmol mol^{-1} P) compared to a factor of 20 for other bioactive metals such as Fe, Mn, Zn and Cu (Ho et al., 2003; Twining and Baines, 2013). As a result, Cd cycling may be significantly influenced by the local phytoplankton community. In an effort to better understand the link between Cd distributions and local phytoplankton community assemblages we calculate the uptake and remineralisation ratios at each station (Figure 6) and compare with available cellular Cd quotas for various species. The uptake ratio describes the slope of correlation between dCd/PO_4 in the SML while the remineralisation ratio describes the slope of correlation between pCd/P in the remineralisation zone (see section 3.1.3). dCd/PO_4 slope values were between 434 - 513 pmol μmol^{-1} in the STZ and SAZ and increased to between 886 - 1058 pmol μmol^{-1} in the PFZ and AAZ. A similar spatial trend was observed for pCd/P, where slope values were between 0.25 – 0.67 pmol $nmol^{-1}$ in the STZ and SAZ and increased to slope values between 1.48 – 1.76 pmol $nmol^{-1}$ in the PFZ and AAZ. This is consistent with global estimates showing a distinct pCd enrichment on particles exported from the surface layer south of 45 – 50 °S (Quay et al., 2015). The significant correlation ($P < 0.05$) between dCd/PO_4 and pCd/P across the transect suggests that the surface dCd to PO_4 uptake stoichiometry is reflected in the particulate material exported below the SML and that the regeneration of this signal dominates the dCd and PO_4 increases in subsurface waters.

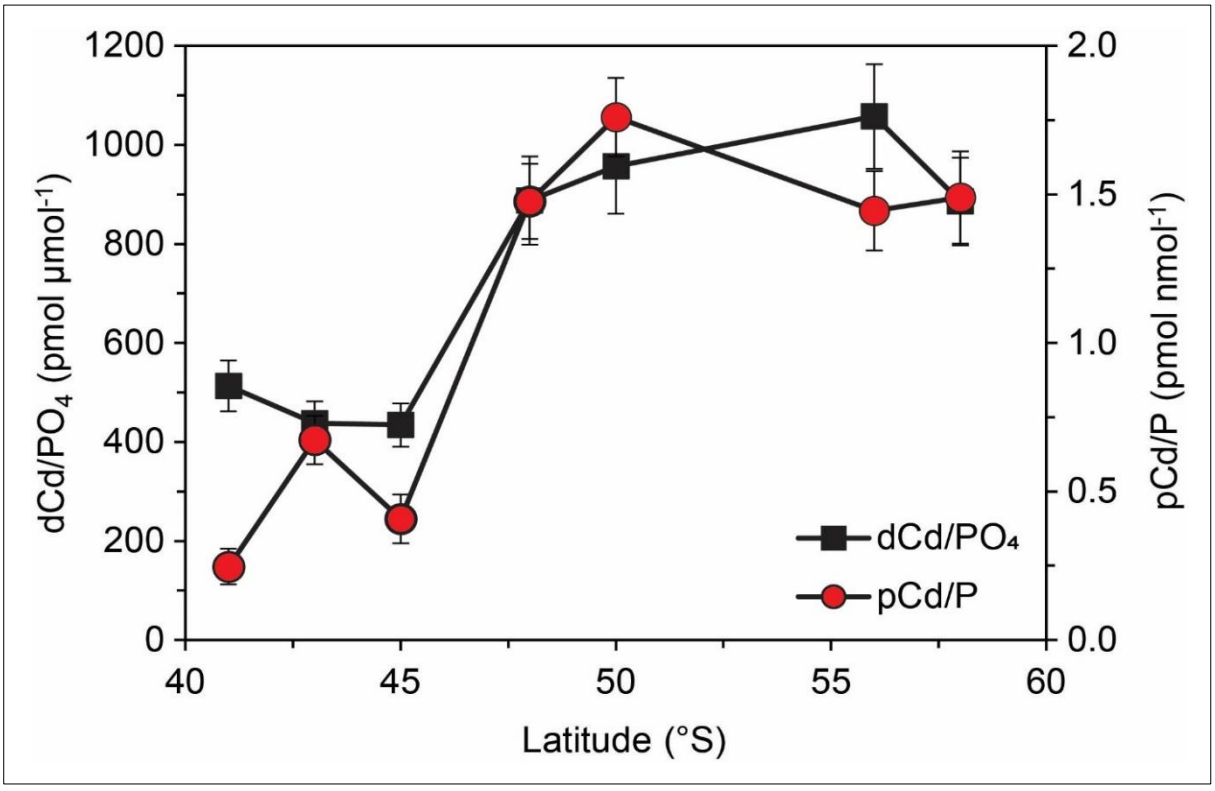

Figure 6. *dCd/PO_4 uptake ratios and pCd/P remineralisation ratios calculated for each station. Uptake ratios calculated as the slope of correlation between dCd and PO_4 in the SML. Remineralisation ratios calculated as the slope of correlation between pCd and P between the SML and bottom of the remineralisation zone. Error bars represent ± one standard deviation.*

Furthermore, spatial trends in dCd/PO_4 and pCd/P systematics reflect the uptake characteristics of the local phytoplankton community. A pCd/P ratio of 0.51 mmol mol^{-1} was reported for a flagellate dominated assemblage in the North Atlantic Ocean (Kuss and Kremling, 1999) and falls within the range of our pCd/P ratios in the STZ and SAZ. Indeed, flagellates were dominant in the low $Si(OH)_4$ (< 3 µmol kg^{-1}) surface waters of the STZ and SAZ (Weir et al., in revision), and their lower cellular Cd quotas compared to diatoms (Twining and Baines, 2013) provides a probable explanation for the low pCd/P ratios at the northern stations. Further south, the elevated pCd/P remineralisation ratios suggest a dominance of diatoms in the $Si(OH)_4$ replete (> 25 µmol kg^{-1}) surface waters of the AAZ and also in the PFZ where $Si(OH)_4$ was > 5 µmol kg^{-1}, in agreement with phytoplankton community data (Weir et al., in revision). Open ocean diatoms are characterised by high cellular Cd quotas in relation to other phytoplankton groups likely driving the elevated ratios in the PFZ and AAZ. For example, a pCd/P ratio of 1.29 pmol $nmol^{-1}$ (Cullen et al., 2003) has been reported for a diatom dominated Southern Ocean phytoplankton assemblage, comparable to our pCd/P ratios from the PFZ and AAZ (1.48 - 1.76 pmol $nmol^{-1}$). Reasons for the enriched cellular Cd in diatoms appear related to Fe availability (Cullen et al., 2003; Lane et al., 2009, 2008) and Mn and Zn availability (Cullen and Sherrell, 2005; Lee et al., 1995; Sunda and Huntsman, 2000). Here we discuss only Fe availability considering that surface dMn (> 0.4 nmol kg^{-1}) and dZn (> 2.5 nmol kg^{-1}), analysed concurrently with dCd but discussed elsewhere, within the PFZ and AAZ were high and increased southwards.

The availability of Fe in surface waters has been shown to impact the dCd to PO_4 uptake dynamics of diatoms whereby diatoms under Fe-limitation either preferentially remove dCd relative to PO_4 in surface waters via growth biodilution (Cullen et al., 2003; Sunda and Huntsman, 2000) or via an additional dCd requirement through a non-specific Fe(II) transporter which is up-regulated under Fe-limitation (Lane et al., 2009, 2008). Both mechanisms are plausible considering that surface dFe was low (< 0.1 nmol kg^{-1}) throughout the PFZ and AAZ, potentially at or near limiting availability, and that both result in increased dCd/PO_4 and pCd/P. While dFe in the surface remained low in the STZ and SAZ, the effect of (near)-limiting dFe concentrations on Cd/PO_4 uptake and pCd/P regeneration dynamics of non-diatom phytoplankton assemblages is not well understood. However the lower dCd/PO_4 and pCd/P calculated at the northern stations suggest that flagellates have lower Cd requirements compared to diatoms.

4.3. Upwelling and physical resupply of dCd through deep winter mixing

Considering the strong preferential uptake of dCd in the PFZ and AAZ, we would expect surface dCd to remain low throughout the southern section of the transect. However, the mean SML dCd concentration in the PFZ and AAZ was between 327 to 722 pmol kg^{-1} and significantly higher compared to stations to the north (Figure 3a). The strong surface dCd gradient was likely the result of the upwelling of underlying water masses, primarily UCDW, which supply dCd enriched waters to the surface layer.

Upwelling of UCDW occurs in the AAZ, where UCDW was sampled between 300 – 600 m, and is laterally transported northwards into the PFZ (Orsi et al., 1995). Importantly, UCDW carried a high mean dCd:PO_4 spot ratio of 370 pmol µmol^{-1} (Figure 7a), similar to the previous summer spot ratios (365 pmol µmol^{-1}; Baars et al., 2014). The dCd:PO_4 spot ratios in UCDW increased southwards and reached a maximum of ~ 500 pmol µmol^{-1} below the SML in the AAZ. The source of the 'excess' dCd relative to PO_4 was predominantly from the remineralisation of particles with high pCd:P (Figure 7b) which, in turn, was set during biological uptake within the SML.

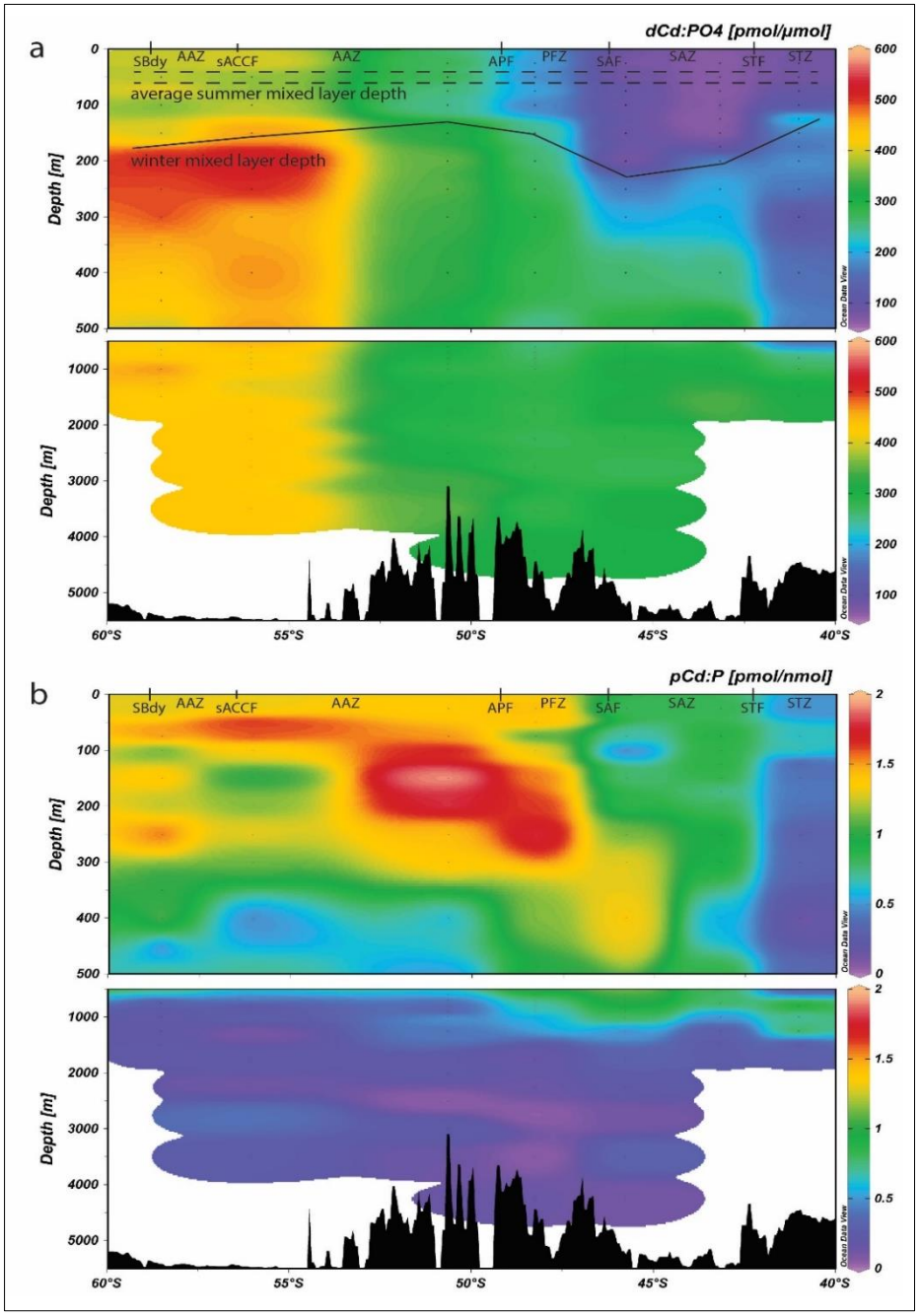

Figure 7. *Distribution plots of a) dCd:PO_4 spot ratios and b) pCd:P spot ratios. Each plot is separated into upper 500 m (upper panel) and below 500 m (bottom panel). Frontal position and corresponding zones are shown. In 7a, dotted lines represent the average range of the summer mixed layer depth (data from WOCE Global Data Resource, (2018)). Solid line represents the calculated winter mixed layer depth during this study. Figure constructed using Ocean Data View (ODV; Schlitzer, 2017). Dots represent depths sampled. Data displayed using weighted average gridding.*

In addition to the strong latitudinal trends in dCd:PO_4 spot ratios, we observed a significant increase with depth (Figure 7a). Increasing dCd:PO_4 spot ratios with depth supports the notion of a physical resupply of dCd to the SML through deep winter mixing. While our sampling took place before the period of maximum nutrient recharge, between August and November (Johnson et al., 2017), the early winter MLDs in the SAZ were similar to the maximum values (~200m) expected in west Indian sector (Sallée et al., 2010) suggesting deep winter mixing and nutrient recharge was ongoing. Deep winter mixing is an important nutrient resupply mechanism in the Southern Ocean as shown previously for Fe (Mtshali et al., 2019; Tagliabue et al., 2014) and other trace metals (Cloete et al., 2019). Here, deeper mixing during the winter months allows access to more nutrient rich waters (i.e. with higher dCd:PO_4) found below the depleted summer mixed layer, potentially resupplying dissolved nutrients which may aid and sustain local phytoplankton production through the spring and summer months. For example, in the STZ and SAZ, dCd:PO_4 increased by 2 -3 fold from 66 - 96 pmol μmol^{-1} at the depth of the average summer mixed layer in this region (between 60 – 80 m; WOCE Global Data Resource, 2018), to values between 169 - 223 pmol μmol^{-1} at the base of the winter mixed layer (~ 200 m; Figure 7a). Winter deep mixing may be of particular importance in the STZ and SAZ where summer surface dCd can be depleted to < 10 pmol kg^{-1} (Boye et al., 2012).

4.4. Export of Cd signatures to the low-latitude ocean

The Southern Ocean plays a central role in the global thermohaline circulation such that water masses formed in the high latitude Southern Ocean spread throughout the Southern Hemisphere and North Atlantic Ocean (Carter et al., 2009). Of particular importance here is SAMW which forms from wintertime cooling and mixing of STSW and SASW (McCartney, 1977). SAMW is the main conduit of nutrients for the low latitude ocean (Sarmiento et al., 2004) and therefore has the potential to influence low latitude productivity (Marinov et al., 2006). Our data suggest that SAMW, sampled between 300 – 500 m in the STZ, is characterised by low dCd* and pCd* signatures relative to other water masses (Figure 8). The net result is that SAMW exports waters that are depleted in dCd relative to PO_4. Furthermore, as a result of the relatively low pCd in the particles, remineralisation of particles is not likely to preferentially enrich SAMW in dCd during transport. These observations are consistent with the low dCd:PO_4 and low pCd:P measured in the upper ocean at lower latitudes (Quay et al., 2015).

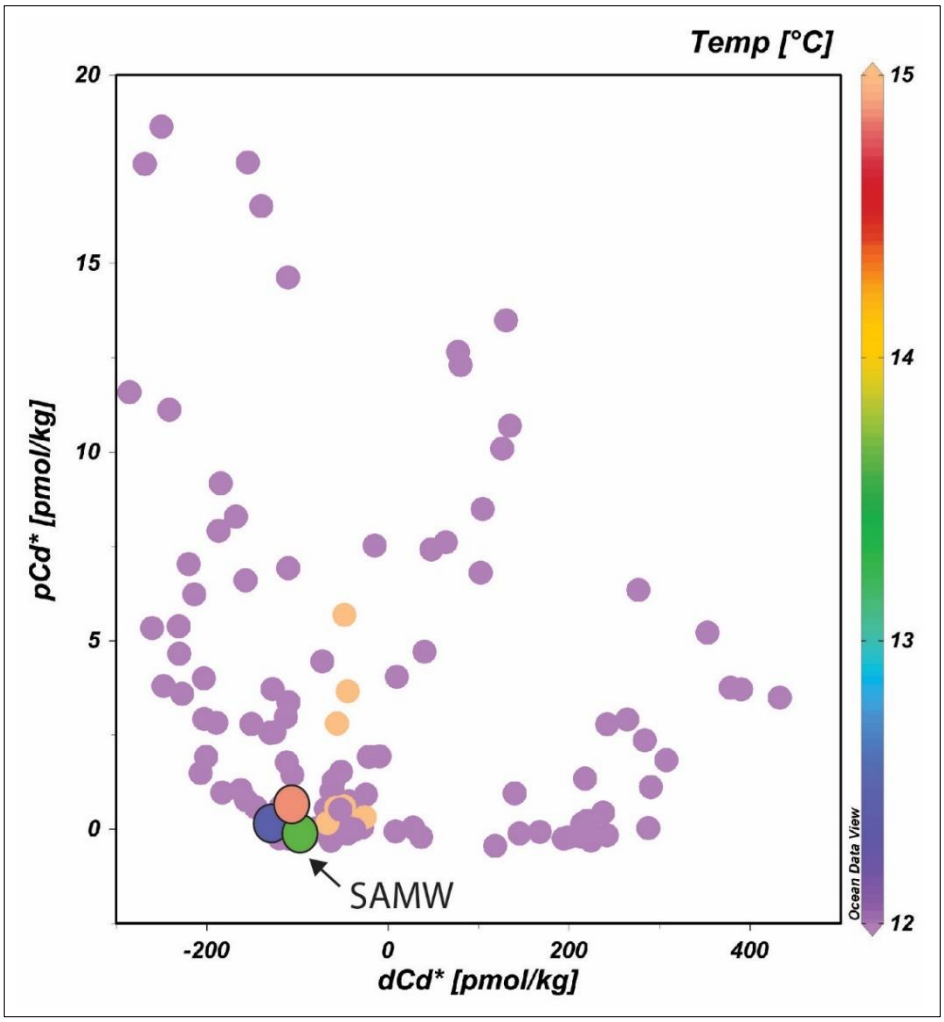

Figure 8. *Plot of pCd* vs dCd* with data points for SAMW (12 - 15°C; Anilkumar et al., 2006) enlarged and coloured according to the temperature scale. Calculations for pCd*, dCd* described in text (section 2.5). Figure constructed using Ocean Data View (ODV; Schlitzer, 2017).*

4.5. dCd in intermediate and deep waters and the importance of water mass mixing

While dCd and PO_4 are well correlated, our data show a change in the steepness of the dCd/PO_4 slope at PO_4 > 1.0 µmol kg^{-1} (Figure 9), a feature commonly referred to as the 'kink', and which is evident in the global dCd/dPO_4 relationship (Middag et al., 2018) which was derived from the GEOTRACES 2017 Intermediate Data Product (IDP 2017; Schlitzer et al., 2018). The samples with low dCd and PO_4 represent surface waters from the STZ and SAZ and plot on a relatively shallow linear slope (61 ± 9 µmol mol^{-1}) with a slightly negative intercept indicating a slight preferential uptake of Cd relative to PO_4. Our winter slope value is higher compared to summer STZ and SAZ surface waters (31 ± 6 µmol mol^{-1}; Baars et al., 2014; Boye et al., 2012) likely reflecting preferential dCd recharge (relative to PO_4) as a result of deep winter mixing (see section 4.3). The higher dCd/PO_4 signatures of intermediate and deep water masses are collectively represented by the steep linear slope (Frew and Hunter, 1992). We calculate a dCd/PO_4 slope value of 453 ± 9 µmol mol^{-1} (n = 73) for these waters which is similar to

slopes observed in previous Southern Ocean winter measurements (444 ± 11 µmol mol^{-1}; Ellwood, 2008), and lower compared to slope values in the Atlantic sector of the Southern Ocean (590 ± 12 µmol mol^{-1}; Baars et al., 2014; Boye et al., 2012). The high slope values and negative intercepts in our winter data suggest a combination of preferential uptake (and subsurface regeneration) of dCd relative to PO_4 but also strong upwelling of dCd enriched water masses in the AAZ (Baars et al., 2014). Furthermore, we identify that in fact multiple linear equations compose data from the steep slope (Figure 9) as shown previously in the Atlantic (Middag et al., 2018). Each slope represents a different water mass and it is assumed that mixing between water masses with different origins and hence, different preformed nutrient components, results in a new equation where the slope value falls between the slope values of the water mass end-members being mixed. For example, NADW has a dCd/dPO_4 slope value of 250 µmol mol^{-1} at its source in the high latitude North Atlantic (Bruland and Franks, 1983) compared to a slope value of 311 ± 5 µmol mol^{-1} (n = 8) measured here. As NADW flows southward across the equator, the increase in slope value arises from mixing with northward flowing AAIW (340 ± 15 µmol mol^{-1}; n = 30) at intermediate depths and at deeper depths with CDW (344 ± 11 µmol mol^{-1}; n = 38) and AABW (2934 ± 22 µmol mol^{-1}; n = 4). These Antarctic derived water masses have higher dCd/dPO_4 slope values such that the slope for NADW observed here lies between its source waters and the waters it interacted with.

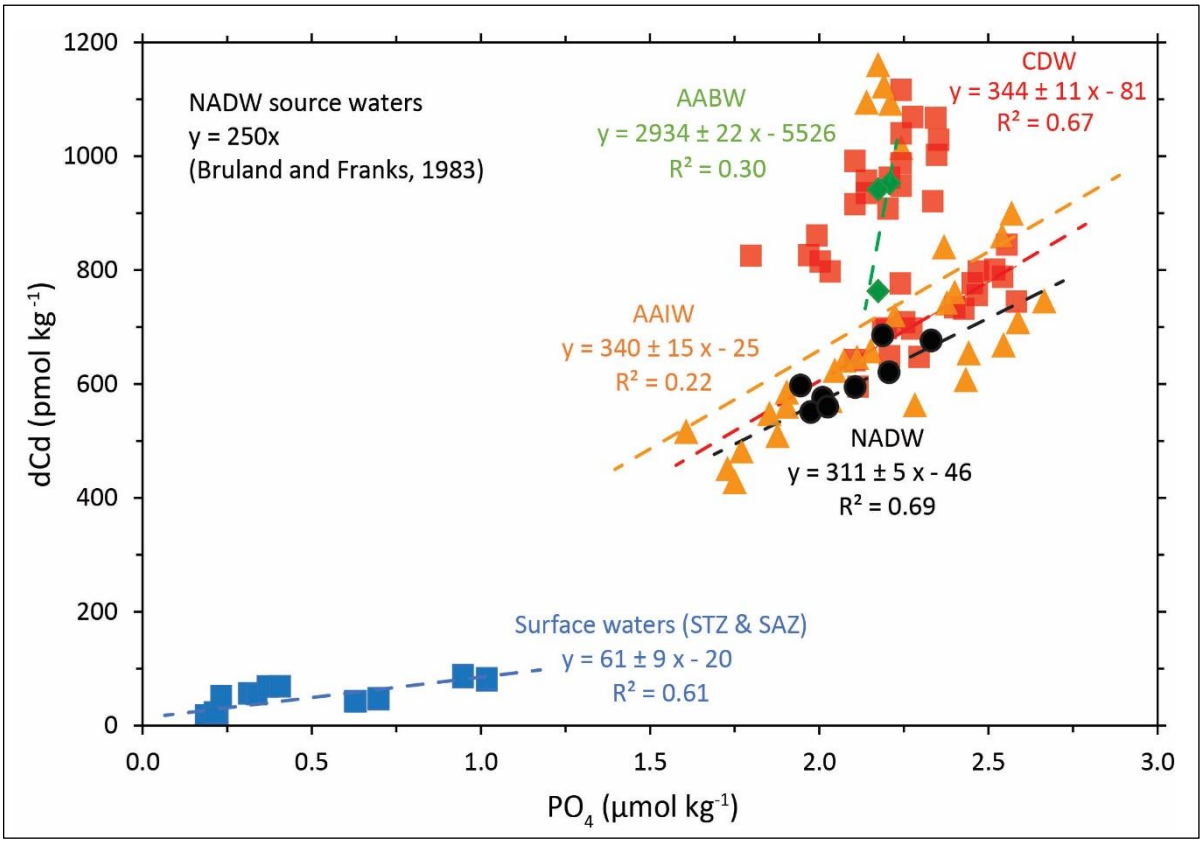

Figure 9. *Plot of dCd/dPO_4 ratios, defined as the correlation of the slope between dCd and PO_4, for various water masses.*

5. Conclusion

This study presents the first winter measurements of dissolved cadmium (dCd) and particulate cadmium (pCd) along the 30°E longitude in the Indian Sector of the Southern Ocean. The results provided a unique opportunity to investigate Cd cycling over seasonal cycles and to characterise the Southern Ocean winter reset state. Our data suggests that biological uptake of trace metals is an important factor to consider during the winter season despite unfavourable growth conditions for phytoplankton. Close correlations between dCd and PO_4, as well as pCd and P, were maintained throughout the transect. At all stations, dCd was lowest in the SML and increased with depth. Conversely, pCd was highest in the SML and decreased rapidly with depth. The vertical behaviours of both dCd and pCd are consistent with biological uptake in surface waters and remineralisation in the sub surface. Concentrations of dCd in the SML were higher compared to summer measurements likely reflecting a combination of weaker biological uptake and increased recharge through deep winter mixing.

Furthermore, there were distinct regional trends in uptake and remineralisation ratios likely reflecting changes in phytoplankton community structures. Uptake ratios in the SML, (dCd/PO_4) were lower in the STZ and SAZ and increased by ~ 2 fold in the PFZ and AAZ. Remineralisation ratios calculated between the SML and remineralisation depth (pCd/P) showed a similar southward increase suggesting a change from a phytoplankton community with lower Cd requirements in the STZ and SAZ (e.g. flagellates) to a community with higher Cd requirements in the PFZ and AAZ (e.g. diatoms). Preferential uptake and assimilation of Cd by diatoms may be linked to Fe availability. The combined effect of preferential uptake and regeneration of diatoms with high Cd content and the upwelling of watermasses in the AAZ resulted in the strong southward increase in surface dCd. In the SAZ, the formation and export of SAMW with low dCd* and pCd* signatures has potential implications for low latitude Cd cycling and productivity. In the intermediate and deep waters, where dCd dominated Cd cycling, there were distinct water mass dependent correlations between plots of dCd versus dPO_4 which suggested that dCd distributions are largely the result of mixing between northward travelling waters of Antarctic origin with high dCd/dPO_4 slopes and southward travelling NADW with an inherently low dCd/dPO_4 signature.

6. Acknowledgements

We would like to thank the South African National Antarctic Programme (SANAP) as well as Captain Knowledge Bengu and the crew of the R/V SA Agulhas II for their professionalism and support during the winter 2017 voyage. We acknowledge Chief Scientist Marcello Vichi and all the participants involved in the expedition. We are grateful to the “Iron” team for their help in collecting trace-clean seawater samples. We would like to thank Gideon Henderson, Eric Achterberg, Angela Milne, Maeve Lohan, Andrew Bowie, Yoshiki Sohrin and Michael Ellwood for allowing permission to use data that are not published outside of the IDP2017. Ryan Cloete was supported through the National Research

Foundation (NRF) Innovation PhD studentship. This research was supported by NRF grants (UID# 93069, 105826 and 110715) to AR. S.F. acknowledges funding from NRF (UID 111210, 110731).

7. References

Abouchami, W., Galer, S.J.G., De Baar, H.J.W., Middag, R., Vance, D., Zhao, Y., Klunder, M., Mezger, K., Feldmann, H., Andreae, M.O., 2014. Biogeochemical cycling of cadmium isotopes in the Southern Ocean along the Zero Meridian. Geochim. Cosmochim. Acta 127, 348–367. https://doi.org/10.1016/j.gca.2013.10.022

Anilkumar, N., Luis, A.J., Somayajulu, Y.K., Ramesh Babu, V., Dash, M.K., Pednekar, S.M., Babu, K.N., Sudhakar, M., Pandey, P.C., 2006. Fronts, water masses and heat content variability in the Western Indian sector of the Southern Ocean during austral summer 2004. J. Mar. Syst. 63, 20–34. https://doi.org/10.1016/j.jmarsys.2006.04.009

Baars, O., Abouchami, W., Galer, S., Boye, M., Croot, P., 2014. Dissolved cadmium in the Southern Ocean: Distribution, speciation, and relation to phosphate. Limnol. Ocean. 59, 385–399. https://doi.org/10.4319/lo.2014.59.2.0385

Becquevort, S., Menon, P., Lancelot, C., 2000. Differences of the protozoan biomass and grazing during spring and summer in the Indian sector of the Southern Ocean. Polar Biol. 23, 309–320. https://doi.org/10.1007/s003000050450

Belkin, I.M., Gordon, A.L., 1996. Southern Ocean fronts from the Greewich meridion to Tasmania. J. Geophys. Res. 101, 3675–3696. https://doi.org/https://doi.org/10.1029/95JC02750

Boye, M., Wake, B.D., Lopez Garcia, P., Bown, J., Baker, A.R., Achterberg, E.P., 2012. Distributions of dissolved trace metals (Cd, Cu, Mn, Pb, Ag) in the southeastern Atlantic and the Southern Ocean. Biogeosciences 9, 3231–3246. https://doi.org/10.5194/bg-9-3231-2012

Boyle, E.A., Sclater, F., Edmond, J.M., 1976. On the marine geochemistry of cadmium. Nature 263, 42–44. https://doi.org/10.1038/263042a0

Broecker, W.S., 1991. The Great Ocean Conveyor. Oceanography 4, 79–89. https://doi.org/10.1016/s0262-4079(08)61198-7

Bruland, K.W., Franks, R.P., 1983. Mn, Ni, Cu, Zn and Cd in the Western North Atlantic. Trace Met. Sea Water. 9, 395–396. https://doi.org/10.1007/978-1-4757-6864-0_23

Bruland, K.W., Knauer, G.A., Martin, J.H., 1978. Cadmium in Northeast Pacific Waters. Limnol. Oceanogr. 23, 618–625. https://doi.org/https://doi.org/10.4319/lo.1978.23.4.0618

Butler, E.C. V, O'Sullivan, J.E., Watson, R.J., Bowie, A.R., Remenyi, T.A., Lannuzel, D., 2013. Trace metals Cd, Co, Cu, Ni, and Zn in waters of the subantarctic and Polar Frontal Zones south of Tasmania during the "SAZ-Sense" project. Mar. Chem. 148, 63–76. https://doi.org/10.1016/j.marchem.2012.10.005

Carter, L., McCave, I.N., Williams, M.J.M., 2009. Chapter 4: Circulation and Water Masses of the Southern Ocean: A Review, in: Florindo, F., Siegert, M. (Eds.), Developments in Earth and Environmental Sciences Series. Antarctic Climate Evolution. Elsevier, Amsterdam, pp. 85–114. https://doi.org/10.1016/S1571-9197(08)00004-9

Cloete, R., Loock, J.C., Mtshali, T., Fietz, S., Roychoudhury, A.N., 2019. Winter and summer distributions of Copper, Zinc and Nickel along the International GEOTRACES Section GIPY05: Insights into deep winter mixing. Chem. Geol. 511, 342–357. https://doi.org/10.1016/j.chemgeo.2018.10.023

Conway, T.M., John, S.G., 2015. Biogeochemical cycling of cadmium isotopes along a high-resolution

section through the North Atlantic Ocean. Geochim. Cosmochim. Acta 148, 269–283. https://doi.org/10.1016/j.gca.2014.09.032

Cullen, J.T., 2006. On the nonlinear relationship between dissolved cadmium and phosphate in the modern global ocean : Could chronic iron limitation of phytoplankton growth cause the kink ? Limnol. Oceanogr. 51, 1369–1380. https://doi.org/10.4319/lo.2006.51.3.1369

Cullen, J.T., Chase, Z., Coale, K.H., Fitzwater, S.E., Sherrell, R.M., 2003. Effect of iron limitation on the cadmium to phosphorous ratio of natural phytoplankton assemblages from the Southern Ocean. Limnol. Oceanogr. 48, 1079–1087. https://doi.org/10.4319/lo.2003.48.3.1079

Cullen, J.T., Sherrell, R.M., 2005. Effects of dissolved carbon dioxide, zinc, and manganese on the cadmium to phosphorus ratio in natural phytoplankton assemblages. Limnol. Oceanogr. 50, 1193–1204. https://doi.org/10.4319/lo.2005.50.4.1193

Cutter, G.A., Bruland, K.W., 2012. Rapid and noncontaminating sampling system for trace elements in global ocean surveys. Limnol. Oceanogr. Methods 10, 425–436. https://doi.org/10.4319/lom.2012.10.425

de Boyer Montégut, C., Madec, G., Fischer, A.S., Lazar, A., Iudicone, D., 2004. Mixed layer depth over the global ocean: An examination of profile data and a profile-based climatology. J. Geophys. Res. C Ocean. 109, 1–20. https://doi.org/10.1029/2004JC002378

de Jong, E., Vichi, M., Mehlmann, C.B., Eayrs, C., De Kock, W., Moldenhauer, M., Audh, R.R., 2018. Sea Ice conditions within the Antarctic Marginal Ice Zone in winter 2017, onboard the SA Agulhas II, in: PANGAEA. University of Cape Town. https://doi.org/https://doi.org/10.1594/PANGAEA.885211

Dong, S., Sprintall, J., Gille, S.T., Talley, L., 2008. Southern ocean mixed-layer depth from Argo float profiles. J. Geophys. Res. Ocean. 113, 1–12. https://doi.org/10.1029/2006JC004051

Duce, R.A., Liss, P.S., Merrill, J.T., Atlas, E.L., Hicks, B.B., Millertl, J.M., Prospero, J.M., Arimoto, R., Church, T.M., Ellis, W., Galloway, J.N., Hansen, L., Knap, A.H., Reinhardt, K.H., Soudine, A., Tsunogai, S., Wollast, R., Zhou, M., 1991. The atmospheric input of trace species to the world ocean. Global Biogeochem. Cycles 5, 193–259. https://doi.org/10.1029/91gb01778

Elderfield, H., Rickaby, R.E.M., 2000. Oceanic Cd/P ratio and nutrient utilization in the glacial Southern Ocean. Nature 405, 305–310. https://doi.org/10.1038/35012507

Ellwood, M.J., 2008. Wintertime trace metal (Zn, Cu, Ni, Cd, Pb and Co) and nutrient distributions in the Subantarctic Zone between 40-52°S; 155-160°E. Mar. Chem. 112, 107–117. https://doi.org/10.1016/j.marchem.2008.07.008

Ellwood, M.J., 2004. Zinc and cadmium speciation in subantarctic waters east of New Zealand. Mar. Chem. 87, 37–58. https://doi.org/10.1016/j.marchem.2004.01.005

Frew, R.D., Hunter, K.A., 1992. Influence of Southern Ocean waters on the cadmium-phosphate properties of the global ocean. Nature 360, 144–146. https://doi.org/10.1038/360144a0

Grasshoff, K., 1983. Automated chemical analysis, in: Grasshoff, K., Ernhardt, M., Kremling, K. (Eds.), Methods of Seawater Analysis. Verlag Chemie Weinhein, New York, pp. 263–289. https://doi.org/10.1002/9783527613984

Hayes, C.T., Black, E.E., Anderson, R.F., Baskaran, M., Buesseler, K.O., Charette, M.A., Cheng, H., Cochran, J.K., Edwards, R.L., Fitzgerald, P., Lam, P.J., Lu, Y., Morris, S.O., Ohnemus, D.C., Pavia, F.J., Stewart, G., Tang, Y., 2018. Flux of Particulate Elements in the North Atlantic Ocean Constrained by Multiple Radionuclides. Global Biogeochem. Cycles 32, 1738–1758. https://doi.org/10.1029/2018GB005994

Ho, T.-Y., Quigg, A., Finkel, Z. V., Milligan, A.J., Wyman, K., Falkowski, P.G., Morel, F.M.M., 2003. The elemental composition of some marine phytoplankton. J. Phycol. 39, 1145–1159.

https://doi.org/10.1111/j.0022-3646.2003.03-090.x

Hölemann, J.A., Schirmacher, M., Prange, A., 1999. Dissolved and Particulate Major and Trace Elements in Newly Formed Ice from the Laptev Sea (Transdrift III, October 1995), Land-Ocean Systems in the Siberian Arctic. Springer-Verlag, Berlin. https://doi.org/10.1007/978-3-642-60134-7_11

Janssen, D.J., Conway, T.M., John, S.G., Christian, J.R., Kramer, D.I., Pedersen, T.F., Cullen, J.T., 2014. Undocumented water column sink for cadmium in open ocean oxygen-deficient zones. Proc. Natl. Acad. Sci. U. S. A. 111, 6888–6893. https://doi.org/10.1073/pnas.1402388111

Janssen, D.J., Sieber, M., Ellwood, M.J., Conway, T.M., Barrett, P.M., Chen, X., de Souza, G.F., Hassler, C.S., Jaccard, S.L., 2020. Trace metal and nutrient dynamics across broad biogeochemical gradients in the Indian and Pacific sectors of the Southern Ocean. Mar. Chem. 221, 103773. https://doi.org/10.1016/j.marchem.2020.103773

John, S.G., Helgoe, J., Townsend, E., 2017. Biogeochemical cycling of Zn and Cd and their stable isotopes in the Eastern Tropical South Pacific. Mar. Chem. 201, 256–262. https://doi.org/10.1016/j.marchem.2017.06.001

Johnson, K.S., Plant, J.N., Dunne, J.P., Talley, L.D., Sarmiento, J.L., 2017. Annual nitrate drawdown observed by SOCCOM profiling floats and the relationship to annual net community production. J. Geophys. Res. Ocean. 122, 6668–6683. https://doi.org/10.1002/2017JC012839

Kuss, J., Kremling, K., 1999. Particulate trace element fluxes in the deep northeast Atlantic Ocean. Deep. Res. Part I Oceanogr. Res. Pap. 46, 149–169. https://doi.org/10.1016/S0967-0637(98)00059-4

Lam, P.J., Marchal, O., 2015. Insights into Particle Cycling from Thorium and Particle Data. Ann. Rev. Mar. Sci. 7, 159–184. https://doi.org/10.1146/annurev-marine-010814-015623

Lambelet, M., Rehkämper, M., van de Flierdt, T., Xue, Z., Kreissig, K., Coles, B., Porcelli, D., Andersson, P., 2013. Isotopic analysis of Cd in the mixing zone of Siberian rivers with the Arctic Ocean-New constraints on marine Cd cycling and the isotope composition of riverine Cd. Earth Planet. Sci. Lett. 361, 64–73. https://doi.org/10.1016/j.epsl.2012.11.034

Lane, E.S., Jang, K., Cullen, J.T., Maldonado, M.T., 2008. The interaction between inorganic iron and cadmium uptake in the marine diatom Thalassiosira oceanica. Limnol. Oceanogr. 53, 1784–1789. https://doi.org/10.4319/lo.2008.53.5.1784

Lane, E.S., Semeniuk, D.M., Strzepek, R.F., Cullen, J.T., Maldonado, M.T., 2009. Effects of iron limitation on intracellular cadmium of cultured phytoplankton: Implications for surface dissolved cadmium to phosphate ratios. Mar. Chem. 115, 155–162. https://doi.org/10.1016/j.marchem.2009.07.008

Lane, T.W., Morel, F.M.M., 2000. A biological function for cadmium in marine diatoms. Proc. Natl. Acad. Sci. U. S. A. 97, 4627–4631. https://doi.org/https://doi.org/10.1073/pnas.090091397

Lane, T.W., Saito, M.A., George, G.N., Prince, R.C., Pickering, I.J., Morel, F.M.M., 2005. A cadmium enzyme from a marine diatom. Nature 435, 42–42. https://doi.org/10.1038/435042a

Lee, J.G., Morel, F.M.M., 1995. Replacement of zinc by cadmium in marine phytoplankton. Mar. Ecol. Prog. Ser. 127, 305–309. https://doi.org/10.3354/meps127305

Lee, J.G., Roberts, S.B., Morel, F.M.M., 1995. Cadmium: A nutrient for the marine diatom Thalassiosira weissflogii. Limnol. Oceanogr. 40, 1056–1063. https://doi.org/10.4319/lo.1995.40.6.1056

Lee, J.M., Heller, M.I., Lam, P.J., 2018. Size distribution of particulate trace elements in the U.S. GEOTRACES Eastern Pacific Zonal Transect (GP16). Mar. Chem. 201, 108–123. https://doi.org/10.1016/j.marchem.2017.09.006

Marinov, I., Gnanadesikan, A., Toggweiler, J.R., Sarmiento, J.L., 2006. The Southern Ocean

biogeochemical divide. Nature 441, 964–967. https://doi.org/10.1038/nature04883

McCartney, M.S., 1977. Subantarctic Mode Water, in: Angel, M.V. (Ed.), A Voyage of Discovery. Oxford, Pergamon, pp. 103–119.

Middag, R., van Heuven, S.M.A.C., Bruland, K.W., de Baar, H.J.W., 2018. The relationship between cadmium and phosphate in the Atlantic Ocean unravelled. Earth Planet. Sci. Lett. 492, 79–88. https://doi.org/10.1016/j.epsl.2018.03.046

Minami, T., Konagaya, W., Zheng, L., Takano, S., Sasaki, M., Murata, R., Nakaguchi, Y., Sohrin, Y., 2015. An off-line automated preconcentration system with ethylenediaminetriacetate chelating resin for the determination of trace metals in seawater by high-resolution inductively coupled plasma mass spectrometry. Anal. Chim. Acta 854, 183–190. https://doi.org/10.1016/j.aca.2014.11.016

Mtshali, T.N., Horsten, N.R., Thomalla, S.J., Ryan-Keogh, T.J., Nicholson, S. -A., Roychoudhury, A.N., Bucciarelli, E., Sarthou, G., Tagliabue, A., Monteiro, P.M.S., 2019. Seasonal depletion of the dissolved iron reservoirs in the sub-Antarctic zone of the Southern Atlantic Ocean. Geophys. Res. Lett. 2018GL081355. https://doi.org/10.1029/2018GL081355

Orsi, A.H., Whitworth, T., Nowlin, W.D., 1995. On the meridional extent and fronts of the Antarctic Circumpolar Current. Deep. Res. Part I 42, 641–673. https://doi.org/10.1016/0967-0637(95)00021-W

Planquette, H., Sherrell, R.M., 2012. Sampling for particulate trace element determination using water sampling bottles: Methodology and comparison to in situ pumps. Limnol. Oceanogr. Methods 10, 367–388. https://doi.org/10.4319/lom.2012.10.367

Pollard, R.T., Lucas, M.I., Read, J.F., 2002. Physical controls on biogeochemical zonation in the Southern Ocean. Deep. Res. Part II Top. Stud. Oceanogr. 49, 3289–3305. https://doi.org/10.1016/S0967-0645(02)00084-X

Price, N.M., Morel, F.M.M., 1990. Cadmium and Cobalt substitution for Zn in a marine diatom. Nature 344, 658–660. https://doi.org/https://doi.org/10.1038/344658a0

Quay, P., Cullen, J., Landing, W., Morton, P., 2015. Processes controlling the distributions of Cd and PO4 in the ocean. Global Biogeochem. Cycles 29, 830–841. https://doi.org/10.1002/2014GB004998

Rembauville, M., Blain, S., Caparros, J., Salter, I., 2016. Particulate matter stoichiometry driven by microplankton community structure in summer in the Indian sector of the Southern Ocean. Limnol. Oceanogr. 61, 1301–1321. https://doi.org/10.1002/lno.10291

Sallée, J.B., Speer, K., Rintoul, S., Wijffels, S., 2010. Southern Ocean Thermocline Ventilation. J. Phys. Oceanogr. 40, 509–529. https://doi.org/10.1175/2009JPO4291.1

Sarmiento, J.L., Gruber, N., Brzezinski, M.A., Dunne, J.P., 2004. High-latitude controls of thermocline nutrients and low latitude biological productivity. Nature 427, 56–60. https://doi.org/10.1038/nature10605

Schlitzer, R., 2017. Ocean Data View. https://doi.org/10.1017/CBO9781107415324.004

Schlitzer, R., Anderson, R.F., Dodas, E.M., Lohan, M., Geibert, W., Tagliabue, A., Bowie, A., Jeandel, C., Maldonado, M.T., Landing, W.M., Cockwell, D., Abadie, C., Abouchami, W., Achterberg, E.P., Agather, A., Aguliar-Islas, A., van Aken, H.M., Andersen, M., Archer, C., Auro, M., de Baar, H.J., Baars, O., Baker, A.R., Bakker, K., Basak, C., Baskaran, M., Bates, N.R., Bauch, D., van Beek, P., Behrens, M.K., Black, E., Bluhm, K., Bopp, L., Bouman, H., Bowman, K., Bown, J., Boyd, P., Boye, M., Boyle, E.A., Branellec, P., Bridgestock, L., Brissebrat, G., Browning, T., Bruland, K.W., Brumsack, H.J., Brzezinski, M., Buck, C.S., Buck, K.N., Buesseler, K., Bull, A., Butler, E., Cai, P., Mor, P.C., Cardinal, D., Carlson, C., Carrasco, G., Casacuberta, N., Casciotti, K.L., Castrillejo, M., Chamizo, E., Chance, R., Charette, M.A., Chaves, J.E., Cheng, H., Chever, F., Christl, M., Church, T.M., Closset, I., Colman, A., Conway, T.M., Cossa, D., Croot, P., Cullen, J.T., Cutter, G.A., Daniels, C., Dehairs, F., Deng, F., Dieu, H.T., Duggan, B., Dulaquais, G., Dumousseaud, C., Echegoyen-Sanz, Y., Edwards,

R.L., Ellwood, M., Fahrbach, E., Fitzsimmons, J.N., Russell Flegal, A., Fleisher, M.Q., van de Flierdt, T., Frank, M., Friedrich, J., Fripiat, F., Fröllje, H., Galer, S.J.G., Gamo, T., Ganeshram, R.S., Garcia-Orellana, J., Garcia-Solsona, E., Gault-Ringold, M., George, E., Gerringa, L.J.A., Gilbert, M., Godoy, J.M., Goldstein, S.L., Gonzalez, S.R., Grissom, K., Hammerschmidt, C., Hartman, A., Hassler, C.S., Hathorne, E.C., Hatta, M., Hawco, N., Hayes, C.T., Heimbürger, L.E., Helgoe, J., Heller, M., Henderson, G.M., Henderson, P.B., van Heuven, S., Ho, P., Horner, T.J., Hsieh, Y. Te, Huang, K.F., Humphreys, M.P., Isshiki, K., Jacquot, J.E., Janssen, D.J., Jenkins, W.J., John, S., Jones, E.M., Jones, J.L., Kadko, D.C., Kayser, R., Kenna, T.C., Khondoker, R., Kim, T., Kipp, L., Klar, J.K., Klunder, M., Kretschmer, S., Kumamoto, Y., Laan, P., Labatut, M., Lacan, F., Lam, P.J., Lambelet, M., Lamborg, C.H., Le Moigne, F.A.C., Le Roy, E., Lechtenfeld, O.J., Lee, J.M., Lherminier, P., Little, S., López-Lora, M., Lu, Y., Masque, P., Mawji, E., Mcclain, C.R., Measures, C., Mehic, S., Barraqueta, J.L.M., van der Merwe, P., Middag, R., Mieruch, S., Milne, A., Minami, T., Moffett, J.W., Moncoiffe, G., Moore, W.S., Morris, P.J., Morton, P.L., Nakaguchi, Y., Nakayama, N., Niedermiller, J., Nishioka, J., Nishiuchi, A., Noble, A., Obata, H., Ober, S., Ohnemus, D.C., van Ooijen, J., O'Sullivan, J., Owens, S., Pahnke, K., Paul, M., Pavia, F., Pena, L.D., Peters, B., Planchon, F., Planquette, H., Pradoux, C., Puigcorbé, V., Quay, P., Queroue, F., Radic, A., Rauschenberg, S., Rehkämper, M., Rember, R., Remenyi, T., Resing, J.A., Rickli, J., Rigaud, S., Rijkenberg, M.J.A., Rintoul, S., Robinson, L.F., Roca-Martí, M., Rodellas, V., Roeske, T., Rolison, J.M., Rosenberg, M., Roshan, S., Rutgers van der Loeff, M.M., Ryabenko, E., Saito, M.A., Salt, L.A., Sanial, V., Sarthou, G., Schallenberg, C., Schauer, U., Scher, H., Schlosser, C., Schnetger, B., Scott, P., Sedwick, P.N., Semiletov, I., Shelley, R., Sherrell, R.M., Shiller, A.M., Sigman, D.M., Singh, S.K., Slagter, H.A., Slater, E., Smethie, W.M., Snaith, H., Sohrin, Y., Sohst, B., Sonke, J.E., Speich, S., Steinfeldt, R., Stewart, G., Stichel, T., Stirling, C.H., Stutsman, J., Swarr, G.J., Swift, J.H., Thomas, A., Thorne, K., Till, C.P., Till, R., Townsend, A.T., Townsend, E., Tuerena, R., Twining, B.S., Vance, D., Velazquez, S., Venchiarutti, C., Villa-Alfageme, M., Vivancos, S.M., Voelker, A.H.L., Wake, B., Warner, M.J., Watson, R., van Weerlee, E., Alexandra Weigand, M., Weinstein, Y., Weiss, D., Wisotzki, A., Woodward, E.M.S., Wu, J., Wu, Y., Wuttig, K., Wyatt, N., Xiang, Y., Xie, R.C., Xue, Z., Yoshikawa, H., Zhang, J., Zhang, P., Zhao, Y., Zheng, L., Zheng, X.Y., Zieringer, M., Zimmer, L.A., Ziveri, P., Zunino, P., Zurbrick, C., 2018. The GEOTRACES Intermediate Data Product 2017. Chem. Geol. 493, 210–223. https://doi.org/10.1016/j.chemgeo.2018.05.040

Sieber, M., Conway, T.M., Souza, G.F. De, Hassler, C.S., Ellwood, M.J., Vance, D., 2019. High-resolution Cd isotope systematics in multiple zones of the Southern Ocean from the Antarctic Circumnavigation Expedition. Earth Planet. Sci. Lett. 527, 115799. https://doi.org/10.1016/j.epsl.2019.115799

Sunda, W.G., Huntsman, S.A., 2000. Effect of Zn, Mn, and Fe on Cd accumulation in phytoplankton: Implications for oceanic Cd cycling. Limnol. Oceanogr. 45, 1501–1516. https://doi.org/10.4319/lo.2000.45.7.1501

Swart, S., Thomalla, S.J., Monteiro, P.M.S., 2015. The seasonal cycle of mixed layer dynamics and phytoplankton biomass in the Sub-Antarctic Zone: A high-resolution glider experiment. J. Mar. Syst. 147, 103–115. https://doi.org/10.1016/j.jmarsys.2014.06.002

Tagliabue, A., Sallée, J.B., Bowie, A.R., Lévy, M., Swart, S., Boyd, P.W., 2014. Surface-water iron supplies in the Southern Ocean sustained by deep winter mixing. Nat. Geosci. 7, 314–320. https://doi.org/10.1038/ngeo2101

Thi Dieu Vu, H., Sohrin, Y., 2013. Diverse stoichiometry of dissolved trace metals in the Indian Ocean. Sci. Rep. 3, 1–5. https://doi.org/10.1038/srep01745

Turekian, K.K., 1977. The fate of metals in the oceans. Geochim. Cosmochim. Acta 41, 1139–1144. https://doi.org/10.1016/0016-7037(77)90109-0

Twining, B.S., Baines, S.B., 2013. The trace metal composition of marine phytoplankton. Ann. Rev. Mar. Sci. 5, 191–215. https://doi.org/10.1146/annurev-marine-121211-172322

Weir, I., Fawcett, S., Smith, S., Walker, D., Bornman, T., Fietz, S., in revision. Winter biogenic silica

and diatom distribution in the Indian Sector of the Southern Ocean. Deep Sea Res. Part I Oceanogr. Res. Pap.

WOCE Global Data Resource, 2018. Natl. Oceanogr. Data Cent. Home Page. URL https://www.nodc.noaa.gov/woce/wdiu/

Xie, R.C., Galer, S.J.G., Abouchami, W., Frank, M., 2018. Limited impact of eolian and riverine sources on the biogeochemical cycling of Cd in the tropical Atlantic. Chem. Geol. 511, 371–379. https://doi.org/10.1016/j.chemgeo.2018.10.018

Xie, R.C., Galer, S.J.G., Abouchami, W., Rijkenberg, M.J.A., De Jong, J., De Baar, H.J.W., Andreae, M.O., 2015. The cadmium-phosphate relationship in the western South Atlantic - The importance of mode and intermediate waters on the global systematics. Mar. Chem. 177, 110–123. https://doi.org/10.1016/j.marchem.2015.06.011

Xu, Y., Tang, D., Shaked, Y., Morel, F.M.M., 2007. Zinc, cadmium, and cobalt interreplacement and relative use efficiencies in the coccolithophore Emiliania huxleyi. Limnol. Oceanogr. 52, 2294–2305. https://doi.org/10.2307/4502377

Chapter 4

Winter dissolved and particulate zinc in the Indian Sector of the Southern Ocean: distribution and relation to major nutrients (GEOTRACES GIpr07 transect)

A presentation of the prepared research paper

This research manuscript has been prepared for submission to Marine Chemistry. I am the lead author of the manuscript. J.C. Loock, N.R. van Horsten, J-L. Menzel Barraqueta, S. Fietz, T.N. Mtshali, H. Planquette, M. I. Garcia-Ibanez and A.N. Roychoudhury are co-authors.

This manuscript contributes the first winter measurements of dissolved zinc (dZn) and particulate zinc (pZn) along the 30°E longitude in the Indian sector of the Southern Ocean. Along with major nutrient data, phosphate (PO_4), phosphorous (P), silicic acid ($Si(OH)_4$) and biogenic silica (bSi), this paper investigates Zn biogeochemical cycling in a season generally considered to be biologically dormant. As a result, we attempt to gain a better understanding of Zn cycling over seasonal timescales.

I was responsible for the collection and analysis of seawater samples for dZn, data processing and writing of the manuscript.

Winter dissolved and particulate zinc in the Indian sector of the Southern Ocean: Distribution and relation to major nutrients (GEOTRACES GIpr07 transect)

R. Cloete[a], J.C. Loock[a], N.R. van Horsten[a,b,c], J-L. Menzel Barraqueta[a], S. Fietz[a], T.N. Mtshali[a,b], H. Planquette[c], M. I. Garcia-Ibanez[d], A.N. Roychoudhury[a, *]

[a]Centre for Trace Metal and Experimental Biogeochemistry (TracEx), Department of Earth Sciences, Stellenbosch University, Stellenbosch 7600, South Africa.

[b]Southern Ocean Carbon and Climate Observatory, Natural Resources and Environment, CSIR, Stellenbosch, 7600, South Africa.

[c]CNRS, Univ. Brest, IRD, Ifremer, Laboratoire des Sciences de l'environnement marin, Technopôle Brest-Iroise, Plouzané, France.

[d]School of Environmental Sciences, University of East Anglia, Norwich Research Park, Norwich, NR4 7TJ

Abstract

First winter measurements of dissolved zinc (dZn) and particulate zinc (pZn) are presented from seven locations, between 41 and 58°S, occupied along the 30°E longitude in the Indian Sector of the Southern Ocean. This unique spatial and seasonal dataset provided the opportunity to investigate Zn biogeochemical cycling in a region which is extremely data scarce and during a period when conditions are unfavourable for phytoplankton growth. Our results support an important biological control for Zn cycling in the upper water column, albeit weaker than in summer. For example, winter dZn in the surface mixed layer (SML) was between 0.15 and 1.46 nmol kg^{-1} higher compared to previous summer measurements reflecting reduced biological uptake by phytoplankton as well as increased recharge through deep winter mixing. Furthermore, there were distinct biologically driven changes in Zn cycling across the transect. In the Antarctic Zone (AAZ), high uptake rates of dZn relative to phosphate (PO_4) in the SML ($dZn/PO_{4\ SML}$ = 6.36 ± 1.66 nmol μmol^{-1}), characteristic of Southern Ocean diatoms, were reflected by high ratios of pZn to phosphorous (P) in the SML (pZn/P_{SML} = 4.78 ± 1.64 pmol $nmol^{-1}$). High SML concentrations of dZn in the AAZ (2.66 – 3.66 nmol kg^{-1}) were maintained through upwelling of Upper Circumpolar Deep Water (UCDW) preferentially enriched in dZn relative to PO_4 as a result of diatom export to the remineralisation zone (pZn/P_{remin} = 4.90 pmol $nmol^{-1}$). Because of their requirement for $Si(OH)_4$, diatoms play a major role in the observed coupling between dZn and $Si(OH)_4$ [dZn (nmol kg^{-1}) = 0.064 $Si(OH)_4$ + 0.69; r^2 = 0.92; n = 120] and pZn and biogenic silica (bSi) [pZn (pmol kg^{-1}) = 131 bSi (µmol kg^{-1}) + 36; r^2 = 0.75; n = 30]. In the region of upwelling, the northward flow of Antarctic Surface Waters (AASW) depleted in dZn (and $Si(OH)_4$) relative to PO_4, sets the lower $dZn/PO_{4\ SML}$ (0.90 – 1.91 nmol μmol^{-1}) and pZn/P_{SML} (1.28 – 2.35 pmol $nmol^{-1}$) ratios observed in surface waters north of the AAZ. As these waters are the source of Sub-

Antarctic Mode Waters (SAMW), the northward flow of this dZn and $Si(OH)_4$ deficient water mass has potential implications for Zn cycling in the global low latitude ocean (Vance et al., 2017). In the deep waters, elevated concentrations of dZn and $Si(OH)_4$ below 3000 m in the AAZ may reflect nutrient accumulation in waters whose northward flow is inhibited by the Indian mid-Ocean ridge.

1. Introduction

Zinc (Zn) is an essential trace metal micronutrient for marine phytoplankton and its availability in the surface ocean has potential implications for biological productivity which, in turn, influences the biogeochemistry of non-metals such as carbon and nitrogen (Morel et al., 1991; Morel and Price, 2003). While zinc is a critical component in numerous enzymes involved in metabolism, perhaps the most important are the metalloproteins carbonic anhydrase and alkaline phosphatase, which enable efficient carbon fixation and the uptake of dissolved organic phosphorous respectively (Shaked et al., 2006; Twining and Baines, 2013). However, high concentrations of dissolved Zn (dZn; > 10 nmol kg^{-1}), which can be found in estuarine and coastal upwelling settings, are known to be toxic to phytoplankton (Sunda and Huntsman, 1998, 1996). On the other hand, low dZn concentrations (< 0.01 nmol kg^{-1}), typical of open ocean settings, could be potentially bio-limiting (Brand et al., 1983).

Owing to an increase in reliable data in the last few decades, and particularly since the onset of the GEOTRACES era (Anderson, 2020), our understanding of the processes controlling the exchange between dissolved and particulate trace metal phases are better constrained. In the surface ocean, assimilation of dZn by phytoplankton is the primary process resulting in the exchange between inorganic dZn (< 0.2µm pore size filtered seawater) and organic particulate zinc (pZn; > 0.45µm pore size filter) phases. Subsequent processes, e.g. zooplankton grazing, result in the formation of larger particles which either sink and contribute to the vertical export of pZn, or disaggregate (via remineralisation, desorption and dissolution) back to smaller particles contributing a source of dZn to the surface ocean (Lam and Marchal, 2015). Scavenging (or adsorption) of dZn onto organic particle surfaces may enhance export of Zn through formation of more dense and more rapidly sinking particulate phases (John and Conway, 2014). Similarly, authigenic Zn sulphide precipitation has been suggested in low oxygen environments with implications for pZn export in localised regions (Conway and John, 2015; Janssen and Cullen, 2015). As a result of the interplay between uptake and regeneration processes, an increase in the dZn pool typically leads to a decrease in the pZn pool. However, the exchange between dissolved and particulate phases is not necessarily proportional considering that biological and physical processes lead to differences in their residence times i.e. years to thousands of years for dissolved phases compared with days to months for particulate phases (Lam and Marchal, 2015).

Comparing the distribution of zinc to those of the major nutrients, silicic acid ($Si(OH)_4$) and phosphate (PO_4), has proven a useful tool in constraining processes governing Zn distribution. For example, there is a tight correlation between global dZn and $Si(OH)_4$ distributions with water column concentrations of both elements characterised by surface depletion and enrichments at depth (Bruland, 1980; Ellwood,

2008; Janssen et al., 2020, Middag et al., 2019; Wyatt et al., 2014; Zhao et al., 2014). The depths at which dZn and $Si(OH)_4$ reach their greatest enrichment are deeper compared to the intermediate depth maxima displayed by global PO_4 distributions (Bruland, 1980; Middag et al., 2018; Quay et al., 2015). The relationship between dZn, $Si(OH)_4$ and PO_4 appears at odds considering that Zn and organic phosphorous (P) are associated with the organic matter of phytoplankton cells (Twining et al., 2004, 2003), while a negligible amount of Zn is incorporated into the siliceous frustules of diatoms (Ellwood and Hunter, 2000). It would therefore be expected that dZn, like PO_4, is regenerated at shallower depths from the rapidly dissolvable organic material and that there is no direct mechanism linking dZn and $Si(OH)_4$. Recently, two hypotheses have sought to explain this phenomenon. The first suggests that the coupling of dZn and $Si(OH)_4$ is a consequence of the natural interaction between ocean biogeochemistry and physical circulation through the Southern Ocean hub (Vance et al., 2017). In sum, Antarctic surface waters are preferentially stripped of dZn and $Si(OH)_4$ relative to PO_4, consistent with the known uptake stoichiometry of diatoms in this region. Physical circulation dictates that the dZn and $Si(OH)_4$ depleted surface waters are transported to the low latitude thermocline thereby setting the low dZn, low $Si(OH)_4$ biogeochemical signature throughout much of the upper ocean (Sarmiento et al., 2004). Furthermore, the export of diatom cells beneath the winter mixed layer traps the majority of dZn and $Si(OH)_4$ in the deep ocean despite variances in their regeneration length scales. The second hypothesis adopts a more mechanistic approach whereby a secondary, deeper dZn source is inferred. The reversible scavenging model suggests that dZn is released at shallow depths from decomposing organic particles at the same rate as PO_4, however dZn is then reversibly scavenged (adsorbed) onto sinking organic particles resulting in its enhanced flux, relative to non-scavenged elements like PO_4, to the deep ocean (John and Conway, 2014; Weber et al., 2018).

Another aspect of Zn cycling requiring attention relates to seasonality. To date, the vast majority of Zn data represent spring/summer seasons, when conditions (e.g. increased light levels, shallow mixed layers) are favourable for phytoplankton growth. However, little is known about Zn cycling during winter months with only two studies reporting winter Zn data for the Atlantic (Cloete et al., 2019) and Pacific (Ellwood, 2008) sectors of the Southern Ocean. Of particular interest is winter deep mixing, a seasonally constrained physical supply mechanism whereby deeper mixing in winter compared to summer may tap into to nutrient rich sub-surface water masses found below the summer stratified layer. Resupply of nutrients through deep winter mixing may be critical in initiating and sustaining phytoplankton growth over the subsequent spring and summer seasons, as shown previously for iron (Tagliabue et al., 2014). Furthermore, Sub-Antarctic Mode Water (SAMW), formed in the deep winter mixed layers of the Sub Antarctic Zone, is the primary communication channel between the Southern Ocean and the global low latitude upper ocean (Broecker, 1991). Therefore, investigating Zn cycling in the source region for SAMW may have important and far reaching implications as shown previously for Zn (Vance et al., 2017), $Si(OH)_4$ (Sarmiento et al., 2004) and cadmium (Middag et al., 2018; Xie et

al., 2015). This study aims to address these knowledge gaps by contributing the first winter measurements of dZn and pZn from the Indian sector of the Southern Ocean (WOCE meridional section IO6S; GEOTRACES section GIpr07).

2. Methods

2.1. Sample collection

Seawater samples were collected on-board the SA Agulhas II polar research vessel during the 2017 Winter Cruise (28/06/2017 – 13/07/2017). The transect followed the World Ocean Circulation Experiment (WOCE) I06 transect along the 30°E meridian in the Indian sector of the Southern Ocean (Figure 1). Of the nine planned stations, seven, consisting of four deep (< 4500 m) and three shallow stations (> 1500 m) , were sampled between 41°S and 58°30'S allowing observations to be investigated over important frontal systems and in different water masses. Two stations (IO03 and IO09) were cancelled for trace metal sampling due to intense storms present at the time of station occupation.

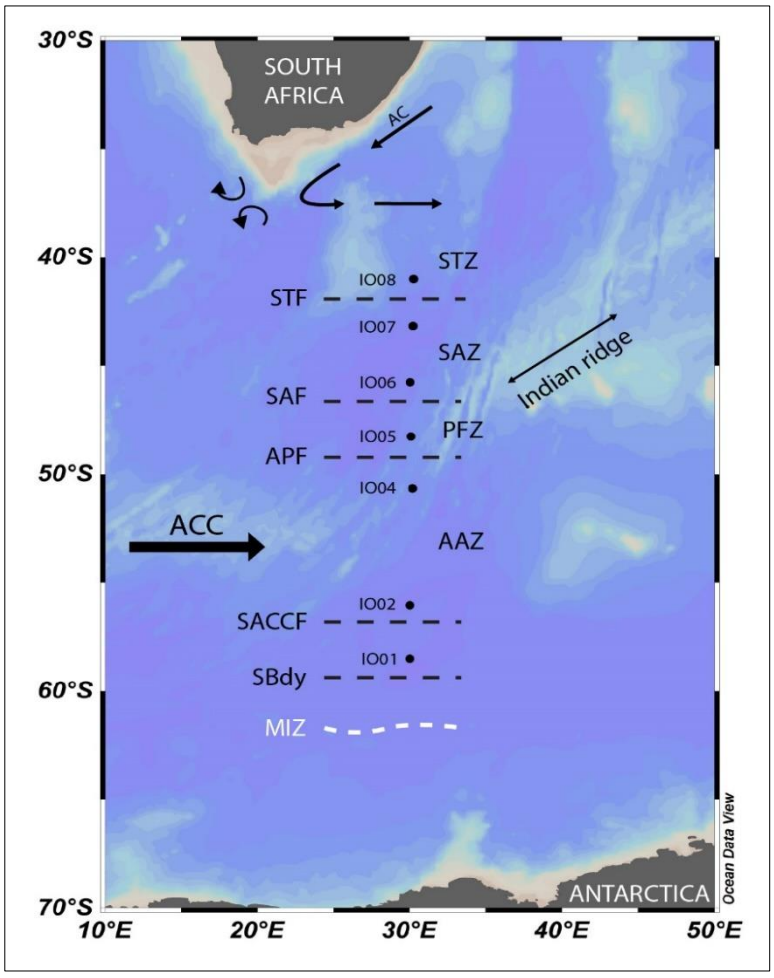

Figure 1. *Sample station locations during the 2017 Winter Cruise along the GEOTRACES GIpr07 transect (30°E longitude). Positions of the frontal systems intersected, and corresponding oceanic zones, are shown as well as the main surface currents. Acronyms in alphabetical order are as follows; AAZ: Antarctic Zone; AC: Agulhas Current; ACC: Antarctic Circumpolar Current; APF: Antarctic Polar Front; PFZ: Polar Frontal Zone; SACCF: Southern Antarctic Circumpolar Current Front; SAZ: Sub-Antarctic Zone; SAF: Sub-Antarctic Front; SBdy: Southern Boundary; STF: Sub-Tropical Front; STZ: Sub-Tropical Zone. Figure constructed using Ocean Data View (ODV; Schlitzer, 2017).*

A vertical profile sampling method, using 24 internally Teflon-coated polyvinyl chloride (PVC) 12l GO-FLO sampling bottles (General Oceanics), was employed at all sampling stations. Seawater samples were collected following a strict 'trace metal clean' protocol using a GEOTRACES compliant CTD (conductivity, temperature and depth) recorder and rosette (Cutter and Bruland, 2012). A Kevlar hydrowire with internal signal cables allowed for the transfer of data between the CTD and the on-board control room. The GO-FLO bottles were triggered at pre-determined depths during the up cast. Directly upon recovery of the rosette, the GO-FLO bottles were covered in a PVC plastic wrap in addition to their ends being covered in plastic (PVC) shower caps, and were transported into a class 100 clean lab for sub-sampling. Samples for dissolved trace metal determination were collected in 125 ml acid-cleaned low density polyethylene (LDPE, Nalgene) bottles after online filtration through 0.2 µm Sartobran filters and under slight N_2 (99.9999% N_2, BIP technology) overpressure. Samples were acidified (pH = 1.7) on-board under a laminar flowhood using hydrochloric acid (Ultrapur HCL, Merck) and stored for later analysis. Thereafter, previously cleaned filters (25mm diameter, Supor, 0.45µm pore size) were mounted on acid-washed swinnex (Millipore) filter holders which were then attached to the GO-FLO spigots and used for filtration (recorded between 5 - 10 L) of samples for particulate trace metal determination (Planquette and Sherrell, 2012). After filtration, filter holders were removed and disassembled before the sampled filter was transferred to an acid-washed polystyrene Petri-dish using clean plastic forceps. Sampled filters were subsequently frozen at -20°C for transport back to land. All handling of filters, filter holders and samples was done under a laminar flow hood.

2.2. Dissolved Zn determination

2.2.1. sea*FAST* and ICP-MS

Seawater samples were first preconcentrated by Solid Phase Extraction (SPE) on a sea*FAST* SC-4 DX module prior to quantification by Inductively Coupled Plasma Mass Spectrometry (ICP-MS, Agilent 7900). During preconcentration, 10 ml of seawater was buffered to a pH of 6.0 ± 0.2 with an ammonium acetate buffer. The buffered solution was then loaded onto a column containing a high affinity metal chelating resin (Nobias PA1) where the Zn ions were bound to the resin and separated from the seawater matrix elements e.g. Na, Mg and Cl which passed through the column. The Zn ions were subsequently eluted from the resin column in low volumes (250 µl) resulting in a preconcentration factor of 40. After preconcentration, the analyte was introduced into the ICP-MS using a low self-aspirating perfluoroalkoxy (PFA) nebulizer with a flow rate of 0.2 µl min^{-1}. Isotopes of ^{66}Zn were measured using the instruments Octopole Reaction System (ORS) in helium (He) collision mode to eliminate plasma and matrix based interferences although the latter was extensively reduced by the seaFAST matrix removal system. Online internal standard addition for drift correction was not possible using the self-aspirating nebulizer. Instead, instrument drift was monitored by running a multi-element standard (MES; verified by Inorganic Ventures) calibration standard every 6 samples. Where drift exceeded 5%

relative to the starting concentration of the MES for a specific element, a drift correction was applied using equation 1:

eq. 1. $2*Conc_{MES\_start}/ (Conc_{MES\_a} + Conc_{MES\_b})*Conc_{Sample}$

where *a* and *b* are the MES before and after each set of 6 samples.

2.2.2. Accuracy and precision

The accuracy of the dZn analyses was verified by way of comparison with GEOTRACES reference seawater (https://www.geotraces.org/standards-and-reference-materials/) and NASS-7 certified reference material (Table 1). For the GEOTRACES SAFe D2, GSC and GSP reference seawater, our dZn values were within analytical uncertainty confirming the methods accuracy over oceanographically relevant concentrations. For the NASS-7, our dZn value was in good agreement with the certified value.To monitor ICP-MS precision, the Winter Indian Southern Ocean Seawater (WISOS) internal reference seawater was placed in the analysis sequence and results compared against each other and the calibrated mean (Table 1). The WISOS reference seawater (0.2 µm filtered seawater) was collected from surface water at 55°S; 28°E during the 2017 Winter Cruise. The calibrated mean concentration (9.67 ± 0.23 nmol kg^{-1}) was established by replicate analysis (n = 10) of the WISOS in conjunction with the SAFe and NASS-7 reference materials. The in-sequence analysis of the WISOS (n > 30) yielded a value of 9.63 ± 0.24 nmol kg^{-1} confirming the methods precision.

2.2.3. Blanks and limits of detection

The instrument (ICP-MS) blank was quantified by introducing a solution of un-preconcentrated 2% HNO_3, identical to the seaFAST eluent, in ultra-pure deionized water. The instrument blank was 0.07 nmol kg^{-1} for Zn (Table 1). To determine the blank contribution from the method, a solution of HNO_3 (ultrapur, Merck) diluted to 2% with ultra-pure deionized water, the same composition as the eluent used in sample pre-concentration, was analysed. The blank was subjected to the same pre-concentration procedure as the seawater samples. The method blank was 0.09 ± 0.02 nmol kg^{-1} and was subtracted from sample values. The limit of detection (LOD), calculated as 3 times the standard deviation of the preconcentrated blank, was 0.02 nmol kg^{-1}.

2.2.4. Data processing

Samples for dZn was analysed in duplicate. The final values represent the mean of duplicate measurements. In cases where the percentage relative standard deviation (%RSD) between the duplicate measurements was > 10% (n = 13), one of the values was deemed a suspected outlier and not used further. This was determined by curve fitting the data points based on the values above (shallower depth) and below (deeper depth) the suspect value as well as by comparison with other parameters (salinity, temperature, and nutrients) measured from the same GO-FLO bottle.

Table 1. *Results from the ICP-MS analysis of GEOTRACES SAFE D2, GSC and GSP seawater reference materials (https://www.geotraces.org/standards-and-reference-materials/), NASS-7 certified seawater reference material and our own WISOS internal reference seawater are compared with respective consensus values. Consensus values for SAFe D2 as of 2013 and GSC and GSP as of 2019. Certified values for NASS-7 as of 2018. Calibrated mean values for WISOS calculated by repeat analysis (n > 10) of a large volume surface seawater sample collected from 55°S; 28°E. Instrument and method blanks as well as ICP-MS detection limits are also shown.*

	dZn nmol kg^{-1}
SAFe D2	
Consensus	7.43 ± 0.25
TracEx (n = 5)	7.23 ± 0.25
TracEx %RSD	3.46
GSC	
Consensus	1.40 ± 0.10
TracEx (n = 5)	1.41 ± 0.10
TracEx %RSD	7.09
GSP	
Consensus	0.03 ± 0.05
TracEx (n = 5)	0.10 ± 0.02
TracEx %RSD	20.00
NASS-7	
Certified	6.27 ± 1.22
TracEx (n = 5)	6.59 ± 0.07
TracEx %RSD	1.06
WISOS reference seawater	
TracEx Calibration (n = 10)	9.67 ± 0.23
TracEx (n >30)	9.63 ± 0.24
TracEx %RSD	2.49
Blanks	
Instrument (n = 5)	0.07 ± 0.01
Method (n = 5)	0.09 ± 0.01
LOD	0.02

2.3. Phosphate and silicic acid determination

Macronutrient concentrations were described previously (Weir et al., in revision). Here, we briefly summarise the analytical methods. Seawater samples for phosphate (PO_4) and silicic acid ($Si(OH)_4$) analysis were collected from GO-FLO bottles, filtered immediately after collection using a 0.2 µm pore size syringe filter into 50 mL Falcon® tubes and frozen at -20°C. Macronutrient analysis was done at the Marine Biogeochemistry Laboratory at the University of Cape Town (MBL-UCT). PO_4 was determined manually by colorimetric method (Grasshoff, 1983) with an analytical error of ± 0.06 µmol kg^{-1}. $Si(OH)_4$ was analysed using a Lachat Quick-Chem flow injection analyser (Wolters, 2002) with an analytical error of ± 0.2 µmol kg^{-1}.

2.4. Particulate Zn and P determination

Samples for particulate trace metals were analysed at the Université de Bretagne Occidentale (UBO). Details of the analytical procedure have been previously described (Planquette and Sherrell, 2012) and are presented briefly here. Collected filters were digested by total acid reflux digestion in an equal part mixture of 8.0M HNO_3 and 2.9M HF (both Fisher Optima grade), in 15 ml trace-metal clean Teflon PFA vials (Savillex®), on a hot plate at ~110°C for 4 hours, under a fume hood. To eliminate HF, 100 µl of concentrated ultra pure HNO_3 was added to the vials and evaporated to near dryness. Samples were then taken up in a 3.0 mL solution of 0.080 M HNO_3, spiked with 1 µg L^{-1} indium (In) to monitor instrumental drift, heated at 60°C for 1 hour to ensure complete redissolution of any dried residue and then transferred into acid-cleaned 15 ml PP tubes (Corning®) before analysis. Trace element analysis was performed using a Sector Field Inductively coupled Plasma Mass Spectrometer (SF-ICP-MS; Element XRTM ThermoFisher Scientific) at the Pole Spectrométrie Océans. Three certified reference materials (PACS 3, MESS 4 and BCR 414) were processed as samples and analysed for pZn and P to assess the accuracy of the methodology (Table 2). The certified reference materials yielded mean percentage recoveries of 108%, 100% and 97% for pZn and 100%, 106% and 95 % for P (PACS 3, MESS 4 and BCR 414, respectively). Filter blanks were determined by digesting and analysing an acid washed filter. The detection limits, defined as three times the standard deviation of the blanks, for pZn and P were 2.82 pmol kg^{-1} and 0.03 nmol kg^{-1}, respectively (n = 5).

Table 2. *Results for pZn and P from the ICP-MS analysis of PACS 3, MESS 4 and BCR 414 certified references materials. Filter blanks as well as ICP-MS limit of detection are also shown.*

	pZn *mmol kg^{-1}*	**P** *mmol kg^{-1}*
PACS 3		
Certified	5.80 ± 0.23	29.38 ± 2.91
Measured	6.24 ± 0.72	29.41 ± 0.31
% recovery	108	100
MESS 4		
Certified	2.25 ± 0.09	33.58 ± 5.17
Measured	2.25 ± 0.59	35.58 ± 0.51
% recovery	100	106
BCR 414		
Certified	1.71 ± 0.04	428.84 ± 51.20
Measured	1.66 ± 0.21	409.34 ± 52.14
% recovery	97	95
Filter Blank	1.47 pmol kg^{-1}	0.08 nmol kg^{-1}
Limit of Detection	2.82 pmol kg^{-1}	0.03 nmol kg^{-1}

2.5. Biogenic silica

Biogenic silica (bSi) concentrations were described previously (Weir et al., in revision). Here, we briefly summarise the analytical method. Seawater (2 L) was filtered through a 47 mm diameter, 0.8 µm pore size cellulose acetate membrane filter (Sartorius Stedim Biotech). The filter was then folded, placed in a plastic petri dish and oven-dried for 12 hrs at 60°C. Filters were subsequently analysed for bSi using a NaOH digestion method and a Genesys 10-S UV spectrophotomometer. The instruments detection limit was 0.19 µmol kg^{-1} and blank interferences (0.04 ± 0.002 µmol kg^{-1}) were subtracted from final reported bSi concentrations. For all samples, the lithogenic fraction was found to be below the detection limit of the hydrofluoric acid digestion method (1.8 µmol kg^{-1}).

2.6. extended optimum multiparameter (eOMP) analysis

An extended optimum multiparameter (eOMP) analysis (Karstensen and Tomczak, 1998) was used to solve the water mass structure of the section. Briefly, OMP analyses consider that the observed physicochemical properties of a given water sample can be formulated as a linear combination of a finite number of water masses represented by the so-called source water types (SWTs; Tomczak, 1999). The SWTs are points in the n-dimensional parameter space, where n is the number of properties that characterize SWTs. In this work, the SWTs are characterized by potential temperature, salinity, oxygen, nitrate, phosphate and silicic acid (Table 3). Once the SWTs and their physicochemical properties are defined, the goal of an OMP analysis is to find the fractions of each SWT (X_i) in each water sample and does so by a least-square method constrained to be positive definite:

$$d = G * X_i + \Delta O_{2bio}/R + \varepsilon$$

where d is the observed property in a water sample, G is the matrix containing the properties defining the SWTs, Xi is the relative contributions of each SWT to the sample, ΔO_{2bio} accounts for the changes in oxygen due to the synthesis and/or remineralisation of the organic matter, R are the Redfield-like stoichiometric ratios and ε is the residual. In this study we used an R of 12 for silicic acid (Perez et al., 1993; Castro et al., 1998), 175 for phosphate and 10.5 for nitrate (Takahashi et al., 1985; Anderson and Sarmiento, 1994). The OMP analysis was restricted to water samples with pressure >1000 dbar. The eOMP analysis was reliable since it explained 99% of the changes in the conservative tracers.

The X_is strongly depend on the characterization of the SWTs (Tomczak, 1981), the choice of which is a key step of the analysis. In this work, we selected the properties for Upper Circumpolar Deep Water (UCDW) from Carter et al. (2014); and those of CDW, North Atlantic Deep Water (NADW), and Antarctic Bottom Water (AABW) from Liu and Tanhua (2019).

Table 3. *Properties characterizing the source water types (SWTs[a]) considered in this study. The square of correlation coefficients (R^2) between the observed and estimated properties are also given.*

	Potential temperature (°C)	Salinity PSU	O_2^0 (µmol kg^{-1}) [b]	NO_3^0 (µmol kg^{-1}) [b]	PO_4^0 (µmol kg^{-1}) [b]	SiO_4^0 (µmol kg^{-1}) [b]
UCDW	3.67	34.31	319.00	20.67	1.52	36.51
CDW	0.40	34.68	345.17	19.99	1.50	115.18
NADW	2.93	34.91	323.28	12.48	0.84	13.21
AABW	-0.47	34.66	353.12	21.92	1.62	124.91
R^2	0.99	0.99	0.97	0.91	0.82	0.93

[a] uCDW: upper Circumpolar Deep Water; CDW: Circumpolar Deep Water; NADW: North Atlantic Deep Water; and AABW: Antarctic Bottom Water.
[b] Oxygen (O_2^0), nitrate (NO_3^0), phosphate (PO_4^0) and silicic acid (SiO_4^0) represent preformed values; note that O_2 represent saturation.

3. Results

3.1. Description of the study area

3.1.1. Frontal positions

The Southern Ocean encircles Antarctica and is dominated by the uninterrupted, eastward flowing Antarctic Circumpolar Current (ACC). Another major current, the Agulhas current (AC) flows southward along the east coast Africa before retroflecting at the southern tip of the continent due to shear interactions with the ACC. A number of important oceanographic fronts run parallel with the ACC and divide the Southern Ocean into distinct biogeochemical zones (Figure 1). Frontal positions were determined were determined previously (Weir et al., in revision) following temperature, salinity and oxygen criteria outlined in several sources (Belkin and Gordon, 1996; Orsi et al., 1995; Pollard et al., 2002). These parameters were measured using a Seabird 9+ conductivity-temperature-depth (CTD) recorder attached to the rosette. To the north of the transect, the Sub-Tropical Front (STF) at 42.4°S separated the Sub-Tropical Zone (STZ) to the north from the Sub-Antarctic Zone (SAZ) to the south. Likewise, the Sub-Antarctic Front (SAF) at 46.2°S separated the SAZ in the north from the Polar Frontal Zone (PFZ) to the south which, in turn, was bounded in the south by the Antarctic Polar front (APF) at 49.3°S. Further south, the Antarctic Zone (AAZ) extended until the Southern Boundary (SBdy) at 58.5°S, incorporating the Southern Antarctic Circumpolar Current Front (SACCF) at 56.5°S. The Marginal Ice Zone (MIZ), defined as 30% ice cover, was encountered at 61.7°S (de Jong et al., 2018).

3.1.2. Water mass characterisation

The hydrography of the Southern Ocean is largely defined by the upwelling and ventilation of deep waters at the higher latitudes (Orsi et al., 1995). As a consequence of wind driven forcing, nutrient rich Upper Circumpolar Deepwater (UCDW) upwells south of the APF (Figure 2). Near the surface, a portion of the upwelled water moves south, as Antarctic Surface Water (AASW; < 5.0°C; Anilkumar et al., 2006), where continued cooling and sea-ice formation increase water density initiating subduction

and eventual formation of cold (θ = ~ 0°C) Antarctic Bottom Water (AABW) which flows northward along the basin floor (Orsi et al., 1999). In the upwelling region, the remaining portion of upwelled UCDW flows northward via Ekman drift. Here, surface waters warm rapidly toward the north forming Sub-Antarctic Surface Water (SASW; 5 - 9°C) and Sub-Tropical Surface Water (STSW; 14 - 24°C; Anilkumar et al., 2006). Subducting northward below the surface water masses were Antarctic Intermediate Water (AAIW) and Sub-Antarctic Mode Water (SAMW; 12 - 15°C; 26.4 - 26.8 kg m^{-3}; Anilkumar et al., 2006). Intermediate waters were comprised of two varieties, namely the Indian variety (i-AAIW), transported from the east via the AC and identified by a salinity minimum (S < 34.25 PSU), and the colder, more saline Atlantic variety (a-AAIW), transported from the west via the ACC. Together with mode waters, intermediate waters are the chief communicators between the major ocean basins exporting their biogeochemical signatures to the lower latitude oceans (Gordon et al., 1992). Deeper in the water column, North Atlantic Deep Water (NADW), identified by a deep salinity and oxygen maximum (S > 34.80 PSU; $\delta^{18}O$ > 0.25; Aken et al., 2004) was generally characterised by lower concentrations of all major nutrients in relation to the overlying UCDW and underlying Lower Circumpolar Deepwater (LCDW).

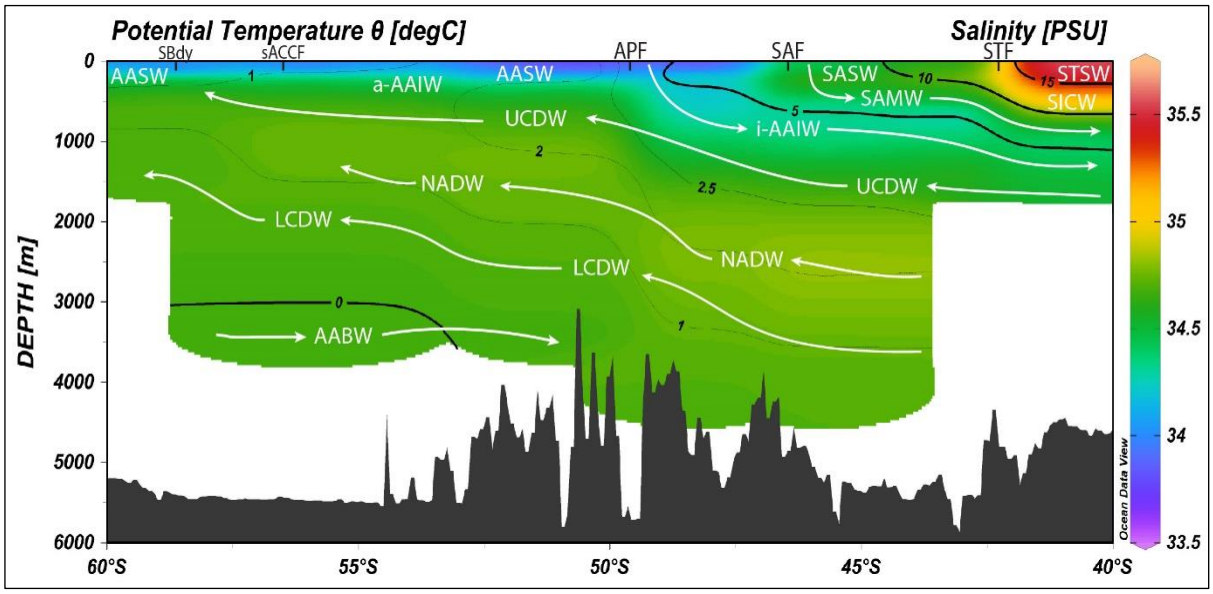

Figure 2. *Distribution plot of salinity overlain by potential temperature used to characterise the water mass regime. Acronyms in alphabetical order are as follows; AABW: Antarctic Bottom Water; AASW: Antarctic Surface Water; a-AAIW: Antarctic Intermediate Water of Atlantic origin; i-AAIW: Antarctic Intermediate Water of Indian origin; ISW: Intermediate Surface Water; LCDW: Lower Circumpolar Deepwater; NADW: North Atlantic Deepwater; SASW: Sub-Antarctic Surface Water; SAMW: Sub-Antarctic Mode Water; SICW: South Indian Central Water; STSW: Sub-Tropical Surface Water; UCDW: Upper Circumpolar Deepwater; WW: Winter Water. Figure constructed using Ocean Data View (ODV; Schlitzer, 2017). Data displayed using weighted average gridding.*

3.1.3. Surface mixed layer and remineralisation depth

The Surface Mixed Layer (SML) at each station is defined as the area between the sea surface and the Mixed Layer Depth (MLD) which was calculated according to the fixed density criterion (Δσθ = 0.03 kg m^{-3}) using 10 m as a reference depth (de Boyer Montégut et al., 2004). Along this transect, the STZ

had the shallowest MLD (122 m) while the SAZ was characterised by the deepest MLD's observed (190 - 220 m). Further south, the MLD generally increased from 134 m in the PFZ to between 125 and 161 m in the AAZ. The remineralisation depth was defined as the depth interval for which O_2 decreased for a corresponding PO_4 increase. Remineralisation depths decreased from north to south, however physical mixing associated with upwelling of UCDW in the AAZ may overprint the actual depth of remineralisation in this zone. In the STZ, the remineralisation depth was between the SML and 1500 m, in the SAZ between SML and 1250 m, in the PFZ between SML and 1000 m and in the AAZ between SML and 250 - 450 m.

3.2. Distribution of dissolved elements

3.2.1. dZn

The distribution of dZn is shown in Figure 3a. At each station, dZn was lowest in surface waters and increased to local maxima in the deepest water mass sampled. The lowest measured dZn was in STSW (0.44 ± 0.28 nmol kg^{-1}) while highest concentrations were observed in AABW (8.67 ± 0.42 nmol kg^{-1}), sampled south of the Indian ridge below 3000 m depth. Surface water dZn concentrations increased southwards by approximately 8-fold between STSW in the north and AASW (3.37 ± 0.28 nmol kg^{-1}) to the south. This trend was also observed in the intermediate and deep waters with distinct increases across the APF. For example, dZn was 2.49 ± 0.92 nmol kg^{-1} in intermediate waters north of the APF (i-AAIW) and 6.01 ± 0.74 nmol kg^{-1} in intermediate waters south of the APF (a-AAIW). Similarly, the dZn in UCDW increased from 4.85 ± 1.05 to 6.49 ± 0.37 nmol kg^{-1} across the APF. In general, NADW was characterised by slightly lower dZn concentrations relative to surrounding water masses. For example, in the PFZ (St. IO05; 48°S), dZn in NADW was 4.91 ± 0.20 nmol kg^{-1}, 5.14 ± 0.89 nmol kg^{-1} in the overlying UCDW and 6.62 ± 0.03 nmol kg^{-1} in the underlying LCDW. In deep waters (> 2500 m) north of the Indian ridge (St. IO05 and IO06), dZn was 5.71 ± 1.18 nmol kg^{-1} while to the south (St. IO04 and IO02) dZn was 8.51 ± 0.37 nmol kg^{-1}.

3.2.2. Phosphate, silicic acid and relations to dZn

Concentrations of PO_4 and $Si(OH)_4$ have been previously reported (Weir et al., in revision) and are shown in Figure 3b and 3c respectively. Here we focus the ratios of dZn to PO_4 and dZn to $Si(OH)_4$. For the full dataset, dZn (nmol kg^{-1}) = 2.93 PO_4 (µmol kg^{-1}) -1.33 (nmol kg^{-1}); $r^2 = 0.55$; n = 120) and dZn (nmol kg^{-1}) = 0.064 $Si(OH)_4$ (µmol kg^{-1}) + 0.69 (nmol kg^{-1}); $r^2 = 0.92$; n = 120). The slopes of correlation between dZn and PO_4 in the SML ($dZn/PO_{4\,SML}$) and between dZn and $Si(OH)_4$ in the SML ($dZn/Si(OH)_{4\,SML}$) varied over the transect suggesting differences in dZn to macronutrient uptake rates. $dZn/PO_{4\,SML}$ was 0.90 ± 0.14 nmol μmol^{-1} in the STZ and SAZ and increased southwards to values of 1.91 ± 0.12 and 6.36 ± 1.66 nmol μmol^{-1} in the PFZ and AAZ respectively. For $dZn/Si(OH)_{4\,SML}$, slope

values were 0.11 ± 0.02 nmol µmol^{-1} in the PFZ and between 0.05 ± 0.01 and 0.18 ± 0.01 nmol µmol^{-1} in the AAZ.

3.3. Distribution of particulate elements

3.3.1. pZn

Depth profiles of pZn (Figure 3d) typically had highest concentrations near the surface, particularly in the AAZ where surface water pZn was 106 ± 29 pmol kg^{-1}. Surface water pZn decreased northward with mean values of 68 ± 9 pmol kg^{-1} in the PFZ, 37 ± 12 pmol kg^{-1} in the SAZ and 21 ± 6 pmol kg^{-1} in the STZ. There was no clear trend in intermediate and deep water pZn distributions. However, below 1000 m depth, pZn was generally higher south of the APF (33 ± 16 pmol kg^{-1}) compared to north of the APF (22 ± 11 pmol kg^{-1}).

3.3.2. Phosphorous and relation to pZn

The distribution of P (Figure 3e) was characterised by high surface concentrations, rapid decreases through sub surface water masses and low concentrations at depth. There were no clear latitudinal trends in surface water P distributions. High surface water P concentrations were measured in the PFZ (22.07 ± 3.32 nmol kg^{-1}) and SAZ (21.05 ± 5.79 nmol kg^{-1}). In the AAZ, surface water P was (14.23 ± 4.62 nmol kg^{-1}) while lowest surface water P was measured in the STZ (10.62 ± 8.44 nmol kg^{-1}). With depth, mean P concentrations decreased consistently between UCDW (2.47 ± 1.40 nmol kg^{-1}), LCDW (1.93 ± 0.87 nmol kg^{-1}) and AABW (1.48 ± 0.25 nmol kg^{-1}). The slope of correlation between pZn and P in the SML (pZn/P_{SML}) increased southwards from 1.28 ± 0.63 pmol nmol^{-1} in the STZ and SAZ, 2.35 ± 0.21 pmol nmol^{-1} in the PFZ and 4.78 ± 1.64 pmol nmol^{-1} in the AAZ. Similarly, the slope of correlation between pZn and P between the SML and depth of remineralisation (pZn/P_{remin}) increased southwards from 1.08 ± 0.27 pmol nmol^{-1} in the STZ and SAZ, 2.14 ± 0.46 pmol nmol^{-1} in the PFZ and 4.90 ± 0.43 pmol nmol^{-1} in the AAZ.

3.3.3. Biogenic silica and relation to pZn

Concentrations of bSi (Figure 3f) are only available for the upper 150 m of the water column and have been previously reported (Weir et al., in revision). The slope of correlation between pZn and bSi in the SML (pZn/bSi_{SML}) was 1292 ± 48 nmol µmol^{-1} at 48°S in the PFZ and between 583 ± 16 (58°S) and 1559 ± 14 (56°S) nmol µmol^{-1}in the AAZ. We assume 150 m as representative of the SML for stations where the MLD is deeper i.e. in the SAZ

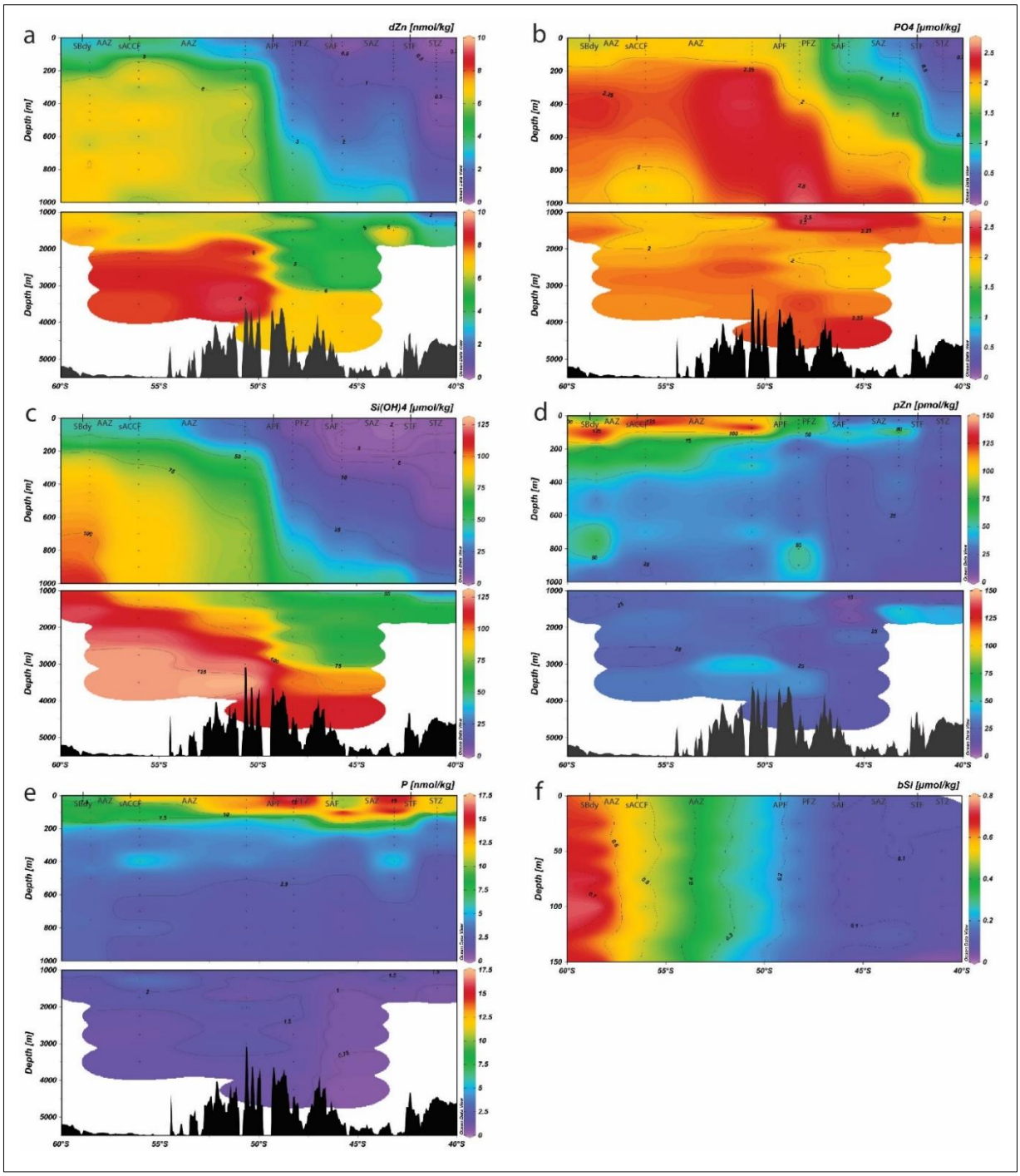

Figure 3. *Distribution plots of a) dZn b) PO_4, c) $Si(OH)_4$, d) pZn, e) P and f) bSi. Each figure is separated into upper 1000 m (upper panel) and below 1000 m (bottom panel). Frontal position and corresponding zones are shown. PO_4, $Si(OH)_4$ and bSi data from Weir et al., in revision. Figure constructed using Ocean Data View (ODV; Schlitzer, 2017). Dots represent depths sampled. Data displayed using weighted average gridding.*

4. Discussion

4.1 Comparison with previously reported dZn and pZn

The data presented here contributes the first winter measurements of dZn and pZn from the 30°E longitude in the Indian sector of the Southern Ocean. For comparative purposes, a global compilation

of dZn and pZn measurements (Figure 4) has been created from all available data included in the GEOTRACES Intermediate Data Product (IDP) 2017 (Schlitzer et al., 2018; see figure caption for dataset references). The data, portrayed as box and whisker plots, was separated into full depth profiles from surface to near seafloor for dZn (Figure 4a) and pZn (Figure 4b) and profiles from surface to 1000 m depth for dZn (Figure 4c) and pZn (Figure 4d).

For dZn, concentrations measured in the Indian sector of the Southern Ocean (this study) fell within the range of measurements from as other ocean basins. There is a global commonality in the vertical distributions of dZn where low surface concentrations, as low as 0.002 nmol kg^{-1} in the South Pacific Ocean (Bowie and Ellwood, unpublished), increase with depth to values above 10 nmol kg^{-1} for most ocean basins, typical vertical behaviour for a 'nutrient type' element. For full depth profiles, the Indian sector of the Southern Ocean dZn data had a range between 0.16 – 9.12 nmol kg^{-1} which compared most similarly to the Indian Ocean (0.16 – 11.14 nmol kg^{-1}; Thi Dieu Vu and Sohrin, 2013) and Atlantic sector of the Southern Ocean (0.32 – 7.79 nmol kg^{-1}; Croot et al., 2011). However, in the upper 100 m, winter dZn from the Indian sector of the Southern Ocean was between 0.6 and 1.2 nmol kg^{-1} higher compared to the summer values from the Atlantic sector (Croot et al., 2011). In the intermediate and deep waters, our dZn data from 48°S (St. IO05) was in good agreement with dZn data from the same latitude in the Atlantic sector (Station PS71-104-2; (Zhao et al., 2014). There were also differences in surface dZn between the Indian and Pacific sectors of the Southern Ocean with dZn from the Indian sector approximately 0.1 – 0.2 nmol kg^{-1} higher compared to summer (Butler et al., 2013) and winter dZn concentrations (Ellwood, 2008).

For pZn, concentrations in the Indian sector of the Southern Ocean (this study) fell within the range of concentrations measured in the Atlantic and Pacific basins. Highest pZn concentrations were found in surface waters of all datasets while extremely lower values were typically measured in the deep ocean. The pZn maximum for the Southern Ocean (147 pmol kg^{-1}) was far lower compared to the maxima from the Pacific (208 pmol kg^{-1}; Ohnemus et al., 2017) and Atlantic (415 – 717 pmol kg^{-1}; Schlitzer et al., 2018). The increased particle load in the Pacific and Atlantic basins coincided with stations closest to the continental margin and therefore likely reflected suspension of shelf sediments and external inputs associated with atmospheric deposition (e.g. Saharan dust in the tropical and North Atlantic Ocean). More recently (i.e. produced after the release of GEOTRACES IDP 2017), surface pZn distributions (< 50 m) have been measured in summer along the 30°E line in the Indian sector of the Southern Ocean (Barrett et al., 2018), overlapping with our transect. Reported pZn concentrations were low north of the APF (< 200 pmol kg^{-1}) increased in the AAZ (200 - 500 pmol kg^{-1}). Summer surface pZn was therefore higher compared to our winter surface pZn north of the APF (< 75 pmol kg^{-1}) and in the AAZ (75 – 147 pmol kg^{-1}).

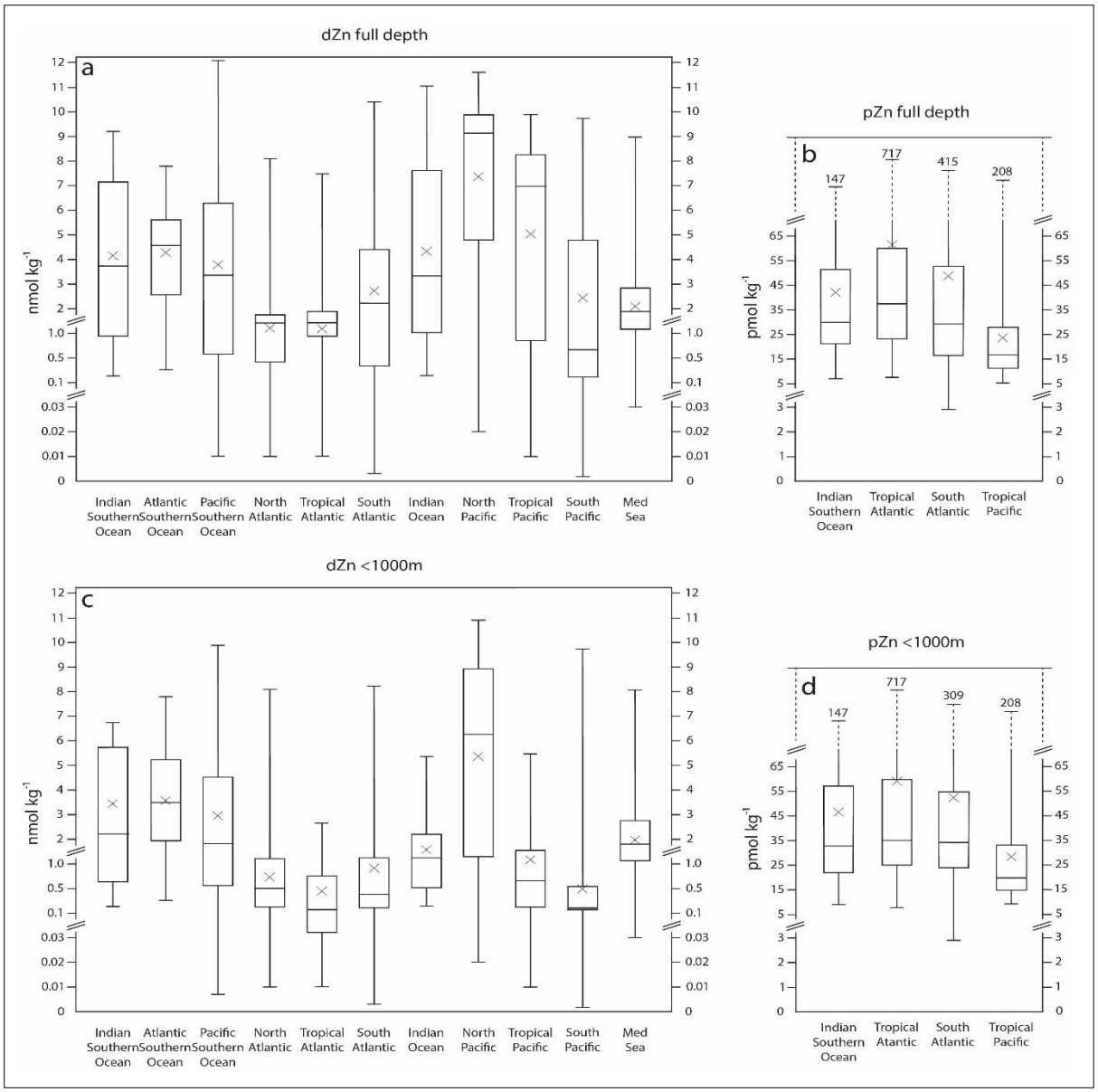

Figure 4. *Box and whisker plots of a) dZn for full depth profiles, b) pZn for full depth profiles, dZn for profiles to 1000, and d) pZn for profiles to 1000 m. Data compiled from all available data from the GEOTRACES intermediate data product (IDP) 2017 (Schlitzer et al., 2018). Plots in bold are data from this study. From bottom to top, plots are structured as follows: minimum, quartile 1, median, quartile 3, maximum. The cross (x) represents the mean value. Note the changes in the vertical scale. For dZn, data references are as follows, Indian Southern Ocean data [this study (n=120 full depth; 91 <1000m)], Atlantic Southern Ocean [transect GIPY05 (n=164 full depth; 105 <1000m) (Croot et al., 2011)], Pacific Southern Ocean [transect GIPY06 (n=82 full depth; 224 <1000m) (Butler et al., 2013), transect GIPY02 (n=0 full depth; 108 <1000m) (Butler et al., 2013), transect GPpr01 (n=0 full depth; 28 <1000m) (Ellwood, unpublished), transect GPpr02 (n=69 full depth; 96 >1000m) (Ellwood, 2008)], North Atlantic Ocean [transect GA02 (n=407 full depth; 227 <1000m) (Middag et al., 2019), transect GA03 (n=589 full depth; 304 <1000m) (Conway and John, 2014)], Tropical Atlantic Ocean [transect GA02 (n=475 full depth; 255 <1000m) (Middag et al., 2019)], South Atlantic Ocean [transect GA02 (n=429 full depth; 235 <1000m) (Middag et al., 2019), transect GA10 (n=596 full depth; 308 <1000m) (Wyatt et al., 2014)], Indian Ocean [transect GI04 (n=168 full depth; 95 <1000m) (Thi Dieu Vu and Sohrin, 2013)], North Pacific Ocean [transect GP02 (n=319 full depth; 170 <1000m) (Kim et al., 2017) , transect GP18 (n=94 full depth; 49 <1000m) (Minami et al., 2015), transect GPpr07 (n=24 full depth; 46 <1000m) (Janssen and Cullen, 2015)], Tropical Pacific Ocean [transect GP16 (n=663 full depth; 340 <1000m) (John et al., 2017)], South Pacific Ocean [transect GP13 (n=316 full depth; 368 <1000m) (Bowie and Ellwood, unpublished)] and Mediterranean Sea [transect GA04 (n=1371 full depth; 1052 <1000m) (Frank, unpublished)]. For pZn, data references are as follows, Indian Southern Ocean data [this study (n=122 full depth; 94 <1000m)], North Atlantic Ocean [transect GA03 (n=0 full depth; 34 <1000m) (Boyle, Bruland, Conway, John, Middag, Wu, unpublished)], Tropical Atlantic Ocean [transect GA06 (n=103 full depth; 82 <1000m) (Achterberg, Milne, Lohan, unpublished)], South Atlantic Ocean [transect GA10 (n=231 full depth; 134 <1000m) (Henderson, Achterberg, Milne, Lohan, unpublished)] and Tropical Pacific Ocean [transect GP16 (n=703 full depth; 397 <1000m) (Ohnemus et al., 2017)].*

4.2. Differences between winter and summer dZn distributions

In an attempt to gain insights into the seasonal cycling of dZn, we compare our winter data to recent summer measurements from the SAZ, PFZ and AAZ within the western Indian sector and eastern Atlantic sector of the Southern Ocean (St. 3, 4, 5, 6, 7, 24; Janssen et al., 2020; Sieber et al., 2019). Produced subsequent to the GEOTRACES IDP 2017, these datasets were chosen as they had a similarly high sampling resolution (6 – 8 measurements in the upper 200 m) to our dataset. Comparisons were made over the depth of the winter mixed layer and comparative summer stations were chosen so as to best resemble our winter stations e.g. similar latitude and remote from any continental or island influences. In all zones, the mean winter dZn was higher compared to summer measurements. For example, seasonal dZn differences were lowest in the SAZ (0.17 nmol kg^{-1}), intermediate in the PFZ (0.68 nmol kg^{-1}) and highest in the AAZ (1.09 nmol kg^{-1}). The seasonal differences here are slightly higher compared with previous observations in the PFZ and AAZ from the Atlantic sector where winter dZn was between 1.15 – 1.24 nmol kg^{-1} higher compared to summer (Cloete et al., 2019). Seasonal differences in dZn concentrations over the winter mixed layer are consistent with winter – summer differences in PO_4 concentrations over the same depth interval. For example, based on a dZn/PO_4 slope value of 2.93 nmol μmol^{-1} (derived from our overall dZn/PO_4 winter relationship), a PO_4 drawdown of 0.04, 0.20 and 0.30 $\mu mol\ kg^{-1}$ (the observed winter – summer PO_4 difference in the SAZ, PFZ and AAZ respectively), equates to a dZn drawdown of between 0.12 and 0.88 nmol kg^{-1}, which roughly equates to the observed seasonal dZn signal (0.17 - 1.09 nmol kg^{-1}). This suggests that reduced biological uptake during winter accounts significantly for the higher surface dZn compared to summer.

In addition to reduced biological uptake, deep winter mixing may also contribute to higher surface dZn observed in the winter mixed layer. Increasing dZn concentrations with depth provides the basis for physical resupply to the SML through deep winter mixing. Typically, the period of maximum nutrient recharge is between August and November (Johnson et al., 2017) however our early winter MLD's were similar to the maximum depths (~200 m) expected for the west Indian sector (Sallée et al., 2010), suggesting deep winter mixing and nutrient recharge were ongoing. When comparing average dZn:PO_4 ratios for the summer and winter mixed layer, we noticed distinct increases below the summer mixed layer. For example, dZn:PO_4 ratios increased by values between 0.12 nmol μmol^{-1} in the PFZ and 0.45 nmol μmol^{-1} in the AAZ (Figure 5). The net result of deep winter mixing is the preferential resupply of dZn through access to waters which are enriched in dZn relative to PO_4, particularly in the AAZ.

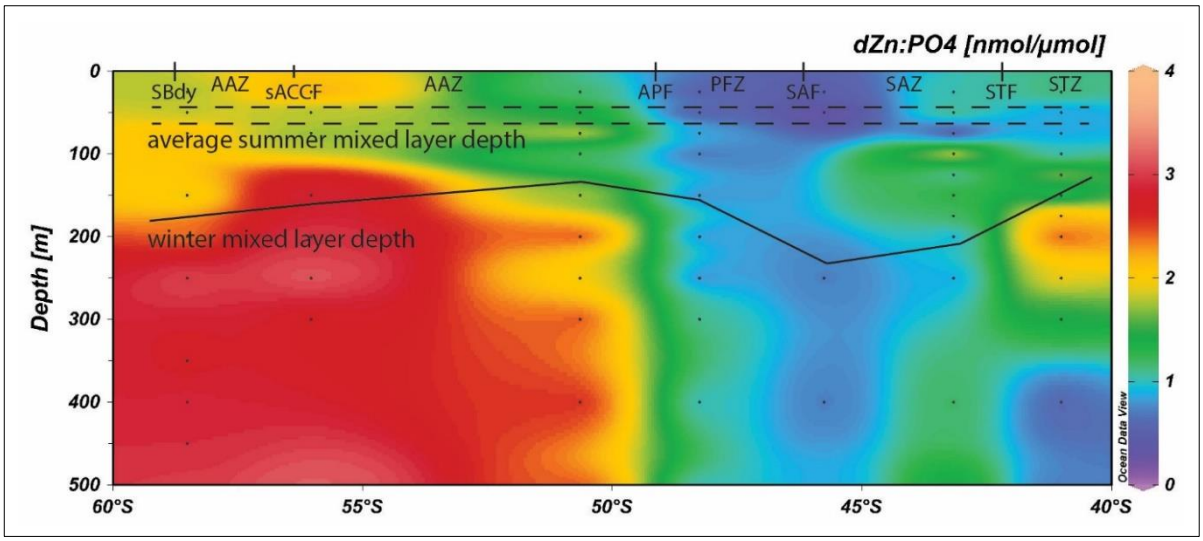

Figure 5. *Distribution plots of dissolved dZn:PO_4 spot ratios for the upper 500 m of the water column. Frontal positions and corresponding zones are shown. Dotted lines represent the average range of the summer mixed layer depth (60 – 80 m; data from WOCE Global Data Resource, (2018)). Solid line represents the calculated winter mixed layer depth during this study. Figure constructed using Ocean Data View (ODV; Schlitzer, 2017). Figure constructed using Ocean Data View (ODV; Schlitzer, 2017). Dots represent depths sampled. Data displayed using weighted average gridding.*

4.3. Processes driving Zn cycling

4.3.1 Zonal trends in dZn - PO_4 and pZn - P systematics

We observed distinct differences in Zn cycling across the different Southern Ocean zones (Figure 6). To illustrate these differences, we compare ratios of dZn and PO_4 in the SML ($dZn/PO_{4\,SML}$) with ratios of pZn to P in the SML (PZn/P_{SML}) and between the SML and remineralisation depth (pZn/P_{remin}). In the STZ and SAZ, $dZn/PO_{4\,SML}$ followed a shallow linear slope (0.90 ± 0.14 nmol µmol^{-1}; Figure 6a) which increased through the PFZ (1.91 ± 0.12 nmol µmol^{-1}; Figure 6b) and AAZ (6.36 ± 1.66 nmol µmol^{-1}; Figure 6c). In the STZ and SAZ, our slope value is higher than that calculated in summer for SAZ surface waters in the Indian sector (0.31 ± 0.20 nmol µmol^{-1}; Janssen et al., 2020) however if we apply the same PO_4 constraints (PO_4 < 1.20 µmol kg^{-1}) to our data the resulting $dZn/PO_{4\,SML}$ slope (0.44 ± 0.12 nmol µmol^{-1}) is more consistent. Our $dZn/PO_{4\,SML}$ slope value in the AAZ is consistent with a slope value of 6.5 nmol µmol^{-1} measured in the Atlantic and Pacific sectors (Sieber et al., 2019). In subsurface waters of the STZ, SAZ and PFZ, there is a distinct change toward steeper dZn/PO_4 slopes reflecting vertical mixing with intermediate and deep waters with high dissolved Zn to PO_4 spot ratios. In the AAZ, vertical mixing follows the steep dZn/PO_4 slope set by diatoms in the SML, consistent with previous observations (Sieber et al., 2019). For pZn/P_{SML}, a similar southward increasing trend in slope values was observed where pZn/P_{SML} was low in the STZ and SAZ (1.28 ± 0.63 pmol nmol^{-1}; Figure 6d), increased in the PFZ (2.35 ± 0.21 pmol nmol^{-1}; Figure 6e) and was highest in the AAZ (4.78 ± 1.64 pmol nmol^{-1}; Figure 6f). Our winter pZn/P_{SML} slope of 4.78 ± 1.64 pmol nmol^{-1} in the AAZ was comparable to a summer slope of 3.00 ± 0.90 pmol nmol^{-1} measured in the AAZ (Barrett et al., 2018). Considering that P-normalised cellular Zn quotas in phytoplankton range by a factor of 20 (1 – 20 mmol

(mol P)$^{-1}$; Twining and Baines, 2013), the strong zonal differences in dZn-PO_4 and pZn-P systematics are partly driven by variations in the local phytoplankton community. During our transect, there was a shift from a flagellate dominated phytoplankton assemblage in the STZ and SAZ to a diatom dominated assemblage in the AAZ with a significant contribution from both groups in the PFZ (Weir et al., in revision). Consistent with our data, Southern Ocean flagellates are characterised by P-normalised cellular Zn quotas which are 4 - 5 times lower compared to those measured in Southern Ocean diatoms (Twining and Baines, 2013). Furthermore, pZn/P_{remin} ratios were 1.08 ± 0.27, 2.14 ± 0.46 and 4.90 ± 0.43 pmol nmol^{-1} in the STZ + SAZ, PFZ and AAZ respectively (Figure 6d - f), and were therefore very similar to pZn/P_{SML}. While remineralisation is likely taking place within the SML, the tight correlation between pZn/P_{SML} and pZn/P_{remin} suggests that a significant portion of sinking phytoplankton cells were exported and remineralised together below the winter mixed layer as suggested previously for the Southern Ocean (Sieber et al., 2019; Twining et al., 2014; Vance et al., 2017). In sum, we suggest that the dZn and PO_4 uptake characteristics in each zone (STZ + SAZ, PFZ and AAZ) are a reflection of the local phytoplankton community, that the uptake signatures are reflected in the particulate phases and that the particulate phases are exported in a near proportional manner below the winter mixed layer.

4.3.2 Zonal trends in dZn – $Si(OH)_4$ and pZn - bSi systematics

We gain further insights into Zn cycling by investigating the relationship between dZn - $Si(OH)_4$ and pZn - bSi (Figure 7). Because $Si(OH)_4$ and bSi in open ocean settings are largely controlled by diatoms, we focus on the PFZ (where diatoms contribute significantly to phytoplankton biomass) and the AAZ (where diatoms dominate phytoplankton biomass). Despite the close correlation between dZn and $Si(OH)_4$ over the whole dataset (r^2 = 0.92; n = 120), there were slight differences between $dZn/Si(OH)_{4\ SML}$ uptake ratios for stations in the PFZ and AAZ. $dZn/Si(OH)_{4\ SML}$ was 0.11 nmol µmol^{-1} at 48°S in the PFZ (Figure 7a) and ranged between 0.05 nmol µmol^{-1} (58°S) and 0.18 nmol µmol^{-1} (56°S) in the AAZ (Figure 7b). While no obvious latitudinal trend was observed, $dZn/Si(OH)_{4\ SML}$ ratios co-varied with pZn/bSi_{SML}. Here, pZn/bSi_{SML} at 48°S (PFZ) was 1292 pmol µmol^{-1} (Figure 7c), intermediate between values of 583 pmol µmol^{-1} (58°S) and 1559 pmol µmol^{-1} (56°S) in the AAZ (Figure 7d). This suggests that the ratio in which diatoms utilise dZn and $Si(OH)_4$ is well represented by their cellular composition. Changes in Zn uptake may be related to the incorporation into diatom frustules. Culture experiments showed that the Zn content of diatom frustules is negligible (1 - 3%; Ellwood and Hunter, 2000), however, recent work suggests this value could increase to 30% under Fe-limitation (Ellwood et al., 2018). Indeed, surface dissolved iron (dFe; ~ 0.1 nmol kg^{-1}; analysed concurrently with dZn) in the AAZ was potentially bio-limiting, providing a possible mechanism linking $dZn/Si(OH)_4$ uptake to pZn/bSi incorporation by diatoms. In sum, our data suggests that dZn cycling is intimately linked with $Si(OH)_4$ despite the lack of spatial association within diatom cells i.e. dZn being associated with PO_4 in

the organic material of phytoplankton cells and $Si(OH)_4$ being used to build the siliceous external diatom frustules.

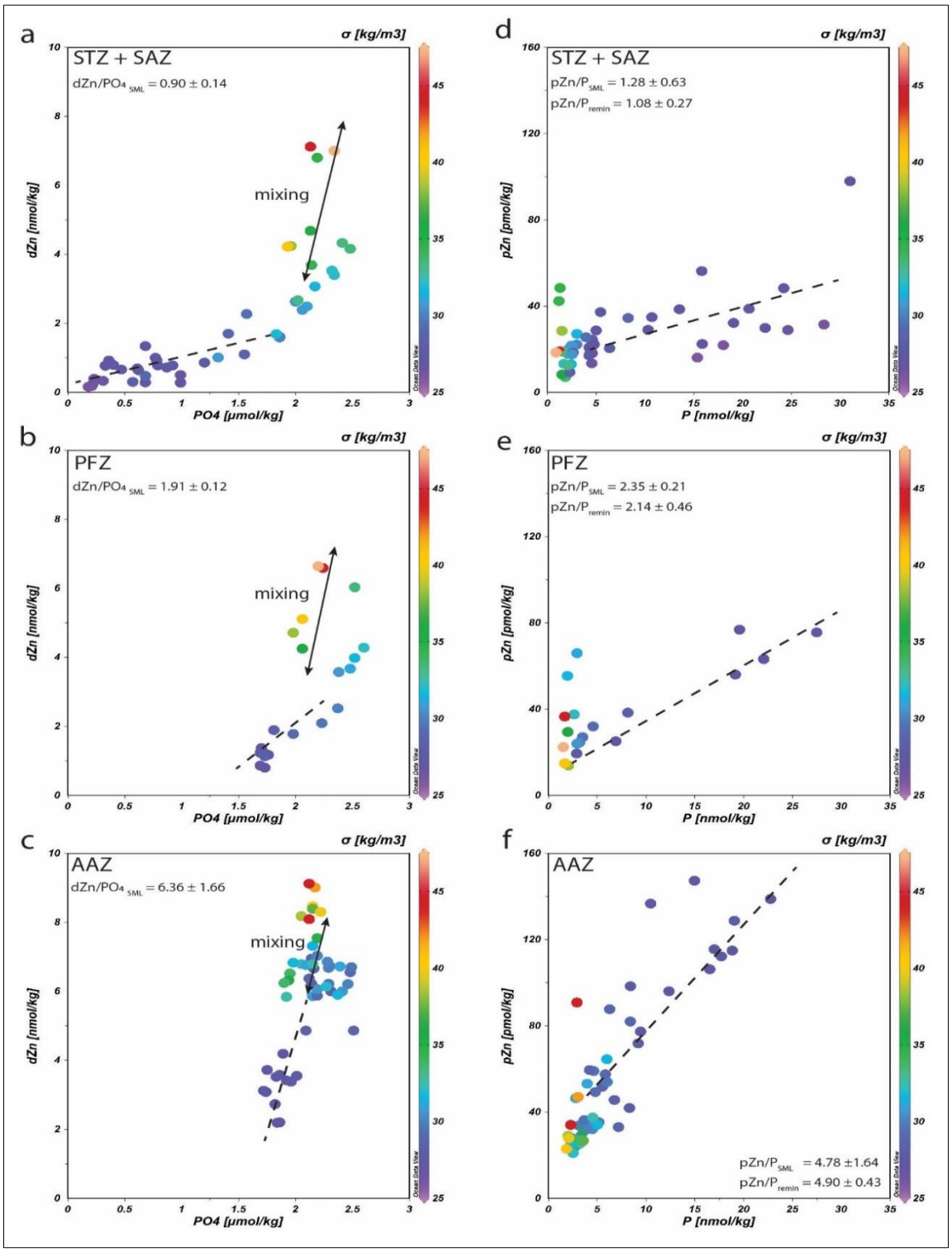

Figure 6. *Scatter plots of a) dZn vs PO_4 in the STZ + SAZ, b) dZn vs PO_4 in the PFZ, c) dZn vs PO_4 in the AAZ, d) pZn vs P in the STZ + SAZ, e) pZn vs P in the PFZ and f) pZn vs P in the AAZ. Each plot represents data from the full water column. Plots are overlain with seawater density (σ; kg m^{-3}). Dashed lines represent the slope of correlation derived from the surface mixed layer (SML) or the depth interval between the SML and the remineralisation depth (remin). Figure constructed using Ocean Data View (ODV; Schlitzer, 2017).*

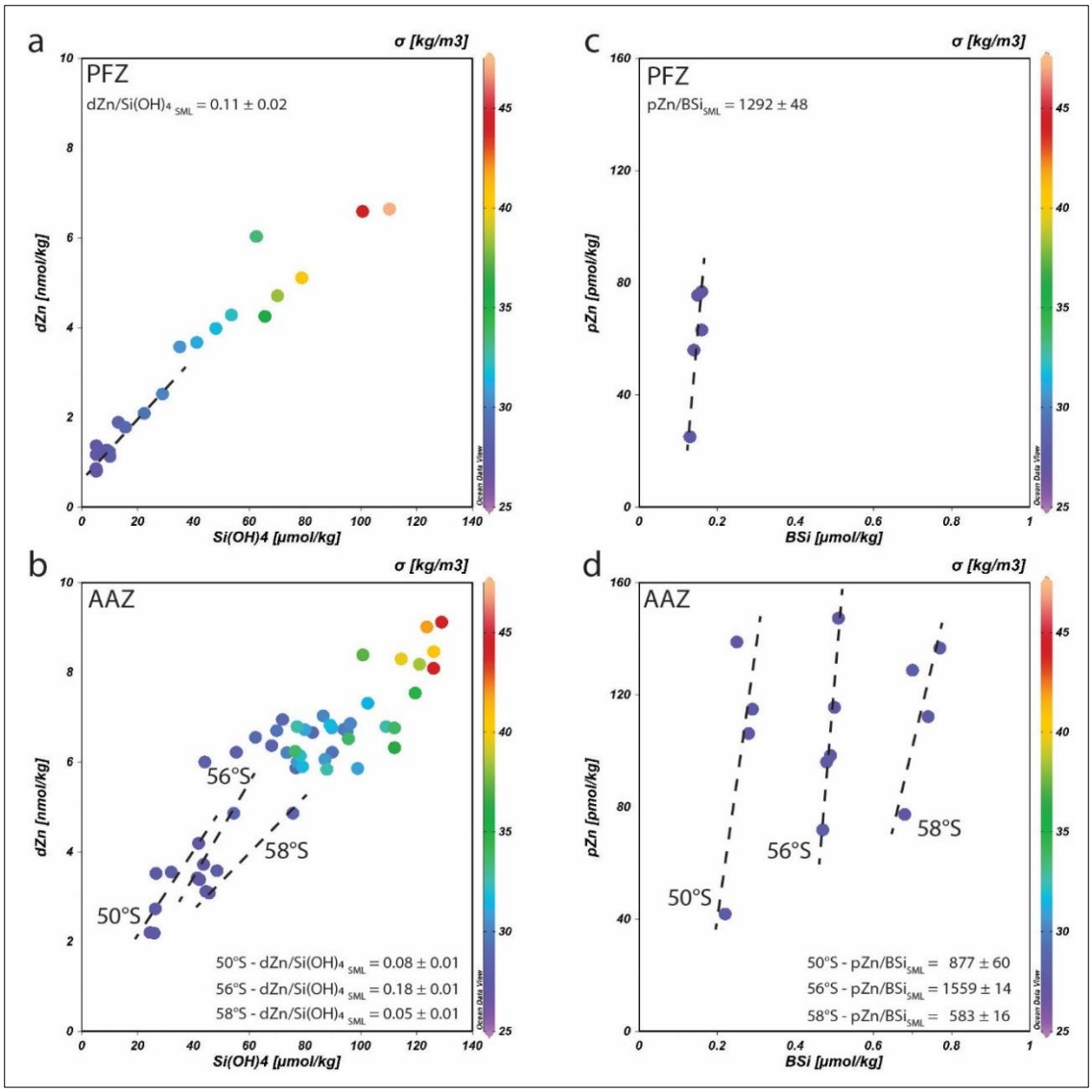

Figure 7. *Scatter plots of a) dZn vs $Si(OH)_4$ in the PFZ, b) dZn vs $Si(OH)_4$ in the AAZ, c) pZn vs bSi in the PFZ and d) pZn vs bSi in the AAZ. Each plot represents data from the full water column. Plots are overlain with seawater density (σ; kg m^{-3}). Dashed lines represent the slope of correlation derived from the surface mixed layer (SML). Figure constructed using Ocean Data View (ODV; Schlitzer, 2017).*

4.3.3. Upwelling and lateral transport of Zn signatures

We have shown that diatoms in the PFZ and AAZ play a significant role in Zn cycling as a result of their strong preferential requirements for dZn relative to PO_4 in comparison to other phytoplankton groups. Considering only biological uptake, this would suggest that surface waters dominated by diatoms should be depleted in dZn, however dZn in the SML increased southwards and was highest in the AAZ (2.84 - 3.66 nmol kg^{-1}) where diatoms were most abundant. The strong surface dZn gradient was likely the result of upwelling of dZn-enriched UCDW to near surface in the AAZ. UCDW had a high mean dZn:PO_4 spot ratio which increased southwards in the AAZ, from 2.54 – 3.00 nmol $µmol^{-1}$. The net result of upwelling UCDW is the progressive enrichment of surface water dZn with latitude. The source of the 'excess' dZn relative to PO_4 was predominantly from the remineralisation of particles

with high pZn:P spot ratios which, in turn, was set by the high dZn/PO_4 uptake stoichiometry of diatoms within the SML.

When considering the physical water mass circulation pattern in the Southern Ocean, it is clear that the influential role that diatoms play in dZn and $Si(OH)_4$ cycling extends beyond the surface waters in which they are found and provides a plausible reason for the global similarity between dZn and $Si(OH)_4$ distributions. Here, our observations build on the initial hypothesis (Vance et al., 2017) and more recent works on dZn cycling in the Southern Ocean (Sieber et al., 2020; Janssen et al., 2020). To elaborate, the net result of biological uptake by diatoms in the AAZ are surface waters that are depleted in dZn and $Si(OH)_4$ with respect to PO_4. Physical circulation dictates that the resulting dZn and $Si(OH)_4$ deficient surface waters are transported northwards across the APF (Figure 8a). Furthermore, a portion of the northward flowing surface water subducts in the PFZ and SAZ, forming SAMW with inherently low dZn and $Si(OH)_4$ concentrations relative to PO_4 (Figure 8b). Considering that SAMW is the main communication channel to the global low latitude ocean (Sarmiento et al., 2004), the northward transport of SAMW provides a likely mechanism for the observed dZn and $Si(OH)_4$ depleted waters of the low latitude upper ocean. Critically, our particulate data suggest that diatoms are exported below the winter mixed layer where remineralisation and rigorous mixing would resolve the deep water dZn - $Si(OH)_4$ correlation despite their different regeneration length scales (Vance et al., 2017).

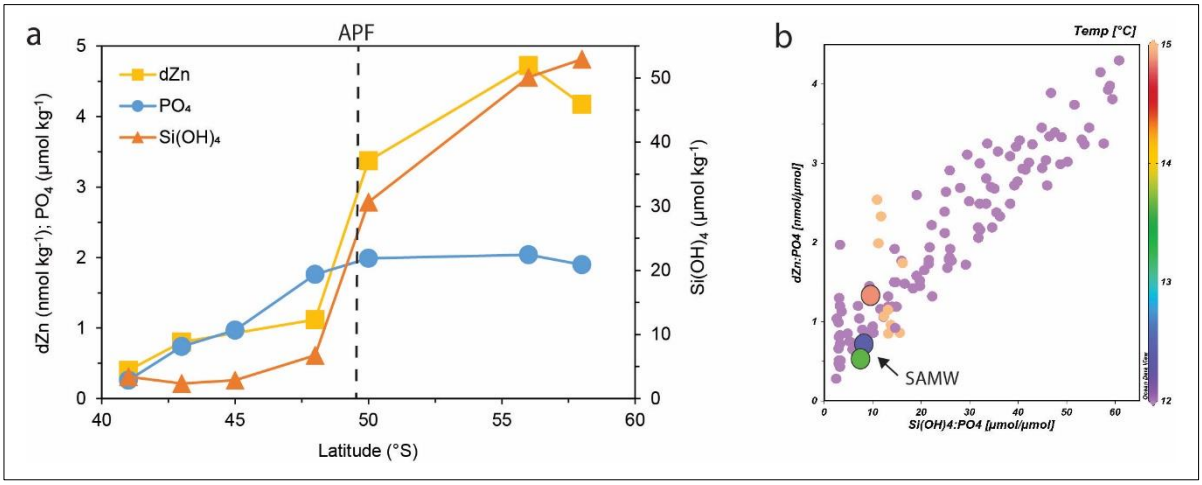

Figure 8. *Plot of a) average dZn, PO_4 and $Si(OH)_4$ in the surface mixed layer (SML) at each station. The location of the Antarctic Polar Front (APF) is shown. b) Scatter plot of showing the low dZn/PO_4 and $Si(OH)_4$/PO_4 signatures of Sub Antarctic Mode Water (SAMW; 12 - 15°C; Anilkumar et al., 2006). Points enlarged for samples within SAMW and coloured according to the temperature scale. Figure constructed using Ocean Data View (ODV; Schlitzer, 2017).*

4.4. Inhibited mixing south of the Indian ridge

Highest concentrations of dZn were measured in deep waters south of the mid-Ocean ridge (hereafter Indian ridge). At 50°S and 56°S dZn was 9.07 ± 0.06 (n = 2) and 8.27 ± 0.18 nmol kg^{-1} (n = 2) below 3000 m respectively. While dZn data for bottom waters in the Southern ocean is extremely limited, our concentrations appear higher compared to average values of 7.25 ± 0.58 nmol kg^{-1} (n = 6; Zhao et al.,

2014). In addition, dZn measured below 3000 m at stations north of the Indian ridge was 6.84 ± 0.23 nmol kg^{-1} (n = 4). The high dZn south of the Indian ridge was associated with the highest measured $Si(OH)_4$ (129 ± 2 µmol kg^{-1}) suggesting that the resuspension of opal-rich sediment may be contributing to elevated dZn and $Si(OH)_4$ as observed in the South Atlantic (Wyatt et al., 2014). While the deepest sampled depth at 50°S was in close proximity to the surface of the southern flank of the Indian ridge, resuspension of opal rich sediment is unlikely at 56°S where the deepest sampled depth (3500 m) was well above the seafloor depth (~5500 m; Figure 4a). Instead we propose that inhibited mixing to the south of the Indian ridge may increase the residence time of 'true' AABW thereby allowing for the accumulation of dZn and $Si(OH)_4$ and other nutrients with deep regeneration cycles. Importantly, the long residence time of dZn, between 3000 - 11000 years (Little et al., 2014; Roshan et al., 2016) and $Si(OH)_4$ (~ 10000 years; Tréguer and De La Rocha, 2013) in the ocean, longer than the timescales used to measure oceanic overturning circulation (centennial timescales; Matsumoto, 2007), support the idea of nutrient accumulation in bottom waters. True AABW refers to AABW in the absence of any mixing with watermasses directly above. True bottom waters in this region have been shown to not extend northward past the Indian ridge (Anilkumar et al., 2006) and that deep waters north of the Indian ridge are instead an altered variety of LCDW resulting from diapycnal mixing between true AABW and LCDW (Mantyla and Reid, 1995). In an effort to further validate these observations, we performed an optimum multiparameter (OMP) analysis which computes the contributions of pre-defined end-member water masses to each measured sample. Consistent with our hypothesis, results of the OMP suggest that samples below 3000 m south of the Indian ridge are composed predominantly of AABW, up to 80% at the deepest sampled depth (Figure 9). It therefore appears plausible that inhibited mixing and increased residence times of deep waters south of the Indian ridge may contribute to elevated dZn and $Si(OH)_4$ concentrations in this region. We do however acknowledge that more deep water measurements are necessary to confirm this.

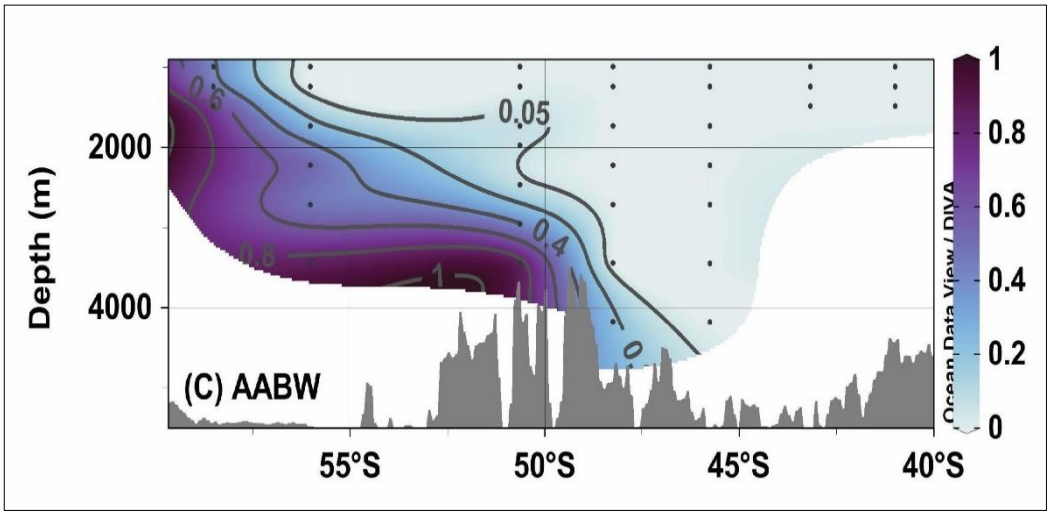

Figure 9. *Results of the optimum multiparameter analysis (OMP) optimised for resolving the contribution of Antarctic Bottom Water (AABW) to each measured sample. Figure constructed using Ocean Data View (ODV; Schlitzer, 2017). Dots represent depths sampled. Data displayed using weighted average gridding.*

5. Conclusion

For the first time, winter measurements of dissolved zinc (dZn) and particulate zinc (pZn) are presented along the 30°E longitude in the Indian sector of the Southern Ocean. The results provided the unique opportunity to investigate Zn cycling over seasonal cycles and to gain insights into the Southern Ocean winter reset state. In the SML, winter dZn was higher compared to summer measurements (derived from previously published datasets), consistent with reduced biological uptake by phytoplankton. In addition, waters below the summer mixed layer and with higher dZn:PO_4 spot ratios may be entrained during winter leading to preferential resupply of dZn to summer surface waters. While biological activity may be reduced in winter, our data suggest that biological uptake and regeneration remain key controls of Zn in the upper ocean. At all stations, dZn was lowest in the SML and increased with depth. Conversely, pZn was highest in the SML and decreased below the SML. The vertical behaviours of both dZn and pZn are consistent with biological uptake in surface waters and remineralisation in the sub surface. Furthermore, we observed distinct differences in Zn cycling across the various Southern Ocean zones. Slope values of dZn and PO_4 in the SML ($dZn/PO_{4\ SML}$) increased 7-fold between the STZ and AAZ reflecting the preferential requirement of dZn relative to PO_4 by diatoms in the AAZ. Variations in $dZn/PO_{4\ SML}$ were reflected in the particulate phase data where slope values of pZn and P in the SML (pZn/P_{SML}) increased southward in a similar fashion to $dZn/PO_{4\ SML}$. Furthermore, extending our pZn/P_{SML} calculation to the remineralisation zone (pZn/P_{remin}) suggests that sinking phytoplankton cells are exported beneath the winter mixed layer with implications for resolving the deepwater dZn-$Si(OH)_4$ correlation (Vance et al., 2017). dZn and $Si(OH)_4$ as well as pZn and bSi were well correlated over the whole dataset. However minor deviations were observed in the SML within the PFZ and AAZ and related to diatom uptake. The preferential uptake and regeneration of diatoms with high Zn content combined with the physical upwelling of water masses in the AAZ resulted in the strong southward increase in surface dZn. Consequently, surface waters flowing north and contributing to the formation of SAMW, were characterised by dZn and $Si(OH)_4$ depletion relative to PO_4 which ultimately has potential consequences for low latitude Zn cycling. Lastly, inhibited mixing leading to increased residence times of bottom waters south of the Indian ridge may partly explain the elevated dZn and $Si(OH)_4$ in comparison to deep waters to the north of the Indian ridge.

6. Acknowledgements

We would like to thank the South African National Antarctic Programme (SANAP) as well as Captain Knowledge Bengu and the crew of the R/V SA Agulhas II for their professionalism and support during the winter 2017 voyage. We acknowledge Chief Scientist Marcello Vichi and all the participants involved in the expedition. We are grateful to the “Iron” team for their help in collecting trace-clean seawater samples. We would like to thank Eric Achterberg, Angela Milne, Andrew Bowie, Gideon

Henderson, Yoshiki Sohrin, Maeve Lohan and Michael Ellwood for allowing permission to use data that are not published outside of the IDP2017. Ryan Cloete was supported through the National Research Foundation (NRF) Innovation PhD studentship. This research was supported by NRF grants (UID# 93069, 105826 and 110715) to AR. S.F. acknowledges funding from NRF (UID 111210, 110731).

7. References

Aken, H.M. Van, Ridderinkhof, H., Ruijter, W.P.M. De, 2004. North Atlantic deep water in the south-western Indian Ocean. Deep Sea Res. Part I Oceanogr. Res. Pap. 51, 755–776. https://doi.org/10.1016/j.dsr.2004.01.008

Anderson, R.F., 2020. GEOTRACES: Accelerating Research on the Marine Biogeochemical Cycles of Trace Elements and Their Isotopes. Ann. Rev. Mar. Sci. 12, 9.1-9.37. https://doi.org/10.2138/gselements.14.6.377

Anderson, L. A. and Sarmiento, J. L.: Redfield ratios of remineralization determined by nutrient data analysis, Global Biogeochem. Cy., 8, 65–80, https://doi.org/10.1029/93GB03318, 1994.

Anilkumar, N., Luis, A.J., Somayajulu, Y.K., Ramesh Babu, V., Dash, M.K., Pednekar, S.M., Babu, K.N., Sudhakar, M., Pandey, P.C., 2006. Fronts, water masses and heat content variability in the Western Indian sector of the Southern Ocean during austral summer 2004. J. Mar. Syst. 63, 20–34. https://doi.org/10.1016/j.jmarsys.2006.04.009

Barrett, P.M., Resing, J.A., Grand, M.M., Measures, C.I., Landing, W.M., 2018. Trace element composition of suspended particulate matter along three meridional CLIVAR sections in the Indian and Southern Oceans: Impact of scavenging on Al distributions. Chem. Geol. 502, 15–28. https://doi.org/10.1016/j.chemgeo.2018.06.015

Belkin, I.M., Gordon, A.L., 1996. Southern Ocean fronts from the Greewich meridion to Tasmania. J. Geophys. Res. 101, 3675–3696. https://doi.org/https://doi.org/10.1029/95JC02750

Brand, L.E., Sunda, W.G., Guillard, R.R.L., 1983. Limitation of marine phytoplankton reproductive rates by zinc, manganese, and iron. Limnol. Oceanogr. 28, 1182–1198. https://doi.org/https://doi.org/10.4319/lo.1983.28.6.1182

Broecker, W.S., 1991. The Great Ocean Conveyor. Oceanography 4, 79–89. https://doi.org/10.1016/s0262-4079(08)61198-7

Bruland, K.W., 1980. Oceanographic distributions of cadmium, zinc, nickel, and copper in the north pacific. Earth Planet. Sci. Lett. 47, 176–198. https://doi.org/https://doi.org/10.1016/0012-821X(80)90035-7

Butler, E.C. V, O'Sullivan, J.E., Watson, R.J., Bowie, A.R., Remenyi, T.A., Lannuzel, D., 2013. Trace metals Cd, Co, Cu, Ni, and Zn in waters of the subantarctic and Polar Frontal Zones south of Tasmania during the "SAZ-Sense" project. Mar. Chem. 148, 63–76. https://doi.org/10.1016/j.marchem.2012.10.005

Carter, B. R., Talley, L. D., and Dickson, A.G.: Mixing and remineralization in waters detrained from the surface into Subantarctic Mode Water and Antarctic Intermediate Water in the southeastern Pacific, J. Geophys. Res. Oceans, 119, 4001–4028, https://doi.org/10.1002/2013JC009355, 2014.

Castro, C. G., Pérez, F. F., Holley, S. E., and Ríos, A. F.: Chemical characterisation and modelling of water masses in the Northeast Atlantic, Prog. Oceanogr., 41, 249–279, https://doi.org/10.1016/S0079-6611(98)00021-4, 1998.

Cloete, R., Loock, J.C., Mtshali, T., Fietz, S., Roychoudhury, A.N., 2019. Winter and summer distributions of Copper, Zinc and Nickel along the International GEOTRACES Section GIPY05: Insights into deep winter mixing. Chem. Geol. 511, 342–357. https://doi.org/10.1016/j.chemgeo.2018.10.023

Conway, T.M., John, S.G., 2015. The cycling of iron, zinc and cadmium in the North East Pacific Ocean - Insights from stable isotopes. Geochim. Cosmochim. Acta 164, 262–283. https://doi.org/10.1016/j.gca.2015.05.023

Croot, P.L., Baars, O., Streu, P., 2011. The distribution of dissolved zinc in the Atlantic sector of the Southern Ocean. Deep. Res. Part II Top. Stud. Oceanogr. 58, 2707–2719. https://doi.org/10.1016/j.dsr2.2010.10.041

Cutter, G.A., Bruland, K.W., 2012. Rapid and noncontaminating sampling system for trace elements in global ocean surveys. Limnol. Oceanogr. Methods 10, 425–436. https://doi.org/10.4319/lom.2012.10.425

de Boyer Montégut, C., Madec, G., Fischer, A.S., Lazar, A., Iudicone, D., 2004. Mixed layer depth over the global ocean: An examination of profile data and a profile-based climatology. J. Geophys. Res. C Ocean. 109, 1–20. https://doi.org/10.1029/2004JC002378

de Jong, E., Vichi, M., Mehlmann, C.B., Eayrs, C., De Kock, W., Moldenhauer, M., Audh, R.R., 2018. Sea Ice conditions within the Antarctic Marginal Ice Zone in winter 2017, onboard the SA Agulhas II, in: PANGAEA. University of Cape Town. https://doi.org/https://doi.org/10.1594/PANGAEA.885211

Ellwood, M.J., 2008. Wintertime trace metal (Zn, Cu, Ni, Cd, Pb and Co) and nutrient distributions in the Subantarctic Zone between 40-52°S; 155-160°E. Mar. Chem. 112, 107–117. https://doi.org/10.1016/j.marchem.2008.07.008

Ellwood, M.J., Grün, R., Samanta, M., Tagliabue, A., 2018. Iron limitation of Southern Ocean diatoms influences the oceanic cycling of zinc, in: Ocean Sciences Meeting. Portland, OR, p. Abstract [MM41A-08].

Ellwood, M.J., Hunter, K.A., 2000. The incorporation of zinc and iron into the frustule of the marine diatom Thalassiosira pseudonana. Limnol. Oceanogr. 45, 1517–1524. https://doi.org/10.4319/lo.2000.45.7.1517

Gordon, A.L., Weiss, R.F., Smethie, W.M., Warner, M.J., 1992. Thermocline and intermediate water communication between the South Atlantic and Indian Oceans. J. Geophys. Res. 97, 7223–7240. https://doi.org/10.1029/92jc00485

Grasshoff, K., 1983. Automated chemical analysis, in: Grasshoff, K., Ernhardt, M., Kremling, K. (Eds.), Methods of Seawater Analysis. Verlag Chemie Weinhein, New York, pp. 263–289. https://doi.org/10.1002/9783527613984

Janssen, D.J., Cullen, J.T., 2015. Decoupling of zinc and silicic acid in the subarctic northeast Pacific interior. Mar. Chem. 177, 124–133. https://doi.org/10.1016/j.marchem.2015.03.014

Janssen, D.J., Sieber, M., Ellwood, M.J., Conway, T.M., Barrett, P.M., Chen, X., de Souza, G.F., Hassler, C.S., Jaccard, S.L., 2020. Trace metal and nutrient dynamics across broad biogeochemical gradients in the Indian and Pacific sectors of the Southern Ocean. Mar. Chem. 221, 103773. https://doi.org/10.1016/j.marchem.2020.103773

John, S.G., Conway, T.M., 2014. A role for scavenging in the marine biogeochemical cycling of zinc and zinc isotopes. Earth Planet. Sci. Lett. 394, 159–167. https://doi.org/10.1016/j.epsl.2014.02.053

Johnson, K.S., Plant, J.N., Dunne, J.P., Talley, L.D., Sarmiento, J.L., 2017. Annual nitrate drawdown observed by SOCCOM profiling floats and the relationship to annual net community production. J. Geophys. Res. Ocean. 122, 6668–6683. https://doi.org/10.1002/2017JC012839

Karstensen, J. and Tomczak M.: Age determination of mixed water masses using CFC and oxygen data, J. Geophys. Res., 103, 18599–18609, https://doi.org/10.1029/98JC00889, 1998.

Lam, P.J., Marchal, O., 2015. Insights into Particle Cycling from Thorium and Particle Data. Ann. Rev. Mar. Sci. 7, 159–184. https://doi.org/10.1146/annurev-marine-010814-015623

Liu, M. and Tanhua, T.: Characteristics of Water Masses in the Atlantic Ocean based on GLODAPv2 data, Ocean Sci. Discuss., https://doi.org/10.5194/os-2018-139, in review, 2019.

Mantyla, A.W., Reid, J.L., 1995. On the origins of deep and bottom waters of the Indian Ocean. J. Geophys. Res. 100, 2417–2439.

Middag, R., de Baar, H.J.W., Bruland, K.W., 2019. The Relationships Between Dissolved Zinc and Major Nutrients Phosphate and Silicate Along the GEOTRACES GA02 Transect in the West Atlantic Ocean. Global Biogeochem. Cycles 4, 63–84. https://doi.org/10.1029/2018GB006034

Middag, R., van Heuven, S.M.A.C., Bruland, K.W., de Baar, H.J.W., 2018. The relationship between cadmium and phosphate in the Atlantic Ocean unravelled. Earth Planet. Sci. Lett. 492, 79–88. https://doi.org/10.1016/j.epsl.2018.03.046

Minami, T., Konagaya, W., Zheng, L., Takano, S., Sasaki, M., Murata, R., Nakaguchi, Y., Sohrin, Y., 2015. An off-line automated preconcentration system with ethylenediaminetriacetate chelating resin for the determination of trace metals in seawater by high-resolution inductively coupled plasma mass spectrometry. Anal. Chim. Acta 854, 183–190. https://doi.org/10.1016/j.aca.2014.11.016

Morel, F.M.M., Hudson, R.J.M., Price, N.M., 1991. Limitation of productivity by trace metals in the sea. Limnol. Oceanogr. 36, 1742–1755. https://doi.org/10.4319/lo.1991.36.8.1742

Morel, F.M.M., Price, N.M., 2003. The Biogeochemical Cycles of Trace Metals. Science (80-.). 300, 944–948. https://doi.org/10.1126/science.1083545

Ohnemus, D.C., Rauschenberg, S., Cutter, G.A., Fitzsimmons, J.N., Sherrell, R.M., Twining, B.S., 2017. Elevated trace metal content of prokaryotic communities associated with marine oxygen deficient zones. Limnol. Oceanogr. 62, 3–25. https://doi.org/10.1002/lno.10363

Orsi, A.H., Johnson, G.C., Bullister, J.L., 1999. Circulation, mixing, and production of Antarctic Bottom Water. Prog. Oceanogr. 43, 55–109. https://doi.org/10.1016/S0079-6611(99)00004-X

Orsi, A.H., Whitworth, T., Nowlin, W.D., 1995. On the meridional extent and fronts of the Antarctic Circumpolar Current. Deep. Res. Part I 42, 641–673. https://doi.org/10.1016/0967-0637(95)00021-W

Perez, F. F., Mouriño, C., Fraga, F., and Rios, A. F.: Displacement of water masses and remineralization rates off the Iberian Peninsula by nutrient anomalies, J. Mar. Res., 51, 869–892, https://doi.org/10.1357/0022240933223891, 1993.

Planquette, H., Sherrell, R.M., 2012. Sampling for particulate trace element determination using water sampling bottles: Methodology and comparison to in situ pumps. Limnol. Oceanogr. Methods 10, 367–388. https://doi.org/10.4319/lom.2012.10.367

Pollard, R.T., Lucas, M.I., Read, J.F., 2002. Physical controls on biogeochemical zonation in the Southern Ocean. Deep. Res. Part II Top. Stud. Oceanogr. 49, 3289–3305. https://doi.org/10.1016/S0967-0645(02)00084-X

Quay, P., Cullen, J., Landing, W., Morton, P., 2015. Processes controlling the distributions of Cd and PO4 in the ocean. Global Biogeochem. Cycles 29, 830–841. https://doi.org/10.1002/2014GB004998

Sallée, J.B., Speer, K., Rintoul, S., Wijffels, S., 2010. Southern Ocean Thermocline Ventilation. J. Phys. Oceanogr. 40, 509–529. https://doi.org/10.1175/2009JPO4291.1

Sarmiento, J.L., Gruber, N., Brzezinski, M.A., Dunne, J.P., 2004. High-latitude controls of thermocline nutrients and low latitude biological productivity. Nature 427, 56–60.

https://doi.org/10.1038/nature10605

Schlitzer, R., 2017. Ocean Data View. https://doi.org/10.1017/CBO9781107415324.004

Schlitzer, R., Anderson, R.F., Dodas, E.M., Lohan, M., Geibert, W., Tagliabue, A., Bowie, A., Jeandel, C., Maldonado, M.T., Landing, W.M., Cockwell, D., Abadie, C., Abouchami, W., Achterberg, E.P., Agather, A., Aguliar-Islas, A., van Aken, H.M., Andersen, M., Archer, C., Auro, M., de Baar, H.J., Baars, O., Baker, A.R., Bakker, K., Basak, C., Baskaran, M., Bates, N.R., Bauch, D., van Beek, P., Behrens, M.K., Black, E., Bluhm, K., Bopp, L., Bouman, H., Bowman, K., Bown, J., Boyd, P., Boye, M., Boyle, E.A., Branellec, P., Bridgestock, L., Brissebrat, G., Browning, T., Bruland, K.W., Brumsack, H.J., Brzezinski, M., Buck, C.S., Buck, K.N., Buesseler, K., Bull, A., Butler, E., Cai, P., Mor, P.C., Cardinal, D., Carlson, C., Carrasco, G., Casacuberta, N., Casciotti, K.L., Castrillejo, M., Chamizo, E., Chance, R., Charette, M.A., Chaves, J.E., Cheng, H., Chever, F., Christl, M., Church, T.M., Closset, I., Colman, A., Conway, T.M., Cossa, D., Croot, P., Cullen, J.T., Cutter, G.A., Daniels, C., Dehairs, F., Deng, F., Dieu, H.T., Duggan, B., Dulaquais, G., Dumousseaud, C., Echegoyen-Sanz, Y., Edwards, R.L., Ellwood, M., Fahrbach, E., Fitzsimmons, J.N., Russell Flegal, A., Fleisher, M.Q., van de Flierdt, T., Frank, M., Friedrich, J., Fripiat, F., Fröllje, H., Galer, S.J.G., Gamo, T., Ganeshram, R.S., Garcia-Orellana, J., Garcia-Solsona, E., Gault-Ringold, M., George, E., Gerringa, L.J.A., Gilbert, M., Godoy, J.M., Goldstein, S.L., Gonzalez, S.R., Grissom, K., Hammerschmidt, C., Hartman, A., Hassler, C.S., Hathorne, E.C., Hatta, M., Hawco, N., Hayes, C.T., Heimbürger, L.E., Helgoe, J., Heller, M., Henderson, G.M., Henderson, P.B., van Heuven, S., Ho, P., Horner, T.J., Hsieh, Y. Te, Huang, K.F., Humphreys, M.P., Isshiki, K., Jacquot, J.E., Janssen, D.J., Jenkins, W.J., John, S., Jones, E.M., Jones, J.L., Kadko, D.C., Kayser, R., Kenna, T.C., Khondoker, R., Kim, T., Kipp, L., Klar, J.K., Klunder, M., Kretschmer, S., Kumamoto, Y., Laan, P., Labatut, M., Lacan, F., Lam, P.J., Lambelet, M., Lamborg, C.H., Le Moigne, F.A.C., Le Roy, E., Lechtenfeld, O.J., Lee, J.M., Lherminier, P., Little, S., López-Lora, M., Lu, Y., Masque, P., Mawji, E., Mcclain, C.R., Measures, C., Mehic, S., Barraqueta, J.L.M., van der Merwe, P., Middag, R., Mieruch, S., Milne, A., Minami, T., Moffett, J.W., Moncoiffe, G., Moore, W.S., Morris, P.J., Morton, P.L., Nakaguchi, Y., Nakayama, N., Niedermiller, J., Nishioka, J., Nishiuchi, A., Noble, A., Obata, H., Ober, S., Ohnemus, D.C., van Ooijen, J., O'Sullivan, J., Owens, S., Pahnke, K., Paul, M., Pavia, F., Pena, L.D., Peters, B., Planchon, F., Planquette, H., Pradoux, C., Puigcorbé, V., Quay, P., Queroue, F., Radic, A., Rauschenberg, S., Rehkämper, M., Rember, R., Remenyi, T., Resing, J.A., Rickli, J., Rigaud, S., Rijkenberg, M.J.A., Rintoul, S., Robinson, L.F., Roca-Martí, M., Rodellas, V., Roeske, T., Rolison, J.M., Rosenberg, M., Roshan, S., Rutgers van der Loeff, M.M., Ryabenko, E., Saito, M.A., Salt, L.A., Sanial, V., Sarthou, G., Schallenberg, C., Schauer, U., Scher, H., Schlosser, C., Schnetger, B., Scott, P., Sedwick, P.N., Semiletov, I., Shelley, R., Sherrell, R.M., Shiller, A.M., Sigman, D.M., Singh, S.K., Slagter, H.A., Slater, E., Smethie, W.M., Snaith, H., Sohrin, Y., Sohst, B., Sonke, J.E., Speich, S., Steinfeldt, R., Stewart, G., Stichel, T., Stirling, C.H., Stutsman, J., Swarr, G.J., Swift, J.H., Thomas, A., Thorne, K., Till, C.P., Till, R., Townsend, A.T., Townsend, E., Tuerena, R., Twining, B.S., Vance, D., Velazquez, S., Venchiarutti, C., Villa-Alfageme, M., Vivancos, S.M., Voelker, A.H.L., Wake, B., Warner, M.J., Watson, R., van Weerlee, E., Alexandra Weigand, M., Weinstein, Y., Weiss, D., Wisotzki, A., Woodward, E.M.S., Wu, J., Wu, Y., Wuttig, K., Wyatt, N., Xiang, Y., Xie, R.C., Xue, Z., Yoshikawa, H., Zhang, J., Zhang, P., Zhao, Y., Zheng, L., Zheng, X.Y., Zieringer, M., Zimmer, L.A., Ziveri, P., Zunino, P., Zurbrick, C., 2018. The GEOTRACES Intermediate Data Product 2017. Chem. Geol. 493, 210–223. https://doi.org/10.1016/j.chemgeo.2018.05.040

Shaked, Y., Xu, Y., Leblanc, K., Morel, F.M.M., 2006. Zinc availability and alkaline phosphatase activity in Emiliania huxleyi : Implications for Zn – P co-limitation in the ocean. Limnol. Ocean. 51, 299–309. https://doi.org/https://doi.org/10.4319/lo.2006.51.1.0299

Sieber, M., Conway, T.M., Souza, G.F. De, Hassler, C.S., Ellwood, M.J., Vance, D., 2019. Cycling of zinc and its isotopes across multiple zones of the Southern Ocean : Insights from the Antarctic Circumnavigation Expedition. Geochim. Cosmochim. Acta. https://doi.org/10.1016/j.gca.2019.09.039

Sunda, W.G., Huntsman, S.A., 1998. Interactive effects of external manganese, the toxic metals copper and zinc, and light in controlling cellular manganese and growth in a coastal diatom. Limnol. Oceanogr. 43, 1467–1475. https://doi.org/https://doi.org/10.4319/lo.1998.43.7.1467

Sunda, W.G., Huntsman, S.A., 1996. Antagonisms between cadmium and zinc toxicity and manganese limitation in a coastal diatom. Limnol. Ocean. 41, 373–387. https://doi.org/https://doi.org/10.4319/lo.1996.41.3.0373

Tagliabue, A., Sallée, J.B., Bowie, A.R., Lévy, M., Swart, S., Boyd, P.W., 2014. Surface-water iron supplies in the Southern Ocean sustained by deep winter mixing. Nat. Geosci. 7, 314–320. https://doi.org/10.1038/ngeo2101

Takahashi, T., Broecker, W. S., and Langer, S.: Redfield ratio based on chemical data from isopycnal surfaces, J. Geophys. Res., 90, 6907–6924, https://doi.org/10.1029/JC090iC04p06907, 1985.

Thi Dieu Vu, H., Sohrin, Y., 2013. Diverse stoichiometry of dissolved trace metals in the Indian Ocean. Sci. Rep. 3, 1–5. https://doi.org/10.1038/srep01745

Tomczak, M.: A multi-parameter extension of temperature/salinity diagram techniques for the analysis of non-isopycnal mixing, Prog. Oceanogr., 10 (3), 147–171, http://dx.doi.org/10.1016/0079-6611(81)90010-0, 1981.

Tomczak, M.: Some historical, theoretical and applied aspects of quantitative water mass analysis, J. Mar. Res., 57, 275–303, https://doi.org/10.1357/002224099321618227, 1999.

Twining, B.S., Baines, S.B., 2013. The trace metal composition of marine phytoplankton. Ann. Rev. Mar. Sci. 5, 191–215. https://doi.org/10.1146/annurev-marine-121211-172322

Twining, B.S., Baines, S.B., Fisher, N.S., 2004. Element stoichiometries of individual plankton cells collected during the Southern Ocean Iron Experiment (SOFeX). Limnol. Oceanogr. 49, 2115–2128. https://doi.org/10.4319/lo.2004.49.6.2115

Twining, B.S., Baines, S.B., Fisher, N.S., Maser, J., Vogt, S., Jacobsen, C., Tovar-Sanchez, A., Sañudo-Wilhelmy, S.A., 2003. Quantifying trace elements in individual aquatic protist cells with a synchrotron X-ray fluorescence microprobe. Anal. Chem. 75, 3806–3816. https://doi.org/10.1021/ac034227z

Twining, B.S., Nodder, S.D., King, A.L., Hutchins, D.A., Lecleir, G.R., Debruyn, J.M., Maas, E.W., Vogt, S., Wilhelm, S.W., Boyd, P.W., 2014. Differential remineralization of major and trace elements in sinking diatoms. Limnol. Oceanogr. 59, 689–704. https://doi.org/10.4319/lo.2014.59.3.0689

Vance, D., Little, S.H., De Souza, G.F., Khatiwala, S., Lohan, M.C., Middag, R., 2017. Silicon and zinc biogeochemical cycles coupled through the Southern Ocean. Nat. Geosci. 10, 202–206. https://doi.org/10.1038/ngeo2890

Weber, T., John, S., Tagliabue, A., Devries, T., 2018. Biological uptake and reversible scavenging of zinc in the global ocean. Science (80-.). 361, 72–76. https://doi.org/10.1126/science.aap8532

Weir, I., Fawcett, S., Smith, S., Walker, D., Bornman, T., Fietz, S., in revision. Winter biogenic silica and diatom distribution in the Indian Sector of the Southern Ocean. Deep Sea Res. Part I Oceanogr. Res. Pap.

Wolters, M., 2002. Quickchem Method 31-114-27-1-D – Silicate in Brackish or Seawater. Colorado, USA.

Wyatt, N.J., Milne, A., Woodward, E.M.S., Rees, A.P., Browning, T.J., Bouman, H.A., Worsfold, P.J., Lohan, M.C., 2014. Biogeochemical cycling of dissolved zinc along the GEOTRACES South Atlantic transect GA10 at 40°S. Global Biogeochem. Cycles 28, 44–56. https://doi.org/10.1002/2013GB004637

Xie, R.C., Galer, S.J.G., Abouchami, W., Rijkenberg, M.J.A., De Jong, J., De Baar, H.J.W., Andreae, M.O., 2015. The cadmium-phosphate relationship in the western South Atlantic - The importance of mode and intermediate waters on the global systematics. Mar. Chem. 177, 110–123. https://doi.org/10.1016/j.marchem.2015.06.011

Zhao, Y., Vance, D., Abouchami, W., de Baar, H.J.W., 2014. Biogeochemical cycling of zinc and its isotopes in the Southern Ocean. Geochim. Cosmochim. Acta 125, 653–672.

https://doi.org/10.1016/j.gca.2013.07.045

Chapter 5
Synopsis

1. Summary and key contributions

Understanding the processes responsible for controlling the distributions of key trace metals is critical given their importance as micronutrients in the marine food web. Trace metal micronutrients serve essential roles in the metabolic and photosynthetic functioning of phytoplankton and their availability in the surface ocean has been shown to influence phytoplankton productivity and community composition (Sunda, 2012; William G. Sunda, 1989; Viljoen et al., 2019). Considering that phytoplankton drive carbon export, the distribution of micronutrients plays an important role in the functioning of the biological carbon pump. Thus far, the vast majority of investigations into trace metal cycling have been conducted in the spring/summer months (Schlitzer et al., 2018) when conditions theoretically favour phytoplankton growth. To date, only a handful of winter trace metal measurements have been published (e.g. Ellwood, 2008) thus our understanding of trace metal cycling over key seasonal transitions is extremely limited. This knowledge is particularly important in polar ocean settings i.e. the Southern Ocean, where seasonality is most pronounced and large environmental fluctuations are expected as a result of climate change (Deppeler and Davidson, 2017). To address these knowledge gaps, multiple expeditions were conducted in the Southern Ocean, where measurements of copper (Cu), zinc (Zn), nickel (Ni) and cadmium (Cd), key trace metal micronutrients, were made over biologically contrasting seasons (summer vs winter). In doing so, a number of significant contributions were made to the scientific community. First winter measurements of dissolved (0.2 µm filtered seawater) copper (dCu), zinc (dZn) and nickel (dNi) were presented from the Atlantic sector of the Southern Ocean (46° - 54°S; 0°) and compared to the respective summer measurements (46° - 68°S; 0°) which in turn, represented the first summer dNi data from this transect. In the Indian sector of the Southern Ocean (41° - 58°S; 30°E), first winter measurements of dissolved and particulate (0.45 µm filter paper) Zn and Cd provided the foundation to further investigate winter trace metal cycling and also the export of their particulate phases to the sub surface ocean.

The data presented in this thesis indicates that, in the Atlantic sector of the Southern Ocean, the winter season is characterised by reduced trace metal requirements by phytoplankton compared to spring/summer periods and augmentation through remineralisation in deep winter mixed layers. Correspondingly, trace metal concentrations in the biologically active mixed layer were higher in winter and showed greatest seasonal differences at higher latitudes in the Antarctic Zone (AAZ) of the Southern Ocean. In addition to reduced biological uptake during winter months, several factors including phytoplankton adaption strategies to seasonal light regimes, limitation of productivity by

other nutrients e.g. iron (Fe) and seasonal differences in zooplankton grazing habits are also likely to contribute to the observed trace metal seasonality. It is important to note that while biological activity might be reduced, the winter Southern Ocean is far from biologically dormant as previously hypothesized (Nelson and Smith, 1991). Further, the Southern Ocean reset state was characterised by deep mixed layers in winter compared to summer. For example, at the Antarctic Polar Front (APF), a particularly productive region in summer, the winter mixed layer was ~200 m deep, roughly double that of the comparative summer season. By comparing differences in trace metal inventories within the respective seasonal mixed layers, our data suggested that mixing of nutrient depleted summer surface waters with more enriched sub-surface waters i.e. deep winter mixing, could potentially resupply Cu, Zn and Ni to the surface ocean constituting an important supply mechanism for the initiation of spring phytoplankton blooms and maintenance of productivity throughout the summer season.

A subsequent winter expedition to the Indian sector of the Southern Ocean, with higher sampling resolution and the measurement of both dissolved (dCd, dZn) and particulate (pCd, pZn) phases, allowed for a more detailed investigation into processes controlling the distribution and biogeochemical cycling of these micronutrients. In agreement with observations in the Atlantic sector, our data suggest that biological uptake of dCd and dZn in surface waters, and remineralisation in the sub surface, play a major role in driving winter trace metal cycling. In addition, we observed distinct differences in Cd and Zn cycling within the various biogeochemical zones sampled along the transect. Of particular importance is the strong preferential uptake and assimilation of Cd and Zn, relative to the major nutrient phosphate (PO_4), by diatoms in the AAZ. The northward transport of the resulting Cd and Zn depleted surface waters significantly impacts trace metal cycling north of the Antarctic Polar front (APF) and has potential implications for low latitude trace metal supply via the northward flow of Sub Antarctic Mode Water (SAMW). The combined effect of preferential uptake and regeneration of diatoms with high Cd and Zn content and the upwelling of water masses at higher latitudes results in high surface dCd and dZn in the AAZ. Furthermore, Zn distributions are intimately related with those of silicic acid ($Si(OH)_4$) and biogenic silica (bSi), implicating diatoms as key controllers of their biogeochemical cycling. Overall, these results suggest that Cd and Zn distributions in the Southern Ocean are significantly impacted by winter phytoplankton communities and highlights the combined effect of ocean biogeochemistry and physical water mass circulation as key drivers of their cycling.

2. Recommendations and future work

By exploring the biogeochemical cycling of key trace metals in different seasons, the research presented in this dissertation has contributed toward a better understanding of trace metal seasonality. It has also however, highlighted a number of areas that future research should aim to address.

The distributions of trace metals presented here represent snapshot scenarios of the biogeochemical status of the ocean. In reality the ocean is a highly dynamic ecosystem and a much higher temporal resolution is necessary to capture processes occurring on timescales of hours to days. Of particular relevance here is the impact of intense storm activity on mixed layer dynamics (Swart et al., 2015) and the potential for increased turbulence to temporarily enhance trace metal supply to the upper surface water through deeper mixing with nutrient enriched subsurface water masses. In addition, expanding sampling efforts to also include spring and autumn seasons, particularly at the time of seasonal transition, will enable a more complete understanding of seasonal trace metal cycling. While advanced biogeochemical models have become useful tools in predicting trace metal seasonal cycling on regional scales (e.g. Tagliabue et al., 2014), they lack the ability to reproduce field observations at finer scales and highlight the need for field observations that are directed toward smaller meso- and sub-mesoscale processes. For example, mesoscale eddies, prominent in the Southern Ocean (Swart et al., 2008), show evidence of distinct trace metal cycling within their cores and may transport these signatures large distances as shown recently for the trace metal Fe (Ellwood et al., 2020). However our understanding of how these eddies influence the cycling Cu, Zn, Ni and Cd is extremely limited, particularly when eddies cross frontal zones and enter contrasting biogeochemical domains compared to their origin. Akin to eddy activity, little attention has been given to the potential role of melting seasonal ice and icebergs in supplying to trace metals to high latitude Southern Ocean surface waters. Considering future climate driven changes to polar environments (Deppeler and Davidson, 2017), increased ice and iceberg melting are anticipated to drive changes in trace metal supply and productivity in the Southern Ocean as shown for Fe (Hopwood and Cantoni, 2017; Lannuzel et al., 2016). In terms of sub-mesoscale processes, the recent use of trace metal isotopic data has proved extremely useful in understanding processes at the cellular uptake scale (Abouchami et al., 2014; Zhao et al., 2014) and highlights the advantages of using multi-parameter datasets particularly in regions as diverse as the Southern Ocean.

The difficulty in capturing higher spatial and temporal resolution trace metal measurements lies in a host of challenges including the rigorous sample collection protocols, ship time, research cost and manpower. The development of autonomous observing systems for micronutrient trace metals (see review by Grand et al., 2019) may provide the key to addressing current knowledge gaps. Already, the application of autonomous technologies such as gliders have proven effective in capturing physical and biological properties in the upper ocean at unprecedented spatial and temporal scales (du Plessis et al., 2017; Little et al., 2018). Future efforts should include working with the engineering and robotics industries to develop infrastructure that combines the analytical requirements and robustness necessary for deployment in highly variable and remote marine environments.

3. References

Abouchami, W., Galer, S.J.G., De Baar, H.J.W., Middag, R., Vance, D., Zhao, Y., Klunder, M., Mezger,

K., Feldmann, H., Andreae, M.O., 2014. Biogeochemical cycling of cadmium isotopes in the Southern Ocean along the Zero Meridian. Geochim. Cosmochim. Acta 127, 348–367. https://doi.org/10.1016/j.gca.2013.10.022

Deppeler, S.L., Davidson, A.T., 2017. Southern Ocean phytoplankton in a changing climate. Front. Mar. Sci. 4. https://doi.org/10.3389/fmars.2017.00040

du Plessis, M., Swart, S., Ansorge, I.J., Mahadevan, A., 2017. Submesoscale processes promote seasonal restratification in the the Subantarctic Ocean. J. Geophys. Res. Ocean. 122, 1–22. https://doi.org/10.1002/2016JC012494

Ellwood, M.J., 2008. Wintertime trace metal (Zn, Cu, Ni, Cd, Pb and Co) and nutrient distributions in the Subantarctic Zone between 40-52°S; 155-160°E. Mar. Chem. 112, 107–117. https://doi.org/10.1016/j.marchem.2008.07.008

Ellwood, M.J., Strzepek, R.F., Strutton, P.G., Trull, T.W., Fourquez, M., Boyd, P.W., 2020. Distinct iron cycling in a Southern Ocean eddy. Nat. Commun. 11, 1–8. https://doi.org/10.1038/s41467-020-14464-0

Grand, M.M., Laes-Huon, A., Fietz, S., Resing, J.A., Obata, H., Luther, G.W., Tagliabue, A., Achterberg, E.P., Middag, R., Tovar-Sánchez, A., Bowie, A.R., 2019. Developing autonomous observing systems for micronutrient trace metals. Front. Mar. Sci. 6. https://doi.org/10.3389/fmars.2019.00035

Hopwood, M.J., Cantoni, C., 2017. The heterogeneous nature of Fe delivery from melting icebergs. https://doi.org/10.7185/geochemlet.1723

Lannuzel, D., Vancoppenolle, M., Van Der Merwe, P., De Jong, J., Meiners, K.M., Grotti, M., Nishioka, J., Schoemann, V., 2016. Iron in sea ice: Review & new insights. Elementa 4, 1–19. https://doi.org/10.12952/journal.elementa.000130

Little, H.J., Vichi, M., Thomalla, S.J., Swart, S., 2018. Spatial and temporal scales of chlorophyll variability using high-resolution glider data. J. Mar. Syst. 187, 1–12. https://doi.org/10.1016/j.jmarsys.2018.06.011

Nelson, D.M., Smith, W.O., 1991. Sverdrup revisited: Critical depths, maximum chlorphyll levels, and the control of Southern Ocean productivity by the irradiance-mixing regime. Limnol. Ocean. 36, 1650–1661. https://doi.org/https://doi.org/10.4319/lo.1991.36.8.1650

Scambos, T.A., Hulbe, C., Fahnestock, M., Bohlander, J., 2000. The link between climate warming and break-up of ice shelves in the Antarctic Peninsula. J. Glaciol. 46, 516–530. https://doi.org/10.3189/172756500781833043

Schlitzer, R., Anderson, R.F., Dodas, E.M., Lohan, M., Geibert, W., Tagliabue, A., Bowie, A., Jeandel, C., Maldonado, M.T., Landing, W.M., Cockwell, D., Abadie, C., Abouchami, W., Achterberg, E.P., Agather, A., Aguliar-Islas, A., van Aken, H.M., Andersen, M., Archer, C., Auro, M., de Baar, H.J., Baars, O., Baker, A.R., Bakker, K., Basak, C., Baskaran, M., Bates, N.R., Bauch, D., van Beek, P., Behrens, M.K., Black, E., Bluhm, K., Bopp, L., Bouman, H., Bowman, K., Bown, J., Boyd, P., Boye, M., Boyle, E.A., Branellec, P., Bridgestock, L., Brissebrat, G., Browning, T., Bruland, K.W., Brumsack, H.J., Brzezinski, M., Buck, C.S., Buck, K.N., Buesseler, K., Bull, A., Butler, E., Cai, P., Mor, P.C., Cardinal, D., Carlson, C., Carrasco, G., Casacuberta, N., Casciotti, K.L., Castrillejo, M., Chamizo, E., Chance, R., Charette, M.A., Chaves, J.E., Cheng, H., Chever, F., Christl, M., Church, T.M., Closset, I., Colman, A., Conway, T.M., Cossa, D., Croot, P., Cullen, J.T., Cutter, G.A., Daniels, C., Dehairs, F., Deng, F., Dieu, H.T., Duggan, B., Dulaquais, G., Dumousseaud, C., Echegoyen-Sanz, Y., Edwards, R.L., Ellwood, M., Fahrbach, E., Fitzsimmons, J.N., Russell Flegal, A., Fleisher, M.Q., van de Flierdt, T., Frank, M., Friedrich, J., Fripiat, F., Fröllje, H., Galer, S.J.G., Gamo, T., Ganeshram, R.S., Garcia-Orellana, J., Garcia-Solsona, E., Gault-Ringold, M., George, E., Gerringa, L.J.A., Gilbert, M., Godoy, J.M., Goldstein, S.L., Gonzalez, S.R., Grissom, K., Hammerschmidt, C., Hartman, A., Hassler, C.S., Hathorne, E.C., Hatta, M., Hawco, N., Hayes, C.T., Heimbürger, L.E., Helgoe, J., Heller, M.,

Henderson, G.M., Henderson, P.B., van Heuven, S., Ho, P., Horner, T.J., Hsieh, Y. Te, Huang, K.F., Humphreys, M.P., Isshiki, K., Jacquot, J.E., Janssen, D.J., Jenkins, W.J., John, S., Jones, E.M., Jones, J.L., Kadko, D.C., Kayser, R., Kenna, T.C., Khondoker, R., Kim, T., Kipp, L., Klar, J.K., Klunder, M., Kretschmer, S., Kumamoto, Y., Laan, P., Labatut, M., Lacan, F., Lam, P.J., Lambelet, M., Lamborg, C.H., Le Moigne, F.A.C., Le Roy, E., Lechtenfeld, O.J., Lee, J.M., Lherminier, P., Little, S., López-Lora, M., Lu, Y., Masque, P., Mawji, E., Mcclain, C.R., Measures, C., Mehic, S., Barraqueta, J.L.M., van der Merwe, P., Middag, R., Mieruch, S., Milne, A., Minami, T., Moffett, J.W., Moncoiffe, G., Moore, W.S., Morris, P.J., Morton, P.L., Nakaguchi, Y., Nakayama, N., Niedermiller, J., Nishioka, J., Nishiuchi, A., Noble, A., Obata, H., Ober, S., Ohnemus, D.C., van Ooijen, J., O'Sullivan, J., Owens, S., Pahnke, K., Paul, M., Pavia, F., Pena, L.D., Peters, B., Planchon, F., Planquette, H., Pradoux, C., Puigcorbé, V., Quay, P., Queroue, F., Radic, A., Rauschenberg, S., Rehkämper, M., Rember, R., Remenyi, T., Resing, J.A., Rickli, J., Rigaud, S., Rijkenberg, M.J.A., Rintoul, S., Robinson, L.F., Roca-Martí, M., Rodellas, V., Roeske, T., Rolison, J.M., Rosenberg, M., Roshan, S., Rutgers van der Loeff, M.M., Ryabenko, E., Saito, M.A., Salt, L.A., Sanial, V., Sarthou, G., Schallenberg, C., Schauer, U., Scher, H., Schlosser, C., Schnetger, B., Scott, P., Sedwick, P.N., Semiletov, I., Shelley, R., Sherrell, R.M., Shiller, A.M., Sigman, D.M., Singh, S.K., Slagter, H.A., Slater, E., Smethie, W.M., Snaith, H., Sohrin, Y., Sohst, B., Sonke, J.E., Speich, S., Steinfeldt, R., Stewart, G., Stichel, T., Stirling, C.H., Stutsman, J., Swarr, G.J., Swift, J.H., Thomas, A., Thorne, K., Till, C.P., Till, R., Townsend, A.T., Townsend, E., Tuerena, R., Twining, B.S., Vance, D., Velazquez, S., Venchiarutti, C., Villa-Alfageme, M., Vivancos, S.M., Voelker, A.H.L., Wake, B., Warner, M.J., Watson, R., van Weerlee, E., Alexandra Weigand, M., Weinstein, Y., Weiss, D., Wisotzki, A., Woodward, E.M.S., Wu, J., Wu, Y., Wuttig, K., Wyatt, N., Xiang, Y., Xie, R.C., Xue, Z., Yoshikawa, H., Zhang, J., Zhang, P., Zhao, Y., Zheng, L., Zheng, X.Y., Zieringer, M., Zimmer, L.A., Ziveri, P., Zunino, P., Zurbrick, C., 2018. The GEOTRACES Intermediate Data Product 2017. Chem. Geol. 493, 210–223. https://doi.org/10.1016/j.chemgeo.2018.05.040

Sunda, W.G., 2012. Feedback interactions between trace metal nutrients and phytoplankton in the ocean. Front. Microbiol. 3, 1–22. https://doi.org/10.3389/fmicb.2012.00204

Sunda, W.G., 1989. Trace metal interactions with marine phytoplankton. Biol. Oceanogr. 6, 411–442. https://doi.org/10.1080/01965581.1988.10749543

Swart, N.C., Ansorge, I.J., Lutjeharms, J.R.E., 2008. Detailed characterization of a cold Antarctic eddy. J. Geophys. Res. Ocean. 113, 1–15. https://doi.org/10.1029/2007JC004190

Swart, S., Thomalla, S.J., Monteiro, P.M.S., 2015. The seasonal cycle of mixed layer dynamics and phytoplankton biomass in the Sub-Antarctic Zone: A high-resolution glider experiment. J. Mar. Syst. 147, 103–115. https://doi.org/10.1016/j.jmarsys.2014.06.002

Tagliabue, A., Sallée, J.B., Bowie, A.R., Lévy, M., Swart, S., Boyd, P.W., 2014. Surface-water iron supplies in the Southern Ocean sustained by deep winter mixing. Nat. Geosci. 7, 314–320. https://doi.org/10.1038/ngeo2101

Viljoen, J.J., Weir, I., Fietz, S., Cloete, R., Loock, J., Philibert, R., Roychoudhury, A.N., 2019. Links between the phytoplankton community composition and trace metal distribution in summer surface waters of the Atlantic southern ocean. Front. Mar. Sci. 6, 1–17. https://doi.org/10.3389/fmars.2019.00295

Woodward, S., Roberts, D.L., Betts, R.A., 2005. A simulation of the effect of climate change-induced desertification on mineral dust aerosol. Geophys. Res. Lett. 32, 1–4. https://doi.org/10.1029/2005GL023482

Zhao, Y., Vance, D., Abouchami, W., de Baar, H.J.W., 2014. Biogeochemical cycling of zinc and its isotopes in the Southern Ocean. Geochim. Cosmochim. Acta 125, 653–672. https://doi.org/10.1016/j.gca.2013.07.045

Appendix A

This appendix contains a detailed description of the methodology employed in order to produce the dissolved trace metal data presented in Chapters 2, 3, 4. The method can be separated into two major components namely the seawater sample collection and the seawater analysis. The analytical complexities associated with trace metal geochemistry are notorious. Implementing this particular methodology for the first time on South African soil necessitated the need for a full method validation. The work described in this appendix was not solely my own and represents equal contributions from myself and fellow PhD candidate Jean Loock.

1. Introduction

Understanding the biogeochemical cycling of trace metals in marine systems has proven paramount given their importance as micronutrients, toxins, tracers of anthropogenic input and potential paleoproxies. It is well established that Manganese (Mn), Iron (Fe), Cobalt (Co), Nickel (Ni), Copper (Cu), Zinc (Zn) and Cadmium (Cd) play essential roles in the metabolic functioning of marine phytoplankton (Bruland et al., 1991; Frew et al., 2001; Moffett and Ho, 1996; Sunda and Huntsman, 1995) Conversely, elevated levels of certain metals, e.g. Cu and Cd, can be toxic to individual phytoplankton species (Brand et al., 1986). Lead (Pb), while not recognised as a bioactive trace metal, has demonstrated usefulness as a tracer of anthropogenic inputs (Boyle et al., 2014). Similarly, Mn and Fe are useful tracers of hydrothermal and riverine inputs, as well as redox cycling (Klunder et al., 2011; Middag et al., 2011). Thus, the initiation of current collaborative platforms such as the GEOTRACES program, and its precursor programs e.g. JGOFS (joint global ocean flux study) and WOCE (world ocean circulation experiment), have proved central to our progressive understanding of biogeochemical cycles whilst also providing a framework for collaborative reporting. The Centre for Trace Metal and Experimental Biogeochemistry (TracEx) at Stellenbosch University was developed to lead South Africa's contribution to the global ocean database. However, given the analytical difficulties associated with marine trace metal chemistry, data contribution requires the full validation of the scientific method.

Analytical difficulties arise from the seawater matrix and the resultant polyatomic interferences, triggered by the presence of mmol kg^{-1} concentrations of cations (e.g. Na^{+}) and anions (e.g. Cl^{-}), as well as instrument capabilities in detecting ultra-low trace metal concentrations in open ocean samples (Milne et al., 2010). Fortunately, recent advancements in the field of analytical chemistry have resulted in the availability of numerous methods with the required sensitivity to measure the inherently low (nmol kg^{-1} to pmol kg^{-1}) concentration ranges exhibited by trace metals in the open ocean. To circumvent matrix derived issues, modern techniques employ a preconcentration step to separate the seawater matrix from the trace elements prior to quantification. Separation and preconcentration methods include solvent extraction (Bruland and Franks, 1979), co-precipitation with magnesium hydroxide ($MgOH_2$; Wu and Boyle, 1997) and solid phase extraction (SPE) using a suitable chelating resin (Wells and Bruland, 1998). While solvent extraction is extremely labour intensive, co-precipitation methods have shown severe matrix effects at high salinities (Komjarova and Blust, 2006). Recently, the SPE technique using the automated sea*FAST* preconcentration system has been employed with great effect (Jackson et al., 2018; Rapp et al., 2017). SPE involves a high affinity metal chelating resin column designed to separate metal ions from their seawater matrix. A variety of chelating resins, each containing various functional groups, are available however some of these resins, such as the silica-immobilized 8-hydroxyquinoline (8-HQ), must be synthesized from scratch and are therefore not commercially available (Mclaren et al., 1985). Commercially available resins containing the

nitriloacetate (NTA) (Lee et al., 2011) and iminodiacetic acid (IDA; (Ho et al., 2010; Milne et al., 2010) functional groups have proved successful in the metal extraction procedure. Several more recent studies have, to great effect, used a chelating resin containing the IDA functional group in combination with the ethylenediaminetriacetic acid (EDTriA) functional group in the simultaneous multi-element extraction of trace metals from seawater (Jackson et al., 2018; Minami et al., 2015; Quéroué et al., 2014).

Similarly, numerous methods have been employed in the quantification of trace metals e.g. Flow Injection Analysis (FIA; Bowie et al., 1998; Croot and Laan, 2002), Cathodic Stripping Voltammetry (CSV; Colombo and van den Berg, 1997; Saito and Moffett, 2001), Graphite Furnace Atomic Adsorption Spectrometry (GFAAS; Kingston et al., 1978) and spectrophotometry (Blain and Tregeur, 1995; King et al., 1991). However, many of the methods are constrained by single element determination and lack the required sensitivity and reproducibility essential in trace metal analysis. Consequently, variations of mass spectrometry including Inductively coupled plasma mass spectrometry (ICP-MS), have proven attractive as these methods combine simultaneous multi-element detection capabilities with the sensitivity required for extremely low analyte signals (Jerez Veguería et al., 2013; Rahmi et al., 2007). Historically, the major drawback of this technique was the occurrence of spectral interferences on the analyte signal (Tan and Horlick, 1986). In order to mitigate the interferences, more advanced mass spectrometers have been developed and applied with great success e.g. Sector-Field (SF) ICP-MS (Minami et al., 2015; Quéroué et al., 2014; Rapp et al., 2017), Multicollector (MC) ICP-MS (De Jong et al., 2012; Takano et al., 2017) and ICP-tandem mass spectrometry (ICP-MS/MS) (Jackson et al., 2018). For SF ICP-MS, by operating the instrument at a higher mass resolution (e.g. R = 10 000), the analyte can be separated from interfering ions that have the same nominal mass yet small differences in their exact masses (e.g. $^{40}Ar^{16}O^{+}$ and $^{56}Fe^{+}$) (Balcaen et al., 2015). A major drawback of this method is the decreased ion transmission, and hence instrument sensitivity, with increasing mass resolution (Jakubowski et al., 1998). By using multiple collectors (Faraday cups), MC ICP-MS can simultaneously detect a range of isotopes, eliminating sources of uncertainty common to quadrupole based instruments that arise from sequential isotope scanning (Moldovan et al., 2004). This variation of ICP-MS is however highly susceptible to instrumental mass bias (Walczyk, 2004). Traditionally, standard quadrupole ICP-MS instruments lacked the ability to completely remove interferences on the analyte signal. Improvements saw the original quadrupole instrument fitted with a collision/reaction cell (CRC) (Tanner and Baranov, 1999) e.g. an octopole collision cell (Yamada et al., 2002). Instruments fitted with a CRC rely on gas phase reactions within the pressurised cell, as opposed to collision-induced dissociation for the other methods. Two types of gas phase reactions are responsible for removing interferences. Firstly, the reaction of the analyte and/or interfering ion(s) with a reactive gas (e.g. H_2; Feldmann et al., 1999), and secondly, a collision reaction between the ions and a non-reactive gas (e.g. He; Yamada et al., 2002). Both reaction types take place

in combination with Kinetic Energy Discrimination (KED), an added means of controlling cell-formed interferences and reducing polyatomic ion interferences (Yamada, 2015). By applying a decelerating potential across the cell, KED is able to separate the polyatomic ions based on their greater energy loss during the collision when compared to the analyte ions. The addition of a CRC to ICP-MS instruments is a simple, cost effective technique in the field of marine trace metal geochemistry. More recent advancements have seen the addition of an extra quadrupole (ICP-MS/MS) before the CRC giving the operator more control over the reactions taking place in the cell (Balcaen et al., 2015). The added complexity of ICP-MS/MS instruments however means they are extremely expensive.

Presented here is a rapid and economical method for the precise, simultaneous determination of Mn, Fe, Co, Ni, Cu, Zn, Cd and Pb in seawater. The method combines the commercially available sea*FAST* preconcentration and matrix removal module, with a single quadrupole ICP-MS for the offline quantification of trace metals. Validation of the method's accuracy and precision was achieved by analysis of SAFe and GEOTRACES inter-comparison samples and internal seawater reference material.

2. Analytical Methods

2.1. Reagents and Materials

All plastic ware, containers and sample bottles used for the storage of seawater and reagents were extensively acid cleaned according to strict protocols outlined by GEOTRACES. Cleaning consisted of soaking in Extran® (Merck) alkaline detergent for 1 week, 6M HCl (reagent grade, uniLAB®, Merck) for 1 month and 1M HCl (Suprapur®, Merck) for 1 month. Ultra-high purity water (UHPW), produced with the Milli-Q® Advantage A10 system (Millipore), was used to rinse sample bottles in between cleaning stages. An ammonium acetate buffer solution (pH = 6.0 ± 0.2) was prepared from ammonium hydroxide (25% diluted to 22% NH4OH; Suprapur®, Merck) and glacial acetic acid (100% CH3COOH; Suprapur®, Merck). The eluent was prepared using nitric acid (60% HNO3; Ultrapur®, Merck). All reagents were prepared in UHPW inside a fume hood housed within a class 100 clean laboratory. Seawater samples were collected and stored in 125 ml low density polyethylene (LDPE) bottles. Aliquots of seawater were transferred into 14 ml polypropylene (PP) Falcon™ tubes (Fischer Sci.) prior to preconcentration.

2.2. Automated Preconcentration using sea*FAST* module

A commercially available sea*FAST*-pico SC-4 DX module (Fig. 1, Elemental Scientific Inc.) was used to strip the seawater samples of their bulk seawater matrix via solid phase extraction (SPE). The preconcentration module is an ultra-clean, automated, low-pressure ion chromatography system capable of picogram L^{-1} detection limits. Samples were introduced into the manifold via a combined sample probe (1.0mm inner diameter) and vacuum pump system. The S400V syringe pump controlled four syringes (S1, S2, S3 and S4) dedicated to reagent distribution while their flowpath was controlled by

the FAST DX 3 valve module. The sea*FAST* module includes a metal chelating resin column (200 µL bed volume; 20 µEq column capacity) comprising ethylenediaminetriacetic acid (EDTriA) and iminodiacetic acid (IDA) functional groups immobilized on a hydrophilic methacrylate polymer (60 µm bead diameter). The system was pressurized using clean air (99.999% O_2; Air Products).

The closed system was set up in a class 100 clean lab and controlled using the ESI software and protocols. Ultrapure Sodium Chloride (3% NaCl, Elemental Sci.) was used to condition the resin column prior to preconcentration of an internal control and subsequent samples. Samples were preconcentrated in the offline configuration mode. Here, 10 ml of acidified seawater was vacuum pumped to fill the sample line while a syringe pump filled the buffer line. The sample was then buffered and pumped across the resin column, chelating the metal ions while washing the matrix ions from the column. The chelated metal ions were eluted into acid cleaned Falcon™ tubes during 4 elution cycles for a final elution volume of 250 µL, achieving a preconcentration factor of 40. This enabled picogram per litre detection limits whilst minimising sample preconcentration time to 20 minutes per sample. After each sample, the probe was rinsed in a 2% HNO_3 (Ultrapur®, Merck) solution followed by UHPW.

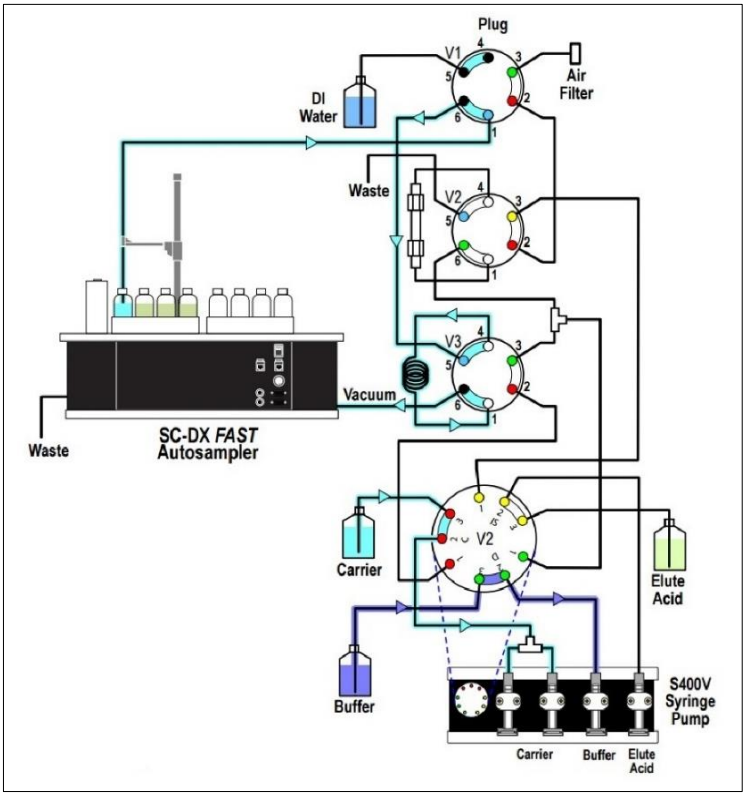

Figure 1. *Schematic illustration of the seaFAST (SX-4) preconcentration system. 10 ml of seawater is taken up by the probe, located on the autosampler, which is controlled by the S400V vacuum syringe pump. The sample is buffered before it is pumped through the metal chelating resin column. The chelated metal ions are then eluted from the resin column with an elution acid, in low volumes (250 µl), into acid cleaned falcon tubes via the sample probe. Figure taken from the ESI SC-4 DX manual.*

2.3. ICP-MS

Sample analysis was performed on an Agilent 7900 quadrupole Inductively Coupled Plasma Mass Spectrometer (ICP-MS) with operating conditions outlined in Table 1. The instrument was optimized for sensitivity and low oxide ratios (<0.3%). Due to the small sample volume (250 µl), samples were introduced using a low flow self-aspirating PFA nebulizer with a flow rate of ~0.2 µl min^{-1}. Isotopes of Mn^{55}, Co^{59}, Ni^{60}, Cu^{63}, Zn^{66}, Cd^{111}, Cd^{112} and Pb^{208} were measured using the Agilent Octopole Reaction System (ORS) in He collision mode, while Fe^{56} was analysed in H_2 reaction mode, to eliminate plasma and matrix-based interferences; though the latter was extensively reduced by using the ESI seaFAST system to remove the seawater matrix.

The instrument was calibrated using a custom blend ICP-MS multi-element standard (MES) from Inorganic Ventures, containing only metals and no alkali ions, and verified with the IV-28 MES standard from Inorganic Ventures. All standards and controls were prepared in 2% HNO_3 (Ultrapure®, Merck); having the same matrix as eluted sea*FAST* samples. A 4-point calibration curve was constructed over a wide concentration range using: 0 ppb, 1 ppb, 10 ppb and 20 ppb concentrations. Instrument detection limits (DL) were determined from 10 blank measurements and calculated as (blank + 3σblank)/sensitivity.

Online internal standard addition for drift correction was not possible using the self-aspirating nebulizer. Analysis was therefore carried out in a standard sample bracketing format by running the MES calibration standard every 6 samples. Where drift exceeded 5% relative to the starting concentration of the MES for a specific element, a drift correction was applied using the formula: 2*ConcMES_start/(ConcMES_a + ConcMES_b)*ConcSample, where a and b are the MES before and after each set of 6 samples. The instrument was re-calibrated if the drift exceeded 20%, or after 4 hours of instrument run time. To reduce contaminant risk, preconcentrated samples were opened ± 5 seconds prior to autosampler probe uptake.

Table 1. *Agilent 7900 ICP-MS instrument parameters.*

ICP-MS operating parameters	
Nebulizer	200µl PFA
Skimmer cone	Ni plated
Sensitivity	>10^9 cps/ppm at <2% CeO
RF power (W)	1600
Carrier gas (L min^{-1})	0.90
Sample probe depth (mm)	10
Make-up gas (L min^{-1})	0.25
He gas flow (ml min^{-1})	4.50
H_2 gas flow (ml min^{-1})	6

2.4. Reference Materials

2.4.1. GEOTRACES and NASS

The accuracy of the method was evaluated using the community verified SAFe (D2-98) deep ocean GEOTRACES reference material (RM) collected during the 2004 Sampling and Analysis of Fe (SAFe) intercalibration cruise. Accuracy was also verified using the commercial NASS-7 (National Research Council, Canada) certified reference material (CRM). Additionally, the GEOTRACES RM's, GSP (62) and GSC (1-19), collected during the 2009 GEOTRACES North Pacific Intercalibration cruise, were analysed.

2.4.2. Internal Controls

Given the scarcity of community RM's and their low volumes, the TracEx lab developed two internal seawater controls namely: Trace Metal 4 (TM4A) and Winter Indian Southern Ocean Standard (WISOS). The TM4A control constitutes bulk seawater collected from the surface at 36°S; 13°E during the SANAE 54 cruise whilst the WISOS control was collected from surface waters at 55°S; 28°E during the 2017 Indian Ocean cruise. Seawater was filtered through a 0.2 µm filter (see section 2.8 for details) into acid cleaned 20L LDPE containers. Sub-samples (1 L) of the bulk seawater were then acidified (pH = 1.7). A "calibrated" mean concentration was established for all trace metals by replicate analysis (n = 10) of the internal controls in conjunction with the GEOTRACES RM's and NASS CRM. The internal controls were subjected to the same analytical methods as the field seawater samples and inserted at regular intervals (12 samples) during preconcentration and analysis of samples. Given the similarity to field samples the controls were ideal proxies to monitor the precision and repeatability of the method in its entirety. Additionally, the IV-28 MES (not subjected to preconcentration) was inserted at 6 sample interludes during ICP-MS analysis functioning as a quality control (QC) check for the instrument during ICP-MS analysis.

2.5. Blanks

The method blank incorporates the potential contribution of the reagents, materials, instrument manifolds and arbitrary incidents, to the field sample. This was quantified by preconcentrating 10ml of Milli-Q using the same analytical technique employed for field samples. The instrument (ICP-MS) blank was quantified by introducing a solution of 2% HNO_3 (identical to the seaFAST eluent) in Milli-Q without the preconcentration step.

2.6. Recovery and Carry Over

The recovery of the seaFAST resin was quantified through replicate analysis of a preconcentrated internal control, with and without the addition of a 200 ppt multi-element spike (Inorganic Ventures IV-28). The internal control used was the Winter Indian Southern Ocean Standard (WISOS).

Furthermore, the relatively high trace metal concentrations in the NASS 7 CRM permitted the evaluation of method (resin or ICP-MS) carry over at concentrations in excess of one order of magnitude greater than the working field sample. Here, results from the analysis of the TM4A internal control samples that were preconcentrated prior to, and post NASS 7 on the seaFAST module, and analysed in the same order, were compared.

2.7. Sample Collection

Seawater samples were collected along the Cape Town–Antarctica transect using twenty-four 12L Teflon coated GO-FLO bottles (General Oceanics) mounted on a GEOTRACES compliant CTD rosette (Figure 2a). A vertical depth profile sampling method was executed according to GEOTRACES compliant clean protocol (Cutter and Bruland, 2012). Directly upon recovery of the rosette, the GO-FLO bottles were transported into a class 100 clean lab for sub-sampling (Figure 2b). Samples for dissolved trace metal determination were collected in 125 ml acid-cleaned, Nalgene™ (Thermo Scientific™) LDPE bottles after online filtration through 0.2 µm Acropak™ Capsule (Supor® 500) filters under slight N_2 gas (99.999% N_2, BIP technology) assistance (Figure 2c). Samples were acidified (pH=1.7) on-board under a class 10 laminar flowhood using hydrochloric acid (HCl, Ultrapur®, Merck) and stored for later analysis in Stellenbosch, South Africa.

3. Results

3.1. ICP-MS Performance

3.1.1. Blanks and Detection Limits

Instrument (ICP-MS) blanks, method blanks and detection limits are compiled and compared to previous methods in Table 2. The ICP-MS instrument blanks were below the detection limit for all elements except Ni (0.024 nmol kg^{-1}) and Zn (0.070 nmol kg^{-1}). The method blank contribution was quantified at picomolar (e.g. Cd) or sub-picomolar (e.g. Mn, Fe, Co, Ni, Cu, Zn and Pb) levels, contributing between 0.20% (Cd) and 4.28% (Fe) of the typical open ocean concentrations presented in Sohrin et al., 2008. Similarly, detection limits for all metals were at sub-picomolar concentrations.

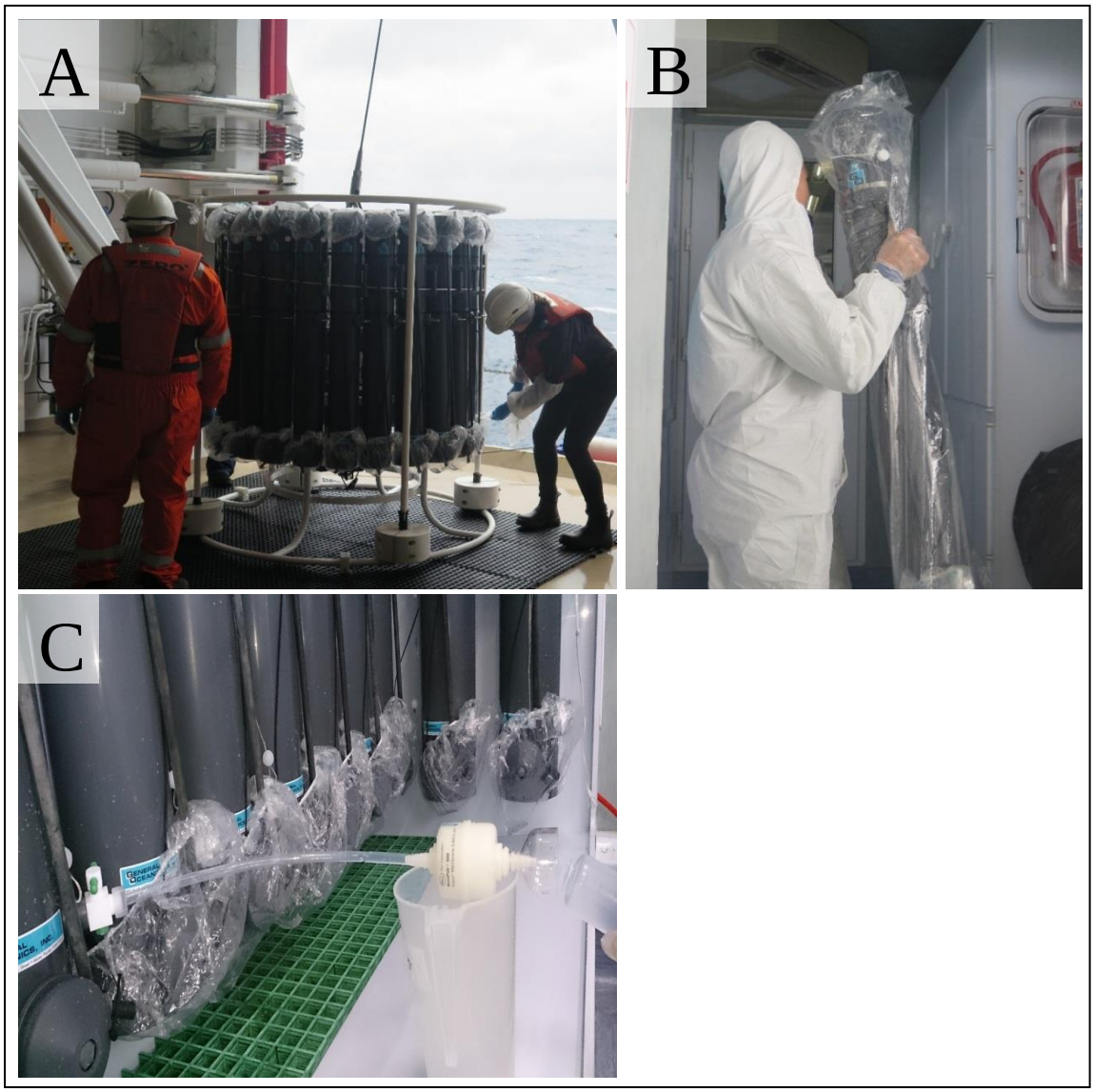

Figure 2. *A) removal of shower caps from GO-FLO bottles before the rosette is launched. B) transportation of GO-FLO bottles to and from the on-board class 100 clean lab. Note the PVC lining enclosing the GO-FLO bottles. C: filtering (0.2 µm) seawater for the determination of the dissolved trace metal fraction.*

***Table 2**. Observed instrument and method blank values with comparisons to relevant literature. Calculated detection limits were also compared to relevant literature values. All values in nmol kg^{-1}. *values in pmol kg $^{-1}$. [a] Typical open ocean trace metal concentrations from Sohrin et al., (2008). [b] Detection limits calculated as (blank + 3σ_{blank})/sensitivity.*

					Method Blank comparisons						Detection limit comparisons			
			Method Blank											
Element	Isotope	Instrument Blank	n	mean	Minami et al.	Sohrin et al.	Quéroué et al.	Jackson et al.	Open Ocean[a]	Detection Limit[b]	Minami et al.	Sohrin et al.	Quéroué et al.	Jackson et al.
Mn	55	<0.000	9	0.001	0.001	<0.010	0.004	0.006	0.4	0.001	0.003	0.010	0.002	0.002
Fe	56	<0.000	9	0.023	0.032	0.033	0.250	0.140	0.5	0.019	0.090	0.040	0.090	0.029
Ni	60	0.024	9	0.033	0.017	<0.010	0.013	0.053	8.5	0.011	0.070	0.010	0.003	0.030
Cu	63	<0.000	9	0.086	0.017	<0.005	0.053	0.030	3.1	0.020	0.020	0.005	0.030	0.008
Zn	66	0.070	9	0.089	0.120	0.071	n.a.	0.025	4.6	0.014	0.100	0.060	n.a.	0.017
Co*	59	<0.000	9	0.687	0.500	<2.000	1.700	n.a.	17.0	0.485	2.000	2.000	0.700	n.a.
Cd*	111	<0.000	9	1.217	<2.000	<9.000	0.190	0.340	622.7	0.888	2.000	9.000	0.120	0.600
Pb*	208	<0.000	9	0.218	0.300	1.600	0.720	0.460	9.7	0.201	0.900	1.000	0.200	0.300

3.1.2. Precision – Internal Control

The method precision was evaluated on the results of the internal and quality control solutions shown in Table 3. The analytical precision was quantified at the 95% confidence interval using the in-run TM4A internal control results in comparison to their "calibrated" mean concentration (TracEx calibration). Results are presented ± 1 standard deviation while the percentage relative standard deviation (%RSD) value was calculated as: (standard deviation/mean metal concentration)*100. The mean method precision, calculated as the mean of each individual metals precision value (Table 3), was 5.74 %RSD across all elements for the TM4A internal control. The results substantiate highly precise measurements with concentrations falling within the analytical error of the "calibrated" value. Comparatively, the precision of the ICP-MS instrument proved within 1% of the certified value for the trace metal suite under replicate analysis of the IV-28 MES (Table 3).

3.1.3. Accuracy – GEOTRACES and NASS

Method accuracy was established using the reference and certified reference materials shown in Table 3. Analytical accuracy was assessed using the results of the GEOTRACES RM's in comparison to the established consensus values. Results were within analytical uncertainty, with the exception of Co and Cu for SAFe D2 (see section 4.1.4), and Zn and Cd for GSP although the large analytical uncertainties observed at these extremely low concentrations are noted. Cobalt (Co) consensus values for GSC and GSP have yet to be established therefore results were compared with recently published values from Wuttig et al., (2019). The NASS-7 CRM results demonstrate good agreement with the certified values across the suite of trace metals.

3.1.4. Recovery and Carry-Over

The recovery of the seaFAST resin ranged between 100 – 109% (±5) for all metals supporting quantitative recovery (Table 4). Moreover, a simple sample carry-over test was performed by the repeat in sequence preconcentration and analysis of the low concentration TM4A internal control after the NASS-7 CRM. NASS-7 has markedly higher trace metal concentrations; more than an order of magnitude greater for Mn, Fe, and Co, relative to the TM4A internal control. The results of the internal control post NASS-5 were compared to the established mean of the "calibrated" TM4A internal control. TM4A concentrations of 0.29 and 0.34nmol kg^{-1} for Mn and Fe respectively and 17.50 pmol kg^{-1} for Co were within the analytical uncertainty of the calibrated mean values of 0.26 nmol kg^{-1}, 0.34 nmol kg^{-1} and 18.23 pmol kg^{-1} for Mn, Fe and Co respectively. Ultimately this indicated no carry-over (memory) effect which may arise if metals from the previous sample were not wholly eluted from the resin column.

Table 3. *Results of analysed reference seawater compared to available consensus data. The Co results for the GSC and GSP reference seawater were compared to Wuttig et al., 2019 as consensus values have yet to be established. Results of the in-run internal and quality control (QC) materials compared to the calibrated mean and certified values respectively. All results indicate mean values over a number of analyses (n) ±1 standard deviation. UV irradiation was not performed on samples therefore Co and Cu are reported as the labile dissolved fraction as opposed to the total dissolved fraction for all other metals.*

	Mn *nmol kg^{-1}*	**Fe** *nmol kg^{-1}*	**Ni** *nmol kg^{-1}*	**Cu** *nmol kg^{-1}*	**Zn** *nmol kg^{-1}*	**Co** *pmol kg^{-1}*	**Cd** *pmol kg^{-1}*	**Pb** *pmol kg^{-1}*
SAFe D2								
Consensus	0.35 ± 0.05	0.93 ± 0.04	8.63 ± 0.25	2.28 ± 0.15	7.43 ± 0.25	45.7 ± 2.90	986 ± 23	28.5 ± 1.2
TracEx (n=5)	0.40 ± 0.035	0.96 ± 0.025	8.05 ± 0.10	2.04 ± 0.03	7.23 ± 0.25	32.7 ± 0.44	955 ± 60	28.5 ± 1.2
TracEx %RSD	8.75	3.13	1.24	1.47	3.46	1.35	6.28	4.21
NASS-7								
Certified	13.47 ± 1.09	6.16 ± 0.47	4.14 ± 0.31	3.07 ± 0.22	6.27 ± 1.22	242.65 ± 23.76	141.50 ± 14.40	12.07 ± 3.86
TracEx (n=5)	13.43 ± 0.78	5.77 ± 0.28	3.90 ± 0.07	3.11 ± 0.08	6.59 ± 0.07	261.40 ± 5.40	132.69 ± 3.08	15.19 ± 1.87
TracEx %RSD	5.81	4.85	1.79	2.57	1.06	2.07	2.32	12.31
GSC								
Consensus	2.18 ± 0.08	1.54 ± 0.12	4.39 ± 0.21	1.10 ± 0.15	1.43 ± 0.10	84 ± 4	364 ± 22	39 ± 4
TracEx (n=5)	1.96 ± 0.18	1.51 ± 0.08	3.91 ± 0.16	1.14 ± 0.04	1.41 ± 0.10	82 ± 4	345 ± 21	40 ± 1.9
TracEx %RSD	9.18	5.3	4.09	3.51	7.09	4.97	6.09	4.81
GSP								
Consensus	0.78 ± 0.03	0.16 ± 0.05	2.60 ± 0.10	0.58 ± 0.05	0.03 ± 0.05	5 ± 0.7	2 ± 2	62 ± 5
TracEx (n=5)	0.73 ± 0.06	0.20 ± 0.02	2.42 ± 0.11	0.57 ± 0.02	0.10 ± 0.02	5 ± 0.5	6 ± 0.3	65 ± 2
TracEx %RSD	8.22	10.00	4.55	3.51	20.00	10.57	4.84	2.30
TM4A Internal Control								
TracEx Calibration (n=10)	0.26 ± 0.01	0.34 ± 0.03	5.80 ± 0.11	1.57 ± 0.03	5.83 ± 0.07	18.23 ± 0.74	625.08 ± 12.15	6.78 ± 0.13
TracEx (n>50)	0.26 ± 0.01	0.29 ± 0.03	5.91 ± 0.19	1.63 ± 0.06	5.79 ± 0.22	19.64 ± 2.42	637.78 ± 21.1	6.62 ± 0.27
TracEx %RSD	4.17	11.18	3.18	3.81	3.82	12.32	3.31	4.09
IV-28 QC (ppt)								
Certified	964	964	964	964	964	964	964	964
TracEx (n>20)	962.91 ± 10.64	969.73 ± 20.96	965.15 ± 9.05	963.17 ± 13.85	966.07 ± 10.44	963.75 ± 10.76	963.98 ± 12.18	962.49 ± 12.47

***Table 4**. Elemental recovery for the seaFAST resin column quantified by spiking a 200 ng L^{-1} (ppt) MES into the WISOS internal control.*

ng L^{-1} (ppt)	**Mn**	**Fe**	**Ni**	**Cu**	**Zn**	**Co**	**Cd**	**Pb**
WISOS (n = 5)	23.21 ± 1.11	17.79 ± 0.07	379.59 ± 0.21	92.32 ± 0.21	543.66 ± 5.74	0.54 ± 0.03	98.39 ± 1.75	1.91 ± 0.01
WISOS + 200ng L^{-1} spike (n=5)	232.70 ± 7.24	228.21 ± 5.15	598.46 ± 15.47	309.47 ± 6.53	746.84 ± 11.54	206.64 ± 4.73	299.13 ± 4.99	207.20 ± 2.99
Spike recovery	209.9	210.41	218.88	217.15	203.18	206.1	200.75	205.28
Spike recovery (%)	105	105	109	108	101	103	100	102
200 ng L^{-1} molar eq. (nmol kg^{-1})	3.55	3.49	3.32	3.07	2.98	3.31	1.76	0.94

4. Discussion

4.1. ICP-MS Performance

4.1.1. Interference Removal

Traditionally, the use of a quadrupole ICP-MS in the simultaneous quantification of trace metals in seawater has proven complicated due to difficulties in resolving spectral interferences (oxide and matrix) compounded at the low nano-to pico-molar concentrations exhibited by these metals in high salt matrices. The precipitation of seawater matrix elements (Na, K, Ca, Mg and Cl) on the instrument cones also results in compromised ion-transmission, affecting sensitivity and recovery. Furthermore, matrix elements introduce matrix-based polyatomic interferences, most notably the interference of $Mo^{16}O^{+}$ on Cd^{111} (Wu and Boyle, 1997), as well as signal suppression from the easily ionised elements such as Na and K. In this study, multiple strategies were employed to minimise the interference effects on the analyte signal. The Agilent 7900 ICP-MS was equipped with an Octopole Reaction System (ORS), a collision/reaction cell (CRC) enabling interference removal using Kinetic Energy Discrimination (KED) in He collision mode. A second gas line was added to permit the use of reactive cell gases (e.g. H_2) which enabled enhanced control over interference reactions taking place within the cell. With regards to negating specific polyatomic interferences, the buffer pH of 6.00 ± 0.2 used on the preconcentration module ensured poor recovery of Mo and thereby limited the MoO^{+} polyatomic interferences on Cd^{111} during ICP-MS analysis (Biller and Bruland, 2012). Monitoring of Cd^{112} further verified that the resulting concentration does not suffer from any oxide interferences contributed by Mo. Additional matrix based interferences, e.g. $^{40}Ar^{23}Na^{+}$ on ^{63}Cu (Wu and Boyle, 1997), were eliminated through the preconcentration step whereby matrix ions such as Na^{+} were removed. Interferences may also arise from the use of argon (Ar) gas plasma during sample ionisation. Of particular concern here is the resulting spectral overlap of $^{40}Ar^{16}O^{+}$ on Fe^{56}. To negate the interferences on the analysis of Fe^{56}, the instrument was run in H_2 reaction mode where the more efficient removal of the ArO^{+} background resulted in improved sensitivity compared to He mode as used for the other elements. In H_2 reaction mode the $^{40}Ar^{16}O^{+}$ interference is eliminated when ArO^{+} is converted to Ar and $ArOH^{+}$ enabling Fe^{56} to be measured interference-free (Arnold et al., 2008).

4.1.2. ICP-MS Calibration Accuracy

Establishing calibration accuracy was crucial in eliminating a variable potentially attributed to this step. The calibration data substantiates a working range conforming to the requirements outlined by GEOTRACES. Further, the concentration range over which the calibration was performed (0 – 20ppb) ensured the expected seawater concentrations fell well within the calibration guaranteeing precision, accuracy and linearity over the full working concentration range. The linearity of the element calibration curve remained within the following parameters: $r > 0.999$, y-intercept within 0 - 5% of target concentration and the RSD of the calibration curve <1.5 - 2%. The accurate quantification of the QC

standards substantiate accurate calibration (Table 3). However, the data does indicate that there may be large (in relative pico-molar terms) differences in the detection limit stemming from day to day calibration. Nonetheless, the QC data precision suggests that detection limits were sufficient. Moreover, the low Background Equivalent Concentrations (BEC), e.g. 0.97 pmol kg^{-1}, illustrate that resolving the highly preconcentrated sample (40 times) from the background value was readily achieved and not likely to inhibit detection.

4.1.3. Blanks and Detection limits

The observed instrument blanks for Ni (0.024 nmol kg^{-1}) most likely stem from the Ni plated skimmer cones used on the instrument; however the Ni blanks associated with the cones were determined not to be significant (<0.4%) in relation to the Ni signal of the samples (Table 2). A possible source for the Zn instrument blank (0.024 nmol kg^{-1}) were the PP sample vials used for preconcentration. Although extensively acid cleaned (see section 2.1), initial experiments conducted on 2% HNO_3 in the sample tubes prior to acid cleaning implicate Zn as the principal contaminant suggesting the acid cleaning process may not have extensively removed Zn. Despite this, the Zn blank was insignificant (<2%) in relation to open ocean Zn concentrations (Table 2). For the remainder of the metals, the instrument blank was below the detection limit. The method blanks and detection limits quantified for this study were compared with the results from four other studies (Jackson et al., 2018; Minami et al., 2015; Quéroué et al., 2014; Sohrin et al., 2008). These studies were chosen for comparison as, in parallel with this study, all made use of the NOBIAS Chelate-PA1 resin, comprising both ethylenediaminetriacetic acid (EDTriA) and iminodiacetic acid (IDA) functional groups, during preconcentration coupled with a variation of ICP-MS for trace metal quantification. With the exception of Cu, method blanks for all metals were within or below the blanks reported in the comparative literature. The Cu blank (0.086 nmol kg^{-1}) was marginally higher than the studies considered however the blank contribution was still insignificant, contributing <3% of typical open ocean Cu concentrations. The Fe blank (0.086nmol kg^{-1}) further supported the elimination of polyatomic interferences on Fe^{56}. The data suggests that the analyte preconcentration factor of 40, sufficiently circumvented the challenge of detectability on low level elements such as Fe, Co, Cd and Pb.

4.1.4. Reference materials

The results of the deep water SAFe D2 RM (Table 3) provide strong evidence for the methods suitability in accurate trace metal quantification at realistic open ocean concentration ranges. The TM4A internal control with characteristic open ocean surface concentrations, proved useful in evaluating the precision of the method at lower concentrations, most notably for Fe and Co. For the SAFe D2 RM, the underestimation of Co (~30%) and Cu (~7%) with respect to their consensus values stems from the omission of an ultra-violet (UV) irradiation pre-treatment procedure deemed necessary to dissociate metal ions from strong organic complexes specific to these two metals (Milne et al., 2010). Typically,

seawater samples for total dissolvable trace metal analysis are acidified (pH 1.7) in order to dissociate any organically bound trace metals, that is trace metals associated with colloids or organometallic complexes. However, evidence suggests that some Co and Cu complexes persist even after sample acidification leading to an inert metal fraction that is not chelated by the resin column during preconcentration and hence not quantified (Biller and Bruland, 2012; Vega and Berg, 1997). The pre-treatment of samples with UV irradiation effectively destroys these metal complexes (Buck and Bruland, 2005; Saito and Moffett, 2001). Samples were not UV irradiated in this study meaning the labile dissolved fraction was quantified for Co and Cu, as opposed to the total dissolved fraction for the remaining trace metals. Implications for this in terms of biological interpretations are uncertain considering that the strongly complexed Co and Cu may not present as bio-available to all phytoplankton taxa. Nonetheless, the resulting underestimation of Co and Cu are similar to previous measurements (24.00 pmol kg^{-1} Co; 2.09 nmol kg^{-1} Cu) of the SAFe D2 reference material without UV irradiation (Milne et al., 2010). In addition, results of the NASS-7 CRM, which has been gamma irradiated, are within the uncertainty estimates for all trace metals (Table 3) and further suggest that Co and Cu were accurately quantified by the method. The IV-28 Quality Control (QC) results (Table 3) support the ICP-MS instruments accuracy and precision over an entire analysis session (approximately 4 hours per station). Iron was the most susceptible to variation during analyses however the relative standard deviation (3% RSD) was well within acceptable limits. All other metals had RSD <1% for the IV-28 QC.

5. Conclusion

A more affordable method for the simultaneous quantification of key GEOTRACES trace metals (Mn, Fe, Co, Ni, Cu, Zn, Cd and Pb) in seawater is presented. By combining solid phase extraction, using the sea*FAST* preconcentration module, with quadrupole ICP-MS, accurate and precise measurements at the extremely low trace metal levels inherent in open ocean seawater samples were possible. By removing the seawater matrix elements e.g. Na and Mg, the sea*FAST* module was effective in eliminating the source of many matrix-based polyatomic interferences on the ICP-MS. To minimise the interference of $^{40}Ar^{16}O^{+}$ on Fe^{56}, H_2 was used as the reaction gas which resulted in the more efficient removal of $^{40}Ar^{16}O_{+}$ compared to He mode as used for the other elements. Blanks and calculated detection limits were comparable to recent studies using the same chelating resin during preconcentration yet with variations of ICP-MS technique e.g. SF-ICP-MS and ICP-MS/MS. Furthermore, the resin demonstrated quantitative recovery of all trace metals considered. The SAFe D2 RM and NASS-7 CRM were analysed showing agreement with established consensus values and confirmed the methods accuracy. The continuous in-run analysis of an internal seawater standard ensured the instruments precision during analyses. The application of the method was demonstrated by way of full depth profiles from

the Southern Ocean. This method proves, through careful instrument optimisation, that quadrupole ICP-MS is a viable analytical technique suitable for the demands of the GEOTRACES program.

6. References

Arnold, T., Harvey, J.N., Weiss, D.J., 2008. An experimental and theoretical investigation into the use of H2 for the simultaneous removal of ArO+ and ArOH+ isobaric interferences during Fe isotope ratio analysis with collision cell based Multi-Collector Inductively Coupled Plasma Mass Spectrometry. Spectrochim. Acta Part B 63, 666–672. https://doi.org/10.1016/j.sab.2008.04.009

Balcaen, L., Bolea-fernandez, E., Resano, M., Vanhaecke, F., 2015. Inductively coupled plasma - Tandem mass spectrometry (ICP-MS / MS): A powerful and universal tool for the interference-free determination of (ultra) trace elements - A tutorial review. Anal. Chim. Acta 894, 7–19. https://doi.org/10.1016/j.aca.2015.08.053

Biller, D. V., Bruland, K.W., 2012. Analysis of Mn, Fe, Co, Ni, Cu, Zn, Cd, and Pb in seawater using the Nobias-chelate PA1 resin and magnetic sector inductively coupled plasma mass spectrometry (ICP-MS). Mar. Chem. 130–131, 12–20. https://doi.org/10.1016/j.marchem.2011.12.001

Blain, S., Tregeur, P., 1995. Iron (II) and iron (III) determination in sea water at the nanomolar level with selective on-line preconcentration and spectrophotometric determination. Anal. Chim. Acta 308, 425–432. //doi.org/10.1016/0003-2670(94)00456-V

Bowie, A.R., Achterberg, E.P., Mantoura, R.F.C., Worsfold, P.J., 1998. Determination of sub-nanomolar levels of iron in seawater using flow injection with chemiluminescence detection. Anal. Chim. Acta 361, 189–200. https://doi.org/10.1016/S0003-2670(98)00015-4

Bown, J., Boye, M., Baker, A., Duvieilbourg, E., Lacan, F., Le Moigne, F., Planchon, F., Speich, S., Nelson, D.M., 2011. The biogeochemical cycle of dissolved cobalt in the Atlantic and the Southern Ocean south off the coast of South Africa. Mar. Chem. 126, 193–206. https://doi.org/10.1016/j.marchem.2011.03.008

Boyle, E., Kayser, R., Zhang, J., Gamo, T., Obata, H., Norisuye, K., Noble, A., Moos, S., 2014. Anthropogenic lead emissions in the ocean: The evolving global experiment. Oceanography 27, 69–75. http://dx.doi.org/10.5670/oceanog.2014.10

Brand, L.E., Sunda, W.G., Guillard, R.R.L., 1986. Reduction of marine phytoplankton reproduction rates by copper and cadmium. J. Exp. Mar. Bio. Ecol. 96, 225–250. https://doi.org/10.1016/0022-0981(86)90205-4

Bruland, K.W., 1980. Oceanographic distribution of cadmium, zinc, nickel, and copper in the North Pacific. Earth Planet. Sci. Lett. 47, 176–198. https://doi.org/10.1016/0012-821X(80)90035-7

Bruland, K.W., Donat, J.R., Hutchins, D.A., 1991. Interactive influences of bioactive trace metals on biological production in oceanic waters. Limnol. Oceanogr. 36, 1555–1577. https://doi.org/10.4319/lo.1991.36.8.1555

Bruland, K.W., Franks, R.P., 1979. Sampling and analytical methods for the determination of copper, cadmium, zinc and nickel at the nanogram per litre level in seawater. Anal. Chim. Acta 28, 367–376. https://doi.org/10.1016/S0003-2670(01)83754-5

Buck, K.N., Bruland, K.W., 2005. Copper speciation in San Francisco Bay : A novel approach using multiple analytical windows. Mar. Chemsitry 96, 185–198. https://doi.org/10.1016/j.marchem.2005.01.001

Cloete, R., Loock, J.C., Mtshali, T., Fietz, S., Roychoudhury, A.N., 2019. Winter and summer distributions of Copper, Zinc and Nickel along the International GEOTRACES Section GIPY05:

Insights into deep winter mixing. Chem. Geol. 511, 342-357. https://doi.org/10.1016/j.chemgeo.2018.10.023

Colombo, C., van den Berg, C.M.G., 1997. Simultaneous determination of several trace metals in seawater using cathodic stripping voltammetry with mixed ligands. Anal. Chim. Acta 337, 29–40. https://doi.org/10.1016/S0003-2670(96)00401-1

Croot, P.L., Laan, P., 2002. Continuous shipboard determination of Fe(II) in polar waters using flow injection analysis with chemiluminescence detection. Anal. Chim. Acta 466, 261–273. https://doi.org/10.1016/S0003-2670(02)00596-2

Cutter, G., Casciotti, K., Croot, P., Geibert, W., Lohan, M., 2017. Sampling and Sample-handling Protocols for GEOTRACES Cruises.

Cutter, G.A., Bruland, K.W., 2012. Rapid and noncontaminating sampling system for trace elements in global ocean surveys. Limnol. Oceanogr. Methods 10, 425–436. https://doi.org/10.4319/lom.2012.10.425

De Jong, J., Schoemann, V., Lannuzel, D., Croot, P., De Baar, H., Tison, J.L., 2012. Natural iron fertilization of the Atlantic sector of the Southern Ocean by continental shelf sources of the Antarctic Peninsula. J. Geophys. Res. Biogeosciences 117, 1–25. https://doi.org/10.1029/2011JG001679

Feldmann, I., Jakubowski, N., D, S., 1999. Application of a hexapole collision and reaction cell in ICP-MS Part I: Instrumental aspects and operational optimization. Fresenius J. Anal. Chem. 365, 415–421. https://doi.org/10.1007/s002160051633

Frew, R., Bowie, A., Croot, P., Pickmere, S., 2001. Macronutrient and trace-metal geochemistry of an in situ iron-induced Southern Ocean bloom. Deep. Res. Part II Top. Stud. Oceanogr. 48, 2467–2481. https://doi.org/10.1016/S0967-0645(01)00004-2

Ho, T.Y., Chien, C. Te, Wang, B.N., Siriraks, A., 2010. Determination of trace metals in seawater by an automated flow injection ion chromatograph pretreatment system with ICPMS. Talanta 82, 1478–1484. https://doi.org/10.1016/j.talanta.2010.07.022

Jackson, S.L., Spence, J., Janssen, D.J., Ross, A.R.S., Cullen, J.T., 2018. Determination of Mn, Fe, Ni, Cu, Zn, Cd and Pb in quadrupole ICP-MS / MS. J. Anal. At. Spectrom. 33, 304–313. https://doi.org/10.1039/C7JA00237H

Jakubowski, N., Moens, L., Vanhaecke, F., 1998. Sector field mass spectrometers in ICP-MS. Spectrochim. Acta Part B 53, 1739–1763. https://doi.org/10.1016/S0584-8547(98)00222-5

Jerez Veguería, S.F., Godoy, J.M., De Campos, R.C., Gonçalves, R.A., 2013. Trace element determination in seawater by ICP-MS using online, offline and bath procedures of preconcentration and matrix elimination. Microchem. J. 106, 121–128. https://doi.org/10.1016/j.microc.2012.05.032

King, D.W., Lin, J., Kester, D.R., 1991. Spectrophotometric determination of iron (II) in seawater at nanomolar concentrations. Anal. Chim. Acta 247, 125–132. https://doi.org/10.1016/S0003-2670(00)83061-5

Kingston, H.M., Barnes, I.L., Brady, T.J., Rains, T.C., Champ, M.A., 1978. Separation of eight transition elements from alkali and alkaline earth elements in estuarine and seawater with chelating resin and their determination by graphite furnace atomic absorption spectrometry. Anal. Chem. 50, 2064–2070. https://doi.org/10.1021/ac50036a031

Klunder, M.B., Laan, P., Middag, R., Baar, H.J.W. De, Ooijen, J.C. Van, 2011. Dissolved iron in the Southern Ocean (Atlantic sector). Deep. Res. Part II 58, 2678–2694. https://doi.org/10.1016/j.dsr2.2010.10.042

Komjarova, I., Blust, R., 2006. Comparison of liquid-liquid extraction, solid-phase extraction and co-precipitation preconcentration methods for the determination of cadmium, copper, nickel, lead and zinc

in seawater. Anal. Chim. Acta 576, 221–228. https://doi.org/10.1016/j.aca.2006.06.002

Lee, J., Boyle, E.A., Echegoyen-Sanz, Y., Fitzsimmons, J.N., Zhang, R., Kayser, R.A., 2011. Analysis of trace metals (Cu, Cd, Pb, and Fe) in seawater using single batch nitrilotriacetate resin extraction and isotope dilution inductively coupled plasma mass spectrometry. Anal. Chim. Acta 686, 93–101. https://doi.org/10.1016/j.aca.2010.11.052

Mclaren, J.W., Mykytiuk, A.P., Willie, S.N., Berman, S.S., 1985. Determination of Trace Metals in Seawater by Inductively Coupled Plasma Mass Spectrometry with Preconcentration on Silica-Immobilized 8-Hydroxyquinoline. Anal. Chem. 2907–2911. https://doi.org/10.1021/ac00291a037

Middag, R., De Baar, H.J.W., Laan, P., Cai, P.H., Van Ooijen, J.C., 2011. Dissolved manganese in the Atlantic sector of the Southern Ocean. Deep Sea Res. Part II Top. Stud. Oceanogr. 58, 2661–2677. https://doi.org/10.1016/S0967-0645(96)00064-1

Milne, A., Landing, W., Bizimis, M., Morton, P., 2010. Determination of Mn, Fe, Co, Ni, Cu, Zn, Cd and Pb in seawater using high resolution magnetic sector inductively coupled mass spectrometry (HR-ICP-MS). Anal. Chim. Acta 665, 200–207. https://doi.org/10.1016/j.aca.2010.03.027

Minami, T., Konagaya, W., Zheng, L., Takano, S., Sasaki, M., Murata, R., Nakaguchi, Y., Sohrin, Y., 2015. An off-line automated preconcentration system with ethylenediaminetriacetate chelating resin for the determination of trace metals in seawater by high-resolution inductively coupled plasma mass spectrometry. Anal. Chim. Acta 854, 183–190. https://doi.org/10.1016/j.aca.2014.11.016

Moffett, J.W., Ho, J., 1996. Oxidation of cobalt and manganese in seawater via a common microbially catalyzed pathway. Geochim. Cosmochim. Acta 60, 3415–3424. https://doi.org/10.1016/0016-7037(96)00176-7

Moldovan, M., Krupp, E.M., Holliday, A.E., Donard, O.F.X., 2004. High resolution sector field ICP-MS and multicollector ICP-MS as tools for trace metal speciation in environmental studies: a review. J. Anal. At. Spectrom. 19, 815–822. https://doi.org/10.1039/B403128H

Quéroué, F., Townsend, A., van der Merwe, P., Lannuzel, D., Sarthou, G., Bucciarelli, E., Bowie, A., 2014. Advances in the offline trace metal extraction of Mn, Co, Ni, Cu, Cd, and Pb from open ocean seawater samples with determination by sector field ICP-MS analysis. Anal. Methods 6, 2837–2847. https://doi.org/10.1039/c3ay41312h

Rahmi, D., Zhu, Y., Fujimori, E., Umemura, T., Haraguchi, H., 2007. Multielement determination of trace metals in seawater by ICP-MS with aid of down-sized chelating resin-packed minicolumn for preconcentration. Talanta 72, 600–606. https://doi.org/10.1016/j.talanta.2006.11.023

Rapp, I., Schlosser, C., Rusiecka, D., Gledhill, M., Achterberg, E.P., 2017. Automated preconcentration of Fe, Zn, Cu, Ni, Cd, Pb, Co, and Mn in seawater with analysis using high-resolution sector field inductively- coupled plasma mass spectrometry. Anal. Chim. Acta 976, 1–13. https://doi.org/10.1016/j.aca.2017.05.008

Saito, M.A., Moffett, J.W., 2001. Complexation of cobalt by natural organic ligands in the Sargasso sea as determined by a new high-sensitivity electrochemical cobalt speciation method suitable for open ocean work. Mar. Chem. 75, 49–68. https://doi.org/10.1016/S0304-4203(01)00025-1

Sohrin, Y., Urushihara, S., Nakatsuka, S., Kono, T., Higo, E., Minami, T., Norisuye, K., Umetani, S., 2008. Multielemental determination of GEOTRACES key trace metals in seawater by ICPMS after preconcentration using an ethylenediaminetriacetic acid chelating resin. Anal. Chem. 80, 6267–6273. https://doi.org/10.1021/ac800500f

Sunda, W.G., Huntsman, S.A., 1995. Iron uptake and growth limitation in oceanic and coastal phytoplankton. Mar. Chem. 50, 189–206. https://doi.org/10.1016/0304-4203(95)00035-P

Takano, S., Tanimizu, M., Hirata, T., Shin, K., Fukami, Y., Suzuki, K., Sohrin, Y., 2017. A simple and rapid method for isotopic analysis of nickel , copper , and zinc in seawater using chelating extraction

and anion exchange. Anal. Chim. Acta 967, 1–11. https://doi.org/10.1016/j.aca.2017.03.010

Tan, S.H., Horlick, G., 1986. Background Spectral Features in Inductively COupled Plasma/Mass Spectrometry. Appl. Spectrosc. 40, 445–460.

Tanner, S.D., Baranov, V.I., 1999. Theory, Design, and Operation of a Dynamic Reaction Cell for ICP-MS. At. Spectrosc. 20, 45–78.

Vega, M., Berg, C.M.G. Van Den, 1997. Determination of Cobalt in Seawater by Catalytic Adsorptive Cathodic Stripping Voltammetry. Anal. Chem. 69, 874–881. https://doi.org/10.1021/ac960214s

Walczyk, T., 2004. TIMS versus multicollector-ICP-MS: coexistence or struggle for survival? Anal. Bioanal. Chem. 378, 229–231. https://doi.org/10.1007/s00216-003-2053-4

Wells, M.L., Bruland, K.W., 1998. An improved method for rapid preconcentration and determination of bioactive trace metals in seawater using solid phase extraction and high resolution inductively coupled plasma mass spectrometry. Mar. Chem. 63, 145–153. https://doi.org/Doi 10.1016/S0304-4203(98)00058-9

Wu, J., Boyle, E.A., 1997. Low blank preconcentration technique for the determination of lead, copper, and cadmium in small-volume seawater samples by isotope dilution ICPMS. Anal. Chem. 69, 2464–70. https://doi.org/10.1021/ac961204u

Wuttig, K., Townsend, A.T., van der Merwe, P., Gault-Ringold, M., Holmes, T., Schallenberg, C., Latour, P., Tonnard, M., Rijkenberg, M.J.A., Lannuzel, D., Bowie, A.R., 2019. Critical evaluation of a SeaFAST system for the analysis of trace metals in a wide range of marine samples. Talanta in press. https://doi.org/10.1016/j.talanta.2019.01.047

Yamada, N., 2015. Kinetic energy discrimination in collision/reaction cell ICP-MS: Theoretical review of principles and limitations. Spectrochim. Acta Part B At. Spectrosc. 110, 31–44. https://doi.org/10.1016/j.sab.2015.05.008

Yamada, N., Takahashi, J., Sakata, K., 2002. The effects of cell-gas impurities and kinetic energy discrimination in an octopole collision cell ICP-MS under non-thermalized conditions. J. Anal. At. Spectrom. 17, 1213–1222. https://doi.org/10.1039/b205416g

Appendix B

This appendix contains separate data tables for each of the six sampling locations occupied during the 54th South African National Antarctic Expedition (SANAE 54) cruise which took place over the 2014/2015 austral summer in the Atlantic sector of the Southern Ocean (46-68°S; 0-8°E). The labile dissolved copper (LdCu) and dissolved zinc (dZn) and nickel (dNi) data were presented in Chapter 2 alongside physical temperature and salinity data as well as macronutrient (PO_4, NO_3 and Si) data. Values for trace metals represent the mean of duplicate measurements. A value was deemed an outlier when the relative standard deviation (RSD) between duplicate measurements was >10% of their mean value. The rejected value was determined by curve fitting the data points based on the values above (shallower depth) and below (deeper depth) the suspect value as well as by comparison with other parameters (salinity, temperature, and nutrients) measured from the same GO-FLO bottle.

SANAE 54			**Date: 12/01/2015**		**Bottom depth: 4224m**					
Domain (Station)	**Lat/Long**	**Depth (m)**	**Temp (°C)**	**Salinity (PSU)**	**NO_3 (µmol kg^{-1})**	**PO_4 (µmol kg^{-1})**	**Si (µmol kg^{-1})**	**LdCu (nmol kg^{-1})**	**dZn (nmol kg^{-1})**	**dNi (nmol kg^{-1})**
DTM2	46˚ 00' S	14	6.35	33.78	19.34	1.30	5.33	1.00	0.85	5.07
	08˚ 00' E	35	6.35	33.78	21.46	1.28	5.14	0.97	0.90	5.30
		75	6.20	33.79	22.75	1.35	5.48	1.04	0.58	5.36
		100	5.84	33.80	24.95	1.64	6.15	0.91	1.95	5.09
		150	4.20	33.86	28.03	-	10.10	1.02	1.32	5.51
		200	4.02	34.05	30.60	1.83	16.40	1.02	1.80	5.65
		400	3.10	34.14	34.99	-	31.80	1.23	2.85	6.30
		501	2.94	34.20	36.10	2.12	39.90	1.26	3.50	6.22
		622	2.84	34.28	37.30	-	52.30	1.32	3.39	6.11
		1000	2.61	34.53	38.70	2.33	76.70	1.74	4.82	6.77
		1501	2.50	34.71	34.57	2.14	82.60	1.90	5.01	6.63
		2000	2.20	34.77	32.29	1.92	85.70	1.97	5.15	6.27
		3000	1.41	34.75	33.80	2.04	106.00	2.44	5.22	6.47
		4002	0.88	34.71	35.00	2.18	126.00	2.82	6.14	6.68
		4302	0.78	34.70	35.10	2.17	133.00	3.15	6.96	7.26
Max.			6.35	34.77	38.70	2.33	133.00	3.15	6.96	7.26
Min.			0.78	33.78	19.34	1.28	5.14	0.91	0.58	5.07
MLD (79m)			6.30	33.79	21.18	1.31	5.32	1.00	0.78	5.24
Surface (<500m)			4.88	33.93	27.28	1.59	15.04	1.06	1.72	5.56
Inter (500-1500m)			2.72	34.43	36.67	2.20	62.88	1.55	4.18	6.43
Deep (>1500m)			1.55	34.73	34.15	2.09	106.66	2.46	5.70	6.66

Cruise: SANAE54 **Date: 14/01/2015** **Bottom depth: 3248m**

Domain (Station)	Lat/Long	Depth (m)	Temp (°C)	Salinity (PSU)	NO_3 (µmol kg^{-1})	PO_4 (µmol kg^{-1})	Si (µmol kg^{-1})	LdCu (nmol kg^{-1})	dZn (nmol kg^{-1})	dNi (nmol kg^{-1})
TM1	50˚ 00' S	16	3.73	33.79	17.81	1.85	5.56	0.94	0.96	4.98
	02˚ 00' E	31	3.73	33.79	16.28	1.80	5.40	0.94	0.62	5.03
		40	3.73	33.79	14.68	1.76	5.50	0.95	0.62	5.11
		60	3.73	33.79	11.76	1.71	5.49	0.96	1.02	5.25
		78	3.72	33.79	18.10	1.85	4.93	0.96	0.61	5.21
		100	3.61	33.79	19.74	1.76	5.82	1.08	1.19	5.61
		150	2.09	34.03	27.77	2.60	38.10	1.09	2.53	5.65
		198	2.08	34.12	29.90	2.69	46.50	1.15	3.25	5.78
		251	2.15	34.18	33.98	2.39	56.72	1.33	3.51	6.07
		303	2.33	34.28	34.62	2.49	63.80	1.34	4.19	6.19
		400	2.39	34.39	34.62	2.48	68.76	1.41	4.81	6.12
		500	2.42	34.49	34.41	2.42	73.72	1.59	5.42	6.65
		599	2.40	34.55	-	-	-	1.63	6.28	6.33
		800	2.33	34.64	32.69	2.34	80.44	1.75	5.30	6.28
		1002	2.27	34.69	31.84	2.20	82.56	1.77	5.35	6.17
Max.			3.73	34.69	34.62	2.69	82.56	1.77	6.28	6.65
Min.			2.08	33.79	11.76	1.71	4.93	0.94	0.61	4.98
MLD (100m)			3.71	33.79	16.39	1.79	5.45	0.97	0.84	5.20
Surface (<500m)			2.98	34.02	24.47	2.15	31.69	1.14	2.40	5.64
Inter (500-1500m)			2.35	34.59	32.98	2.32	78.90	1.69	5.59	6.36
Deep (>1500m)			-	-	-	-	-	-	-	-

Cruise: SANAE54 **Date: 15/01/2015** **Bottom depth: 2412m**

Domain (Station)	Lat/Long	Depth (m)	Temp (°C)	Salinity (PSU)	NO_3 (µmol kg^{-1})	PO_4 (µmol kg^{-1})	Si (µmol kg^{-1})	LdCu (nmol kg^{-1})	dZn (nmol kg^{-1})	dNi (nmol kg^{-1})
DTM3	54˚ 00' S	15	0.96	33.83	16.14	1.44	28.80	1.45	1.55	5.42
	00˚ 00' E	23	0.86	33.83	18.89	1.43	30.83	1.42	3.01	5.78
		50	0.68	33.83	20.09	1.56	30.87	1.32	2.09	5.41
		75	-0.01	33.86	19.86	1.57	34.43	1.35	2.55	5.23
		101	-0.31	33.90	22.13	1.87	47.80	1.33	2.65	5.50
		151	-0.02	34.16	33.12	2.12	68.90	1.41	4.44	5.68
		250	1.55	34.51	38.50	2.38	93.30	1.60	5.93	6.04
		298	1.62	34.56	36.73	2.42	92.48	1.72	6.22	6.31
		350	1.70	34.60	34.82	2.39	92.67	1.73	5.87	6.13
		398	1.76	34.63	35.33	2.43	91.00	1.70	6.18	6.10
		450	1.74	34.65	35.63	2.33	98.27	1.90	6.32	6.74
		500	1.70	34.66	34.53	2.28	95.47	1.95	6.61	6.59
		549	1.66	34.68	34.95	2.26	102.00	2.07	6.57	6.86
		599	1.62	34.69	33.17	2.22	94.73	2.14	6.68	6.99
		650	1.58	34.69	35.62	2.28	95.57	2.17	6.42	6.94
		749	1.50	34.70	30.94	2.25	105.04	2.21	6.48	6.79
		1000	1.24	34.71	27.06	2.12	97.90	2.30	6.71	6.45
		1250	0.94	34.70	30.22	2.26	124.83	2.17	6.95	6.24
		1502	0.71	34.69	28.73	2.22	118.86	2.28	7.15	6.18
		1749	0.56	34.68	34.69	2.30	118.84	2.30	7.45	6.10
		2001	0.45	34.68	35.00	2.23	108.33	2.34	7.51	6.06
		2249	0.40	34.68	29.06	2.40	122.67	2.55	7.66	6.29
		2400	0.40	34.68	41.56	2.29	131.00	2.46	7.96	6.27
Max.			1.76	34.71	41.56	2.43	131.00	2.55	7.96	6.99
Min.			-0.31	33.83	16.14	1.43	28.80	1.32	1.55	5.23
MLD (101m)			0.44	33.85	19.42	1.57	34.55	1.38	2.37	5.47

Surface (<500m)	1.02	34.25	28.82	2.02	67.07	1.58	4.45	5.91
Inter (500-1500m)	1.37	34.69	31.90	2.24	104.30	2.16	6.69	6.63
Deep (>1500m)	0.50	34.68	33.80	2.29	119.94	2.39	7.55	6.18

Cruise: SANAE54 **Date: 16/01/2015** **Bottom depth: 5174m**

Domain (Station)	Lat/Long	Depth (m)	Temp (°C)	Salinity (PSU)	NO_3 (µmol kg^{-1})	PO_4 (µmol kg^{-1})	Si (µmol kg^{-1})	LdCu (nmol kg^{-1})	dZn (nmol kg^{-1})	dNi (nmol kg^{-1})
TM2	60˚ 00' S	16	0.73	33.75	22.12	1.23	59.90	1.49	1.33	5.98
	00˚ 00' E	41	-1.70	34.13	24.81	1.54	70.10	1.60	3.22	6.09
		58	-1.25	33.97	26.61	2.07	74.80	1.53	2.58	5.89
		60	-1.71	34.13	29.05	1.98	82.50	1.77	3.89	6.17
		79	-1.74	34.19	30.53	1.98	83.80	1.70	3.82	6.02
		100	-1.26	34.34	31.94	2.33	95.60	1.90	4.97	6.16
		150	0.68	34.66	36.95	2.33	126.00	2.25	7.49	6.73
		199	0.64	34.68	36.38	2.33	135.00	2.38	7.38	6.83
		251	0.57	34.68	36.49	2.38	136.00	2.46	7.51	6.80
		300	0.53	34.68	37.09	2.60	139.00	2.51	7.41	6.97
		399	0.46	34.68	37.51	2.60	144.00	2.51	7.93	6.73
		500	0.41	34.68	37.41	2.33	146.00	2.61	7.74	6.73
		599	0.37	34.68	36.99	2.29	155.00	2.63	7.82	6.71
		800	0.27	34.68	43.33	2.24	146.00	2.64	7.54	6.73
		1001	0.18	34.67	-	2.29	-	2.95	8.72	7.28
Max.			0.73	34.68	43.33	2.60	155.00	2.95	8.72	7.28
Min.			-1.74	33.75	22.12	1.23	59.90	1.49	1.33	5.89
MLD (50m)			-0.74	33.95	24.51	1.61	68.27	1.54	2.38	5.99
Surface (<500m)			-0.30	34.38	32.24	2.14	107.73	2.06	5.44	6.42
Inter (500-1500m)			0.31	34.68	39.25	2.29	149.00	2.71	7.96	6.86
Deep (>1500m)			-	-	-	-	-	-	-	-

Cruise: SANAE54 **Date: 18/01/2015** **Bottom depth: 3605m**

Domain (Station)	Lat/Long	Depth (m)	Temp (°C)	Salinity (PSU)	NO_3 (µmol kg^{-1})	PO_4 (µmol kg^{-1})	Si (µmol kg^{-1})	LdCu (nmol kg^{-1})	dZn (nmol kg^{-1})	dNi (nmol kg^{-1})
DTM1	65˚ 00' S	25	-	-	-	-	-	1.29	1.02	4.65
	00˚ 00' E	39	-0.73	34.09	25.02	1.85	74.30	1.45	2.21	4.73
		51	-0.87	34.30	29.92	2.02	95.50	1.48	3.68	4.96
		70	0.40	34.56	31.40	2.20	110.00	1.74	5.22	5.69
		100	1.08	34.67	31.20	2.29	113.00	1.89	5.78	5.76
		151	1.13	34.69	31.70	2.24	118.00	1.95	5.08	5.71
		200	1.10	34.69	30.80	2.20	120.00	1.87	5.05	5.55
		400	0.89	34.70	32.07	2.24	126.00	2.00	5.20	5.49
		498	0.81	34.70	30.79	2.16	130.00	2.03	5.33	5.56
		749	0.61	34.69	30.83	2.20	136.00	2.50	6.05	6.51
		1001	0.47	34.69	32.79	2.29	141.00	2.43	5.53	5.71
		1251	0.34	34.68	31.89	2.29	144.00	2.27	5.46	5.44
		1501	0.24	34.67	39.69	2.38	145.00	2.28	5.35	5.30
		2002	0.05	34.67	38.45	2.24	145.00	2.47	5.97	5.67
		2501	-0.09	34.66	36.09	2.33	145.00	2.37	6.11	5.60
		3001	-0.18	34.66	38.43	2.24	148.00	2.35	5.63	5.40
		3650	-0.26	34.65	35.99	2.20	147.50	2.37	5.02	5.03
Max.			1.13	34.70	39.69	2.38	148.00	2.50	6.11	6.51
Min.			-0.87	34.09	25.02	1.85	74.30	1.29	1.02	4.65
MLD (68m)			-0.40	34.32	28.78	2.02	93.27	1.49	3.04	5.01
Surface (<500m)			0.48	34.55	30.36	2.15	110.85	1.74	4.29	5.35
Inter (500-1500m)			0.49	34.69	33.20	2.26	139.20	2.30	5.54	5.70
Deep (>1500m)			-0.05	34.66	37.73	2.28	146.10	2.37	5.62	5.40

Cruise: SANAE54 **Date: 19/01/2015** **Bottom depth: 4372m**

Domain (Station)	Lat/Long	Depth (m)	Temp (°C)	Salinity (PSU)	NO_3 (µmol kg^{-1})	PO_4 (µmol kg^{-1})	Si (µmol kg^{-1})	LdCu (nmol kg^{-1})	dZn (nmol kg^{-1})	dNi (nmol kg^{-1})
TM3	68˚ 00' S	15	-1.69	33.82	26.32	1.99	89.80	1.83	4.56	6.02
	00˚ 00' E	30	-1.76	34.07	28.12	2.08	92.00	1.81	4.61	6.00
		40	-1.76	34.31	28.22	2.16	93.00	1.90	5.19	6.31
		60	-1.75	34.38	27.42	2.12	89.40	1.86	4.67	6.21
		80	-1.70	34.42	28.34	2.16	91.40	1.85	4.69	6.23
		99	-1.01	34.48	27.36	2.21	88.50	1.89	4.88	6.23
		150	0.62	34.66	30.10	2.25	110.00	2.12	6.43	6.57
		201	0.71	34.67	31.50	2.38	114.00	2.19	6.77	6.58
		250	0.82	34.69	32.69	2.29	119.00	2.35	6.59	6.61
		301	0.82	34.69	31.20	2.33	141.00	2.34	6.79	6.79
		400	0.77	34.69	32.37	2.29	124.00	2.45	6.99	6.88
		501	0.70	34.69	15.16	1.99	89.80	2.38	6.68	6.39
		600	0.65	34.69	31.20	2.33	135.00	2.45	6.89	6.40
		799	0.55	34.69	32.00	2.25	138.00	2.55	7.44	6.60
		1000	0.44	34.68	32.10	2.38	143.00	2.79	7.97	7.04
Max.			0.82	34.69	32.69	2.38	143.00	2.79	7.97	7.04
Min.			-1.76	33.82	15.16	1.99	88.50	1.81	4.56	6.00
MLD (86m)			-1.73	34.20	27.68	2.10	91.12	1.85	4.74	6.15
Surface (<500m)			-0.44	34.46	28.23	2.19	103.49	2.08	5.74	6.40
Inter (500-1500m)			0.58	34.69	27.61	2.24	126.45	2.54	7.25	6.61
Deep (>1500m)			-	-	-	-	-	-	-	-

Appendix C

This appendix contains separate data tables for each of the three sampling locations occupied during the third Southern Ocean Seasonal Cycle Experiment (SOSCEX III) cruise which took place over the 2015 austral winter in the Atlantic Sector of the Southern Ocean (46-54°S; 0-5°E). The three sample locations overlapped with three corresponding stations from the SANAE 54 cruise. The labile dissolved copper (LdCu) and dissolved zinc (dZn) and nickel (dNi) data were presented in Chapter 2 alongside physical temperature and salinity data as well as macronutrient (PO_4, NO_3 and Si) data. Values for trace metals represent the mean of duplicate measurements. A value was deemed an outlier when the relative standard deviation (RSD) between duplicate measurements was >10% of their mean value. The rejected value was determined by curve fitting the data points based on the values above (shallower depth) and below (deeper depth) the suspect value as well as by comparison with other parameters (salinity, temperature, and nutrients) measured from the same GO-FLO bottle.

Cruise: SOSCEX III **Date: 30/07/2015** **Bottom depth: 4224m**

Domain (Station)	Lat/Long	Depth (m)	Temp (°C)	Salinity (PSU)	NO_3 (µmol kg^{-1})	PO_4 (µmol kg^{-1})	Si (µmol kg^{-1})	dCu (nmol kg^{-1})	dZn (nmol kg^{-1})	dNi (nmol kg^{-1})
DTM2	46˚ 00' S	9	5.46	33.88	22.57	1.55	4.78	1.06	0.47	5.05
	05˚ 00' E	29	5.45	33.87	23.73	1.51	4.28	0.94	0.67	5.31
		48	5.44	33.87	22.78	1.55	4.30	1.02	0.49	5.02
		74	5.41	33.87	22.92	1.51	4.32	0.91	0.58	5.21
		149	5.16	34.13	26.48	1.84	9.35	0.93	1.42	5.15
		199	4.46	34.13	27.68	1.80	12.00	0.90	1.51	5.37
		299	3.80	34.13	29.48	1.92	17.80	1.03	2.55	5.55
		398	3.39	34.14	32.18	1.96	23.30	1.11	2.42	5.82
		448	3.22	34.16	31.50	1.92	26.90	1.17	2.37	5.74
		749	2.85	34.34	34.38	2.28	50.40	1.46	3.81	6.13
		999	2.66	34.50	34.38	2.28	65.20	1.63	4.99	6.48
		1498	2.56	34.70	31.78	2.20	69.40	1.82	4.36	6.20
		1999	2.13	34.76	35.18	2.24	66.80	2.08	4.34	6.43
		2998	1.28	34.75	32.40	2.12	95.70	2.88	5.88	6.37
		3999	0.59	34.71	34.48	2.20	115.00	2.82	6.75	6.49
		4099	0.59	34.71	34.08	2.16	115.00	2.83	6.16	6.24
Max.			5.46	34.76	35.18	2.28	115.00	2.88	6.75	6.49
Min.			0.59	33.87	22.57	1.51	4.28	0.90	0.47	5.02
MLD (121m)			5.38	33.93	23.70	1.59	5.41	0.97	0.73	5.15
Surface (<500m)			4.64	34.02	26.59	1.73	11.89	1.01	1.39	5.36
Inter (500-1500m)			2.69	34.52	33.52	2.25	61.67	1.64	4.38	6.27
Deep (>1500m)			1.15	34.73	34.04	2.18	98.13	2.65	5.79	6.38

Cruise: SOSCEX III **Date: 01/08/2015** **Bottom depth: 3248m**

Domain (Station)	Lat/Long	Depth (m)	Temp (°C)	Salinity (PSU)	NO_3 (µmol kg^{-1})	PO_4 (µmol kg^{-1})	Si (µmol kg^{-1})	dCu (nmol kg^{-1})	dZn (nmol kg^{-1})	dNi (nmol kg^{-1})
TM1	50˚ 00' S	9	2.34	33.84	25.44	1.76	17.3	1.16	1.64	5.61
	01˚ 00' E	29	2.34	33.84	25.66	1.76	17.20	1.16	1.75	5.57
		49	2.34	33.84	25.75	1.72	17.30	1.19	1.53	5.72
		72	2.34	33.85	25.70	1.68	17.20	1.15	1.60	5.69
		99	2.34	33.85	25.73	1.68	17.30	1.16	1.80	5.60
		147	2.26	33.88	28.06	2.04	24.40	1.21	2.41	6.04
		198	2.13	34.03	31.33	2.20	37.60	1.27	3.54	6.26
		248	2.24	34.39	31.88	2.32	44.40	1.35	3.86	6.07
		298	2.08	34.47	32.87	2.36	51.50	1.34	4.44	6.28
		349	2.18	34.57	33.20	2.28	56.10	1.49	4.83	6.60
		399	2.36	34.59	33.64	2.40	63.20	1.46	5.07	6.29
		447	2.39	34.62	33.88	2.40	67.60	1.54	5.15	6.26
		499	2.38	34.65	33.97	2.32	71.60	1.60	5.24	6.27
		601	2.37	34.66	33.88	2.24	75.60	1.72	5.65	6.51
		698	2.36	34.68	33.22	2.32	77.10	1.79	5.53	6.58
		797	2.31	34.69	32.67	2.24	81.30	1.81	5.38	6.39
		896	2.26	34.70	32.67	2.24	80.30	1.76	5.49	6.55
		998	2.15	34.71	32.56	2.28	83.30	2.04	5.48	6.64
		1096	2.09	34.71	32.10	2.16	83.90	2.02	5.67	6.75
		1200	2.04	34.71	31.55	2.16	84.50	2.11	6.46	7.18
		1398	1.87	34.70	30.91	2.00	85.50	2.12	5.65	6.68
		1599	1.81	34.69	30.36	1.96	83.90	2.12	5.36	6.41
		1798	1.60	34.68	30.56	2.04	88.00	2.34	6.08	6.79
		2000	1.28	34.68	31.77	2.04	98.80	2.34	6.39	6.57
Max.			2.39	34.71	33.97	2.40	98.80	2.34	6.46	7.18
Min.			1.28	33.84	25.44	1.68	17.20	1.15	1.53	5.57

MLD (193m)	2.30	33.87	26.81	1.83	21.19	1.19	2.04	5.78
Surface (<500m)	2.29	34.19	29.78	2.07	38.67	1.31	3.30	6.02
Inter (500-1500m)	2.18	34.69	32.45	2.20	81.44	1.92	5.66	6.66
Deep (>1500m)	1.56	34.68	30.90	2.01	90.23	2.27	5.95	6.59

Cruise: SOSCEX III **Date: 30/07/2015** **Bottom depth: 2600m**

Domain (Station)	Lat/Long	Depth (m)	Temp (°C)	Salinity (PSU)	NO_3 (µmol kg^{-1})	PO_4 (µmol kg^{-1})	Si (µmol kg^{-1})	dCu (nmol kg^{-1})	dZn (nmol kg^{-1})	dNi (nmol kg^{-1})
DTM3	54˚ 00' S	9	-0.56	33.84	25.63	2.00	-	1.48	3.38	5.99
	00˚ 00' E	30	-0.56	33.84	25.50	2.12	51.00	1.57	3.32	6.19
		49	-0.59	33.84	26.10	2.08	51.70	1.53	3.70	5.96
		74	-0.62	33.84	26.19	2.20	51.90	1.62	4.16	6.01
		99	-0.63	33.85	26.24	2.08	52.10	1.62	3.57	6.17
		123	-0.69	33.93	26.93	2.00	54.20	1.63	3.52	6.07
		148	-0.06	34.15	28.91	2.00	59.90	1.60	4.56	6.18
		173	1.20	34.22	31.97	2.40	74.60	1.71	5.78	6.30
		198	1.44	34.27	32.61	2.36	79.10	1.75	5.98	6.16
		249	1.74	34.32	32.94	2.36	84.20	1.85	6.33	6.57
		299	1.75	34.40	32.54	2.28	86.10	1.88	6.51	6.62
		348	1.76	34.45	32.62	2.44	88.10	1.84	6.24	6.30
		399	1.76	34.49	32.38	2.32	90.00	1.83	5.98	6.61
		448	1.72	34.56	32.33	2.28	90.70	1.96	6.41	6.72
		499	1.68	34.61	32.41	2.28	91.90	2.04	6.49	6.77
		597	1.60	34.64	32.34	2.40	93.50	2.26	6.13	6.76
		698	1.51	34.67	32.25	2.40	95.50	2.04	5.96	6.22
		799	1.41	34.68	31.81	2.16	97.30	2.35	6.39	6.52
		899	1.27	34.70	31.99	2.12	104.00	2.36	6.14	6.34
		999	1.14	34.72	32.41	2.28	103.00	2.17	6.59	6.38
		1249	0.84	34.74	32.84	2.32	109.00	2.42	6.40	6.39
		1499	0.59	34.76	33.38	2.80	115.00	2.46	7.78	6.33
		1999	0.32	34.76	33.68	2.56	122.00	2.45	6.70	6.01
		2488	0.24	34.73	34.42	2.32	128.00	2.90	7.47	6.65
Max.			1.76	34.76	34.42	2.80	128.00	2.90	7.78	6.77
Min.			-0.69	33.84	25.50	2.00	51.00	1.53	3.32	5.96

MLD (128m)	-0.61	33.86	26.10	2.08	52.18	1.58	3.61	6.07
Surface (<500m)	0.62	34.17	29.69	2.21	71.82	1.73	5.06	6.31
Inter (500-1500m)	1.20	34.70	32.43	2.35	102.47	2.29	6.48	6.42
Deep (>1500m)	0.28	34.75	34.05	2.44	125.00	2.67	7.08	6.33

Appendix D

This appendix contains separate data tables for each of the seven sampling locations occupied during the 2017 winter cruise which took place over the 2017 austral winter in the Indian Sector of the Southern Ocean (41-58°S; 30°E). The dissolved cadmium (dCd) particulate cadmium (pCd) are presented in chapter 3 alongside physical temperature and salinity data as well as dissolved macronutrient (PO_4, NO_3 and Si) and particulate phosphorous (P) data. Dissolved zinc (dZn) and particulate zinc (pZn) are also included in the data tables and were presented in chapter 4. Values for trace metals represent the mean of duplicate measurements. A value was deemed an outlier when the relative standard deviation (RSD) between duplicate measurements was >10% of their mean value. The rejected value was determined by curve fitting the data points based on the values above (shallower depth) and below (deeper depth) the suspect value as well as by comparison with other parameters (salinity, temperature, and nutrients) measured from the same GO-FLO bottle. Values in red indicate instances where both measurements were assessed to be outliers, most likely originating from contamination during the sample collection or analytical phase of the investigation. These values were not included in any data interpretation or figures from chapters 3 and 4.

Cruise: Winter 2017 **Date: 07/10/2017** **Bottom depth: 4484m**

Domain (Station)	Lat/Long	Depth (m)	Temp (°C)	Salinity (PSU)	NO_3 (µmol kg^{-1})	PO_4 (µmol kg^{-1})	P (nmol kg^{-1})	Si (µmol kg^{-1})	dCd (pmol kg^{-1})	pCd (pmol kg^{-1})	dZn (nmol kg^{-1})	pZn (pmol kg^{-1})
IO08	41˚ 00' S	25	18,02	35,59	2,55	0,22	11,52	2,92	18,13	5,64	0,25	16,12
	30˚ 00' E	50	18,03	35,59	2,41	0,22	-	2,88	17,77	-	0,18	-
		75	18,03	35,59	3,16	0,19	10,97	2,90	17,99	7,00	0,16	21,84
		100	18,00	35,58	3,14	0,21	16,03	2,94	23,11	10,93	0,20	31,44
		125	17,46	35,56	4,34	0,23	3,52	3,76	51,86	1,17	0,39	13,44
		150	17,24	35,55	4,32	0,31	3,78	3,87	56,77	1,49	0,33	22,25
		175	16,99	35,53	4,99	0,34	3,36	3,96	55,26	1,42	0,77	18,10
		200	16,68	35,52	5,65	0,37	3,29	4,03	68,91	1,30	0,92	20,87
		250	16,01	35,48	6,15	0,41	3,92	4,54	68,98	1,09	0,79	28,71
		300	14,87	35,33	6,42	0,48	3,47	4,78	51,07	1,17	0,66	17,10
		400	13,63	35,28	7,19	0,59	1,84	4,82	91,66	0,25	0,30	9,29
		500	12,41	35,12	12,07	0,70	1,76	5,53	117,60	0,62	0,48	18,44
		800	7,66	34,50	21,18	1,35	2,06	11,96	345,13	1,90	1,01	17,59
		1000	5,46	34,39	29,75	1,88	1,52	27,49	508,70	1,04	1,69	12,99
		1250	4,20	34,43	33,42	2,07	1,10	46,23	640,78	0,90	2,67	12,42
		1500	3,49	34,54	34,75	2,20	0,92	64,21	697,47	0,22	3,69	42,33
Max.			18,03	35,59	34,75	2,20	16,03	64,21	697,47	10,93	3,69	42,33
Min.			3,49	34,39	2,41	0,19	0,92	2,88	17,77	0,22	0,16	9,29
MLD (112m)			18,02	35,59	2,82	0,21	12,84	2,91	19,25	7,85	0,20	23,13
Surface (<500m)			16,45	35,48	5,20	0,36	5,77	3,91	53,26	2,91	0,45	19,78
Inter (500-1500m)			6,64	34,59	26,23	1,64	1,47	31,08	461,93	0,94	1,91	20,75
Deep (>1500m)			-	-	-	-	-	-	-	-	-	-

Cruise: Winter 2017 **Date: 07/10/2017** **Bottom depth: 5528m**

Domain (Station)	Lat/Long	Depth (m)	Temp (°C)	Salinity (PSU)	NO_3 (µmol kg^{-1})	PO_4 (µmol kg^{-1})	P (nmol kg^{-1})	Si (µmol kg^{-1})	dCd (pmol kg^{-1})	pCd (pmol kg^{-1})	dZn (nmol kg^{-1})	pZn (pmol kg^{-1})
IO07	43˚ 00' S	25	10.55	34.58	8.43	0.63	15.30	1.65	42.95	12.85	0.64	28.87
	30˚ 00' E	50	10.55	34.58	10.14	0.63	-	2.25	42.86	-	0.69	-
		75	10.55	34.58	10.79	0.70	13.57	2.27	46.23	12.03	0.29	29.83
		100	10.60	34.60	11.43	0.70	17.17	2.27	48.32	14.91	1.34	97.91
		125	10.79	34.66	11.27	0.81	12.24	2.39	50.51	10.86	0.78	38.75
		150	10.88	34.69	11.40	0.79	11.21	2.45	50.01	9.76	1.00	32.20
		175	10.67	34.66	11.83	0.80	8.27	2.57	62.39	5.90	0.93	28.95
		200	10.66	34.77	11.83	0.89	4.32	2.89	166.80	3.56	0.72	37.21
		250	10.06	34.71	13.46	0.95	3.47	4.59	190.90	3.42	0.78	22.73
		300	9.32	34.61	18.59	1.21	3.85	6.08	254.15	3.64	4.03	24.39
		400	8.36	34.57	22.60	1.45	5.92	10.10	371.73	3.30	1.70	34.45
		500	6.97	34.46	27.00	1.61	3.07	14.96	515.71	2.65	2.27	25.54
		750	4.30	34.25	31.01	2.11	2.17	24.48	645.78	1.74	2.39	21.72
		1000	3.62	34.40	34.65	2.38	1.32	46.89	741.13	0.66	3.53	13.22
		1250	3.22	34.55	35.26	2.47	1.61	63.49	797.53	0.43	4.33	17.85
		1500	2.85	34.62	34.47	2.24	1.05	66.09	776.49	0.28	6.85	48.39
Max.			10.88	34.77	35.26	2.47	17.17	66.09	797.53	14.91	6.85	97.91
Min.			2.85	34.25	8.43	0.63	1.05	1.65	42.86	0.28	0.29	13.22
MLD (228m)			10.59	34.65	11.18	0.76	10.69	2.59	77.88	9.16	0.80	39.55
Surface (<500m)			10.00	34.62	14.06	0.93	8.94	4.54	153.55	7.54	1.01	36.44
Inter (500-1500m)			4.19	34.46	32.48	2.16	1.84	43.18	695.33	1.15	3.87	25.34
Deep (>1500m)			-	-	-	-	-	-	-	-	-	-

Cruise: Winter 2017 **Date: 07/09/2017** **Bottom depth: 5872m**

Domain (Station)	Lat/Long	Depth (m)	Temp (°C)	Salinity (PSU)	NO_3 (µmol kg^{-1})	PO_4 (µmol kg^{-1})	P (nmol kg^{-1})	Si (µmol kg^{-1})	dCd (pmol kg^{-1})	pCd (pmol kg^{-1})	dZn (nmol kg^{-1})	pZn (pmol kg^{-1})
IO06	46˚ 00' S	25	9.56	34.44	12.23	1.02	10.25	3.44	79.57	8.26	0.50	22.45
	30˚ 00' E	50	9.58	34.45	12.37	1.02	-	2.51	83.07	-	0.28	-
		75	9.55	34.44	12.39	0.95	8.81	3.24	88.90	6.09	1.47	38.53
		100	9.64	34.46	12.13	0.95	16.21	2.70	86.08	7.58	11.51	56.25
		150	9.75	34.49	12.10	0.95	12.83	2.59	85.35	9.86	3.01	48.29
		200	10.58	34.70	13.13	0.96	6.86	2.79	73.46	5.78	4.85	34.89
		250	9.92	34.70	15.01	1.23	3.66	4.02	208.31	4.10	0.86	20.47
		300	8.73	34.54	17.39	1.44	2.80	6.65	292.93	3.66	6.77	21.03
		400	7.87	34.52	21.46	1.59	2.83	11.57	417.18	3.80	1.10	19.48
		500	6.06	34.36	25.90	1.90	-	16.00	559.90	-	1.61	-
		600	5.12	34.31	27.85	1.90	1.93	19.28	584.66	2.08	1.59	22.15
		700	4.58	34.32	29.37	2.05	1.47	27.00	622.75	1.46	2.63	20.20
		800	3.93	34.30	30.82	2.15	1.40	32.05	657.19	1.47	2.49	19.57
		900	3.69	34.36	31.97	2.22	1.85	40.73	719.05	1.47	3.07	27.08
		1000	3.31	34.38	32.87	2.40	1.48	47.39	759.74	1.17	3.40	18.72
		1250	2.96	34.53	33.64	2.54	1.10	64.62	787.99	0.52	4.16	7.04
		1750	2.64	34.71	30.95	2.19	0.91	69.47	694.64	0.27	4.68	8.28
		2250	2.47	34.81	27.07	2.01	0.86	64.66	575.91	0.18	4.24	28.53
		2750	2.17	34.81	26.82	1.98	0.86	68.44	550.69	0.10	4.22	18.89
		3500	1.34	34.74	29.97	2.19	0.71	101.65	685.52	0.22	7.12	18.98
		4250	0.81	34.70	32.06	2.40	0.54	116.94	734.60	0.06	7.00	18.43
Max.			10.58	34.81	33.64	2.54	16.21	116.94	787.99	9.86	7.12	56.25
Min.			0.81	34.30	12.10	0.95	0.54	2.51	73.46	0.06	0.28	7.04
MLD (235m)			9.80	34.52	12.77	1.01	9.77	3.04	100.68	6.94	3.21	36.81
Surface (<500m)			9.12	34.51	15.41	1.20	8.03	5.55	197.48	6.14	0.87	32.67
Inter (500-1500m)			4.24	34.36	30.35	2.17	1.54	35.30	670.18	1.36	2.71	19.13
Deep (>1500m)			1.89	34.75	29.37	2.15	0.78	84.23	648.27	0.17	5.45	18.62

Cruise: Winter 2017 **Date: 07/09/2017** **Bottom depth: 5156m**

Domain (Station)	Lat/Long	Depth (m)	Temp (°C)	Salinity (PSU)	NO_3 (µmol kg^{-1})	PO_4 (µmol kg^{-1})	P (nmol kg^{-1})	Si (µmol kg^{-1})	dCd (pmol kg^{-1})	pCd (pmol kg^{-1})	dZn (nmol kg^{-1})	pZn (pmol kg^{-1})
IO05	48˚ 00' S	25	5.10	33.81	22.83	1.74	16.41	5.22	330.26	23.71	0,86	75.52
	30˚ 00' E	50	5.09	33.81	22.91	1.77	14.80	5.28	322.78	21.26	0,80	76.81
		75	5.09	33.81	23.05	1.75	14.46	5.32	341.96	15.20	1,37	63.18
		100	5.10	33.81	23.08	1.80	11.49	5.31	316.67	15.13	1,17	55.98
		150	6.70	34.29	23.54	1.75	5.09	9.17	427.59	7.88	1,27	25.06
		200	6.21	34.26	24.37	1.73	2.60	10.12	450.29	4.26	1,23	19.35
		250	5.62	34.22	25.49	1.77	4.65	10.32	481.34	8.42	1,13	38.34
		300	5.30	34.23	27.58	1.85	-	13.42	546.83	5.42	1,89	-
		400	4.39	34.17	29.02	2.03	3.63	15.98	569.82	4.22	1,78	31.95
		500	4.12	34.22	30.97	2.28	2.58	22.89	562.30	2.57	2,09	26.98
		600	3.62	34.23	32.29	2.43	2.24	29.70	606.42	2.08	2,52	24.55
		700	3.28	34.27	33.75	2.44	2.23	35.96	653.43	1.58	3,57	23.89
		800	3.11	34.32	34.59	2.54	2.30	42.22	667.45	1.52	3,67	65.91
		900	3.07	34.38	35.33	2.59	1.63	49.26	708.35	1.13	3,98	55.35
		1000	2.93	34.43	35.89	2.66	2.04	54.95	744.75	1.06	4,28	37.50
		1250	2.71	34.54	35.80	2.58	-	64.12	744.54	-	6,03	-
		1750	2.60	34.73	32.14	2.12	1.53	67.27	595.08	0.25	4,25	29.39
		2250	2.30	34.78	30.19	2.02	1.54	71.93	560.27	0.25	4,71	13.75
		2750	1.85	34.77	30.62	2.11	1.25	80.79	594.59	0.06	5,11	14.84
		3500	1.13	34.73	32.54	2.30	1.34	103.18	647.47	0.07	6,59	36.49
		4250	0.73	34.70	33.59	2.25	1.15	113.04	708.44	0.17	6,64	22.38
Max.			6.70	34.78	35.89	2.66	16.41	113.04	744.75	23.71	6,64	76.81
Min.			0.73	33.81	22.83	1.73	1.15	5.22	316.67	0.06	0,80	13.75
MLD (137m)			5.42	33.91	23.08	1.76	12.45	6.06	347.85	16.64	1,09	59.31
Surface (<500m)			5.27	34.06	25.29	1.85	9.14	10.30	434.98	10.81	1,36	45.91
Inter (500-1500m)			3.26	34.34	34.09	2.51	2.17	42.73	669.61	1.66	3,74	39.03
Deep (>1500m)			1.72	34.74	31.82	2.16	1.36	87.24	621.17	0.16	5,46	23.37

Cruise: Winter 2017 **Date: 07/08/2017** **Bottom depth: 4020m**

Domain (Station)	Lat/Long	Depth (m)	Temp (°C)	Salinity (PSU)	NO_3 (µmol kg^{-1})	PO_4 (µmol kg^{-1})	P (nmol kg^{-1})	Si (µmol kg^{-1})	dCd (pmol kg^{-1})	pCd (pmol kg^{-1})	dZn (nmol kg^{-1})	pZn (pmol kg^{-1})
IO04	50˚ 00' S	25	1.79	33.77	26.42	1.91	12.91	25.11	526.59	17.68	2,20	106.21
	30˚ 00' E	50	1.79	33.77	26.58	1.87	-	26.94	518.58	-	2,73	-
		75	1.78	33.77	26.81	1.88	13.66	27.27	487.17	20.73	3,52	138.83
		100	1.73	33.78	26.76	1.89	12.37	26.56	477.24	21.16	2,19	114.89
		150	1.43	34.02	31.29	2.06	4.67	32.84	673.21	9.05	3,55	41.89
		200	1.66	34.19	34.63	2.37	4.78	45.20	839.74	8.67	6,00	45.61
		250	2.03	34.33	36.56	2.57	4.29	55.86	898.83	6.03	4,86	32.99
		300	2.09	34.40	37.36	2.54	3.62	63.80	858.83	5.12	6,55	57.54
		400	2.24	34.52	36.64	2.55	4.50	71.58	844.54	2.61	6,70	36.22
		500	2.27	34.60	35.25	2.52	2.40	75.30	800.73	1.25	6,21	32.13
		600	2.27	34.65	34.93	2.47	1.69	79.12	756.07	1.03	6,00	27.22
		700	2.19	34.68	34.24	2.45	2.49	81.95	776.71	0.86	6,72	53.17
		800	2.15	34.70	33.45	2.43	1.56	81.07	731.98	0.50	5,90	26.01
		900	2.11	34.73	32.72	2.33	2.07	80.19	676.50	0.50	6,14	26.95
		1000	2.14	34.75	31.51	2.21	1.81	79.07	620.54	1.01	6,79	37.45
		1250	1.95	34.77	30.74	1.94	1.40	78.35	597.25	0.58	6,24	27.73
		1750	1.35	34.74	32.16	2.11	1.18	97.72	641.77	-	-	25.04
		2000	1.13	34.73	32.56	2.21	2.08	103.28	648.59	0.44	8,39	26.68
		2500	0.76	34.70	33.38	2.27	1.53	117.35	697.08	0.07	8,30	27.91
		3000	0.47	34.69	34.20	2.23	1.90	126.77	752.55	0.50	9,01	47.06
		3500	0.09	34.67	34.15	2.17	1.44	132.22	763.28	0.22	9,12	34.02
Max.			2.27	34.77	37.36	2.57	13.66	132.22	898.83	21.16	9,12	138.83
Min.			0.09	33.77	26.42	1.87	1.18	25.11	477.24	0.07	2,19	25.04
MLD (127m)			1.70	33.82	27.57	1.92	10.90	27.75	536.56	17.16	2,84	100.46
Surface (<500m)			1.88	34.11	31.83	2.21	7.02	45.05	692.55	10.26	4,45	67.37
Inter (500-1500m)			2.16	34.70	33.26	2.34	1.92	79.29	708.54	0.82	6,29	32.95
Deep (>1500m)			0.76	34.71	33.29	2.20	1.62	115.47	700.65	0.31	8,71	32.14

Cruise: Winter 2017 **Date: 07/06/2017** **Bottom depth: 5530m**

Domain (Station)	Lat/Long	Depth (m)	Temp (°C)	Salinity (PSU)	NO_3 (µmol kg^{-1})	PO_4 (µmol kg^{-1})	P (nmol kg^{-1})	Si (µmol kg^{-1})	dCd (pmol kg^{-1})	pCd (pmol kg^{-1})	dZn (nmol kg^{-1})	pZn (pmol kg^{-1})
IO02	56˚ 00' S	25	0.50	33.97	28.74	1.93	12.82	42.91	777.04	16.63	4,19	115.48
	30˚ 00' E	50	0.50	33.97	28.83	1.97	9.36	42.43	735.02	15.43	3,42	147.31
		75	0.51	33.97	28.51	2.01	8.99	43.24	751.37	14.59	3,38	96.01
		100	0.51	33.97	28.94	1.99	7.59	45.57	768.26	10.04	8,43	98.34
		150	0.90	34.18	32.87	2.19	8.04	56.73	1009.08	8.04	6,22	71.84
		200	1.45	34.38	35.69	2.17	3.75	69.74	1159.39	4.27	6,37	59.48
		250	1.85	34.49	35.96	2.19	3.69	73.71	1122.32	4.87	6,95	87.68
		300	1.71	34.51	36.40	2.24	3.38	78.68	1013.86	3.79	5,87	49.28
		400	1.81	34.60	35.78	2.28	6.29	83.56	1068.49	2.78	11,57	35.30
		500	1.77	34.65	35.05	2.24	2.74	88.71	1039.87	1.95	7,03	32.12
		600	1.84	34.69	34.05	2.24	2.58	89.39	986.99	1.21	6,06	33.86
		700	1.69	34.70	33.46	2.14	1.51	91.83	935.20	0.74	6,76	46.42
		800	1.89	34.74	33.12	2.03	3.52	91.18	797.58	0.49	6,83	34.13
		900	1.75	34.74	32.48	1.80	1.75	89.90	825.20	0.39	10,56	20.98
		1000	1.64	34.75	32.14	1.97	1.64	90.04	826.05	0.53	5,84	25.45
		1250	1.40	34.74	32.16	2.00	3.52	97.99	814.95	0.32	6,52	25.05
		1750	0.85	34.71	33.35	1.99	1.96	114.90	860.48	0.42	6,32	31.21
		2250	0.51	34.69	34.49	2.11	1.40	124.07	915.49	0.19	8,18	28.94
		2750	0.29	34.68	34.59	2.21	1.25	129.32	952.67	0.49	8,46	22.94
		3500	0.05	34.67	34.58	2.17	1.33	129.21	941.78	0.34	8,09	90.80
Max.			1.89	34.75	36.40	2.28	12.82	129.32	1159.39	16.63	8,46	147.31
Min.			0.05	33.97	28.51	1.80	1.25	42.43	735.02	0.19	3,38	20.98
MLD (160m)			0.58	34.01	29.58	2.02	9.36	46.18	808.15	12.95	5,13	105.80
Surface (<500m)			1.15	34.27	32.68	2.12	6.67	62.53	944.47	8.24	5,43	79.28
Inter (500-1500m)			1.71	34.72	33.21	2.06	2.46	91.29	889.41	0.81	6,60	31.14
Deep (>1500m)			0.42	34.69	34.25	2.12	1.48	124.38	917.61	0.36	7,76	43.47

Cruise: Winter 2017 **Date: 07/06/2017** **Bottom depth: 5473m**

Domain (Station)	Lat/Long	Depth (m)	Temp (°C)	Salinity (PSU)	NO_3 (µmol kg^{-1})	PO_4 (µmol kg^{-1})	P (nmol kg^{-1})	Si (µmol kg^{-1})	dCd (pmol kg^{-1})	pCd (pmol kg^{-1})	dZn (nmol kg^{-1})	pZn (pmol kg^{-1})
IO01	58° 00' S	25	-0,06	34,00	28,55	1,78	6,63	46,79	697,93	8,54	3,08	77,36
	30° 00' E	50	-0,06	34,00	28,46	1,76	-	45,62	678,40	-	3,12	-
		75	-0,06	34,00	28,65	1,80	9,13	44,73	735,85	13,98	3,72	112,21
		100	-0,06	34,00	28,04	2,00	8,57	53,35	733,61	9,55	6,62	136,67
		150	-0,03	34,01	28,16	1,91	9,84	49,63	764,68	13,61	3,58	128,78
		200	0,63	34,41	34,52	2,14	3,88	77,55	1093,80	4,77	4,86	51,69
		250	0,79	34,49	35,19	2,21	4,27	84,75	1091,81	6,76	6,66	81,98
		300	1,02	34,55	35,23	2,24	3,21	86,42	1116,37	22,41	10,63	110,14
		350	1,29	34,62	35,06	2,34	3,27	91,97	1067,33	3,22	6,22	58,99
		400	1,35	34,64	34,97	2,35	3,31	96,24	1028,63	3,89	6,73	53,95
		450	1,36	34,66	34,67	2,35	4,89	97,45	1002,19	1,91	6,68	33,72
		500	1,32	34,67	34,62	2,34	2,19	98,61	920,81	1,57	6,86	29,15
		550	1,38	34,69	34,16	2,26	12,86	99,14	-	8,11	-	128,41
		650	1,34	34,71	33,60	2,20	-	101,33	907,75	-	5,86	-
		750	1,09	34,70	33,79	2,21	3,07	105,06	962,25	0,81	7,31	64,49
		1000	0,89	34,70	34,10	2,11	3,08	111,84	991,42	0,61	6,79	25,10
		1250	0,65	34,69	34,14	2,14	1,70	114,82	957,14	0,31	6,76	24,36
		1500	0,54	34,69	34,57	2,24	1,49	122,50	947,79	0,31	7,54	24,45
Max.			1,38	34,71	35,23	2,35	9,84	122,50	1116,37	13,98	7,54	136,67
Min.			-0,06	34,00	28,04	1,76	1,49	44,73	678,40	0,31	3,08	24,36
MLD (161m)			-0,05	34,00	28,37	1,85	8,54	48,02	722,09	11,42	3,37	113,76
Surface (<500m)			0,62	34,34	32,18	2,10	5,38	72,76	910,95	6,78	5,15	76,45
Inter (500-1500m)			1,03	34,69	34,14	2,21	2,31	107,61	947,86	0,72	6,85	33,51
Deep (>1500m)			-	-	-	-	-	-	-	-	-	-